PNNL-11450 Rev. 1
UC-2030

Composition and Quantities of Retained Gas Measured in Hanford Waste Tanks 241-AW-101, A-101, AN-105, AN-104, and AN-103

A. Shekarriz
D.R. Rector
L.A. Mahoney
M.A. Chieda
J.M. Bates
R. E. Bauer(a)
N.S. Cannon(a)
B.E. Hey(a)
C.G. Linschooten(a)
F.J. Reitz(a)
E.R. Siciliano(a)

March 1997

Prepared for
the U.S. Department of Energy
under Contract DE-AC06-76RLO 1830

Pacific Northwest National Laboratory
Richland, Washington 99352

(a) Project Hanford Management Contractor

HH

Preface

This report was prepared to satisfy the Defense Nuclear Facility Safety Board (DNFSB) Recommendation 93-5 Implementation Plan (DOE-RL 1996), Milestone 5.4.3.5k, which requires, in part, a "Letter reporting completion of retained gas sampling in tanks AW-101, AN-103, AN-104, AN-105, and U-103." Tank A-101 has been substituted for Tank U-103 by Change No. 1 to this plan. The text of the Recommendation 93-5 Implementation Plan states:

> *The flammable gas hazard will continue to exist until the wastes are retrieved from the tanks. However, DOE plans to resolve the Flammable Gas Safety Issues on a tank-by-tank basis when the following steps are completed: a) determination of the amount and composition of gas retained in the wastes; b) establishment of an adequate understanding of the mechanisms for gas generation, retention, and release; and c) updating the Authorization Basis for the Manage Tank Waste Function.*

The emphasis of this report is on presenting the measurements resulting from retained gas sampling of Tanks AW-101, A-101, AN-105, AN-104, and AN-103, not interpreting the effects of the findings on the understanding of tank behavior or the safety issues. The retained gas sampling information is a direct measurement of the amount and composition of gas retained in these tanks. This information will be combined with information from other sources to develop a better understanding of the mechanisms for gas generation, retention, and release, which will lead to closure of the Flammable Gas Unreviewed Safety Question and resolution of the Flammable Gas Safety Issue.

Executive Summary

This report provides the results obtained for the first five tanks sampled with the Retained Gas Sampler (RGS): Tanks 241-AW-101, A-101, AN-105, AN-104, and AN-103. The RGS is a modified version of the core sampler used at Hanford. It is designed specifically, in concert with the gas extraction equipment in the hot cell, to capture and extrude a gas-containing waste sample in a hermetically sealed system. The retained gases are then extracted and stored in small gas canisters. The composition of the gases contained in the canisters was measured by mass spectroscopy. The total gas volume was obtained from analysis of the extraction process, as discussed in detail throughout this report.

The following are the findings of this research:

- The RGS is a viable approach for measuring retained gases in double- and single-shell waste tanks at Hanford.
- Local measurements of void fraction with the RGS agree with the results obtained with the void fraction instrument (VFI) in most cases .
- In the tanks sampled, more than 16% of the retained gas in the nonconvective layer was nitrogen (N_2). The fraction of nitrogen gas was approximately 60% in Tank 241-AW-101. This finding shows that not all the retained gas mixtures are flammable.
- In the tanks sampled, the ratios of hydrogen to oxidizers were observed to be significantly higher than 1; i.e., these tanks are fuel-rich.

Based on these observations, the RGS will be used to sample for retained gases in several single-shell tanks at Hanford.

The remaining sections of this summary describe the RGS findings for the first five tanks tested. The results are described in the order in which the tanks were sampled, to reflect the increasing experience on which RGS methods were based.

Tank 241-AW-101 (AW-101) Results

Tank AW-101 was the first tank sampled using the RGS system to measure the retained gases. The waste in this tank consists of a nonconvective layer believed to be approximately 260–310 cm in depth, a crust on the surface, and a 710–740 cm supernatant liquid between the crust and nonconvective layer making up the remainder of the 1040 cm total depth of the waste. Six segments were taken with the RGS from two risers in this tank.

Retained gas measurements and estimated solubilities show three major constituents in the gas/vapor phase (free gas) of the nonconvective and convective layers: 60 mol% of nitrogen, 31 mol% hydrogen, and 5.7 mol% nitrous oxide. The remainder of the gas content comprises ammonia, methane, and other hydrocarbons. The measured local ammonia concentrations in AW-101 ranged from 960 to 2900 μmole/liter of waste. Integrating the local concentrations leads to a total amount, if it were vapor (which is improbable), of 120 m^3 (4,200 ft^3) of ammonia at standard temperature and pressure (STP). Based on estimated solubility, more than 99.9% of ammonia is dissolved in the liquid. (Details of integration are in Section 3.4.1.)

The extraction results show that the insoluble gases (other than those in the crust, which RGS did not sample) were primarily retained in the lower 170 cm (70 in.) of the tank, or the lower two-thirds of the nonconvective layer. Based on estimated solubilities and RGS measurements of gas concentrations, about 3.1% by volume (in-situ) of the nonconvective layer was filled with free gas, while 0.6% by volume (in-situ) of the convective (upper) layer was free gas. The in-situ void fraction in the nonconvective layer ranged between 1.7 and 4.4% by volume, consistent with the data reported for VFI measurements in this tank. Some lateral nonuniformity was apparent from differences in measurements between two risers at similar elevations. The calculated hydrogen inventory in both phases of the nonconvective and convective layers of AW-101, based on integrated RGS measurements, is 28 m^3 (990 ft^3).

Two important results were obtained from examining the x-ray images obtained from various segments. First, mostly round bubbles ranging from 1 to 7 mm in diameter were observed in several of the segments taken from the nonconvective layer. However, most of the gas volume was found to be smaller than the detection threshold (<~1 mm) of the current x-ray imaging system. Thus, based on our examination of the x-ray images taken from various points in the nonconvective layer, the structure of the retained gases in this tank is speculated to be a bubbly mixture. Secondly, the calculated mean supernatant density found from the x-ray densitometry approach discussed in this report is 1.42 g/cc, and the gas-retaining waste density averages about 1.63 g/cc.

Tank 241-A-101 (A-101) Results

Hanford Tank A-101 was the first Flammable Gas Watch List (FGWL) single-shell tank sampled for measurement of the retained gases in the waste. The RGS was used in two risers within this tank to sample seven segments. The waste consists of two distinct layers, the lower, liquid-like layer (~498 cm) and the upper, crust-like layer (~424 cm).

Retained gas measurements and estimated solubilities show three major low-solubility constituents in the gas/vapor phase (free gas) of the upper and lower layers: 18 mol% nitrogen, 72 mol% hydrogen, and 5.6 mol% nitrous oxide. The remainder of the gas content is ammonia, methane, and other hydrocarbons. Although some oxygen and argon gas was detected, these two constituents were believed to result from entrainment of the drill string gases into the sampler nose piece. The measured local ammonia concentrations in Tank A-101 ranged from 3,200 to 33,000 µmole/L of waste, more than 99% of the ammonia is dissolved in the liquid. Integrating the local concentrations leads to a total amount, if it were vapor (which is improbable), of approximately 950 m^3 (33,000 ft^3) of ammonia at STP. (Details of integration are in Section 3.4.1.)

The extraction results show that the insoluble gases were primarily retained in the upper layer. Based on the estimated solubilities and RGS measurements of gas concentrations, about 14% by volume (in-situ) of the upper layer was filled with free gas, while 0.4% by volume (in-situ) of the lower layer was free gas. The compositions and void volumes were consistent between the two risers, suggesting that the waste proportions are laterally uniform in the tank. The calculated hydrogen inventory in both phases of the upper and lower layers of A-101 is 218 m^3 (7,700 ft^3), based on integrated RGS measurements.

Images of the sampler taken with the x-ray imaging system reveal that the lower waste layer is primarily a uniform (homogeneous) mixture, possibly a dense liquid, with density of approximately 1.7 g/cc. On the other hand, the upper layer was made up of gas pockets, fractures, and phase heterogeneities. The density of the upper layer, based on the x-ray images, was less than 1.4 g/cc. When the contribution of retained gases was removed from the average density, the remaining waste density (gas-free) ranged from 1.67 to 1.73 g/cc.

Tank 241-AN-105 (AN-105) Results

Tank AN-105 was the second double-shell tank sampled for retained gases. The RGS was used in two risers within this tank to obtain eight segments. The total depth of waste is ~1040 cm, of which 430 cm makes up the nonconvective layer at the bottom of the tank, 50–100 cm is the crust-like layer on the surface, and the remainder is the supernatant liquid.

Retained gas measurements and estimated solubilities show three major constituents in the gas/vapor phase (free gas) of the nonconvective and convective layers: 27 mol% nitrogen, 60 mol% hydrogen, and 11 mol% nitrous oxide. The remainder is ammonia, methane, and other hydrocarbons. The measured local ammonia concentrations in Tank AN-105 ranged from 890 to 2100 μmole/liter of waste, more than 99.9% of the ammonia is dissolved in the liquid. Integrating the local concentrations leads to a total amount, if it were vapor (which is improbable), of approximately 99 m^3 (3,500 ft^3) of ammonia at STP. (Details of integration are in Section 3.4.1.)

The extraction results show that the insoluble gases were primarily retained in the lower, nonconvective layer. Based on the estimated solubilities and RGS measurements of gas concentrations, about 4.5% by volume (in-situ) of the nonconvective layer was filled with free gas, while 0.3% by volume (in-situ) of the convective (upper) layer was free gas. Local calculated void fractions based on RGS data were in close agreement with the VFI results for the segments above 200 cm (80 in.) elevation. While the lower two segments did not have VFI measurements to compare, the trends pointed to reasonable estimates of the void fraction. The maximum void fraction measured with RGS was approximately 11.1% in this tank. Although the void fractions appear to be consistent for both risers, some variations in the gas composition were observed between the two, indicating some lateral variation. The calculated hydrogen inventory in both phases of the nonconvective and convective layers of AN-105 is 103 m^3 (3,600 ft^3), based on integrated RGS measurements.

The x-ray results are significantly different from those of the previous two tanks in several ways: 1) large gas pockets were observed in Tank AN-105 that account for a large portion of the measured void fraction. This contrasts with the observations made for AW-101 waste, where the major portion of the gas was observed to be smaller than the detection threshold of the x-ray imaging system (<0.5 mm); 2) no fractures or irregularly shaped bubbles were observed in this tank, unlike what was observed in Tank A-101 waste. Densities measured in this tank, based on x-ray images, ranged from 1.65 to 1.83 g/cc.

Tank 241-AN-104 (AN-104) Results

Tank AN-104 was the third double-shell tank sampled for retained gases. The total depth of waste in AN-104 is ~978 cm, of which 445 cm is believed to be the nonconvective layer, and the remainder is considered to be the convective, supernatant liquid layer. No appreciable crust is believed to be present in this tank. The RGS was used in two risers within this tank to obtain seven segments.

Retained gas measurements and estimated solubilities show three major constituents in the gas/vapor phase (free gas) of the nonconvective and convective layers: 33 mol% nitrogen, 46 mol% hydrogen, and 19 mol% nitrous oxide. The remainder of the gas is ammonia, methane, and other hydrocarbons. The measured local ammonia concentrations ranged from 1,100 to 3,700 μmole/L of waste, more than 99.9% of which is dissolved in the liquid. Integrating the local concentrations leads to a total amount, if it were vapor (which is improbable), of approximately 140 m^3 (4,900 ft^3) of ammonia at STP. (Details of integration are in Section 3.4.1.)

The extraction results show that the insoluble gases were primarily retained in the lower, nonconvective layer. Based on the estimated solubilities and RGS measurements of gas concentrations, about 5.7% by volume (in-situ) of the nonconvective layer was filled with free gas, while 0.5% by volume (in-situ) of the convective (upper) layer was free gas. The void fractions calculated from RGS data ranged between 0.5% in the supernatant layer and 13.3% in segment 21, near the bottom of the tank, with a monotonic variation between the two limits. With the exception of segment 21, with which there were no VFI data to compare, all the RGS measurements were in close agreement with the VFI results. Because of scheduling constraints, there were insufficient data from both risers to form any conclusions about lateral uniformity in void fraction and gas composition in this tank. The calculated hydrogen inventory in both phases of the nonconvective and convective layers of AN-104 is 102 m^3 (3,600 ft^3), based on integrated RGS measurements.

The same general x-ray observations are true about Tank AN-104 as about Tank AN-105. Further, densities measured in this tank, based on x-ray images, were 1.41 g/cc for the supernatant layer and ranged from 1.72 to 2.09 g/cc within the nonconvective layer.

Tank 241-AN-103 (AN-103) Results

Tank AN-103 was the fourth double-shell tank sampled for retained gases. The total depth of waste in AN-103 is ~884 cm, of which the nonconvective layer is believed to be about 378 cm, the crust is ~92 cm, and the balance is a supernatant liquid. Seven segments were taken with the RGS in two risers within this tank.

Retained gas measurements and estimated solubilities show three major constituents in the gas/vapor phase (free gas) of the nonconvective and convective layers: 35 mol% nitrogen, 60 mol% hydrogen, and 3.7 mol% nitrous oxide. The remainder of the gas is composed of ammonia, methane, and other hydrocarbons. The composition of the crust free gas was very similar: 29% nitrogen, 63% hydrogen, and 6.7% nitrous oxide. The measured local ammonia concentrations in Tank AN-103 were found to range from 1,300 to 3,800 µmole/liter of waste, more than 99.9% of which is dissolved in the liquid. Integrating the local concentrations leads to a total amount, if it were vapor (which is improbable), of approximately 170 m^3 (6,000 ft^3) of ammonia at STP. (Details of integration are in Section 3.4.1.)

The extraction results show that the insoluble gases were primarily retained in the lower, nonconvective layer. Based on the estimated solubilities and RGS measurements of gas concentrations, about 7.7% by volume (in-situ) of the nonconvective layer was filled with free gas, while 0.4% by volume (in-situ) of the convective (upper) layer was free gas. One crust sample was taken; its void fraction was 14.6%. The void fractions based on RGS data ranged between 0.4% in the supernatant layer and 9.4% in segment 16. These measurements were, in general, lower than what was measured with VFI. Because some samples were lost owing to sampler valve problems, there were insufficient data from both risers to form any conclusions about lateral uniformity in void fraction and gas composition in this tank. The calculated hydrogen inventory in both phases of the nonconvective, convective, and crust layers of AN-103 is 168 m^3 (5,900 ft^3), based on integrated RGS measurements.

The same general x-ray observations are true about Tank AN-103 as those about Tank AN-105. Further, densities measured in this tank were higher than those measured in the other tanks. The measurements, based on x-ray images, suggest the densities range from 1.85 g/cc to 2.12 g/cc in this tank.

Overall Summary for all Tanks

The table below summarizes the void fractions, void volumes, and hydrogen contents of the five tanks discussed in this report. The values in the table are derived from RGS data alone. The ± values represent a standard deviation that results from instrument error and uncertainty in locating (or defining) layer interfaces; they do not include estimates of lateral or temporal variability.

Table S.1. Overview of Tank Gas Contents Based on RGS Data

All values derived from RGS data alone	In-Situ Void Fraction (single-point or **average**)	Maximum In-Situ Void Fraction	Mol% H_2 (single-point or **integrated average**)	Total STP Free Gas (m^3)	Total STP Free Hydrogen (m^3)
AW-101 Convective	0.006±0.001	0.006±0.001	26 ± 7	21 ± 5	5.6 ± 0.8
AW-101 Nonconvective	**0.031±0.006**	0.044±0.004	**32 ± 2**	69 ± 11	22 ± 3
A-101 Lower	**0.004±0.001**	0.006±0.001	**16 ± 1.5**	14 ± 1.3	2.2 ± 0.2
A-101 Upper	**0.142±0.014**	0.178±0.011	**75 ± 4**	290 ± 23	220 ± 14
AN-105 Convective	0.003±0.001	0.003±0.001	24 ± 8	10 ± 3.5	2.3 ± 0.6
AN-105 Nonconvective	**0.045±0.005**	**0.111±0.009**	**62 ± 4**	160 ± 37	97 ± 23
AN-104 Convective	0.005±0.001	0.005±0.001	25 ± 9	10 ± 3.8	2.6 ± 0.4
AN-104 Nonconvective	**0.057±0.010**	**0.133±0.013**	**47 ± 4**	200 ± 26	96 ± 12
AN-103 Crust	0.146±0.015	0.146±0.015	63 ± 2	48 ± 3.0	30 ± 1.5
AN-103 Convective	0.004±0.001	0.004±0.001	18 ± 10	8.8 ± 4.6	1.6 ± 0.3
AN-103 Nonconvective	**0.077±0.012**	**0.094±0.012**	**62 ± 7**	216 ± 22	134 ± 13

Acknowledgments

The authors especially would like to acknowledge the instrumental role played in implementation of the Retained Gas Sampler System by the following Project Hanford Management Contract (PHMC) personnel: Ken Birney, Al Bridges, Dennis Graves, Jerry Johnson, Craig Knight, Bob Kowitz, Jim Weber, Dave Wootan. Many thanks to Milt Goheen and Larry Pederson at Pacific Northwest National Laboratory and Bill Kubic at the Los Alamos National Laboratory. Also, we would like to thank Chuck Stewart, Harry Babad, and Joe Brothers for reviewing the document.

This report is dedicated to the memory of Ken Birney.

Contents

Figures

Tables

1.0 Introduction

Interest in understanding how much and what types of gases are stored in the Hanford waste tanks stems from the fact that the waste in many of the tanks at Hanford has been shown to generate, retain, and release gas in a gradual or episodic fashion. On the basis of the amount and type of gas potentially present and the type of safety hazard they pose, many of the tanks at Hanford have been placed on the Flammable Gas Watch List (FGWL). A concise review of the flammable gas safety issues and the list of the FGWL tanks is provided in Stewart et al. (1996a).

Many studies have been performed to better understand the mechanisms that control the rate of generation of various gases and the modes of retention of gas bubbles in various types of wastes. A comprehensive review of gas generation studies is provided in Pederson and Bryan (1996). Also, a compilation of the results of gas retention studies can be found in Gauglitz et al. (1996). This section contains a summary of the relevant findings provided in these two reports.

Studies with simulants of the Hanford waste tanks (Meisel et al. 1993; Ashby et al. 1994) suggest the following observations: 1) hydrogen was generated by radiolysis of water and radiolytic reactions involving organic solutes; 2) hydrogen was also one of the byproducts of thermal decomposition of chelators, while aluminate and nitrite ions were present and played an important role; 3) nitrogen-containing gas species were formed by thermally or radiolytically induced reactions involving nitrite ions, while aluminate ion was a major catalyzer of decomposition reactions in the absence of radiation; 4) the presence of oxygen enhanced generation of hydrogen in a simulated waste and inhibited production of nitrogen-containing gases.

Studies with actual wastes from Tanks 241-SY-101 (SY-101) (Person 1996) and 241-SY-103 (SY-103) (Bryan et al. 1995, 1996) produced the following observations: 1) thermal nitrous oxide generation was favored at high reaction temperatures, and thermal hydrogen generation was favored at lower temperatures similar to those at which wastes are stored; 2) radiolytic contribution of hydrogen gas generation in Tank SY-103 waste was more than four times greater than the thermal contribution while the cumulative rate of generation matched those reported from head space measurements (Wilkins 1995); 3) while the total organic carbon (TOC) and aluminate ion concentrations are different in SY-101 than in SY-103 waste, the gas generation rates in the two waste samples were comparable. This contrasts with the findings from studies on simulants. 4) results of studies on SY-101 waste showed that presence of oxygen promoted generation of hydrogen, consistent with the studies on simulants, while it essentially had no effect on the rate of generation of nitrogen-containing gases, in contrast to the simulant studies results.

Much less is known about solubility of gases in the waste. Two groups of studies have been performed to address solubility of the major gas constituents in Hanford tank wastes: 1) experimental studies of Norton and Pederson (1994, 1995), validated by the empirical correlations based on Schumpe ion interaction parameters (Hermann et al. 1995); and 2) modeling of solubility by Los Alamos National Laboratory (LANL 1994) based on Pitzer ion interaction model. Pederson and Bryan (1996) summarize the results of both studies and conclude that LANL (1994) estimates are substantially higher than those obtained from the Schumpe model, providing a more conservative approach to estimating gas quantities.

Gas phase reactions were addressed in studies by Bryan and Pederson (1995, 1996). They found that, under typical radiation doses and temperature ranges within the Hanford tank wastes, 1) thermally and radiolytically activated nitrous oxide decomposition was less than 1% per year; 2) nitrous oxide/hydrogen reactions led to less than 2.2% consumption of nitrous oxide per year and even less if waste solids were present; and 3) less than 1% decomposition of ammonia occurred with moist simulated wastes.

Palmer et al. (1996) performed a comprehensive study of the mechanisms of ammonia release from Hanford tank wastes. They considered releases by several mechanisms: 1) diffusion-limited; 2) large releases such as rollovers, limnic eruptions, and earthquakes; 3) small releases such as chimney mudpot and dry-out fractures; and 4) tank operations effects such as intrusion and dilution. They concluded that buoyant displacements and tank operations are the only two mechanisms that may lead to significant ammonia concentrations in the tank head space. Their models showed that the two most important parameters controlling the head space concentrations are ammonia concentrations in the waste and Henry's law constant for ammonia.

Studies on mechanisms of retention of gas bubbles and release summarized in Gauglitz et al. (1996) were directed to classifying the shape of gas bubbles and their retention mechanisms on the basis of several dimensionless parameters. They concluded that gas retention can be yield-strength dominated where the bubbles are particle-displacing, or capillary-force dominated where the bubbles are interstitial liquid-displacing. The experimental observations for all actual waste and most of the simulants studied suggest that the predominant mode of retention is yield-strength dominated. The only results showing capillary-dominated retention were for a slurry of glass beads, which is not representative of the actual wastes. Further, it was observed that the shape of the bubbles is primarily spherical when the surface tension forces dominate the strength of the waste. A dendritic formation or slit-shaped entity of gas was shown to exist when the sludge strength was high.

Although a large number of studies have indirectly or directly estimated the physical and chemical characteristics of the gases stored in the FGWL tanks, the knowledge of actual condition in the various tanks from a direct measurement approach is of paramount importance. Thus the RGS methodology was formulated by which these characteristics are more directly qualified and quantified for the actual waste at the in-tank conditions. This report provides the results for the first five tanks sampled with RGS: AW-101, A-101, AN-105, AN-104, and AN-103. The data for these tanks are presented in the order in which the tanks were sampled.

Section 2 provides an overview of the process by which retained gases in the Hanford tanks are sampled and analyzed. A detailed description of the procedure used to reduce and analyze the data is provided in Section 3. Finally, tank-by-tank results are covered in Section 4. Appendixes A contains details of the sampler design, sampling procedure, gas extraction equipment, and laboratory procedures. Appendix B describes the procedures used to determine the sampler volume and its uncertainty. Appendix C contains detailed laboratory data from each of the five tanks.

2.0 Retained Gas Sampler Data Acquisition System

The RGS is a modified version of the core sampler specifically designed for sampling gas. An overview of the procedure by which the data were analyzed and interpreted is provided in this section. Figure 2.1 provides a graphical diagram of the flow of material and information from the tanks sampled to the end product (this report). The RGS system; sampler preparation, deployment, and retrieval; and the analytical procedure is detailed in Appendix A. Details on the core sampler and modifications and operational constraints of the RGS are contained in Webb (1994).

To obtain an RGS sample, an RGS is installed in the drill string, lowered into the correct vertical position in the tank, and the sample taken by holding the sampler piston in position while pushing the rest of the sampler and drill string down through the waste. When the piston contacts the top end of the sampler, a spring is triggered that closes the sampler ball valve—hermetically sealing the waste sample solids, liquids, and gases in a chamber approximately 1.125 inches in diameter and 19 inches long.

The sampler is then removed from the tank and immediately placed in the x-ray cart for x-ray imaging. The x-ray images provide information about the amount of recovery and subsequent analysis that will be required on the gas phase distribution, void structure (bubble shape, etc.), and density of the waste. After x-raying, the sampler is placed in a transport cask for delivery to the hot cell facilities for extrusion and gas extraction. To extract the gases, the sampler is loaded into the hot cell and installed on a previously evacuated extraction system. A photograph of the extrusion and extraction system is provided in Figure 2.2. The appendix contains more details of the system. The sampler ball valve is opened and the extruder's hydraulic ram pushes the sampler piston all the way forward to move the sampler contents into the extractor. The sample waste is then stirred at the ambient or an elevated temperature (depending on the particular stage of testing), and sample gas is then transferred from the extractor to collector gas sample canisters using a mercury transfer pump. During this process the sampler and canister pressures and temperatures are monitored and recorded. The data files are transmitted for further data reduction and analysis. In parallel, the extracted gases are analyzed via a mass spectrometry system.

An analysis procedure was formulated that uses the temperature, pressure, and volumes during extraction as well as the mass spectrometry data on species concentration as input, and mole fraction of gas constituents, total volume of each gas, vapor phase versus dissolved percentages for all species, and void fraction for each elevation at which the gas was sampled as output. The analysis also provides an estimate of the gas inventory in the nonconvective layer within the tank. The x-ray images are analyzed to provide, in addition to qualitative observations, quantitative information on the density and distribution of the phases in the sampler immediately after removal of the sample from the tank (see Section 3.5).

Shekarriz (1994) performed a series of flow visualization tests to examine the effectiveness of the RGS drill bit in capturing bubbles in the sludge during sampling. A transparent simulant with rheological properties similar to the sludges in the DSTs was used for these tests. Based on these tests, it was concluded that a 60° drill bit provides the optimal conditions for minimizing disturbance of the bubbles and the waste during sampling. Comprehensive studies were performed to quantify the uncertainty in measuring retained gases using RGS (Cannon and Knight 1995, 1996). In these acceptance tests, the procedures for sampling both insoluble (low solubility) gases and ammonia were calibrated. It was found that, while the insoluble components could be measured with high accuracy, ammonia was more problematic because it is absorbed within the system. The tank-by-tank results are given in the order in which sampling was carried out in order to reflect the increasing experience on which RGS methods were based. The details of the difficulties with ammonia measurements are given in Section 3.2.

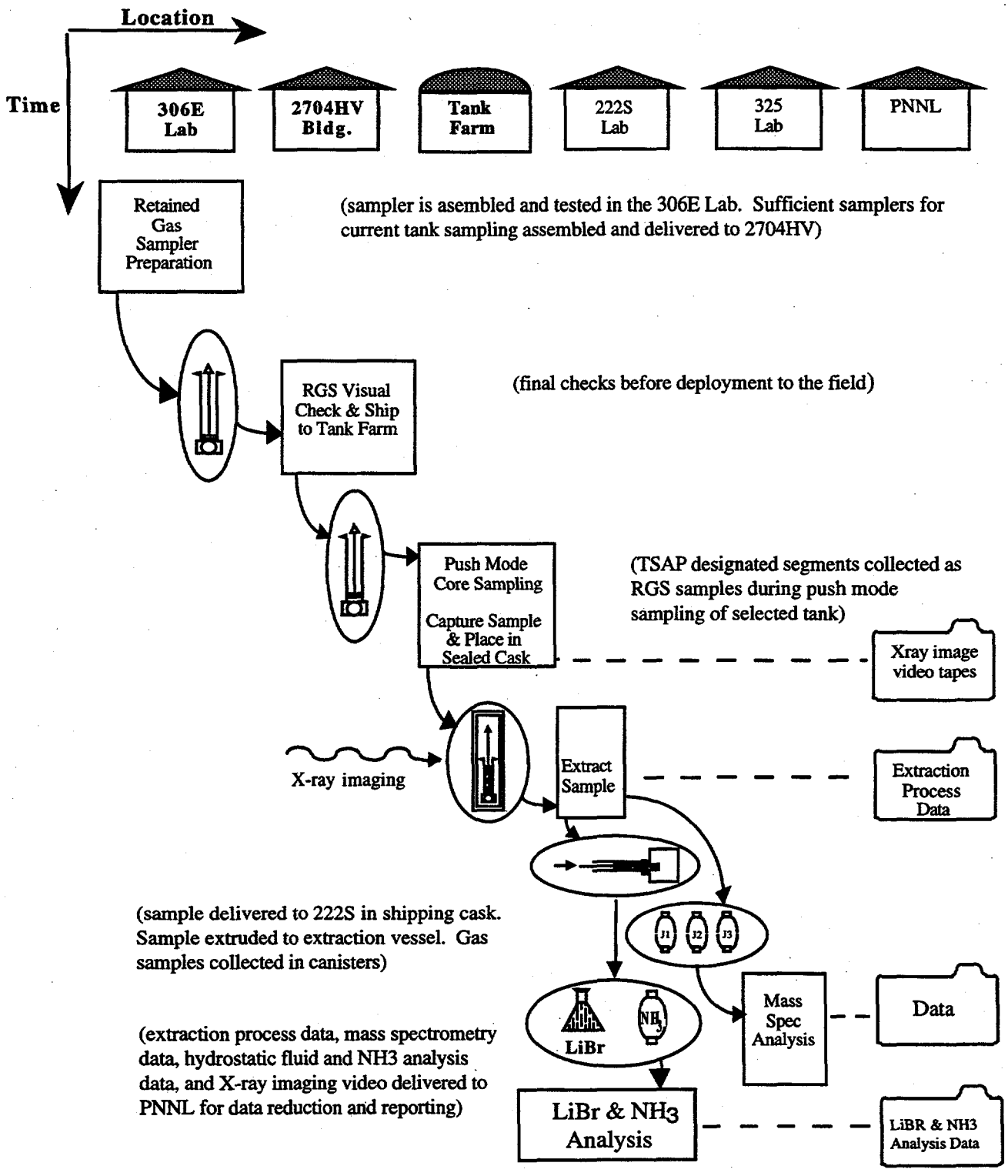

Figure 2.1. RGS Process Flow Diagram

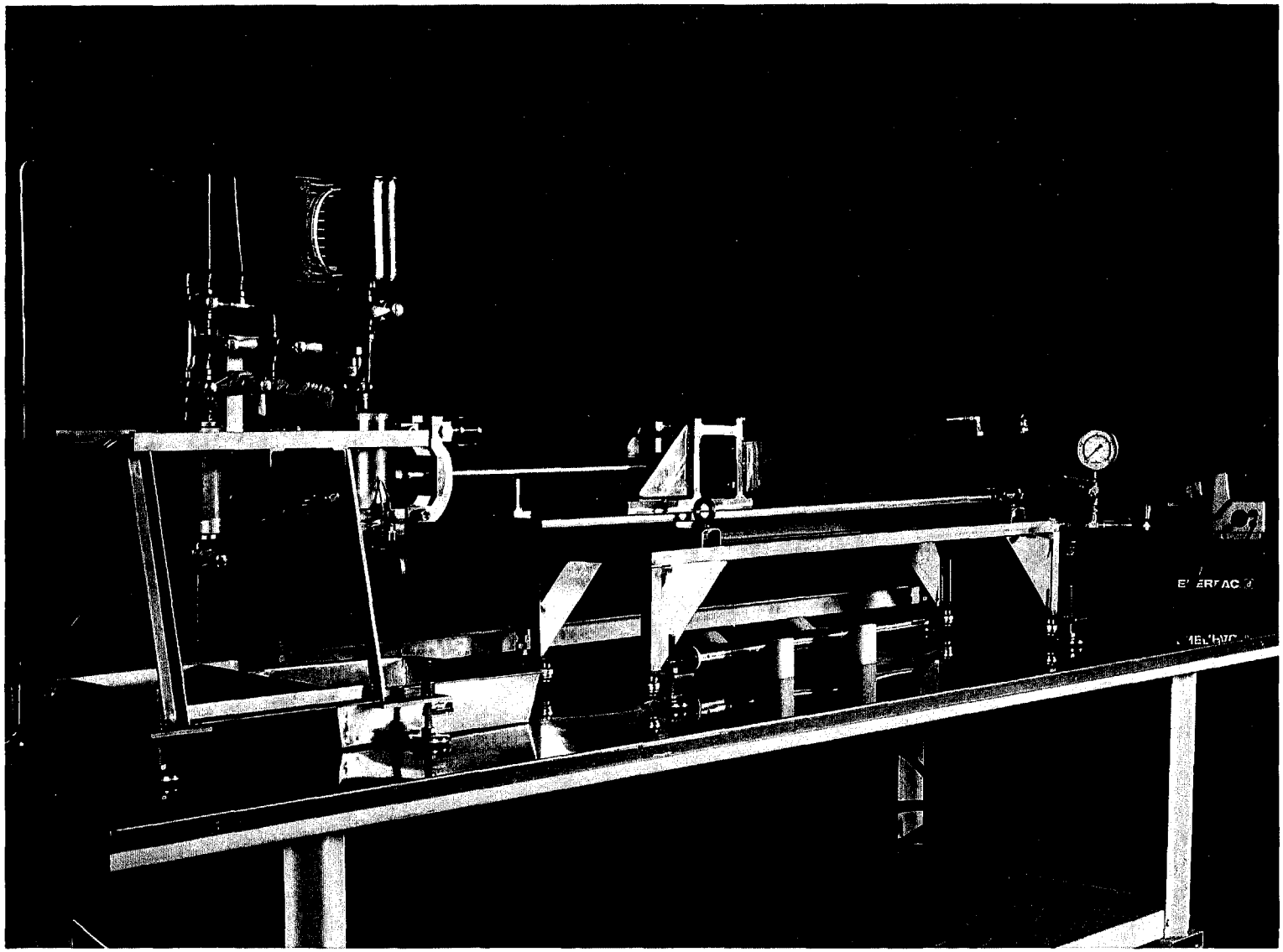

Figure 2.2. Photograph of the RGS Extrusion and Extraction System

3.0 Data Analysis

This section provides the details of the analysis used to process the raw data to determine quantities of interest such as the total concentration of each species of gas in each waste sample. The section describes the inputs, assumptions, and procedures related to each of the analysis tasks. A tank-by-tank discussion of the analysis results is presented in Section 4 and in the appendixes.

The trapped gases in tank waste exist both in the form of bubbles (free gas) and as dissolved gases in the liquid. Section 3.1 describes the procedure for determining the concentrations of low-solubility gases, which exist primarily in the form of "free gas" or bubbles. Section 3.2 describes the procedure for determining the concentration of high-solubility ammonia, which exists both as a vapor and dissolved in the waste solution. The procedure for determining the distribution of the gas constituents between vapor and liquid under in-tank conditions (the total void fraction) are described in Section 3.3. These results are then used to determine the total tank inventory of gases in the liquid and vapor phases, as described in Section 3.4. A description of the procedure for x-ray images is presented in Section 3.5.

3.1 Concentration of Low-Solubility Gases

The objective of this task is to determine the concentration of low-solubility (sometimes called "insoluble") gases in each waste sample as received. A "sample" consists of one 48-cm (19-in.) waste segment; the words "sample" and "segment" are used interchangeably in this report. A sample, as received, may contain not only native tank waste but hydrostatic head fluid (HHF) and entrained gases (potentially a combination of air and argon gas used to purge the drill string). These possible contaminants are discussed in Section 3.4.

The term "low-solubility" implies that the gases are assumed to be primarily in the gas/vapor phase and that a negligible amount is dissolved in the liquid portion of the waste sample. Gases that fall in this category include nitrogen (N_2), hydrogen (H_2), oxygen (O_2), argon (Ar), and methane (CH_4). Although nitrous oxide (N_2O) is partially soluble, analysis results indicate that the residual amount remaining after the final extraction procedure can be considered negligible. Therefore, the data analysis for nitrous oxide concentration is the same as for other low-solubility gases. It should also be noted that the portion of the ammonia that is present in the gas-collection canisters as vapor is calculated in the same way as the low-solubility gases. The rest of the ammonia is calculated by methods described in Section 3.2.

The composition of low-solubility gases (and ammonia vapor) for each sample was determined using data obtained from the extraction process described in Section 2 (and in more detail in Appendix A), in which both low- and high-solubility gases were extracted from the sample and collected in three canisters (often referred to as J canisters) using a mercury vacuum pump. The content of each J canister was analyzed using mass spectrometry to determine the dry mole fraction for each gas component. The total amount of each species of gas in a particular waste sample was determined by calculating the total amount of gas (excluding water vapor) in each canister based on the measured canister pressure and the ideal gas law, partitioning the different components using the measured dry mole fractions, and then summing over all the canisters. The amounts of gas in each J canister, and the per-canister composition, can be found in Tables C.n.6 and C.n.7. (Here "n" is a tank identification index from 1 through 5; it refers to the order in which tanks were analyzed and corresponds to the order in which tank results are discussed in Section 4.)

The procedure described in this section requires input from a variety of sources. The dry mole fraction results (Table C.n.1) are obtained using mass spectrometry analysis, as presented in Appendix A (Section A.3). The collector volumes, determined during the acceptance testing by pressurizing the system with a known quantity of gas, are listed in Appendix C (Tables C.n.2). The collector pressures and temperatures are measured during the procedure as described in Appendix A (Section A.3). The tank-specific collector pressures as a function of pump cycle are presented in Appendix C (Tables C.n.3-5).

The following assumptions are made in the data analysis and interpreted in this section:

- The sampler is entirely filled with tank waste (gas/vapor and slurry). That is, 100% sample recovery is assumed. This assumption is unavoidable because, lacking a method for measuring pressure in the sampler and comparing it to in situ pressure, we cannot tell whether the void spaces in x-ray images result from retained gas volume or from incomplete sample recovery. Thus we cannot quantify the impact of this assumption, but we believe it leads to less than 10% underestimation of gas content in samples with less than complete sample recovery. This belief is based on a qualitative review of x-ray images of samplers and a comparison of the void in them to the extracted gas content.

- The water in pumped J canisters is assumed to have the vapor pressure of pure water. Pumped canisters (see Section A.3 for a detailed description of the pumping procedure) are not in direct contact with the sample, being valved off from it at all times. The actual water vapor pressure in a canister is that of a dilute solution of ammonia in water; preliminary estimates give a water vapor pressure that is more than 50% of the value for pure water. Since the vapor pressure of water at room temperature is about 0.03 atm, the maximum potential error introduced by this assumption is that of underestimating the joint pressure of low-solubility gas and ammonia vapor by 0.015 atm. The total pressures are typically greater than 0.3 atm for the canisters in which the bulk of low-solubility gas is collected (the first two canisters of nonconvective layers), meaning that the underestimation is 5% or less in these cases. In samples from convective layers, which retain much less gas (discussed in Section 4) and produce lower total canister pressures, (averaging about 0.15 atm), the underestimation of low-solubility gas is estimated to be 10%.

- The water vapor pressure for unpumped J canisters (which are directly connected with the extractor side and with the sample) is assumed to be the vapor pressure over the waste. This vapor pressure is calculated based on correlations from simulant data (Mahoney and Trent 1995, Equation 6.2 and Table 6.2). This model relates the experimentally observed water vapor pressure over tank waste simulant to the temperature and concentration of the simulant. The maximum error of the water vapor pressure model was found to be ± 15% over a salt concentration range of 0 to 61 wt%, a dissolved ammonia range of 0 to 3.5 molal, and a temperature range of 25 to 70°C. Because unpumped canisters can have total pressures of less than twice the water vapor pressure, the underestimation of low-solubility gas is probably about 10% for the unpumped canisters. However, these relatively low-pressure canisters typically do not contribute much of the total extracted gas for a sample (as a review of Table C.5.6 will show); so a 10% error in unpumped canisters produces an underestimation of only 1 or 2% in the total sample gas.

- The gas/vapor species collected in the J canisters behave like ideal gases under extraction process temperatures (about 25°C) and pressures (0.02 to 0.95 atm). This assumption holds for ammonia vapor as well as for the low-solubility species; ammonia's critical pressure and temperature are 112.5 atm and 132.5°C. The reduced pressure ($P/P_c < 0.01$) is so low that the compressibility factor of ammonia is effectively unity.

- No significant amount of gas is lost because of system pumpdown between canisters. The amount of gas that is evacuated from the collector during pumpdowns is accounted for by assuming the same gas composition in the collector line volume as in the J canister (whose gas composition is measured). The gas in the collector lines is then included as part of that in the canister by using a combined canister/line volume in calculations (and in Tables C.n.2) instead of using the canister volume alone. Part of the extractor side of the apparatus is also evacuated. This gas loss is not accounted for, but the volume and low pressure of this part of the extractor cause the estimated loss to be less than 2% of the sample total gas.

- The volume of condensate trapped in the J canister is negligible because the density of the liquid is so much greater than that of the vapor. Preliminary estimates indicate that less than 0.3% of the canister volume (or 0.3 ml) is taken up by condensate.

- The low-solubility gases are completely extracted from the sample to the collector; no significant amount is lost as a result of deposition on equipment surfaces, nor is a significant amount lost as a result of dissolution in the canister condensate.

In summary, the assumptions under which the low-solubility gas data analysis is conducted are believed to bias the gas estimate on the low side. The total underestimation is probably 5% or less for samples with gas content above about 3% void fraction, and about 10% for samples with lower gas content. Some further underestimation (believed to be 10% or less) may result from incomplete sample recovery in some cases, but this cannot be well quantified.

The total amount of each insoluble gas constituent in a particular waste sample is determined by calculating the total amount of gas (excluding water vapor) in each canister. Using the measured mole fractions (which are based on dry gas), the amount of each gas constituent in each canister is determined and then summed over all canisters.

The total amount of dry gas in a J canister is determined using the collector pressure and temperature data from the retained gas sampling system and assuming ideal gas behavior:

$$N_j = \frac{(P_j - P_{v_j})V_j}{RT_j} \qquad (3.1.1)$$

where j indicates the canister number, P_j is the total pressure (which includes water vapor pressure) at the end of the extraction process for each canister, P_v is the partial pressure of water at saturation, T_j is the canister temperature, V_j is the volume of the collector, and R is the universal gas constant. Note that the measured total wet pressure is adjusted to a dry basis by subtracting the water vapor pressure in equilibrium with the condensed water in the collector system (for pumped canisters) or in equilibrium with the waste sample (for unpumped canisters). The canister pressures and volumes used in this expression can be found in Tables C.n.2.

The total amount of dry gas, expressed in moles, is divided into separate components using the mass spectrometry data shown in Appendix C (Tables C.n.1). (The mass spectrometry compositions are given as dry-basis mole fractions; that is, they sum to 100% without water included.) The relative quantity of each component, i, is expressed in terms of a mole fraction, f_{ij}. Therefore, in the case of three canisters, the total quantity of each gas component, n_i, is determined by

$$n_i = \sum_{j=1}^{3} f_{ij} \cdot N_j \qquad (3.1.2)$$

Combining Equations 3.1.1 and 3.1.2 yields

$$n_i = \sum_{j=1}^{3} f_{ij} \cdot \frac{(P_j - P_v)V_j}{RT_j} \qquad (3.1.3)$$

The number of moles of each species in each canister can now be calculated using Equation 3.1.3. The total number of moles of each low-solubility gas species extracted from a particular waste sample is the sum of the quantities calculated for the three canisters. These values are then divided by the sampler volume to give the concentration of each low-solubility gas species per liter of waste under in-tank conditions (see Section 4 for results).

It is useful to examine the mole fraction information, provided in Tables C.n.7 as the mass spectrometry results, to determine the extent to which the assumption of complete gas extraction (e.g., low solubility) is consistent with the data. This analysis approach is based on the assumption that the only gas component with significant solubility is ammonia. Gas solubility calculations presented in Section 3.2 indicate that the second most soluble gas component is nitrous oxide, which has a solubility at least two orders of magnitude lower than that of ammonia. One way to verify this assumption is to calculate the relative composition of the insoluble gases (excluding ammonia) for each canister. For truly insoluble gases, the relative composition will not change for a given sample, assuming that all the insoluble gases have come out of the waste and are present in the extractor dome space during the extraction process for all three canisters.

The results of this comparison are presented in Appendix C (Tables C.n.7). Given the measurement uncertainties, the values for hydrogen, nitrogen, oxygen, and argon are relatively constant as a percentage of total. However, it does appear that the fractions of nitrous oxide, methane and the other hydrocarbons increase slightly as the insoluble gases are removed from the sample, indicating the possibility of a solubility effect. The effect is sufficiently small, however, such that it will not significantly affect the total composition results.

The uncertainty in determining the number of moles of each species for each J canister is a function of the uncertainty in the canister pressure measurement, volume measurement, canister temperature measurement, and the mole fraction measurements provided by mass spectrometry. The uncertainty in the pressure measurement is ± 2% of the full range of the instrument, which is 1 atm, or approximately ± 2.0 kPa. The uncertainty in the temperature measurement is approximately ± 2.2°C. The cumulative uncertainty is found using the root mean square approach of Klein and McClintock as described in Holman (1978).

Throughout the data analysis, the assumption is made that the sampler was completely filled with tank waste during the sampling procedure. This assumption is not necessarily true; it depends on the resistance to movement of the waste during sampling, which may be due either to the cohesive strength of the waste or drag along the walls of the sampler. This effect might result

in the waste not filling the sampler and leaving a void at the top of the sample.[a] Such a situation would be observable in the x-ray images discussed in Section 4.n.8. Throughout the analysis, it is assumed that the voids observed in the x-ray images are not due to this phenomenon, but rather to air/argon entrainment into or gas phase redistribution within the sampler.

3.2 Concentration of Ammonia Gas

The objective of RGS sampling is to determine the total amount of gas, both "free" and dissolved, retained in the waste. The gases in the waste sample with a high solubility, such as ammonia, cannot be calculated using the methods described in the previous section because a significant portion remains dissolved in the waste solution at the end of the extraction process. As the gas is pumped from the extractor, dissolved gas comes out of solution to replace it. Unless enough pumping cycles are performed to completely extract the dissolved gas, a method is required to estimate the amount remaining in solution. Because the amounts of soluble gases are not directly observable, it is necessary to use some form of inference to calculate the amounts.

The extraction procedure described in Appendix A is used to obtain information about the concentration of ammonia in the sample. The total amount of ammonia in each sample is determined by summing the amounts of ammonia vapor removed in the gas canisters, using the same methods described in Section 3.1 and adding an estimate of the residual ammonia remaining in the sample, as is described in this section. The residual is determined by comparing the change in partial pressure of ammonia, obtained from the canister pressure versus vacuum pump cycle curves, and the measured change in total ammonia. It should be noted that this method does not rely on the use of any *a priori* Henry's Law constant, theoretical or experimental.

Supplementary information (partial pressure of ammonia over the sample) is obtained by a procedure that uses an initially evacuated canister (referred to as an ammonia, PQ, or wet-chemistry canister) that is connected to the extractor gas space. After the sample comes to equilibrium in the extractor and before extracting the gases with the mercury pump, a sample is taken from the extractor into the ammonia canister. The canister is opened to the extractor gas space and allowed to reach equilibrium; the canister is then isolated and removed from the hot cell. A small amount of acidic solution is injected into the canister, and the solution is allowed to absorb the ammonia gas. The solution is removed from the ammonia canister and analyzed for concentration of ammonia. This information is then used to determine the partial pressure of ammonia in the extractor (Tables C.n.12); it is not used to estimate the amount of ammonia in the sample.

The analysis procedures described in this section require input from a variety of sources. The dry mole fraction for ammonia is obtained using mass spectrometry analysis (Tables C.n.1) of the vapor in the J canisters. The collector volumes are determined during acceptance testing by pressurizing the system with a known quantity of gas, as described in Section 3.1. The collector pressures and temperatures are measured during the procedure described in Appendix A (A.1.3). The collector pressures as a function of pump cycle are presented in Tables C.n.3–5. The supernatant liquid ion concentrations were obtained from various sources, including the Tank Characterization Reports, and can also be found in Tables C.n.10.

The following assumptions were used in the J (extraction) canister data analysis for the amount (moles) of ammonia:

- 100% sample recovery is assumed (as for low-solubility gases, Section 3.1).

(a) Shekarriz A and JD Norton. 1995. *Retained Gas Sampler System Analysis.* PNLFGP:091595, Pacific Northwest Laboratory, Richland, Washington.

- The water in pumped J canisters is assumed to have the vapor pressure of pure water (as for low-solubility gases, Section 3.1).

- The water vapor pressure for unpumped J canisters is assumed to be the vapor pressure over the waste (as for low-solubility gases, Section 3.1).

- Ammonia behaves as an ideal gas (as for low-solubility gases, Section 3.1).

- No significant amount of gas is lost because of system pumpdown between canisters (as for low-solubility gases, Section 3.1).

- The volume of condensate trapped in the J canister is negligible (as for low-solubility gases, Section 3.1).

- No significant amount of ammonia is lost because of deposition on equipment surfaces. Tests have been made using gas standards with low ammonia concentrations and no water. The preliminary findings are that approximately 50 μmol of ammonia are lost. This finding is order- of-magnitude consistent with the maximum of 20 μmol of NH_3 that could be held by a monolayer in the apparatus whose surface area is 0.6 m^2 (± 50%). Based on preliminary tests, the ammonia lost to surfaces (in the absence of condensation) would cause no more than a 10% underestimation for most samples, as review of the ammonia totals in Tables C.n.6 confirms.

- The ammonia dissolved in water condensate on the canister (collector) side of the vacuum pump is neglected. Preliminary estimates indicate that the condensed ammonia is often between 30% and 300% of that in the vapor phase. Neglecting the condensed ammonia is expected to underestimate the total ammonia by a factor of about 2–3 in many cases. This assumption of negligible ammonia condensation is used only because more refined techniques have not yet been developed; the RGS system was designed primarily for gas-phase insolubles measurement, and the data that have been collected do not consistently support calculations of the amount of condensed ammonia. In future work, we will attempt to reduce the uncertainty in estimating the amount of ammonia in a sample by introducing a standard amount of nitrogen-15 tagged ammonia, whose ratio to the normal ammonia from the waste can be measured by the mass spectrometer.

- The ammonia solubility for the waste sample, represented by the effective Henry's Law constant, is assumed not to change significantly as a result of either extraction or the heating and cooling cycle that is part of the extraction procedure (details in Appendix A, Section A.3). However, the Henry's Law constant could change, because the solids that dissolve during heating might not fully re-precipitate by the time the post-cooling extraction is carried out. Should this be the case, the salt concentrations would be higher after the thermal cycling, and the ammonia solubility would be lower. This change would cause an overestimation of the residual ammonia; the amount of overestimation cannot be quantified in a general way.

- The ammonia in the waste sample is assumed to reach equilibrium with the extractor head space before every stroke of the mercury pump. This assumption is partially correct, because pressure-time plots for the extractor show that, after a pump stroke takes gas and vapor out of the extractor and so decreases the pressure, the pressure does not rise all the way to a steady value before the next pump stroke. The impact of this error is unclear. The method of calculating residual (and so total) ammonia does not use a predetermined value for ammonia solubility but only assumes that the solubility is constant throughout extraction. As long as the pump strokes tend

(on average) to always truncate the ammonia equilibration at about the same "distance" from equilibrium, the effect will be to make the ammonia behave as if it had a falsely low partial pressure (high solubility). This by itself might not contribute significantly to the error as long as the false solubility is constant. However, another type of non-equilibrium situation must also be considered. If there is an ammonia concentration gradient within the sample (which is not being stirred for most of the extraction), this could cause a significant (as yet unquantified) underestimation of the residual ammonia.

In summary, there is reason to believe that the ammonia content of samples if substantially underestimated by the RGS analysis methods and assumptions used at this time. The underestimation bias is believed to be a factor of 2 to 3. Further work is planned to gather more complete ammonia data and to improve ammonia estimation methods to put ammonia on the same footing as the low-solubility gases.

The following assumptions were used in the wet chemistry (ammonia) canister analysis to determine the ammonia partial pressure:

- The acid solution completely removes ammonia from the canister surface and volume. If this is not the case, the ammonia content of the wet chemistry canister, and so the partial pressure of ammonia in the extractor, would be underestimated. We have no data to quantify this possible source of bias, but preliminary tests with ammonia standards have shown low underestimates.

- The gas in each wet chemistry canister is in equilibrium with the extractor head space. This assumption is expected to produce little error, since the extractor pressure measurements show extractor pressure reaching its final value rapidly after the wet chemistry canister is opened to the extractor.

- There is no water condensation in the ammonia canister that would concentrate the ammonia (compared to what would be present in vapor alone). This assumption is expected to cause little error because no condensation is expected in the ammonia canister. The ammonia canister is at the same temperature (and so vapor pressure) as the extractor and is not pressurized by pumping (unlike most of the J canisters). The ammonia losses to surface layers are also assumed to be negligible by the same evidence discussed earlier.

Before describing the data analysis procedure for determining the ammonia concentration, it is useful to discuss gas solubility and describe Henry's Law. The distribution of ammonia between the vapor and slurry phases is determined by a parameter referred to as a Henry's Law constant, K_H, which is defined as

$$\chi_i = K_H p_i \qquad (3.2.1)$$

where p_i is the partial pressure of ammonia in atmospheres and χ_i is the concentration of ammonia expressed in terms of moles per liter of waste. This equation differs from the normal definition of the Henry's law constant because it is in terms of unit volume of waste rather than mass. The distribution of ammonia between both the vapor and slurry phases can be determined under any set of conditions if the total ammonia and the effective Henry's Law expression have been determined.

The Henry's Law constant for a gas depends on several variables, including the solution temperature and ion concentrations. A number of expressions have been developed to calculate the

Henry's law constant; these have been reviewed by Norton and Pederson (1994, 1995). (A word of caution: there are two different conventions for expressing the Henry's Law constant; one is the inverse of the other. Our discussion employs the expression which is defined in Equation 3.2.1 and is consistent with Norton and Pederson [1994, 1995].) Of the models reviewed, the Schumpe model (Schumpe 1993) gave the best agreement with experimental values from simulated waste. The Schumpe model is given by

$$\log(c_{G,o}/c_G) = \log\left(\frac{K_{H,G}(\text{water})}{K_{H,G}(\text{solution})}\right) = \sum_i (h_i + h_G)\, c_i \qquad (3.2.2)$$

where $c_{G,o}$ and c_G denotes the gas solubility of gas G in pure water and salt solution, respectively; h_i and h_G are the ion and gas-specific coefficients, respectively; and c_i is the concentration of ion i in the salt solution. The gas-specific constant, h_G, is assumed to be a linear function of temperature

$$h_G = h_{G,o} + h_T(T - 298.15\text{K}) \qquad (3.2.3)$$

where $h_{G,o}$ is the reference value, and h_T is the temperature-specific coefficient.

A calculation of the Henry's law constants for gases in Tank AW-101 is presented in Tables 3.1 and 3.2. The terms Σc_i and $\Sigma h_i c_i$ are calculated using ion concentrations obtained from a variety of sources, including Tank Characterization Reports (tank-specific references are given in Appendix C). The values for the temperature-dependent gas-specific constants are presented in Table 3.1. The values for h_i, $h_{G,o}$, and h_T are taken from Weisenberger and Schumpe (1996). The Henry's Law constants for most of the major gas constituents have been calculated using this information and are presented in Table 3.2. The solubility of ammonia is at least two orders of magnitude greater than that of the next highest solubility species, nitrous oxide. The Henry's Law constants presented in Table 3.2 are not used to calculate the residual ammonia in each sample but are included for the discussion. The actual Henry's Law constants that were used to determine phase distributions in the tanks can be found in Tables C.n.11.

The Henry's Law constant obtained through the above procedure must be converted from a molal basis, moles of solute per kg of solvent (water) in solution, to a basis of moles per volume of gas-free waste (both solution and solids). The conversion is accomplished by calculating

$$K_H\text{, L waste basis} = (K_H\text{, kg water basis})\,(1 - x_s)\rho_L\omega_L \qquad (3.2.4)$$

where x_s is the volume fraction of solids in the gas-free waste, ω_L is the weight fraction of water in the solution, and ρ_L is the solution density. Solids volume fractions are either taken from core sample data (when available) or estimated based on solution density, intrinsic solid density ρ_S (also known as particle density), and gasless bulk waste density, ρ_b:

$$x_s = \frac{\rho_b - \rho_L}{\rho_S - \rho_L} \qquad (3.2.5)$$

Table 3.1. AW-101 Ion Contributions for Determining the Henry's Law Constant

Ion	c_i(μg/mL)	M	c_i(kmole/m^3)	h_i	$h_i c_i$
CO_3^{-2}	12,300	60.01	0.205	0.1423	0.0292
Cl^-	5,180	35.45	0.146	0.0318	0.0046
OH^-	86,200	17.01	5.07	0.0839	0.425
NO_3^-	2.14 E+5	62.00	3.45	0.0128	0.0442
NO_2^-	1.02 E+5	46.01	2.22	0.0795	0.176
PO_4^{-3}	2,110	94.97	0.022	0.2119	0.0047
SO_4^{-2}	1,030	96.06	0.011	0.1117	0.0012
Al^{+3}	27,900	26.98	1.03	0.2174	0.224
Cr^{+3}	161	52.00	0.003	0.0648	0.0002
K^+	41,800	39.10	1.07	0.0922	0.0987
Na^+	2.30 E+5	22.99	10.00	0.1143	1.143
Total			23.23		2.151

Values for the solids fractions and densities used in Equations (3.2.4) and (3.2.5) are given in Tables C.n.9 and the surrounding text. The weight fraction of water in the solution is back-calculated from the solution density using a correlation (from experimental data) that can be found in Equation 4.4 of Mahoney and Trent (1995). The maximum error of this correlation was found to be ± 8% over a salt concentration range of 0 to 70 wt% and a temperature range of 0 to 70°C.

Table 3.2. Henry's Law Constant for Pure Water and AW-101 Supernatant Liquid

	K_H (25°C) (mol/kg water-atm)		K_H (40°C) (mol/kg water-atm)	
Gas	Water*	AW-101 Supernatant	Water*	AW-101 Supernatant
Ammonia	60.75	5.62	30.89	2.86
Nitrous Oxide	2.43 E-2	2.70 E-4	1.65 E-2	2.70 E-4
Methane	1.40 E-3	8.79 E-6	1.14 E -3	1.09 E-5
Oxygen	1.28 E-3	9.04 E-6	1.04 E-3	9.60 E-6
Hydrogen	7.84 E-4	1.78 E-5	7.39 E-4	2.13 E-5
Nitrogen	6.57 E-4	4.90 E-6	5.54 E-4	6.71 E-6
* Calculated using expressions presented in Norton and Pederson (1995).				

The total ammonia in a waste sample is determined by a combination of methods. First, the total amount of ammonia vapor (not condensate) captured by the gas canisters is calculated in a manner similar to that of the insoluble gases (see Section 3.1). Second, the amount of ammonia remaining in solution (the residual ammonia) is calculated from the pressure information taken during the extraction procedure. Summing these contributions gives the total amount of ammonia in the waste sample.

During the extraction process, a series of vacuum pump cycles (or strokes) is performed in which a fraction of the gas in the extractor head space is removed and pumped into the gas canister. The canister pressure rises quickly during the first few cycles but then approaches a constant gradual upward slope. The pressure increases at the beginning of the extraction process are typically dominated by low-solubility gases because water and ammonia vapor pressures are small. As the extraction process continues, the pressure change is expected to be primarily dominated by water and highly soluble ammonia because most of the gas has already been extracted.

According to Dalton's law, the canister pressure is the summation of three partial pressure contributions: water vapor, insoluble gases, and ammonia concentration.

$$p_{can} = p_{H_2O} + p_{ins} + p_{NH_3} \tag{3.2.6}$$

This partitioning of pressure assumes that all components except ammonia and water can be treated as low-solubility gases. This assumption results in a conservative estimate of the total amount of residual ammonia and, potentially, an underestimation of the total nitrous oxide quantities (as was mentioned in Section 3.1).

After the first pump stroke, the water vapor transferred to the collector has a partial pressure that exceeds the vapor pressure for the canister temperature, due to compression by the mercury pump. As a result, a portion of the water vapor condenses. The amount of insoluble gases transferred to the gas canister depends on the volume fraction of the extractor vapor space that is removed by the vacuum pump during each cycle. The remaining pressure is due to water, which is assumed to maintain a constant vapor pressure, and ammonia, which is assumed to re-establish a new equilibrium after each cycle, based on the Henry's law constant and the total of ammonia remaining on the extractor side. For a large amount of ammonia dissolved in the waste, this amount can appear to be a nearly constant quantity of ammonia transferred for each cycle.

The Henry's law expression presented in Equation 3.2.1 states that there is a linear relationship between the ammonia partial pressure and the ammonia concentration in the liquid. Using this relationship, it can be shown that there is a linear relationship between the total ammonia in a given sample and the ammonia partial pressure, assuming that the geometry and gas solubility remain constant. The total amount (moles) of ammonia in the extractor volume, n_{NH_3}, can be expressed as

$$n_{NH_3,tot} = n_{NH_3,v} + n_{NH_3,l} \tag{3.2.7}$$

where $n_{NH_3,v}$ indicates the number of moles in the vapor phase and $n_{NH_3,l}$ indicates the number of moles of ammonia in the liquid (more accurately, slurry) phase. The moles of ammonia vapor are related to the partial pressure by the ideal gas law, so are proportional to the partial pressure:

$$n_{NH_3,v} = \frac{p_{NH_3} V_v}{RT} = C_v p_{NH_3} \tag{3.2.8}$$

where V_v is the vapor volume, R is the ideal gas constant, T is the absolute temperature, and C_v is a vapor proportionality constant. In the same way, the number of moles in the slurry phase can be expressed as proportional to the concentration of ammonia in the slurry.

$$n_{NH_3,l} = C_l \chi_{NH_3} \tag{3.2.9}$$

Here, C_l is the liquid-phase proportionality constant. Using Equation 3.2.1 we can write the total number of moles of ammonia in terms of partial pressure

$$\begin{aligned} n_{NH_3,tot} &= C_v\, p_{NH_3} + C_l p_{NH_3} K_H \\ &= p_{NH_3}\left[C_v + C_l K_H\right] \end{aligned} \tag{3.2.10}$$

As an example, if the total ammonia in a sample is reduced by 10%, the partial pressure of ammonia is reduced by 10%. Further, as the solubility of ammonia increases, K_H increases, and for the same total ammonia quantity in the system, the partial pressure of ammonia decreases. Thus Equation 3.2.10 is consistent with our intuition.

The partial pressure of ammonia in the extractor head space at the end of an extraction cycle is calculated using the change in the moles of ammonia on the collector side for each vacuum pump cycle. The ideal gas law is applied to a single vacuum pump cycle to give the expression

$$p_{NH_3,ext} = \frac{\Delta n_{col} RT}{V_{pump}} \tag{3.2.11}$$

where Δn_{col} is the increase of ammonia in the collector after one vacuum pump cycle, V_{pump} is the volume of a single vacuum pump stroke, and $p_{NH3,ext}$ is the partial pressure of ammonia in the extractor. Therefore, the increase of ammonia in the collector per pump cycle is directly proportional to the total ammonia remaining in the extractor.

The residual total ammonia remaining in the extractor (all phases) after the final extraction process (J_3) can be determined by combining Equation 3.2.10 with Equation 3.2.11 to obtain

$$n_{NH_3,\,tot} = \Delta n_{col}\left[C_g + C_l K_H\right]\left(\frac{RT}{V_{pump}}\right) \tag{3.2.12}$$

in which it must be recognized that the Δn_{col} is that amount of ammonia transferred to the collector in the final pump cycle only. Applying Equation 3.2.12 to both the J3 and the J2 extraction processes, for example, and taking the ratio gives

$$\frac{n_{NH_3,tot}\big|_3}{n_{NH_3,tot}\big|_2} \equiv \frac{n_{res}}{n_{res}+\Delta n_3} = \frac{\Delta n_{col}\big|_3}{\Delta n_{col}\big|_2} \tag{3.2.13}$$

in which the $\Delta n_{col}|_3$ and $\Delta n_{col}|_2$ values are the moles of ammonia transferred to the collector by the final pump cycles for J3 and J2, respectively. The quantity $n_{NH3,tot}|_2$ can be seen to be the sum of $n_{NH3,tot}|_3$ and the entire amount extracted during the J3 process, Δn_3, and that $n_{NH3,tot}|_3$ is the residual ammonia, n_{res}, that we desire to calculate.

If we now assume that, near the end of an extraction process, the Δn_{col} over any single pump cycle does not change much, then the $\Delta n_{col}|_3$ and $\Delta n_{col}|_2$ can be better approximated by taking the average over several of the last pump cycles, $\Delta n_N/N$, which is the total amount extracted over the last ΔN cycles, Δn_N, divided by N. With this, Equation 3.2.13 becomes

$$\frac{n_{res}}{n_{res}+\Delta n_3} = \frac{(\Delta n/N)_3}{(\Delta n/N)_2} \tag{3.2.14}$$

In practice, the ratios (or discrete slopes) in the numerator and denominator of the right-hand side of Equation (3.2.14) are found by performing a linear regression on the last several canister pressures. Related data are found in Tables C.n.8.

The primary advantage of this approach is that the residual ammonia can be determined without first calculating the effective Henry's law constant. In some cases, the fraction of ammonia in the J1 canister for certain segments was sufficiently large to use the J1 canister information rather than the J2 canister. This allows for a greater difference in the final rates of change, which results in a more accurate estimate of the residual ammonia.

The calculation of the moles of residual ammonia is complicated by the presence of insoluble gases in the canisters. The pressure data presented in Tables C.n.3-5, C.n.8) are modified by subtracting the insoluble gas contributions. The canister pressure contribution after each pump stroke, N, is given by

$$p_{ins,N} = p_{ins,tot}[1 - (1 - F_V)^N] \tag{3.2.15}$$

where F_V is the vapor volume fraction removed from the extractor head space for each vacuum pump cycle. The discrete derivative of insoluble gas canister pressure with respect to pump cycle is given by the expression

$$\left(\frac{dp_{ins}}{dN}\right)_N = - p_{ins,tot}\,(1 - F_V)^N\,[\ln(1 - F_V)] \tag{3.2.16}$$

After the residual amount of ammonia has been determined for each waste sample, the partial pressures can be calculated based on the total ammonia concentrations in Tables C.n.6, the effective Henry's law constants (Tables C.n.11), and the sample and extractor volumes. The resulting values presented in Tables C.n.12 are corrected to an extractor temperature of 25°C.

The uncertainty analysis is based on the uncertainties of the derivative (Equation 3.2.16) and the collected amounts of ammonia. The uncertainty of the derivative is calculated as part of the linear regression based on the uncertainties of the individual canister pressures; the method of calculation is standard (Press et al. 1989). The uncertainty in the pressure measurement is ± 2% of the full range of the instrument, which is 1 atm, or approximately ± 2.0 kPa. The cumulative uncertainty of the collected mass of ammonia is calculated using the same root-mean-square procedure used in the insoluble gas data analysis (Holman 1978).

3.3 Phase Distribution of Constituents and Void Fraction

Once the concentrations of low-solubility gases and high-solubility vapors have been determined, the distribution of the different components between the liquid (or slurry) and gas/vapor phases must be determined for each waste sample under in-tank conditions. The quantity of gases in the gas/vapor phase determines the void fraction of the sample.

The phase distribution of the gas constituents is based on the effective Henry's law constants that are calculated for in situ conditions using the Weisenberger and Schumpe model described in Section 3.2. The in-tank pressure for each sample is calculated as a hydrostatic pressure based on the measured waste densities. An iterative procedure is used that matches the sum of partial pressures of all the gas constituents with the in-tank pressure.

The analysis procedures described in this section require input from a variety of sources. The total gas concentrations are determined using the procedures described in Sections 3.1 and 3.2. Several tank waste properties are used in the analysis; these were obtained from a variety of sources, including the Tank Characterization Reports (tank-specific references are given in Section 4 and Appendix C). These properties include the following:

- Molar ion concentrations per liter of water in the waste solution, used to calculate Henry's law constants
- Solid volume fractions and weight fraction of water in solution, used to calculate effective Henry's law constants per liter of waste
- Average bulk densities of convective and nonconvective layers, used to calculate the in-tank hydrostatic pressures at each elevation.

Other inputs include

- Elevations from which the samples were taken (from the sampling plan)
- Location and thickness of convective and nonconvective layers and crust
- Temperature at each sample elevation
- Water vapor pressure at each sample location.

The assumptions used in the phase distribution (void fraction) analysis are the following:

- The gas species collected in the canisters behave like ideal gases under in-tank temperatures and pressures. Because pressures are less than 3 atm, this assumption is accurate for the same reasons stated in Section 3.1 for extractor conditions.

- Gases are in equilibrium between the gas/vapor and slurry phases under tank conditions, and both phases are at the same temperature. This assumption should hold true for undisturbed waste. The effect on equilibrium of the disturbance caused by the sampling process cannot be quantified.

- The Schumpe model provides an accurate estimate of the Henry's law constants for each gas constituent in salt solution, so long as the correct concentrations of ions are used in the waste solution. Norton and Pederson (1995) provide information on the accuracy of this solubility model in predicting oxygen, nitrogen, hydrogen, methane, nitrous oxide, and ammonia solubility in heterogeneous and homogeneous simulants of SY-101 waste. It appears that the Schumpe model predict solubilities of low-solubility gases with less than a factor-of-two error, while it underpredicts ammonia solubility by a factor of as much as 3 at 60-70°C. (For all species the model error increases with temperature.) The effect of this error is discussed in the next bullet, in terms of the overall impact of solubility errors whether caused by solubility models or poor concentration data.

- The ionic concentrations of the waste solutions are accurate and uniform throughout the tank. The accuracy of the concentration values is questionable; complete and consistent data sets were not available at report time. Sensitivity tests that were done for this report have shown that the effect of an error in the solution salt concentration depends on the ammonia concentration in the tank. In a high-ammonia tank, of which A-101 is the only known example, doubling the total salt concentration can increase the void fraction by as much as 50% of its value as ammonia is "salted-out" from solution. In a low-ammonia tank, doubling the total salt increases the void fraction by no more than 5% of its value. In both types of tanks, doubling the salt multiplies the ammonia concentration in the vapor phase by a factor of 4; and in both types of tanks, halving the concentration has substantially less effect than doubling it. The range of variation of the solubility when the total salt is doubled or halved is a factor of 4 to 16, depending on the species.

- The hydrostatic head (in-situ pressure) can be calculated with sufficient accuracy by treating each layer of waste as having a uniform density equal to the average density of the layer. (Waste layers are distinguished from each other, for the purposes of this report, by their thermal behavior [temperature profiles], their physical properties as found in core samples, and their gas retention characteristics. Tank-specific layering details are given in Section 4.) A typical error in calculating hydrostatic head might involve having 1 m less or more of a layer than had been anticipated at a calculated pressure of 1.5 atm. Then the difference in pressure might be 400 kg/m^3 (a typical difference between slurry and liquid densities) times the depth difference times gravity, or about 4 kPa (0.04 atm). Thus the errors from density and layer depth variation probably cause an error contribution of less than 5% of the void fraction (which is inversely proportional to pressure).

- The pressure experienced by the bubbles is that of atmospheric pressure plus the hydrostatic head of the bulk waste; that is, the bubbles are supporting both the particles and the liquid above them. In the alternative case, the bubbles are confined to the pores of the waste and support only the liquid in the pores; the particles are

self-supporting. In this latter case, bubbles experience hydrostatic pressure from the liquid alone. Because most of the waste in the five tanks is fine-grained and the pores are small, the gas bubbles are expected to be particle-supporting (as assumed in calculations). However, bubbles could be confined to pores in three situations: 1) bubbles in extremely strong waste; 2) bubbles near the tank bottom; or 3) bubbles more than 50 cm (20 in.) deep in coarse saltcake (Stewart et al. 1996b, Section 3.1), such as might be present in the upper layer of A-101. We do not have enough information on particle size and waste strength to confirm the assumption of particle-supporting bubbles in all cases. If bubbles in the upper layer of A-101 were not particle-supporting, the in-situ void fraction would be underestimated by less than 15%; if bubbles at the tank bottom were not self-supporting, the in-situ void fraction would be underestimated by about 30%.

In summary, we conclude that the assumptions in the void fraction method have less than ± 10% effect on tanks with low ammonia content. However, errors in the ammonia solubility could easily increase or decrease the void fraction by 20% in high-ammonia tanks (A-101 being the only example to date). Ammonia vapor concentrations are also sensitive to the solubility (proportional to it), in all the tanks measured to date.

The void fraction (phase distribution) analysis begins by determining the in-tank gas pressure, p_z, at each sample elevation. It is assumed to be equal to the hydrostatic pressure, which is obtained by multiplying the average waste density for each layer by the thickness of each layer above that elevation, and summing. Next, the effective Henry's law constant at the in-tank temperature is calculated for each sample elevation using the procedure described in Section 3.2.

The distribution of each gas constituent between the slurry and vapor phases can be determined using Henry's law if the concentration of the gas constituent, the total void fraction, and the effective Henry's law constant for that constituent are known. Using Equations 3.2.8 and 3.2.10, the portion of each gas constituent, i, in the vapor phase is given by the expression

$$\frac{n_{i,v}}{n_{i,tot}} = \frac{\alpha/RT}{\alpha/RT + (1-\alpha)K_{H,i}} \qquad (3.3.1)$$

where α is the void fraction. The partial pressure for each gas constituent is given by the expression

$$p_i = \frac{n_{i,tot}/V_{tot}}{\left[\frac{\alpha}{RT} + (1-\alpha)\cdot K_{H,i}\right]} \qquad (3.3.2)$$

The system is constrained by the fact that the sum of all the gas constituent partial pressures must equal the dry hydrostatic pressure in the tank at that elevation

$$p_{hyd} = p_{H_2O} + \sum p_i \qquad (3.3.3)$$

The void fraction can be calculated using the ideal gas law:

$$\alpha = \frac{\sum n_{i,v} RT}{p_{hyd} V} \qquad (3.3.4)$$

Note that the void fraction is not known *a priori*. It is required to calculate the phase distributions using Equation 3.3.1. As a result, an iterative procedure has been developed that begins with an estimated total void fraction. The phase distribution for each gas component is calculated, and the partial pressures are summed. This sum is compared with the in-tank hydrostatic pressure, and the void fraction is adjusted accordingly. This iteration continues until the sum of partial pressures is within 0.001% of the specified in-tank pressure.

3.4 Tank Inventories and Data Interpretation

The data analysis tasks in Sections 3.1 through 3.3 provide gas concentration and void fraction data at the points where samples were successfully taken. These results require further interpretation to provide overall tank waste properties such as gas inventories and to account for types of sample contamination that might have made the concentration data not fully representative of actual undisturbed tank waste.

3.4.1 Total Tank Gas Inventories

Once the phase distribution of each of the gas constituents has been determined, the total tank inventory of free and dissolved gases can be calculated. The analysis consists of calculating the average void fraction in each of the layers from which samples were taken, calculating the average gas composition in each layer, estimating the total number of moles of each gas constituent in both layers, and summing to determine the total gas inventory.

The analysis procedures described in this section require input from a variety of sources. The free and dissolved gas concentrations at the various sampling locations are determined using the procedure described in Section 3.3. Other inputs include

- Location, thickness, and volume of the convective and nonconvective layers, including estimated variation (uncertainty) in layer thicknesses and location; layers are distinguished from one another by their temperature profiles, core sample physical properties, and gas retention capacities.
- Elevations from which samples were taken.
- Temperature at each sample elevation (obtained from multifunction instrument trees [MITs] or thermocouple [T/C] profiles).
- Pressure at each sample elevation (calculated in Section 3.3).

The assumptions used in the total tank gas inventory analysis are as follows:

- All variables are assumed to be radially uniform; variation between risers is not accounted for in calculations. This assumption is necessary because there are too few data to allow a quantitative assessment of the effects of lateral variability. Calculating "alternative" inventories based on each riser alone would have little meaning because there would be only one or two samples per layer per riser. Therefore, tanks that display substantial differences between risers are noted qualitatively on a tank-by-tank basis (in Section 4).

- The convective layer is assumed to be well-mixed, so temperature and gas concentration (mole/L) are vertically uniform. This is equivalent to assuming a void fraction that varies with the inverse of depth. In most cases this assumption is necessary because samples were concentrated in the nonconvective layer of the tank, where most of the gas is retained, and one sample was taken from the convective layer. Section 4 discusses the few cases where multiple samples allow this assumption to be tested.

- There is assumed to be a linear variation of concentration within the nonconvective layer between the subsequent vertical locations at which samples were taken. Again, we do not have data to permit any more accurate assumptions. VFI results suggest that total gas concentrations (void fractions) may not behave monotonically. One way to attempt to capture some of this fine detail in the void profile is to calculate gas inventories based on average RGS compositions for a layer and on total-gas inventories obtained by VFI (Stewart et al. 1996a). This type of inventory, as well as inventories based entirely on RGS data, is calculated in order to give some idea of the variability that might result from sparse sampling and lateral variability. Both types of inventory are presented in Section 4 on a tank-by-tank, layer-by-layer basis.

As stated, this report contains two kinds of gas inventories: one created from average RGS compositions and VFI void volumes for each layer of waste, and one from RGS data alone. The VFI gas volumes used came from Stewart et al. (1996a); they are based on volume integration of measured void fractions, not on the barometric pressure effect (BPE) method. The calculation methods used for the two types of inventories (RGS/VFI and RGS) are described separately.

3.4.1.1 RGS/VFI Inventories

Two calculation methods are used on RGS concentration data, depending on the type of layer and the availability of data. Where only one sample is available in a layer, as is generally the case with supernatant and crust layers, its data are used without further processing. The composition (mole fractions of species) of the single sample is multiplied by the layer's gas inventory as derived from VFI data. The uncertainty in the VFI gas volume, as given by Stewart et al. (1996a), is taken into account in estimating the uncertainties of the inventories of the constituents of the gas.

When more than one sample is available for a layer, an arithmetic average of all the samples in the layer is used to determine the average gas compositions (mole fractions). This average composition is multiplied by the layer's gas inventory as derived from VFI data.

3.4.1.2 RGS Inventories

In generating RGS inventories, three kinds of calculation methods may be used on RGS concentration data. Where only one RGS sample is available in a layer, its data are used directly. The species concentrations of the single sample are assumed to extend throughout the layer. The gas volume for the layer is calculated from the single gas concentration, in mol/L, and the average pressure in the layer (usually the hydrostatic pressure at the layer midpoint).

When more than one sample is available for a convective layer, the layer is assumed to be well-mixed. An arithmetic average of the samples' concentrations is used to determine the average gas concentrations (mol/L) for the layer. In this case, too, the in-situ gas volume is based on the average pressure in the layer.

When more than one sample is available for a nonconvective layer, the concentrations are integrated over depth to find the average. In addition, the mass-average pressure and temperature of the gas in the layer are found from integrating the temperatures and pressures at sample locations

(multiplied by gas concentration). The STP gas volume for the layer is calculated from the averaged concentration, temperature, and pressure using the ideal gas law to adjust from tank conditions to standard conditions.

The integration method assumes that the concentrations of all the gases are piece-wise linear continuous between samples. This assumption allows Simpson's Rule to be used for integration, with the concentrations between sample centers linearly interpolated. Figure 3.1 shows an example integration for one layer of waste from which three samples (segments 5, 6, and 10, the closed circles) have been taken. The concentrations at the bottom of the layer are set equal to the concentrations from the lowest sample, and similarly for the top of the layer. The four integration intervals are unequal in size, reflecting the different distances between data locations.

3.4.2 Corrections for Contamination

One type of sample contamination is indicated by the measured concentrations of oxygen and argon, which appear to be higher than the essentially zero values that were anticipated. Oxygen contamination can occur during the sampling process due to the leading end of the sampler trapping air. A separate laboratory measurement of the maximum air volume at STP suggests the possibility

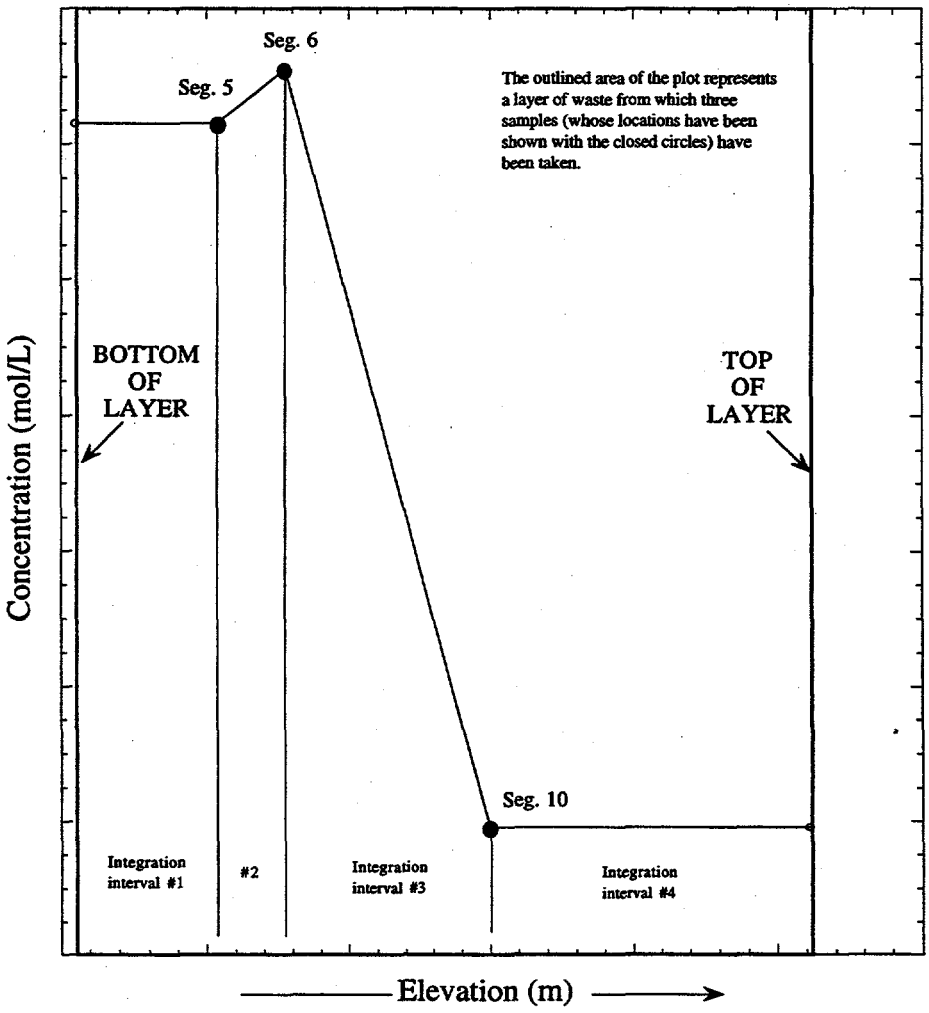

Figure 3.1. Example of Integration Scheme for Averaging RGS Concentrations

of a maximum of 6.1 cc of air trapped in the nose piece.[a] Argon contamination can also occur during the sampling process. When high concentrations of hydrogen are detected during sampling, argon is used to purge the drill string for safe operation. A portion of that argon may be forced into the waste (or, like air, entrained in the sampler nosepiece) and captured in the sampler. The corrected results are based on the assumption that all the argon and oxygen in the sample are from the entrained drill string gases. The argon and oxygen are removed, and the nitrogen is reduced based on the nitrogen-to-oxygen ratio for standard atmospheric air, $N_2/O_2 = 3.71$.

Another type of contamination could result from the HHF, the fluid used during the sampling procedures to balance hydrostatic head, seeping into the sampler and replacing some of the waste volume. If such contamination occurred, the RGS measurements would misrepresent the pure waste in four ways (in order of diminishing importance): 1) for a given volume percent of HHF, the calculated gas content of the waste is reduced by about the same percentage, just as if incomplete sample recovery had occurred; 2) the HHF contains dissolved air constituents with which it contaminates the waste gas; 3) the HHF dilutes the ammonia in the sample, reducing its measured partial pressure (measured by the PQ canister grab sample during extraction) below that of pure waste; 4) the HHF may decrease the ionic strength of the waste liquid, increasing the solubility of ammonia and leading to a further underestimate of the partial pressure of ammonia. However, this depends on whether the solids in the waste are still present and in equilibrium with the solution; if so, the solution concentration will be essentially the same as if no HHF had been added.

As detailed in Appendix A, the HHF has been marked with trace amounts of lithium bromide so a chemical analysis could indicate whether contamination has occurred. Chemical analysis results[b] show that HHF (bromide ion) was present in the waste only in concentrations at or below the Br^- detection limit. In all but three samples, the detection limit corresponds to HHF contamination (and gas underestimation) of 5% or less. For segments 17, 19, and 21 of Tank AN-104, the maximum HHF contamination was about 10%; the actual contamination could be substantially less because the detection limit represents the maximum amount of HHF that could be present, not the actual amount.

3.5 X-Ray Image Analysis

Analyses of x-ray images are expected to yield several pieces of information that will assist in data interpretation and understanding of the waste behavior. The most notable parameter that can be extracted from these images is density. In a less quantitative fashion, the phase distribution can be obtained from these images as well. Furthermore, information on where the gas phase is concentrated or how it is distributed, the structure of the solid matrix/particle agglomerates, and the amount of gas can be inferred.

3.5.1 General Background on X-Ray Image Processing

The current approach yields line-of-sight averaged information on the density of the material which fills the sampler. Such information does not offer the ability to obtain local information along the line-of-sight; the system has no "depth perception." As such, the phases might be distributed in many different ways and still produce the same results. For instance, we can see that

---

(a) Cannon NS. March 1997. *Retained Gas Sampler Interface Volume.* Letter Report HNF-SD-WM-CN-092, SGN Eurisys Services Corporation, Richland, Washington.

(b) Hey BE. February 20, 1997. Data transmittal to LA Mahoney. Spreadsheet RGS7020A.XLS, Numatec Hanford Corporation, Richland, Washington.

there is a void in the waste and measure its size, but we cannot tell where, front to back, the void is. Thus the x-ray image analysis technique offers a two-dimensional map of phase distributions in the core sampler.

Immediately after sampling, each segment is radiographed using the x-ray imaging system described in Appendix A, which is recorded on video tape. The video for each segment is then transferred to a digital image format for analysis. The analysis begins by preparing the calibration standards and extracting the core sample regions of interest from the full-frame video images. Images from each section of the video are then combined into a single composite of the core sample. Attenuation coefficients for the waste and the water standard are then calculated by applying a logarithmic relationship derived from Beer's law (see Subsection 3.5.2.3). Density (in terms of specific gravity) of the waste is then obtained by dividing the attenuation coefficients of the waste by the mean attenuation coefficient for water obtained from the calibration sample. The final step in the analysis is to correct for uneven x-ray exposure in the original image by applying an empirical correction matrix to the data.

Successful analysis of x-ray images depends heavily on the continuity of the radiography system between imaging the standards and the waste sample. If either the x-ray source energy or the iris on the x-ray imaging camera are adjusted between the radiography of the standards and completion of the waste radiography, the standards may no longer be valid and analysis may not yield reliable results. The air standard is required to effectively compensate for the attenuation of the steel RGS sampler walls. The water standard is used to derive the waste density from the attenuation coefficients. There are several assumptions made when processing the x-ray images:

- Sampler content is assumed to be undisturbed.
- The RGS is assumed to be a concentric cylinder with uniform wall thickness of 0.97 cm (0.38 in). This is not the case, however, as the sampler inner and outer walls are not necessarily concentric, varying up to 0.089 cm (0.035 in), or about 9.2%. Random rotational orientation of the sampler and unknown rotational orientation of the calibration standards during the radiography session prevents making an accurate correction for this.
- Image aspect ratio through all the imaging optics is assumed to remain 1:1.
- A featureless supernatant liquid is assumed to have a uniform density (ideal situation). This allows us to create a correction matrix to compensate for the background variations.
- For Tanks AN-103 and AN-104, standards are radiographed less frequently so many segments will share standards. We assume the radiography system's operation is invariant between standards.
- X-rays from the source are the result of electrons accelerated by a high-voltage potential to nonrelativistic energies (< 1 MeV) colliding with atoms in the high-Z target material. Thus we can assume that the x-ray spectrum is consistent with that of bremsstrahlung radiation (Krane 1988) and will have a predictable distribution with the maximum energy proportionate to the x-ray source voltage, typically 140 kV.
- The x-ray interaction in the waste material (primarily low-Z) is assumed to be dominated by Compton scattering.

- The spatial uniformity of x-rays incident over the surface of the RGS sampler is constant given that the same radiography system is used. This allows us to correct for uneven x-ray exposures.

- The spatial and spectral dependence of the attenuation function are separable. The spectral dependence of the attenuation coefficient can be factored out by assuming that we are always working with the *total* attenuation coefficient averaged over the same spectral range of x-rays.

- The attenuation of any given x-ray through any gas phase material in the sampler is negligible.

3.5.2 Detailed Analysis Procedure

3.5.2.1 Image Digitization and Preparation

Images were digitized with a PC using the embedded 16-bit video A/D unit with SVHS I/O. The images were captured at 640x480 pixels at 8-bit grayscale resolution and saved in TIFF format. An eight-frame averaging was used to suppress transient noise in the video signal.

The images were transferred to an Intel 90-MHz 586 PC for further processing with Image Pro Plus 2.0™ from Media Cybernetics. First, the exact position of the left and right interior walls was determined for each image using a horizontal line profile by measuring the distance between the two minima that occur at the sampler cylinder wall to waste interface. The images were then calibrated spatially based on a sample cylinder inside diameter (i.d.) of 2.86 cm (1.125 in) and an assumed image aspect ratio of 1:1. Next we determined the pixel length of the inter-image sampler movement. This was accomplished by computing the value based on the on-screen position notes and the image calibration. When available, tracking notable objects between two sequential images was used to check the inter-image sampler movement value. Once the dimensions of the portion of the core sample unique to each image were determined, that region was extracted and saved to a subimage in TIFF format which was then converted to an ASCII text matrix. Figure 3.2 shows a typical section of an unprocessed radiograph from Tank 241-AN-105, segment 13.

Data are extracted from the calibration images using averaged line profiles confined to the i.d. of the sample cylinder. These profiles are typically averaged over 50 lines of data. Two profiles for air are saved as ASCII text files, one from the air/soil sample and the other from the air/water sample. A water profile is also saved.

3.5.2.2 Data Calibration

The radius (along the horizontal axis) is normalized, which changes the horizontal axis range to [-1,1]. This is done because the calibration images and core images are different sizes due to the calibration standards being slightly farther from the x-ray imaging tube. Since column-by-column arithmetic cannot be done, a normalized scale is introduced. A third-degree polynomial is then fit to the calibration data profile to eliminate local variations while preserving the overall shape of the curve. This curve is used with the water profile data to compute the average experimental attenuation coefficient for water according to the following equation:

$$\sigma_{water}(y) = \frac{-\ln\left(\frac{I_{water}(y)}{I_{cal}(y)}\right)}{L_{water}(y)} \qquad (3.5.1)$$

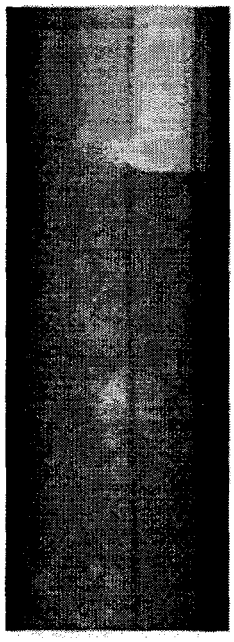

Figure 3.2. Typical Raw X-Ray Image Section (note the two vertical wires [dark] and voids [light] that are visible)

where $I_{water}(y)$ is the intensity (graylevel) of the water profile at position y, $I_{cal}(y)$ is the intensity of the air profile approximation at position y, and $L_{water}(y)$ is the path length through the medium (core of the sampler along the z-axis) at position y along the diameter (refer to Figure 3.5). This will be used later in determining the density of the core sample material. The derivations of Equations 3.5.1 and 3.5.2 are found in Subsection 3.5.2.4.

3.5.2.3 Composite Image Reconstruction and Analysis

The subimage data files are imported into a matrix calculation software package. A composite core sample data set is constructed by stacking the ordered subimages, creating a

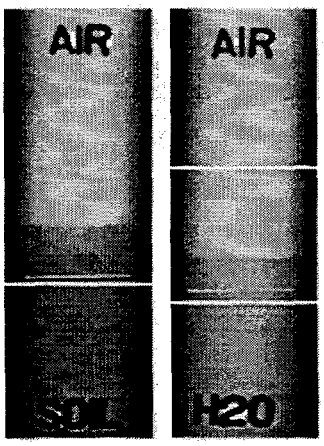

Figure 3.3. X-Ray Images of Calibration Standards—Air, Water, and Dry Soil

full-scale mosaic of the entire core sample. The radius of the core sample (along the x axis) is then normalized. Calculations of local attenuation coefficients are performed row by row at each point of the core using this equation (definition of terms provided in Subsection 3.5.3.4):

$$\sigma_{core}(x,y) = \frac{-\ln\left(\frac{I_{core}(x,y)}{I_{cal}(x)}\right)}{L_{core}(x)} \qquad (3.5.2)$$

The local attenuation values are actually σ/ρ for the core material. These values are then divided by the average experimental attenuation coefficient, σ/ρ, for water. The result is a matrix of local densities (specific gravity) for the core sample material.

The final step is correcting the data for any unevenness in the original x-ray image. This process is done last because until now the grayscale interpretation has included a path-length factor (longer in the center, shorter at the edges). To create a correction matrix, a sample believed to be supernatant liquid, or one with very few features, is selected. The data are normalized to their own mean density to create the matrix of corrections and applied to the other images. Figure 3.4 shows the progression from (left to right) raw x-ray image, attenuation coefficients, density, and corrected density for part of Tank AN-104 segment 14.

3.5.2.4 Density Measurement

The sample x-ray image in Figure 3.2 was produced by transmitting high-energy electromagnetic radiation (~100 KeV), emitted by a source, through the sampler and is viewed by an x-ray imaging tube. Figure A.8 shows the layout of the x-ray imaging system. The light regions in Figure 3.2 are regions of high transmission where, due to low absorption and scattering, a high number of x-rays passed through the sample. Conversely, the dark regions are areas of lower transmission, due to high absorption and scattering of the x-rays, where relatively few x-rays passed through the sample. The gray areas are due to material capable of only moderately attenuating the x-rays and/or some mixture of high- and low-attenuation material.

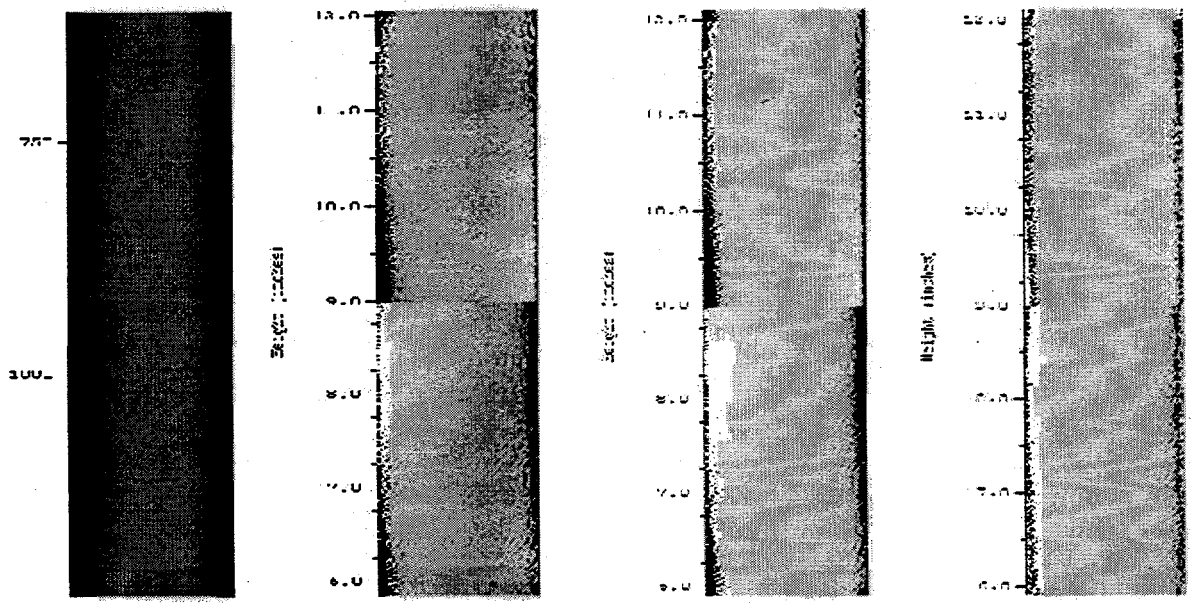

Figure 3.4. Progression of Analysis (from left to right): Raw X-Ray, Attenuation Coefficients, Uncorrected Density, Corrected Density

The mode of scattering of the x-ray energy, known as Compton scattering, is due to interaction of the x-ray with free lattice or bound electrons in a substance (Krane 1988). The amount of scattered energy is governed by the following relationship:

$$\sigma = \rho N \frac{Z}{A} e^{\sigma} \qquad (3.5.3)$$

where σ is the scattering coefficient, ρ is the substance density, N is Avogadro's number, Z is the atomic number, and A is the atomic weight. The parameter e^{σ} is the single-electron scattering cross-section, which is only a function of the frequency of the x-ray beam ($h\nu_o$). For a given source frequency, the single-electron scattering cross-section becomes fixed. Also, for low atomic number elements, the ratio of Z/A is approximately 1/2. Equation 3.5.3 shows that, for a mixture composed of low atomic number elements and molecules, the scattering coefficient is directly proportional to the density of the material.

$$\sigma \cong C \rho \qquad (3.5.4)$$

In the above equation, C is the constant of proportionality and is determined by calibration against a known substance such as water. Equation 3.5.4 reveals that, from knowledge of the attenuation or scattering coefficient of a particular medium, when operating within the Compton scattering domain, one may be able to determine the density of the medium. This is the theoretical basis for the x-ray densitometry approach.

The distribution of grayscale across the x-ray image of the sample represents the intensity of an x-ray after passing through different layers of attenuating media such as the sampler wall and waste liquid. Figure 3.5 shows a cross-section of the sampler and the different layers through which the beam passes. The attenuation of the beam intensity, i_o, at any position y changes according to Beer's law, as shown in Equation 3.5.5:

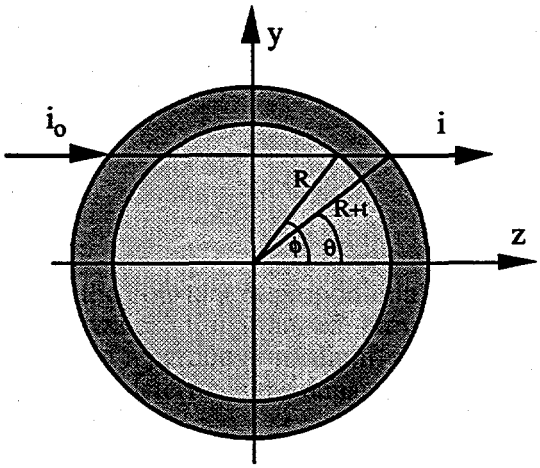

Figure 3.5. Schematic Diagram of Sampler Cross-Section Showing the X-Ray Path

$$\frac{i(y)}{i_o} = \exp\left[-\int_{\lambda_1}^{\lambda_2}\int_{z_1}^{z_2} \sigma(y,z,\lambda)\cdot dz\, d\lambda\right] \qquad (3.5.5)$$

We assume that the spatial (function of y,z) and spectral (function of λ) dependence of the attenuation function are separable. The spectral dependence of the attenuation coefficient can be factored out by assuming that we are always working with the *total* attenuation coefficient averaged over the same spectral range of x-rays. The spatial component in z, (z), will become an average over all z, and the spectral component (λ) will be an average over all the x-ray wavelengths present. Equation 3.5.5 can then be written as

$$\frac{i(y)}{i_o} = \exp\left[-\sigma_s L_s(y) - \langle\sigma_{sl}\rangle L_{sl}(y) - \langle\sigma_g\rangle L_g(y)\right] \qquad (3.5.6)$$

where the subscripts s, sl, and g refer to the solid container (steel sampler cylinder), solid-liquid slurry, and retained gas respectively, and the symvol <> refers to phase-averaged quantities. Note that the attenuation coefficients represented in this equation are phase-averaged in that they are averaged over the entire length of the particular phases along the path of the x-ray. For a given sampler geometry and material, the container contribution is a well-defined function of location *y*. We assume that the x-ray energy is not attenuated by the gas phase. Thus the effect of gas bubbles along the path of the x-ray beam is to reduce the path length along which attenuation takes place. i.e., Lsl. Thus Equation (3.5.6) reduces to

$$\frac{i(y)}{i_o} = f_s(y)\cdot\exp\left[-\langle\sigma_{sl}\rangle L_{sl}(y)\right] \qquad (3.5.7)$$

where fs(y) is the local attenuation function of the container, which is known. Both parameters in the quotient are unknown and, as a result, the problem is under-specified and can be solved. The attenuation coefficient averaged over the entire path length of the beam (sum of Lsl and Lg) should yield the density of the mixture in the sampler. Therefore, the local path-averaged mixture density in the sampler can be determined. The solid-liquid-gas can be treated as one system with no requirement to know the attenuation coefficient of the individual components in the system.

The uncertainty of the system based on the calculation of root-mean-square (RMS) error in density is approximately 5%. This uncertainty was calculated from the attenuation coefficient data of segments sampled from the supernatant liquid. According to the RMS error, the limit of resolution of the calculations is 0.5 mm. Hypothetically, if a homogeneous substance (such as a liquid or a uniformly mixed mixture) is analyzed using this method, in the absence of any measurement error, the probability distribution function (PDF) would be a single spike representing the density of the substance, with the standard deviation of zero. Addition of the measurement error in this case broadens the peak. Also, nonuniformities in density of a mixture contribute to broadening this density peak.

The information embedded in the corrected density image is best visualized in a histogram or PDF of density values in a relevant subsample of the waste. Figure 3.6 is the PDF for the density of the waste in segment 15-5 of Tank A-101. This distribution function is constructed by

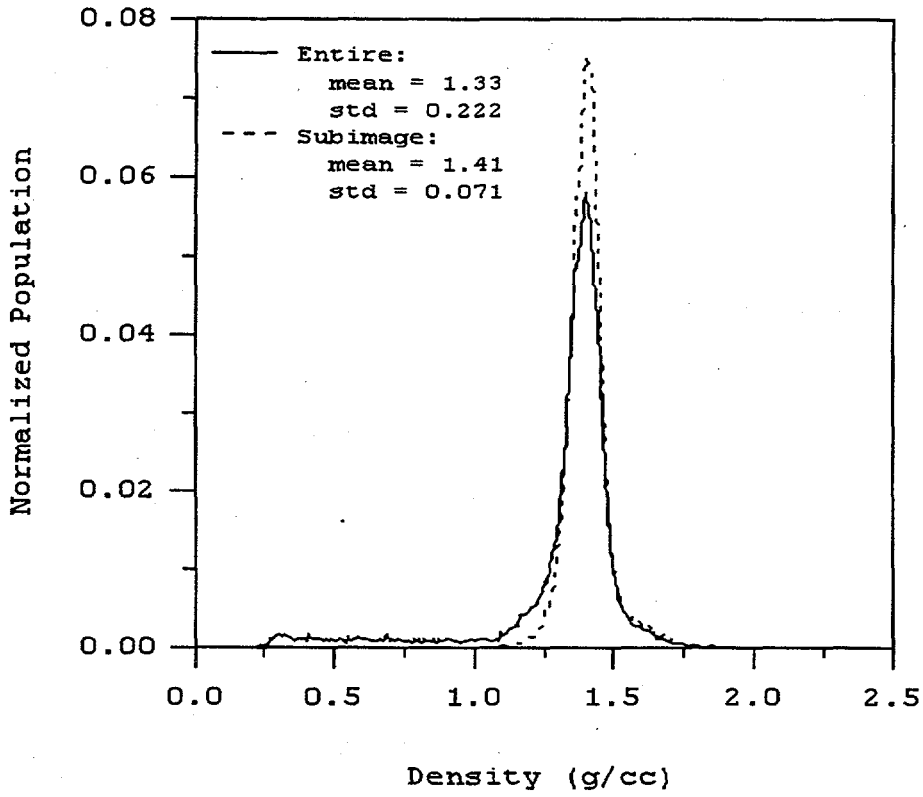

Figure 3.6. Density PDF of Homogenous Liquid Sample

counting the number of pixels in the image with similar densities. This distribution would be single-valued if the entire image was the same exact density. The distribution becomes broader as fluctuations and perturbations about the mean density exist. Hypothetically, if a sample population is selected from a random set in an image, it is expected that the distribution will have a true normal or Gaussian shape. If a smaller object with a uniform density different from the background is superimposed on the hypothetical image, a bimodal distribution will appear where the second mode will provide information on the size of the object and its density. This is the basis for examination of the PDFs.

Two different distributions are provided to illustrate an important point. The sample populations for these distributions were $2x10^4$ and 10^5 for the subimage and the entire image of this segment, respectively. Note that the PDF for the subimage is very clean and close to a normal distribution. Within this subimage some nonuniformity in the density distribution was observed, but overall there did not appear to be any discrete discontinuities associated with gas pockets or bubbles. The entire image, however, included what appeared to be a fracture in the saltcake (see Section 4.2.8 for other images provided for this tank). The lobe on the left side of the solid line distribution is the result of this fracture, which reduces the mean by approximately 6% and increases the standard deviation in the density three-fold.

Figure 3.7(a) and (b) shows examples of PDFs from Tank AN-104, segments 03 and 21. Note the narrow peak in Figure 3.7(a) relating to the homogeneity of the sample. Contrast that with the broad multi-peaked curve in Figure 3.7(b) Here, the smaller sub-peaks are density peaks

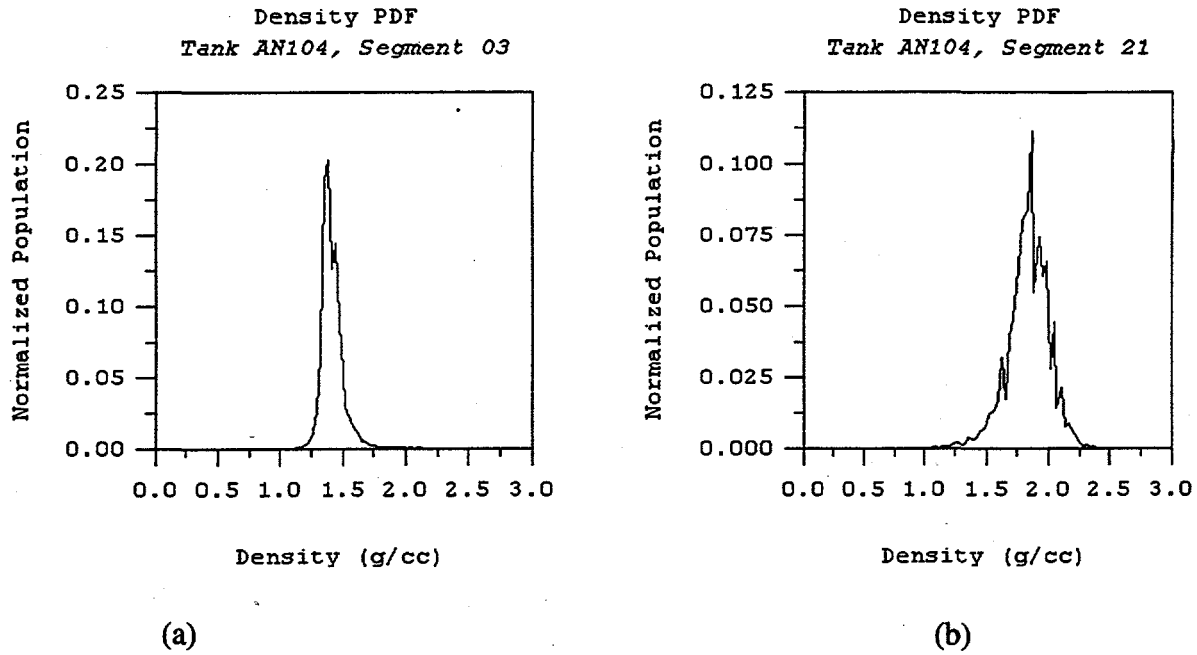

Figure 3.7. Density PDF of Homogenous Liquid Sample

due to bubbles, voids, and higher density inclusions in the waste material. As mentioned before, the void density is not clearly separated from the waste density because the attenuation of an x-ray is averaged over its path through the material that usually encompasses some ratio of waste to void. Further results and discussions will be provided in Section 4 for presentation of tank-by-tank results. It should be mentioned that the validity of this approach has been shown in relation to other methods for actual tank data,(a) as will be discussed further in Section 4.1.8.

3.5.3 Guide for Viewing X-Ray Images

Section 4 contains a number of x-ray images; this section is provided as a guide to their interpretation. Figure 3.8 shows the image subsegments in the sequence in which they were grabbed and processed. These subsegments are marked with Roman numerals to more conveniently identify their relative position in the sampler. These identifiers should be referred to when looking at the tank-specific images provided in Sections 4.1 through 4.5. Note that the lower part of the piston always appears in sub-segment I and the top of the valve housing usually shows up in subsegment VI. Also, the cable for the valve trigger mechanism occasionally shows up in the images.

(a) Shekarriz,A, DR Rector, MA Chieda, M White, and JM Bates. 1996. *Retained Gas Sampler Measurement Results for Hanford Waste Tank 241-AW-101.* TWS-MIT-071996, Pacific Northwest National Laboratory, Richland, Washington.

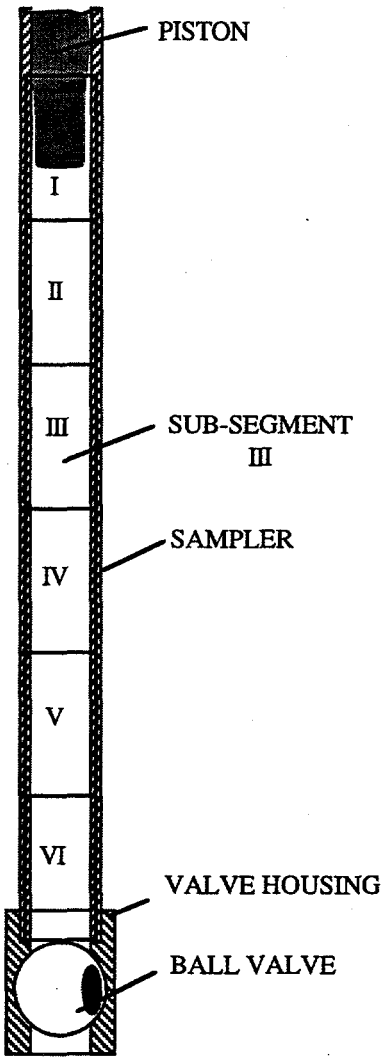

Figure 3.8. Schematic Diagram of X-Ray Subsegments

4.0 Tank-by-Tank RGS Results

This section contains the sampling results obtained with the RGS. A section is devoted to each tank tested. More detailed data are included in the appendixes at the end of the report.

4.1 Tank 241-AW-101

4.1.1 Sampling Locations

Tank 241-AW-101 was the first tank sampled with the RGS. The push-mode sampling was carried out in risers 24A and 24B, whose approximate locations are depicted in Figure 4.1. Various core segments were taken at different elevations and within two different risers to capture some of the lateral and vertical nonuniformities in the gas composition and quantities (Figure 4.2). Riser 24A was sampled because of its proximity to the multifunction instrument tree (MIT) and to correlate the gas composition to local waste temperature. Riser 24B was sampled because it was close to riser 1C, one of the risers used for VFI (Figure 4.1).

The total depth of waste in Tank AW-101 is approximately 1040 cm (410 in.). Figure 4.2 shows the available information on tank content layering as derived from the riser 4A thermocouple tree and riser 15A MIT measured temperature profiles, in concurrence with the VFI/ball rheometer

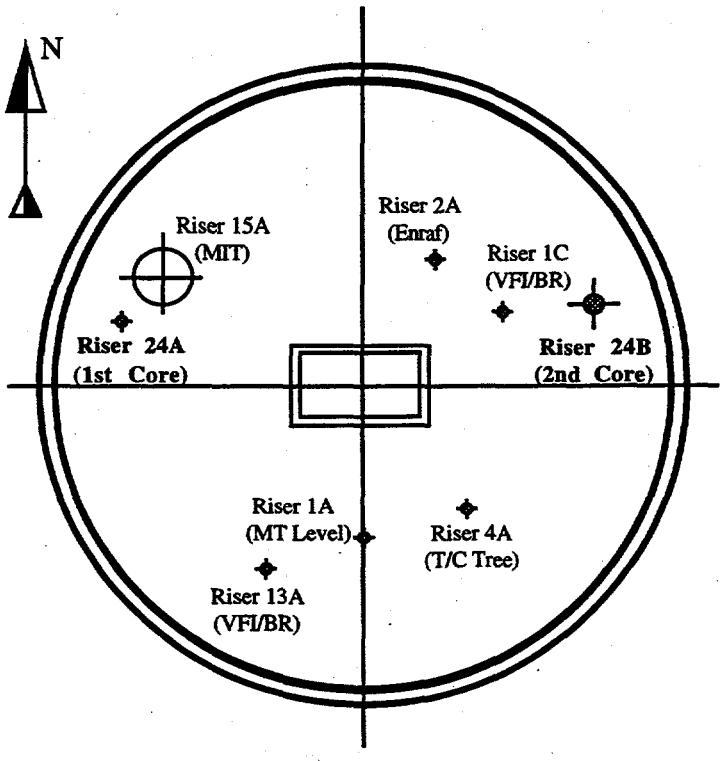

Figure 4.1. Schematic Diagram of Riser Locations in Tank 241-AW-101

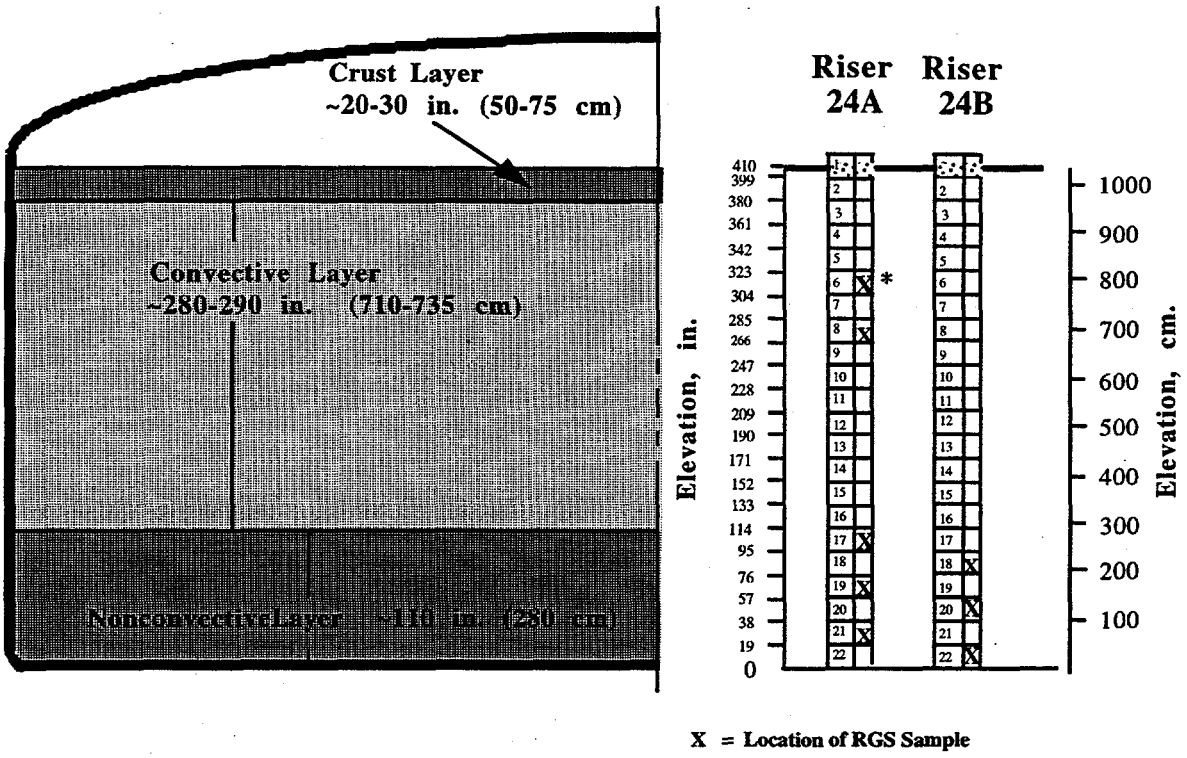

Figure 4.2. Diagram of As-Sampled RGS Sample Elevations for Tank AW-101 (*segment 6 was lost during the extraction process)

data for this tank. The nonconvective layer is believed to be about 260–310 cm (100–120 in.) in depth, with the convective, supernatant liquid layer and a 50–70 cm (20–30 in.) thick crust forming the balance of the contents. Twenty-one full sampler cores and one half-length sampler core were required; of these, the crust occupied all of segment 1 (not an RGS segment) and about one-third of segment 2 in riser 24A. The vertical locations for various RGS segments in each of the two selected risers are depicted in Figure 4.2 (Benar 1996).

4.1.2 Pertinent Tank Characterization Information

Figure 4.3 is a temperature profile taken with the MIT located in riser 15A. The solid circles show the distribution of temperature as measured on February 5, 1996. The thickness of the three zones, crust, supernatant liquid, and nonconvective layers, can be approximated from this temperature profile. The convective layer is the layer throughout which the waste temperature is almost uniform. The temperature throughout the crust drops nearly linearly to that of the dome space. The balance of the waste near the bottom of the tank is assumed to be the nonconvective layer.

The sudden change in the temperature profile at the MIT location after an episodic gas release event (GRE),[a] as shown in Figure 4.3 (closed circles), is noteworthy. If the temperature measurement uncertainty (biased error) is smaller than the temperature change at each location,[b] the local temperature of the nonconvective layer below ~254 cm (100 in.) may have increased after the GRE. This situation is rather unusual; in most cases the temperature in the nonconvective layer decreases after a GRE. The potential mechanisms for such a change have not been identified. Because some local flow or instability may have caused the change, the possibility of high lateral variability of gas content should be considered in reviewing RGS data. The same (unknown) mechanism could also result in significant changes over time, causing RGS and VFI data to differ.

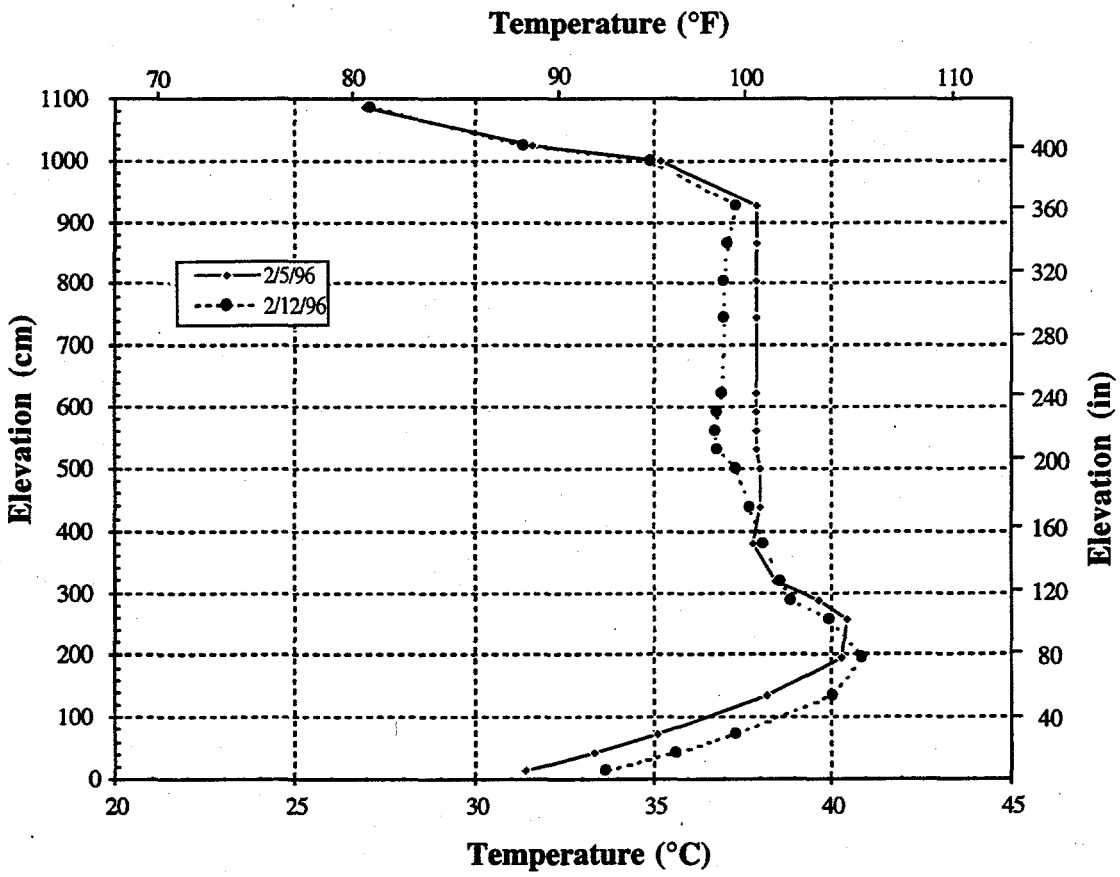

Figure 4.3. Profile of Temperature in Tank 241-AW-101 Taken with MIT

(a) NJ Wilkins, February 1996. Personal communication. Westinghouse Hanford Company, Richland, Washington.

(b) The three temperature readings on top are consistent and show no changes, which suggests that a sudden shift in the reference junction temperature is not the case.

The average density measured in the convective layer using the ball rheometer was found to be 1.42 ± 0.03 g/cc (Stewart et al. 1996a). The same reference gave a density of 1.57 ± 0.03 g/cc for the nonconvective layer from core sample analysis. These densities, rather than densities obtained by x-ray image processing, were used in RGS data analysis for AW-101; this choice was made because ball rheometer and core sample densities are obtained by recognized methods and so are preferred when available.

4.1.3 RGS Sampling Process Information

Segment 6 was lost in the laboratory due to sampler mishandling, and segment 20 was not recovered due to sampler valve problems. The remaining segments analyzed are shown in Table 4.1. This table also shows the lag times (delay between sample acquisition and processing) for these samples. This information is provided in case one is interested in correlating lag time between sampling and extrusion and decomposition or reactions of the various constituents. Further discussion of these data is provided in Section 4.6.

4.1.4 RGS Results Summary

Retained gas measurement data (Table 4.2), after averaging (by integration over the nonconvective layer) and correcting for entrainment (Table 4.5), show three major constituents in the in-situ gas/vapor phase: 56.5 ± 4.6 mol% nitrogen, 32.4 ± 2.4 mol% hydrogen, and 7.0 ± 0.6 mol% nitrous oxide. For the retained gas/vapor in the convective layer (Table 4.6), the major constituents have a composition of 69.4 ± 23 mol % nitrogen, 26.2 ± 6.6 mol % hydrogen, and 1.6 ± 0.5 mol% nitrous oxide. The remainder of the gas is composed of ammonia, methane, and other hydrocarbons.

The lower-bound ammonia concentrations in AW-101 were found to range from 960 ± 160 to 2900 ± 3500 µmol/L of waste (Table 4.3); more than 99.9% of this ammonia is dissolved in the waste. These concentrations integrate to a lower-bound, nonconvective layer ammonia inventory that, if it were present as vapor, would occupy 59 ± 33 m^3 (2100 ± 1100 ft^3) at STP (Table 4.5); the corresponding lower-bound, convective layer ammonia inventory (Table 4.6) would have a volume of 61 ± 11 m^3 (2200 ± 390 ft^3) at STP.(a)

Table 4.1. Lag Times for Processing RGS Samples from Tank AW-101

Sample	Acquisition Date	Processing Date	Lag (days)
24A-8	March 15, 1996	March 26, 1996	11
24A-17	March 21, 1996	March 26, 1996	5
24A-19	March 22, 1996	April 1, 1996	10
24A-21	March 22, 1996	April 10, 1996	19
24B-18	May 22, 1996	May 28, 1996	6
24B-22	May 23, 1996	June 4, 1996	12

(a) Calculations are being performed to further quantify the biased error in these measurements. Based on some preliminary calculations, these lower-bound ammonia values are estimated to be one-half to one-third of the actual in-tank values.

RGS data (Table 4.7, Figure 4.4) gives a corrected in-situ void fraction of 0.006 ± 0.001 for the convective layer and void fractions ranging from 0.017 ± 0.003 to 0.044 ± 0.004 for the nonconvective layer. The volume-averaged void fraction for the nonconvective layer (an average obtained by integrating over the depth of the layer) is 0.031 ± 0.006. The VFI data for the tank show in-situ void fractions of 0.002 to 0.005 in the convective layer and 0.016 to 0.087 in the nonconvective layer (Stewart et al. 1996a).

The STP hydrogen inventory retained in the nonconvective layer of Tank AW-101 is 35 ± 4.6 m^3 (1300 ± 160 ft^3), based on a hydrogen mole fraction that is an arithmetic average of the RGS data for both risers and on a total gas volume of 115 ± 12 m^3 calculated from VFI data by Stewart et al. (1996a). The nonconvective gas volume estimate from RGS data alone is 69 ± 11 m^3 at STP; the STP hydrogen inventory, calculated by integrating RGS hydrogen concentrations over depth and using data from both risers, is 22 ± 3.4 m^3. Table 4.6 contains supporting information.

The STP hydrogen inventory retained in the convective layer of AW-101 is 8.4 ± 9.2 m^3 (300 ± 320 ft^3), based on a hydrogen mole fraction from the single sample taken from this layer and on a total gas volume of 32 ± 34 m^3 that was calculated from VFI data by Stewart et al. (1996a). The convective gas volume estimate from RGS data alone is 21 ± 4.8 m^3 at STP; the STP hydrogen inventory, calculated from the single datum, is 5.6 ± 0.8 m^3. Supporting information can be found in Table 4.7.

Note that the hydrogen concentration differences between the two risers (Table 4.2) strongly indicate lateral variability in hydrogen concentrations. Accordingly, the hydrogen inventory must be considered to contain substantially more uncertainty than the stated ± values (which only account for instrument precision and layer interface uncertainty). The same is true for void fraction and total void volume, as the VFI data further indicate.

4.1.5 Retained Gas Concentrations

Table 4.2 presents the estimated concentrations of the insoluble and low-solubility gases in AW-101. No corrections have been made in Table 4.2 for air entrainment. Such a correction would consist of removing all the O_2 and Ar and subtracting (3.71 x O_2) from the N_2, consistent with the molar N_2/O_2 ratio in atmospheric air.

Table 4.3 presents the total ammonia concentration per liter of waste under in-tank conditions. The average and standard deviation over the nonconvective layer are 2400 ± 390 µmol/L of waste. Because this standard deviation is smaller than the error bands on individual samples, the concentration of ammonia can be considered constant throughout the nonconvective layer. The concentration in the convective layer (segment 8) appears to be significantly lower. These concentrations must be regarded as lower bounds because they do not account for ammonia lost to condensation in the RGS system.(a)

(a) Preliminary analysis to estimate the amount of condensed water and ammonia in the condensate shows that the concentration of ammonia found from the current analysis may have been underestimated by a factor of 2–3. Laboratory results are available that support this argument; however, such results are preliminary and not comprehensive.

Table 4.2. Concentrations of Insoluble Constituents (μmol/liter of waste) in Tank 241-AW-101, Without Air Entrainment Correction

Segment	N_2	H_2	N_2O	O_2	CH_4	Ar	Other Nit. Ox	C_2H_x	C_3H_x	Other Hyd.
24A-8	450±60	94±12	11±2	56±7	3.0±0.7	42±6	1.6±1.6	1.2±0.2	0.69±0.12	2.5±0.5
24A-17	1430±80	530±30	106±7	96±6	29±2	24±2	4.0±4.0	17±2	4.3±0.6	22±3
24A-19	2040±90	1610±70	220±10	74±3	48±3	25±1	0.6±0.6	28±2	6.1±0.8	26±3
24A-21	2430±90	1190±50	320±20	59±2	61±12	24±2	5.7±5.7	37±5	7.1±1.0	33±3
24B-18	1350±90	280±20	120±10	100±10	28±2	69±5	2.4±2.4	20±3	4.8±0.8	28±3
24B-22	1240±80	210±20	230±20	44±3	34±4	44±3	0.3±0.3	28±4	5.3±0.6	39±4

Table 4.3. Total Ammonia Concentrations in Tank 241-AW-101

Segment	NH_3* (μmol/L)
24A-8	960±160
24A-17	2600±1000
24A-19	2000±400
24A-21	2100±800
24B-18	2900±3500
24B-22	2600±1100

* These lower-bound values do not account for ammonia in the condensate in the collector side of the RGS system; they are expected to be 1/2 to 1/3 of the actual in-tank values.

4.1.6 Gas Inventories

Table 4.4 compares the layer gas inventories that are calculated entirely from RGS data, with and without corrections for entrained air, to the gas inventories calculated from VFI data by Stewart et al. (1996a). The RGS error bands in the convective layer contain only the instrument and layer thickness uncertainties for a single point, while the VFI error bands additionally contain the standard deviation for a large number of measurements. The method of calculation was described in detail in Section 3.4.1. Correcting for entrained air makes a greater change in the convective layer inventory than the nonconvective. No RGS value for the crust is provided in this table since there was no RGS sample taken from this layer. With or without correction, the RGS-alone inventory is significantly lower than the VFI inventory, a matter that receives further discussion in Section 4.1.7. Note that calculations of gas inventory for the nonconvective layer do not include segment 8 or any of the information from the convective layer.

Table 4.5 shows estimates of the STP volumes of gas constituents in the nonconvective layer in AW-101. The RGS/VFI inventories were calculated from the concentration data presented in Tables 4.2 and 4.3 by taking an arithmetic average of the mole fractions of constituents in the gas and multiplying that average composition by the volume of gas measured by VFI (Stewart et al. 1996a). The RGS inventories were calculated by integrating RGS data over depth, as discussed in Section 3.4.1. Although a significant difference in hydrogen concentrations was measured in the two risers, data from both risers have been used to generate Table 4.5 without any attempt to account for possible concentration variations in the horizontal plane. Table 4.6 is the same sort of table, but the concentrations for the upper convective layer are based on the single sample taken in that layer. The values in Tables 4.5 and 4.6 include the effect of corrections to remove the (assumed) entrained air. The table gives volume (at standard conditions) and the volume percent of each gas.

Table 4.4. STP Gas Inventories in Tank 241-AW-101, According to Different Methods

Layer	STP Gas Volume (m^3)		
	Uncorrected RGS	Corrected RGS	VFI (Stewart et al. 1996a)
Crust	---	---	63 ± 23
Upper (convective)	41 ± 6.0	21 ± 4.8	32 ± 34
Lower (nonconvective)	79 ± 12	69 ± 11	115 ± 12
Total	120 ± 13 (no crust)	90 ± 12 (no crust)	147 ± 36 (no crust) 209 ± 47 (crust)

Table 4.5. Nonconvective Layer Gas Inventory in Tank 241-AW-101 at STP

Gas	RGS (corrected)		RGS (corrected)/VFI
	m^3 (mole %) in gas/vapor phase	m^3 (mole %) dissolved in liquid phase	m^3 (mole %) in gas/vapor phase
Ammonia	0.042±0.02 (0.06%)	59±33 (98.4%)	0.074 (0.06%)
Nitrogen	39±6.1 (56.5%)	0.13±0.02 (0.2%)	66 (57.8%)
Hydrogen	22±3.4 (32.4%)	0.20±0.03 (0.3%)	35 (30.8%)
Nitrous Oxide	4.8±0.75 (7.0%)	0.65±0.10 (1.1%)	8.1 (7.1%)
Methane	1.1±0.21 (1.6%)	0.006±0.001 (0.01%)	1.8 (1.6%)
C_2H_x*	0.71±0.13 (1.0%)	0	1.2 (1.1%)
C_3H_x*	0.15±0.03 (0.2%)	0	0.26 (0.2%)
Other*	0.84±0.20 (1.2%)	0	1.5 (1.3%)
TOTAL	69±11 m^3	60±30 m^3	115 m^3

* These gases were assumed to be entirely insoluble.

Table 4.6. Convective Layer Gas Inventory in Tank 241-AW-101 at STP

Gas	RGS (corrected)		RGS (corrected)/VFI
	m^3 (mole %) in gas/vapor phase	m^3 (mole %) dissolved in liquid phase	m^3 (mole %) in gas/vapor phase
Ammonia	0.007±0.001 (0.03%)	61±11 (98.3%)	0.0099 (0.03%)
Nitrogen	15±3.7 (69.4%)	0.34±0.08 (0.5%)	22 (69.4%)
Hydrogen	5.6±0.8 (26.2%)	0.40±0.06 (0.6%)	8.4 (26.2%)
Nitrous Oxide	0.35±0.06 (1.6%)	0.32±0.06 (0.5%)	0.53 (1.6%)
Methane	0.18±0.04 (0.9%)	0.007±0.002 (0.01%)	0.28 (0.9%)
C_2H_x*	0.074±0.016 (0.4%)	0	0.11 (0.4%)
C_3H_x*	0.044±0.008 (0.2%)	0	0.066 (0.2%)
Other*	0.26±0.13 (1.2%)	0	0.39 (1.2%)
TOTAL	21±4.8 m^3	62±11 m^3	32 m^3
* These gases were assumed to be entirely insoluble.			

The error bands in Tables 4.5 and 4.6 represent only the uncertainty that carries through from instrument error and uncertainty in layer interface location. Temporal and lateral variability in compositions are not included, and the resulting inventories may not be conservative.

4.1.7 Retained Void Fraction

The method by which the in-situ void fractions were calculated is given in Section 3.3. The results are presented in Table 4.7, showing the difference between (entrained air) corrected and uncorrected in-situ void fractions.

Table 4.7. In-Situ Void Fractions in Tank 241-AW-101

Segment	Sample Central Height (cm)	Hydrostatic Pressure (atm)	Temperature (°C)	Corrected Void Fraction (In-Tank Conditions)	Uncorrected Void Fraction (In-Tank Conditions)
24A-8	700	1.47	40.8	0.006 ± 0.001	0.012
24A-17	265	2.07	42.6	0.022 ± 0.002	0.028
24A-19	169	2.21	43.0	0.044 ± 0.004	0.048
24A-21	72	2.36	37.5	0.042 ± 0.004	0.045
24B-18	217	2.14	43.4	0.017 ± 0.002	0.024
24B-22	24	2.43	35.8	0.017 ± 0.003	0.019

Figure 4.4 presents the corrected void fractions found from RGS. The segment numbers are shown next to each symbol representing the RGS data. On the same plot, the results found using VFI (Stewart et al. 1996a) are shown. This figure shows that the data from the retained gas sampler agree reasonably well with the VFI results. Given that both measurement techniques have finite uncertainty and that the measurements were made at different points in the tank with possible lateral variations, the agreement between the two sets of data is reasonably close. Although the VFI data show a maximum of approximately 0.09 void fraction at approximately 100 cm (40 in.) and the maximum void fraction found with the RGS is 0.044, the differences in the two sets of results are not anomalous and can be explained based on measurement resolution for each system.

RGS segment 24A-19 captured waste between the elevations of 145 and 193 cm. The arithmetic average of the VFI void fractions in this slice of the waste is roughly 0.035, compared to the RGS void of 0.044. RGS segment 24A-21 contained waste located between 48 and 96 cm. In this range, the arithmetic average of the VFI data is about 0.055. Thus the similarity between RGS and VFI results is greater than appears at first glance. Had an RGS sample been taken successfully at segment 20 (96–145 cm elevation), the RGS data might have shown the maximum that the VFI reported. (In this slice of waste, VFI results average to about 0.06.) The RGS data imply that a maximum void might exist between segments 19 and 21, where the VFI data explicitly show a maximum.

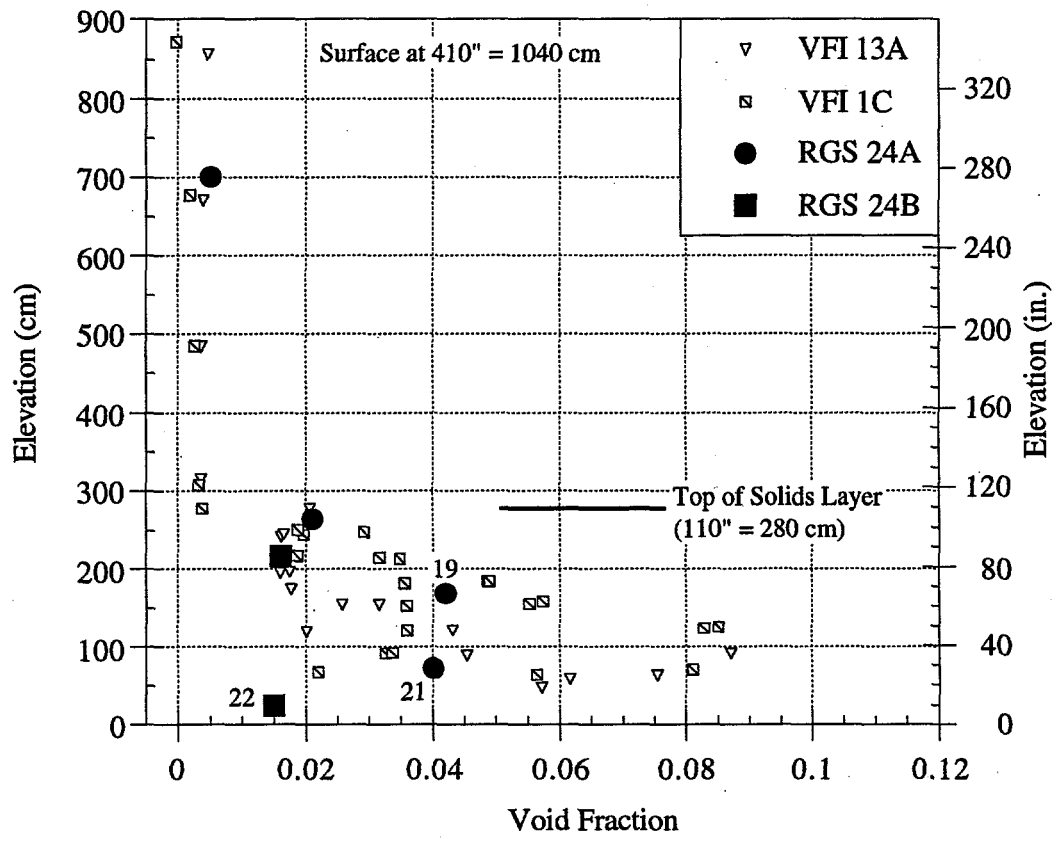

Figure 4.4. Void Fractions in Tank 241-AW-101 (RGS data were taken in riser 24A in March-April and in riser 24B in May-June 1996; VFI data in September 1995)

4.1.8 X-Ray Results

Figure 4.5 shows the region near the top of the sampler for two different segments taken from the supernatant liquid. The lighter region shows the presence of void underneath the piston. Note that both segments 6 and 8 contain the same amount of void approximately 1.8%±0.5%.(a) Without further analysis, this void might be taken to be the gas content of the convective layer. However, a more thorough review of the RGS data shows that this void resulted from air and argon entrainment in the sampler nose piece. This subject is further discussed in Subsection 4.1.9.2 and Section 4.6.1.

Table 4.8 summarizes observations for all the segments analyzed. There were no calibration records for two of the six segments for which x-ray images were recorded. Therefore, quantitative information on these segments could not be obtained from the x-ray images.

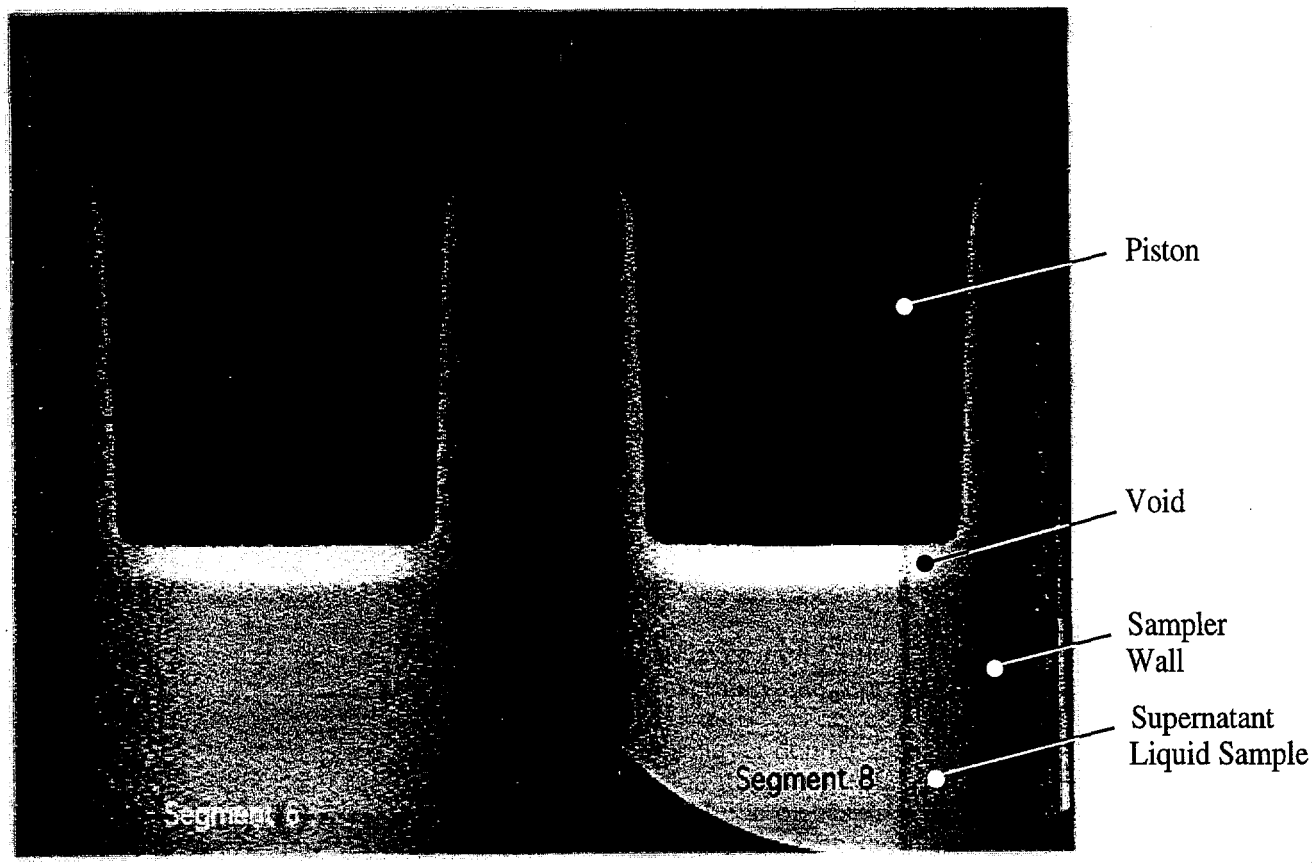

Figure 4.5. X-Ray Images Recorded from RGS Segments 6 and 8 for Tank AW-101 (see Section 3 for relative position of this subsegment in the sampler)

(a) For calculation of void volume, the volume of the annular space around the piston and the "disk-like" volume below the piston were included. This annular region was found to have an attenuation coefficient closer to that of a void than to liquid from image processing. Thus it was assumed that this volume is filled with gas.

4.1.8.1 Phase Distribution

Figures 4.6 and 4.7 are sample reconstructed images of the density distribution of the waste in the RGS samplers (segments 8 and 22). These images are produced using the procedure outlined in Section 3.5. The lighter regions on this image correspond to higher densities, and conversely, the darker regions are the low-density parts of the waste mixture. Thus, if a bubble is located along the path of x-ray, it appears dark on this image. The larger the size of the bubble, the larger and darker it would appear on the image. Figure 4.6 appears to be rather uniform and free of discontinuities, within measurement uncertainty associated with image recording, digitization, and processing, as described in Section 3.5. The homogeneity in the image suggests that no resolvable bubbles are present in the supernatant liquid layer, as expected. However, within segment 22 (Figure 4.7), both darker and lighter regions are observed, suggesting that bubbles, as well as solids of higher density than the local mixture, exist in the nonconvective layer.

Based on our observation of the various segments, which was summarized in Table 4.8, bubbles as large as 7 mm in diameter are clearly present. However, this size is not considered to be the upper limit in the size distribution of the bubbles retained within the nonconvective layer in this tank. Also, close inspection of the images shows that the majority of the visible bubbles are in the order of 1 mm. Whether bubbles smaller than that size exist cannot directly be determined from the current density map due to the detection limit dictated by the signal-to-noise ratio, as discussed in Section 3.5. A preliminary estimate of the volume of visible bubbles in segment 19 shows that more than 90% of the gas volume is in bubbles at the undetectable size level. Based on this observation, the AW-101 sludge is considered to be a bubbly mixture.

4.1.8.2 Waste Density

Table 4.9 provides a summary of the mean and standard deviation (STD) of the density of the waste found from the current x-ray densitometry. The details of the measurement technique are provided in Subsection 3.5.2.4. Note that the mean density in the supernatant layer is very close to what was found with the ball rheometer (Stewart et al. 1996a). The density reported for ball rheometer measurement in the supernatant layer is 1.47 ± 0.03 g/cc (riser 22 data; it is 1.4 ± 0.2 g/cc for riser 17 data). Such agreement further validates the use of this approach.

The densities reported for the nonconvective layer are the most probable average density in each segment (see explanation in Section 3.5). Thus, this value represents the average density over all solid, liquid, and gas phases (i.e., mixture density). The results show an increasing density of the mixture as a function of nonconvective layer depth. The density of the slurry can be determined by removing the gas phase contribution on the mean density (by adjusting the averaging volume provided in Section 4.1.7). The volume of gas used for this calculation was found based on the current estimation of the void fraction in each sampler (see Table 4.7). The results clearly show the effect of slurry compaction as a function of waste depth. That is, as the depth increases, the slurry becomes more dense under a higher hydrostatic or lithostatic pressure. Such variations in density as a function of compaction pressure have previously been shown for SY-102 waste (Onishi et al. 1996).

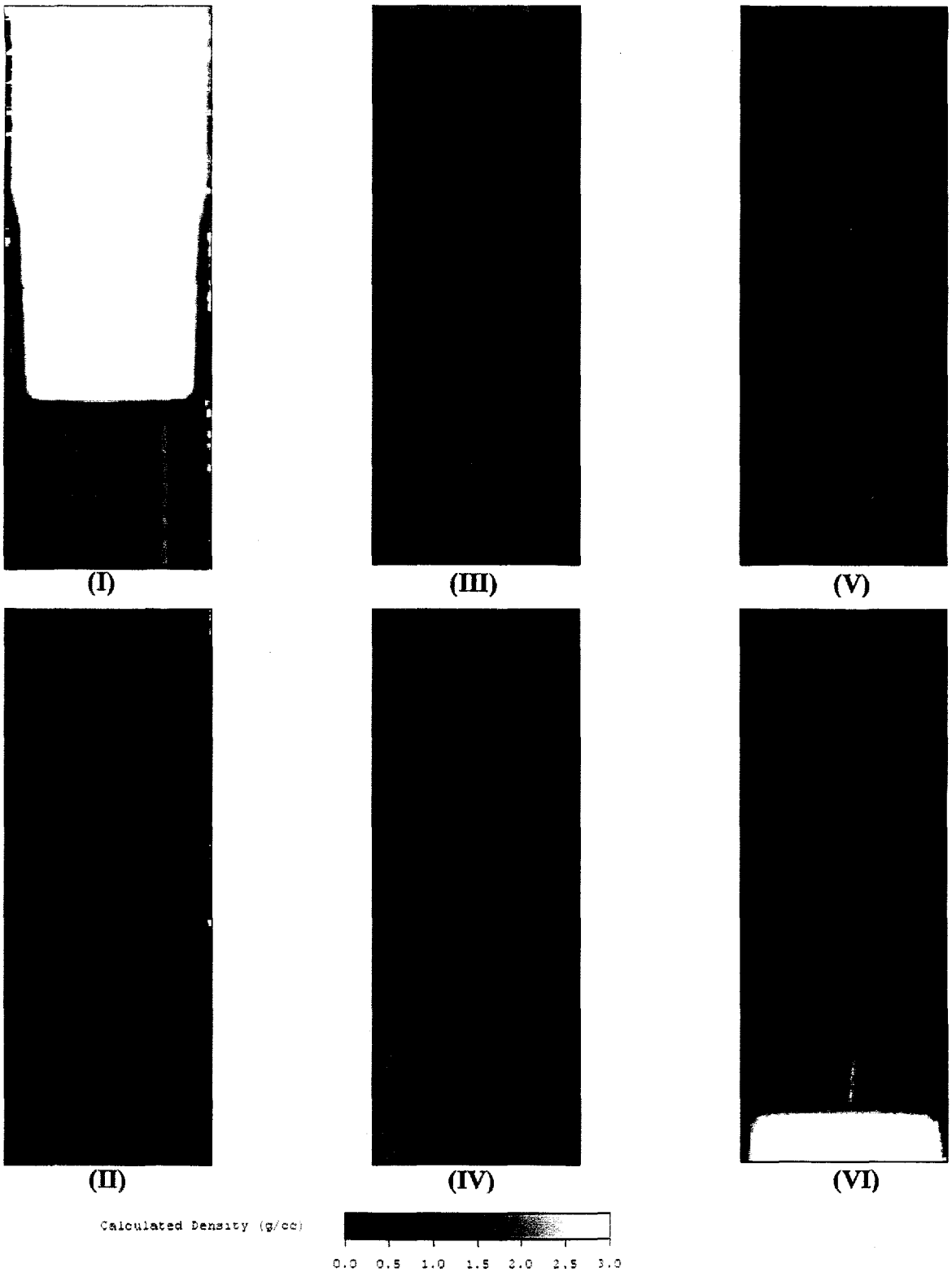

Figure 4.6. Density Image Calculated from X-Ray Images of Segment 8, Riser 24A, Tank AW-101

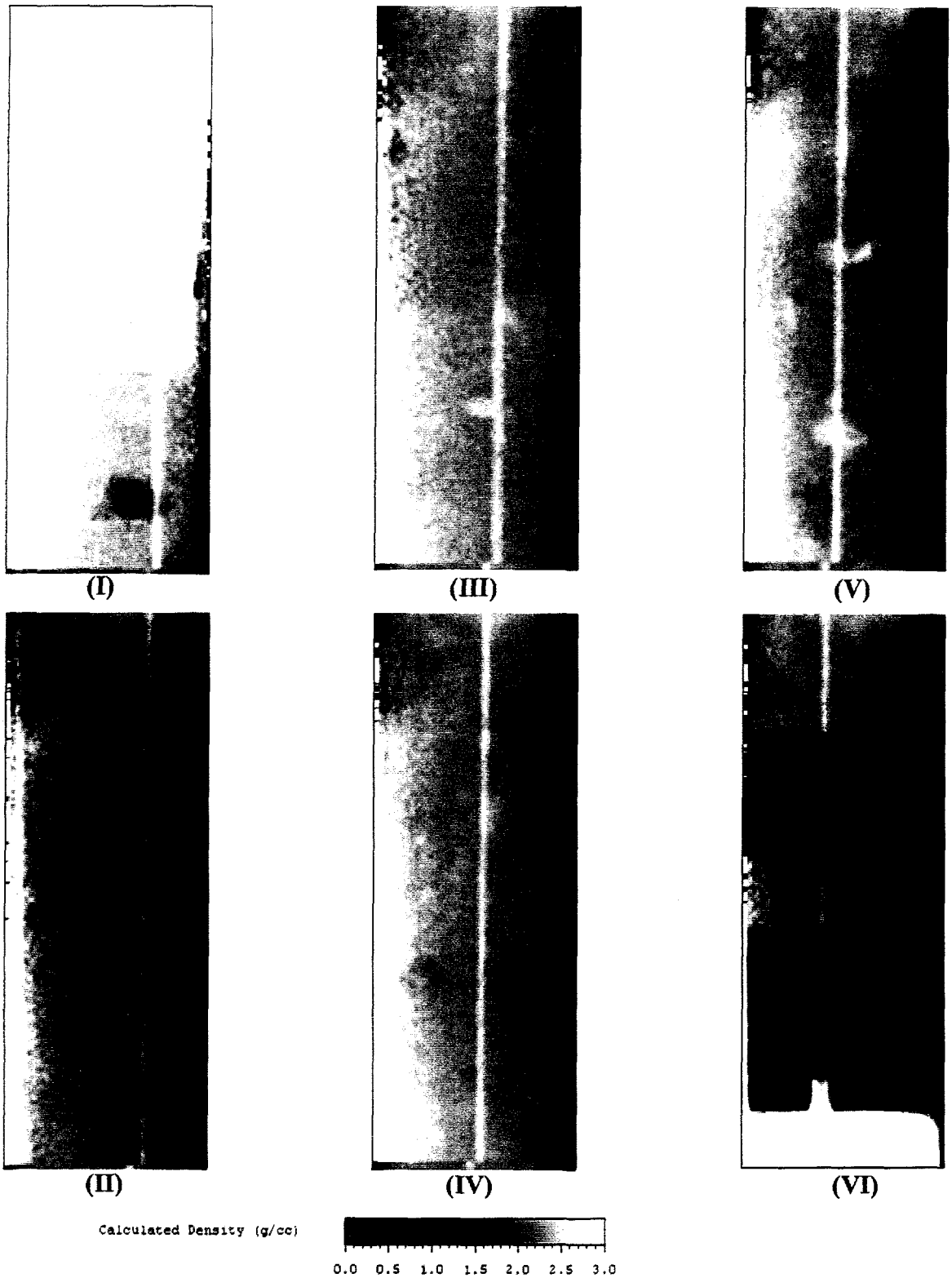

Figure 4.7. Density Image Calculated from X-Ray Images of Segment 22, Riser 24B, Tank AW-101

Table 4.8. Summary of Observations from X-Ray Images of Tank AW-101

Segment	Comments / Observations
24A-8	Homogenous sample, very small void below piston.
24A-17	Fairly homogenous sample with few small bubbles in the upper half of the sample. No noticeable void below piston.
24B-18	No calibration data available for this segment. Homogeneous sample with a small void below the piston.
24A-19	Numerous small bubbles with 2 distinct medium bubbles visible in middle of sample. No noticeable void below piston.
24A-21	Numerous small to medium bubbles throughout sample, increasing in number toward top. No noticeable void below piston.
24B-22	No calibration data available for this segment. Many medium bubbles throughout. No noticeable void below piston.

Table 4.9. Summary of X-Ray Densitometry Results

Segment	Riser	Mean Density (g/cc)	Density STD (%)	Mean Slurry Density (g/cc)	Slurry Density STD (%)
24A-8	24A	1.42	4.7	1.43	4.7
24A-17	24A	1.58	4.4	1.63	4.5
24B-18	24B	N/A	N/A	N/A	N/A
24A-19	24A	1.6	3.9	1.68	4.0
24A-21	24A	1.68	6.4	1.76	6.5
24B-22	24B	N/A	N/A	N/A	N/A

4.1.9 Other Discussions of RGS Results for Tank 241-AW-101

4.1.9.1 Effect of Sample Processing

In processing the waste samples for AW-101, the first tank on which the RGS was deployed, certain processing difficulties were evident that were not characteristic of later tanks. First, on segment 8 (the first one handled) the mercury-pumping was not carried out long enough to extract all of the insoluble gases. Second, on segments 8, 17, 19, and 21 (all of the riser 24A samples), at the end of the bound-vapor extraction, dilution water was added to the sample to improve mixing and to ensure gas release. As a result, the J3 canister results for these samples had to be discarded owing to contamination by dissolved gas in the dilution water.

Because of both of these effects, there is reason to believe that the insoluble and soluble gases for riser 24A may have been underestimated. An upper bound can be found for the degree to which the data were biased. Supposing that the J3 canister contained as much insoluble gas as the J2 canisters did, which probably overestimated the J3 canister. Then Table 4.2 would show an insoluble gas content that was about 20% too low for segment 8 and about 10% too low for segments 17, 19, and 21. It is not so straightforward to find the amount by which the ammonia content of the riser 24A samples is underestimated, but it is probably small by comparison to the underestimation that results from neglecting condensation in the J canisters.

4.1.9.2 Entrainment/Contamination

Table 4.2 shows that the calculated concentrations of oxygen and argon in AW-101 were higher than the anticipated zero values. (Oxygen is believed not to be present as free gases in tank waste, based on current kinetic models, and argon should not be present at all.) The possible sources of RGS contamination are the following:

- air entrainment, in which the sampler captures air during sampling
- argon intrusion, in which argon purge gas either enters the waste or is entrained, as with air
- dissolved gases in the hydrostatic head fluid (HHF), which may mix with waste during sampling
- air in-leakage during sampler handling or gas extraction.

Air entrainment is contamination of the sample with air during the sampling process. The leading edge (nose piece) of the sampler can trap air before becoming fully submerged. The maximum possible volume of this trapped air is estimated at about 6 cc (at STP).(a) This amount of air in about 313 cc of sample would contribute about 4.7 cc (670 µmol/L waste) of N_2, 1.2 cc (180 µmol/L waste) of O_2, and 0.056 cc (8 µmol/L waste) of Ar. This is considered an upper bound on the potential nosepiece air entrainment. In all samples except segment 18, oxygen concentrations are less than half the 6-cc entrainment value. Further discussion is provided in Section 4.6.

The sampling process can also lead to argon contamination. When high concentrations of hydrogen are detected during the sampling process, argon is used to purge the drill string for safe operation. A portion of that argon may be forced into the waste and captured in the sampler or be trapped in the inlet cavity of the sampler and enter the sampler as the piston is retracted. Because argon concentrations were found to be in the range of 40–70 µmol/L, above the concentration possible from air entrainment, it is safe to conclude that argon purge gas entered the sample.

A second possible explanation for the oxygen is that HHF (which consists of a solution of LiBr salt in water) mixed with the sample when it was taken, and this water contained dissolved oxygen and nitrogen. In all samples tested to date, the bromide content has been below the minimum detection limit. Based on the known (analyzed) bromide concentration in the HHF, the detection limit corresponds to a maximum of 30 cc of hydrostatic balance fluid in the roughly 313 cc of total sample.

(a) Cannon NS. March 6, 1997. *Retained Gas Sampler Interface Volume.* Letter report HNF-SD-WM-CN-092, SGN Eurisys Services Corporation, Richland, Washington.

Assuming that the dissolved nitrogen and oxygen are in equilibrium with air at 25°C, and treating the hydrostatic fluid as pure water (to obtain an upper bound on the gas content in the fluid), 30 cc of hydrostatic fluid could contain 15 μmole of N_2 and 8 μmole of O_2. (The inverse Henry's Law constants, respectively 6.6 x 10^{-4} and 1.3 x 10^{-3} mole/(kg water)(atm), were based on correlations presented in Norton and Pederson [1995].) In 313 cc of sample, this dissolved gas contribution would come to about 49 μmole/L waste of N_2 and 26 μmole/L waste of O_2. Again, this is less than the typical oxygen concentration (in AW-101 samples).

A third explanation for the presence of oxygen is the inleakage of air during sample processing (which is carried out at subatmospheric pressure). It makes some difference whether oxygen came from entrainment or inleakage. Leaked air would have an N_2/O_2 ratio of 78/21, as in the atmosphere, while entrained air could have a higher N_2/O_2 ratio because some unknown amount of the oxygen might have reacted with the waste during the lag time. If the wrong ratio is used, too much or too little N_2 may be removed while correcting for sample contamination.

The maximum allowable leak rate is 0.003 μmol/s at full vacuum. The leak rates are calculated from rates of pressure rise in the system (which is at subatmospheric pressures). Nominally the pressure rise all comes from air leaking in, but it may also result from desorption of gas and water vapor from surfaces within the vacuum system. (Out-leakage is not a concern because the system operates at a vacuum.)

A typical set of procedures takes several hours; for example, a total data-collection period of 7.3 hours was recorded for segment 17 of AW-101. An upper-bound estimate of air inleakage would thus be (0.003 μmol/s)(7 hr), or 188 μmol/L waste of N_2, 51 μmol/L waste of O_2, and 2.2 μmol/L waste of argon. The measured oxygen content (40 to 100 μmol/L) is generally higher, indicating that some amount of air entrainment as well as inleakage must have occurred.

In summary, the oxygen levels in AW-101 samples are too high to be explained by either extractor inleakage or HHF contamination alone and are substantially lower than would result from entraining the maximum amount (6 cc) of air during sampling. The observed O_2 concentrations could result from maximum entrainment only if half or more of the O_2 had reacted with the waste during the hold (lag) time.

The main consequence of ambiguity regarding the oxygen source is that there is also ambiguity as to what N_2/O_2 ratio to use in correcting the N_2 concentrations to remove the contribution of air contamination. If oxygen for the contaminants came from leaked air or entrained air that underwent no reaction, N_2/O_2 would be 3.7. If oxygen came from entrained air whose oxygen reacted significantly in the sample, N_2/O_2 would be higher than 3.7.[a] If oxygen came from air constituents dissolved in HHF, calculated N_2/O_2 for the contaminants would be 1.9 in the absence of oxygen reaction, or higher if reaction occurred. In view of these ambiguities and as a result of a lack of better supporting data, we have used a ratio of $N_2/O_2 = 3.7$ to correct for air entrainment. Using a ratio of 3.7 would overestimate the amount of native N_2 if air gases had come from dissolved air.

(a) See discussion provided in Section 1 for argument against substantial reaction of oxygen based on data provided in Person (1996).

4.1.9.3 High Local Hydrogen

In Table 4.2, the hydrogen concentrations for riser 24A (segments 19 and 21) are much higher than for riser 24B (segments 18 and 22). The other insoluble gases, with minor exceptions, do not show such a dramatic difference. Several explanations for this difference are possible. One possibility is the effect of the holding times of the samplers from riser 24B on leakage of hydrogen through the seals and sampler walls.

To determine whether holding time was an issue, the dates the waste samples were taken and the dates the samples were processed in the lab were used to calculate the sample hold times (Table 4.1). The results show that the hold times for segments 18 and 22 were in fact less than those for segments 19 and 21. In addition, the RGS acceptance tests included testing the leakage rate during which a gas mixture with 30% hydrogen was sealed in a sampler. The results showed no detectable leakage when the sampler was held from 24 to 187 hours (Cannon and Knight 1995). Therefore, the leakage of hydrogen (due to extended hold times) does not appear to explain the difference in H_2 concentration. A plausible explanation is lateral variation in the chemical composition of the waste, which affects the rate of generation of hydrogen.

It has been argued that one cause for variation in gas composition within the tank may be due to a gas release event (GRE). However, there is no physical reason to expect that GREs affect gas composition. Rather, a GRE causes the release of all the gas constituents together such that no change in the composition of the gas bubbles or pockets should result. (The void fraction changes, but no gas is preferentially released). Thus a GRE does not seem to be a viable explanation of the variation in the local hydrogen mole fraction that is seen in AW-101.

4.1.9.4 Large Ammonia Error Band

In Table 4.3, considerable variation is seen in the size of the error in ammonia concentration compared with the concentration itself. The high error comes from the calculated ammonia residual; when the ammonia versus cycle slopes ($\Delta n/\Delta N$, described in Section 3.2) are nearly equal for two canisters, the relative error is high for the difference of the slopes (residual ammonia).

4.2 Tank 241-A-101

4.2.1 Sampling Locations

Push-mode sampling was performed in risers 15 and 24 of single-shell Tank A-101, the second tank sampled. The approximate locations of the risers and characterization equipment are depicted in Figure 4.8. Lateral distance between the two risers was approximately 15 m (50 ft).

Three segments of the first core (riser 15) and four segments of the second core (riser 24) were sampled and analyzed to provide data on the multiple layers in the tank and supply information on lateral nonuniformity. The elevations at which different segments within each core were sampled are shown in Figure 4.9.[a]

(a) Shekarriz R and JM Bates. 1996. *Sampling Plan for Tank 241-A-101 Retained Gas Sampler Deployment.* TWS-MIT-071996, Pacific Northwest Laboratory, Richland, Washington.

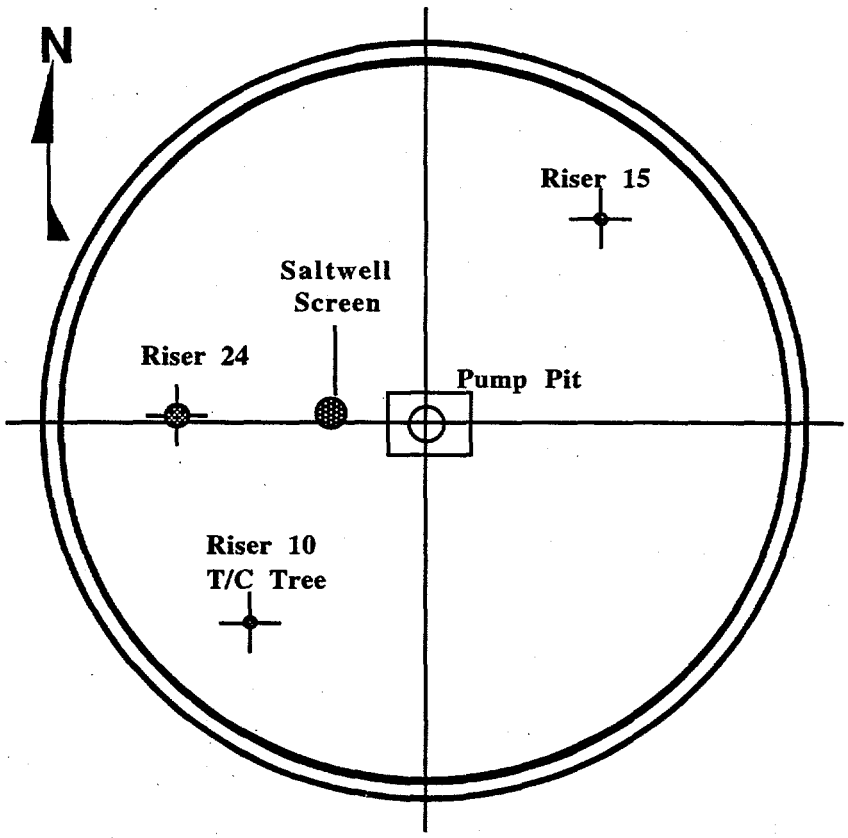

Figure 4.8. Schematic Diagram of Riser Locations for Tank 241-A-101

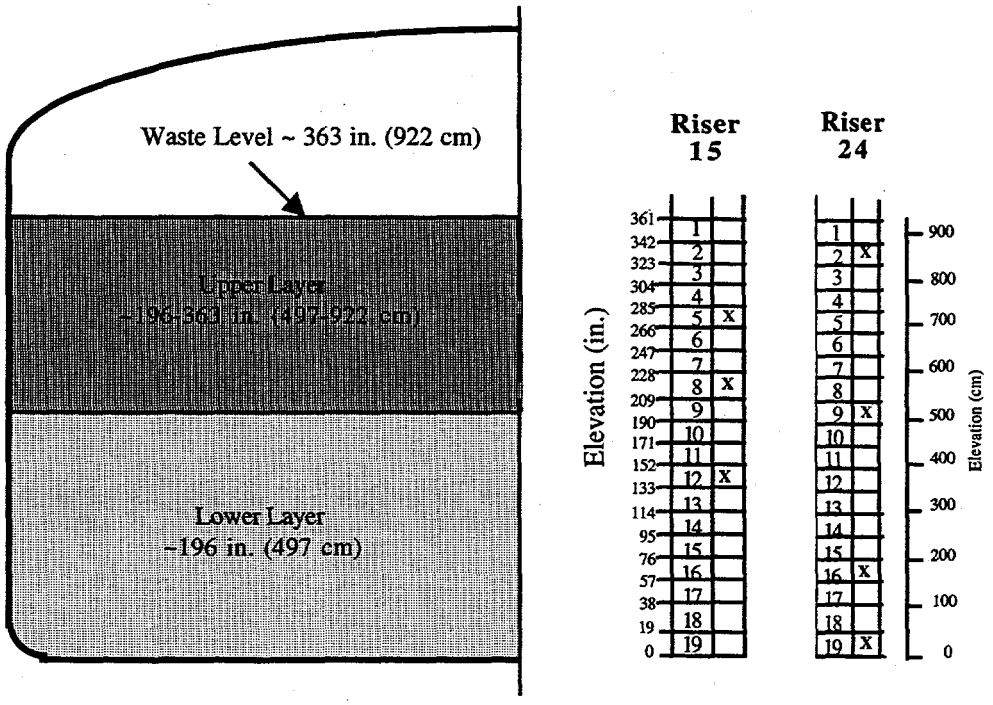

Figure 4.9. Diagram of the As-Sampled RGS Sample Elevations for Tank 241-A-101

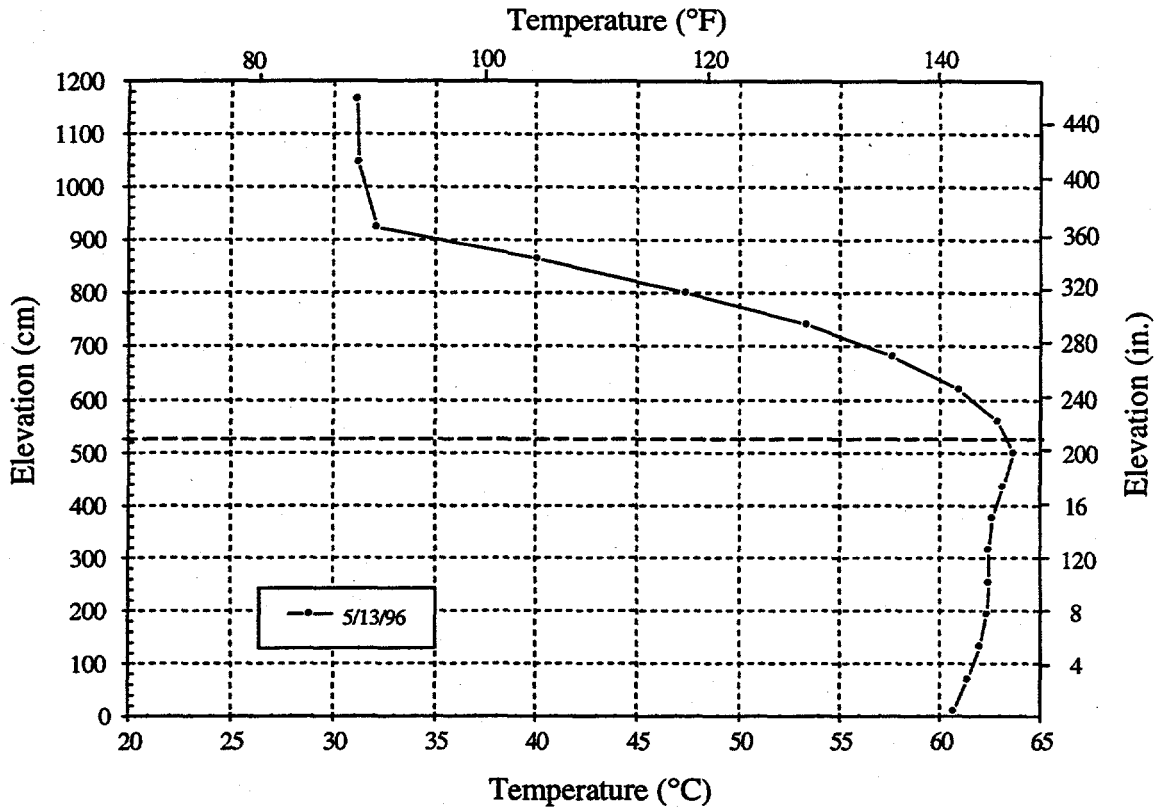

Figure 4.10. Profile of Temperature in Tank A-101 Taken with Thermocouple Tree

4.2.2 Pertinent Tank Characterization Information

The temperature within the waste is monitored using a single thermocouple tree containing 18 thermocouple probes. The vertical distribution of temperature is shown in Figure 4.10. Note that this tank has significantly different thermal characteristics than those reported for DSTs such as AW-101. Based on an extensive analysis, Ogden (1996) surmised the presence of two distinct layers in this tank—a lower layer ~498 cm (196 in.) deep and an upper layer ~424 cm (167 in.) thick. The upper layer shows insulating behavior, while the lower layer has a more uniform temperature associated with its higher conductance (whether in convective or conductive modes). This layering model is consistent with the most recent observations of the sample extrusions, classifying the upper layer material as moist salt or wet salt and the lower layer as salt slurry or liquid.(a) These extrusions indicate that segment 10 is the topmost segment of the layer. However, the tank layer model provided by Brevick et al. (1995) is inconsistent with the above-mentioned observations.

Because no other sources of data were identified for density of the waste, the average densities used in RGS data analysis for A-101 were those determined by x-rays of the sample (see Subsection 4.2.8.2).

(a) Field JG. September 12, 1996. cc:Mail communication. Westinghouse Hanford Company, Richland, Washington.

4.2.3 RGS Sampling Process Information and Field Observations

The lag times (delay between sample acquisition and processing) for the RGS samples for Tank A-101 are shown in Table 4.10. The maximum hold time allowed by the sampling plan is 24 days, based on measured sampler leakage rates during acceptance testing. The hold time for sample 15-5 exceeded this limit, but the sample was accepted based on calculations that indicated the estimated leakage was still negligible.

4.2.4 RGS Results Summary

The retained gas measurement data (Table 4.11), after averaging (by integration over the upper layer) and correcting for entrained air (Table 4.14), show three major constituents in the in-situ gas/vapor phase: 16 ± 0.9 mol% nitrogen, 75 ± 3.8 mol% hydrogen, and 5.6 ± 0.3 mol% nitrous oxide. For the retained gas/vapor in the lower layer (Table 4.15), the major constituents have a composition of 73 ± 8.0 mol% nitrogen, 16 ± 1.5 mol% hydrogen, and 6.8 ± 0.7 mol% nitrous oxide, based on averaging by integration. The remainder of the gas is composed of ammonia, methane, and other hydrocarbons.

The lower-bound ammonia concentrations in A-101 were found to range from 3200 ± 400 to 33000 ± 29000 µmol/L of waste (Table 4.3); more than 99% of this ammonia is dissolved in the waste. These concentrations integrate to a lower-bound, upper-layer ammonia inventory that, if it were present as vapor, would occupy 275 ± 120 m^3 (9900 ± 4200 ft^3) at STP (Table 4.14); the corresponding lower-bound lower-layer ammonia inventory (Table 4.15) would have a volume of 669 ± 180 m^3 (24000 ± 6400 ft^3) at STP. These lower-bound ammonia values are expected to be one-half to one-third of the actual in-tank values.(a)

RGS data (Table 4.16, Figure 4.11) gives void fractions ranging from 0.139 ± 0.011 to 0.178 ± 0.011 (with a volume-averaged void fraction of 0.142 ± 0.014) for the upper layer. Void fractions range from 0.003 ± 0.0004 to 0.006 ± 0.0005 (with a volume-averaged void fraction of 0.004 ± 0.0005) for the lower layer (Stewart et al. 1996a). In each layer, the volume-averaged void fraction is obtained by integrating over the depth of the layer.

The STP hydrogen inventory retained in the upper layer of A-101 is 215 ± 14 m^3 (7800 ± 500 ft^3), based on RGS data alone; the STP retained gas inventory, calculated by integrating RGS gas-phase constituent concentrations over the depth of the layer and using data from both risers, 288 ± 23 m^3. Supporting information can be found in Table 4.14.

Based on RGS data alone, the STP hydrogen inventory retained in the lower layer of A-101 is 2.2 ± 0.15 m^3 (78 ± 5.3 ft^3); calculated by integrating RGS gas-phase constituent concentrations over depth and using data from both risers, the STP retained gas inventory is 14 ± 1.3 m^3. This information can be found in Table 4.15.

The differences in hydrogen concentration between the two risers (Table 4.11) do not conclusively indicate lateral variability in hydrogen concentrations. Nevertheless, the hydrogen inventory could contain more uncertainty than the stated ± values (which account only for instrument precision and layer interface uncertainty). The same is true for void fraction and total void volume.

(a) Calculations are being performed to further quantify the biased error in these measurements. Based on some preliminary calculations, these lower-bound ammonia values are estimated to be one-half to one-third of the actual in-tank values.

Table 4.10. Lag Times for Processing RGS Samples from Tank A-101

Sample	Acquisition Date	Processing Date	Lag (days)
15-5	July 12, 1996	August 7, 1996	26
15-8	July 12, 1996	August 1, 1996	20
15-12	July 17, 1996	August 9, 1996	23
24-2	July 22, 1996	August 12, 1996	21
24-9	July 23, 1996	August 13, 1996	21
24-16	July 24, 1996	August 14, 1996	21
24-19	July 25, 1996	August 15, 1996	21

4.2.5 Retained Gas Concentrations

Table 4.11 presents the estimated concentrations of insoluble and low-solubility gases in A-101; no corrections for air entrainment, which would consist of removing all the O_2 and Ar and subtracting (3.71 x O_2) from the N_2, consistent with the molar N_2/O_2 ratio in atmospheric air, have been made.

Table 4.12 presents total ammonia concentration per liter of waste under in-tank conditions. The average and standard deviation over the upper layer is 16000 ± 15000 µmol/L of waste, with the high (and very uncertain) value from segment 9 dominating the average. By omitting segment 9, the average concentration in the upper layer becomes 7300 ± 430 µmol/L of waste. The concentrations in the lower layer are probably higher, with an average and standard deviation of 13000 ± 2600 µmol/L of waste. All these concentrations must be regarded as lower bounds (probably by a factor of 2–3) because they do not account for ammonia lost to condensation in the RGS system.(a)

Table 4.11. Concentrations of Insoluble Constituents (µmoles/liter of waste) in Tank 241-A-101, Without Entrainment Correction

Segment	N_2	H_2	N_2O	O_2	CH_4	Ar	Other Nit. Ox	C_2H_x	C_3H_x	Other Hyd.
15-5	1200±40	5200±140	410±20	39±2	49.±7	16±2	3.2±1.2	7.0±1.4	4.1±1.2	8.4±1.8
15-8	1490±60	6300±200	450±20	42±2	56±5	10±1	7.5±1.4	8.1±1.4	3.7±1.4	6.0±1.4
15-12	420±20	43±2	82±6	55±3	10±3	200±10	3.0±1.4	0.28±0.12	1.0±0.5	3.2±1.0
24-2	9170±230	3400±100	400±10	2070±60	23±6	111±4	4.0±2.3	8.1±1.5	5.0±1.8	6.9±1.8
24-9	2070±60	6230±150	440±10	11±1	76±9	290±10	1.0±0.5	12.0±1.4	3.2±1.5	5.8±1.8
24-16	320±20	55±2	79±4	26±2	3.0±0.6	310±20	1.9±0.7	0.58±0.21	0.72±0.35	3.1±0.9
24-19	690±30	112±4	103±4	82±3	4.1±0.5	300±10	1.9±0.8	0.91±0.46	0.87±0.42	2.7±1.0

(a) Calculations are being performed to further quantify the biased error in these measurements. Based on some preliminary calculations, these lower-bound ammonia values are estimated to be one-half to one-third of the actual in-tank values.

Table 4.12. Total Ammonia Concentrations in Tank A-101

Segment	NH_3* (μmole/liter)
15-5	7000±600
15-8	7600±2200
15-12	16000±6000
24-2**	3200±400
24-9	33000±29000
24-16	11000±1900
24-19	13000±2000

* These lower-bound values do not account for ammonia in the condensate in the collector side of the RGS system; they are expected to be one-half to one-third of the actual in-tank values.
** Segment 2 data are suspect because of air contamination.

4.2.6 Gas Inventory

Table 4.13 compares the layer gas inventories that are calculated with and without correction for entrained air. Note that the correction for entrained air makes a greater change in the lower layer inventory than the upper.

Table 4.14 shows an estimate of the STP volumes of gas constituents in the upper layer in A-101. The inventory was calculated by integrating RGS data over depth, as was discussed in Section 3.4.1. Data from both risers have been used to generate Table 4.14 without any attempt to account for possible concentration variations in the horizontal plane. Table 4.15 is similar to Table 4.14 but for the lower layer. The values in these tables were corrected for the presumed entrained air. Note that the results show a high concentration of hydrogen, composing approximately 75% of the volume of the free gas in the upper (high-solids) layer. This contrasts with the results found for Tank AW-101, in which only 33% of the free gas was hydrogen. Further, the volume of ammonia in the gas phase (free gas) for the whole tank was higher than what was found in AW-101 (0.75 mol% in A-101 versus 0.02 mol% in AW-101).

Table 4.13. STP Gas Inventories in Tank A-101 According to Different Methods

Layer	STP Gas Volume (m^3)	
	Uncorrected RGS	Corrected RGS
Upper	296 ± 24	288 ± 23
Lower	38 ± 2.8	14 ± 1.3
Total	334 ± 24	302 ± 23

Table 4.14. Upper Layer Gas Inventory in Tank A-101 at STP

Gas	RGS (corrected)	
	m^3 (mol%) in gas/vapor phase	m^3 (mol%) dissolved in liquid phase
Ammonia	6.9±3.8 (2.4%)	275±120 (99.9%)
Nitrogen	46±3.3 (16%)	0.02±0.001 (0.01%)
Hydrogen	215±14 (75%)	0.20±0.01 (0.07%)
Nitrous Oxide	16±1.1 (5.6%)	0.18±0.01 (0.07%)
Methane	2.0±0.3 (0.7%)	0.001±0.0002 (0%)
C_2H_x*	0.30±0.06 (0.1%)	0
C_3H_x*	0.15±0.05 (0.05%)	0
Other*	0.46±0.12 (0.2%)	0
Total	288±23 m^3	276±120 m^3
* These gases were assumed to be entirely insoluble.		

The error bands in Tables 4.14 and 4.15 represent only the uncertainty that carries through from instrument error and uncertainty in layer interface location. Temporal and lateral variability in compositions are not included, and the resulting inventories may not be conservative.

Table 4.15. Lower Layer Gas Inventory in Tank A-101 at STP

Gas	RGS (corrected)	
	m^3 (mol%) in gas/vapor phase	m^3 (mol%) dissolved in liquid phase
Ammonia	0.073±0.020 (0.5%)	669±180 (99.3%)
Nitrogen	10±0.9 (73%)	1.3±0.1 (0.2%)
Hydrogen	2.2±0.15 (16%)	0.56±0.04 (0.08%)
Nitrous Oxide	0.94±0.07 (6.8%)	3.1±0.2 (0.5%)
Methane	0.24±0.07 (1.7%)	0.052±0.015 (0.01%)
C_2H_x*	0.023±0.01 (0.2%)	0
C_3H_x*	0.041±0.02 (0.3%)	0
Other*	0.25±0.09 (1.8%)	0
TOTAL	14±1.3 m^3	674±180 m^3
* These gases were assumed to be entirely insoluble.		

4.2.7 Retained Void Fraction

The method by which the in-situ void fractions were calculated is given in Section 3.3. The results are presented in Table 4.16, showing the difference between entrainment-corrected and -uncorrected in-situ void fractions.

Figure 4.11 presents the corrected void fractions found from RGS. The gas profile in the upper layer apparently increases monotonically with depth. As expected, two distinct layers exist in this tank—the upper layer characterized as having a high free or insoluble gas content and the lower layer characterized as being relatively free of any insoluble or free gas.

4.2.8 X-Ray Results

Seven segments from Tank A-101 were radiographed with x-rays. A summary of the observations of these images is provided in Table 4.17. A discussion of the observations follows. Two of the seven segments radiographed did not have calibration images. As a result, these segments are omitted from quantitative discussions.

4.2.8.1 Phase Distribution

A quick glance at the observations recorded in this table reveals that the structure of the waste observed in Tank A-101 was dramatically different from that of AW-101 waste. In contrast to AW-101 waste, in which a large number of small round bubbles were observed, the A-101 waste appears to contain very irregularly-shaped structures, most of which are slit-shaped.

Figure 4.12 presents two typical subimages taken from segments 24-9 and 24-16.[a] As mentioned before, the magnitude of grayscale or intensity on these images is a measure of the line-of-sight-averaged density in the RGS sample. The darker the region, the lower the material density, perhaps corresponding to a gas pocket or a bubble. The continuous diagonal variation

Table 4.16. In-Situ Void Fractions in Tank A-101

Segment	Sample Central Height (cm.)	Hydrostatic Pressure (atm)	Temperature (°C)	Corrected Void Fraction (In-Tank Conditions)	Uncorrected Void Fraction (In-Tank Conditions)
15-5	700	1.29	46.0	0.139 ± 0.011	0.143
15-8	555	1.48	57.0	0.155 ± 0.015	0.158
15-12	362	1.78	62.0	0.004 ± 0.0004	0.012
24-2	844	1.10	33.0	0.121 ± 0.009	0.349
24-9	507	1.54	63.0	0.178 ± 0.011	0.185
24-16	169	2.09	61.0	0.003 ± 0.0004	0.010
24-19	24	2.33	60.0	0.006 ± 0.0005	0.015

(a) For a description of what a subimage is and how it was obtained and processed, the reader is referred to Section 3.5.

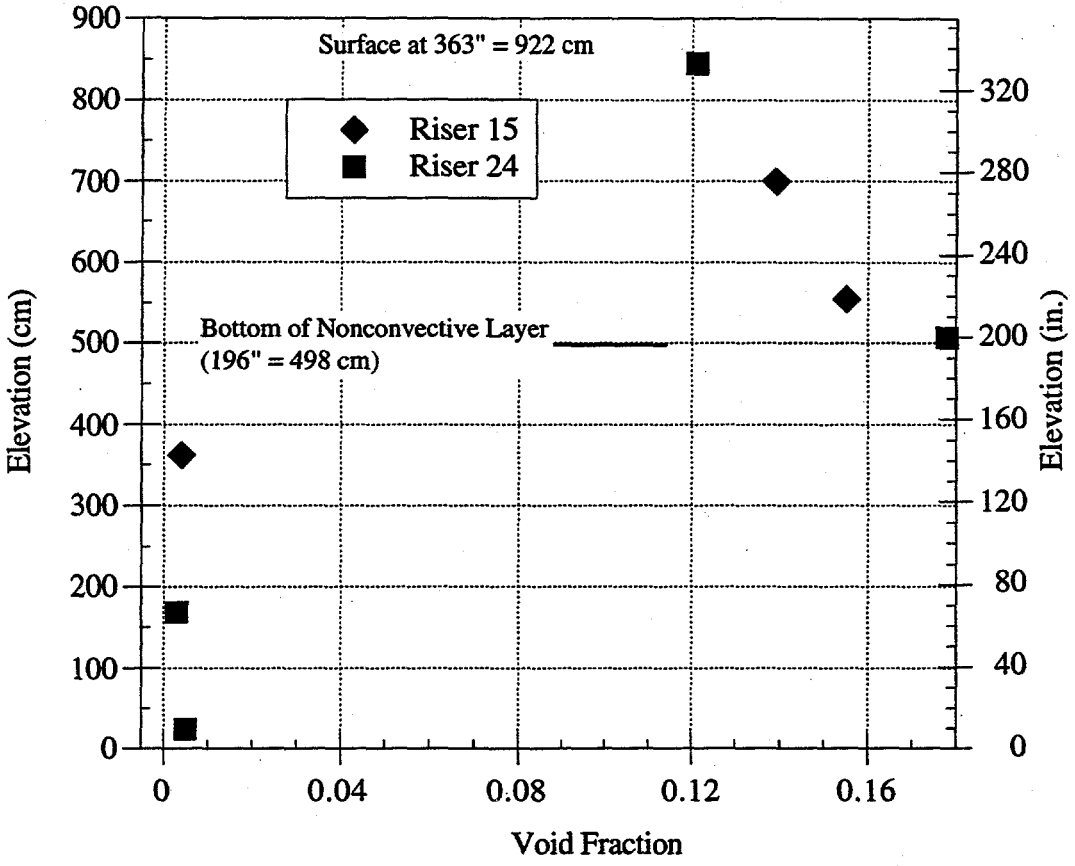

Figure 4.11. Void Fractions in Tank A-101

Table 4.17. Summary of Observations from X-Ray Images for Tank A-101

Segment	Comments / Observations
24-2 center	No calibration data available for this segment. Some small to medium bubbles, small void under piston.
15-5 center	Few small to medium bubbles, some fine structures in waste. Medium fracture near bottom of sample. Medium fracture/void near piston (approx 0.3 in.).
15-8	Many voids and fine structure. Large void at bottom (approx. 4 in.) and at top (approx. 2 in.).
24-9	Many small to medium voids and complex fine structure in waste. Medium fracture near piston. Small void under piston (approx. 0.5 in.).
15-12	Homogenous sample, small void under piston (approx. 0.5 in.).
24-16	Homogenous sample. Very small void under piston.
24-19	No calibration data available for this segment. Homogenous sample, small void under piston.

observed in 24-16 is a measurement artifact caused by the nonuniformity in the source radiation and/or detector response. Although some attempt was made to remove this background by using an appropriate image-processing procedure, this particular attempt was not successful. Despite this gradient, it is important to note that no phase discontinuities are observed on this subimage, and the waste at this location appears to be homogeneous. On the other hand, segment 24-9 shows a large variation in the local density. Unlike the x-ray images of the AW-101 waste, in which the gas phase appeared to be in the shape of round bubbles, the gas phase in segment 24-9 does not appear to be round. However, this observation could be misleading in that a large population of round bubbles may also give the appearance that the gas pockets or bubbles are not round. To resolve this issue, a tomographic x-ray imaging system is required that would provide projections from several directions and enable the spatial distribution and shape of the gas phase to be determined more accurately.

Figure 4.13 shows two images from the entire length of segments 24-9 and 24-16. Two features that appear in these images and that seem to be characteristic of the waste in this tank are fissures or fractures. However, one may question whether such fractures are present in the tank or are artifacts of the measurement approach produced during sampling. It has been shown that the waste sample is under a compressive stress during sampling.(a) Such a stress field would be acting in the opposite direction from that expected for formation of these fractures. Thus it is speculated that the fractures are filled with high pressure gas which sustained the form of the fractures during sampling. Presence of such fractures or fissures was observed for S-102 saltcake and stiff sludge (Gauglitz et al. 1996).

4.2.8.2 Waste Density

The summary of the densities and their standard deviation is provided in Table 4.18. Appropriate calibration data did not exist for segments 15-2 and 24-19 so they were not used for quantitative information. Further, these measurements are extremely sensitive to how meticulously the sampler was radiographed. Movement of the sampler during recording raised the background noise level significantly in many instances. Careful evaluation of the available videos provided some guidelines for selecting the best data set; based on these observations and the consistency of the results, data from some segments were rejected.

Table 4.18 shows that the mean layer density varies from low results in the upper layer of the tank to fairly high results in the lower layer. As shown in Table 4.17, segments 24-12 and 24-16 were homogeneous waste with no observable nonuniformities in the images. The standard deviation of the data in these segments, which is below 6.2%, is simply due to the experimental measurement uncertainty. This variance is the result of nonuniformity in the background radiation and could not be entirely removed from the images. This value can be considered as baseline uncertainty in the measurements.

The standard deviation in the segments from the upper layer, segments 5, 8, and 9, is higher than the baseline uncertainty. This parameter is proportional to the size of discontinuities in the upper layer. For example, if two segments of the upper layer contain similar quantities of gas, the standard deviation in the density measurements (using the current technique) would be higher in the segment with the larger gas pockets or bubbles. Certainly, this is consistent with the visual observations of the images, in that segments 5, 8, and 9 appear to contain more large gas pockets, as discussed in the previous section. Recall that the standard deviations in the values on the density measurements for Tank AW-101 nonconvective layer were within the measurement uncertainty, suggesting that the bubbles observed were smaller than those in the current tank.

(a) Shekarriz A and JD Norton. 1995. *Retained Gas Sampler System Analysis.* PNLFGP:091595, Pacific Northwest Laboratory, Richland, Washington.

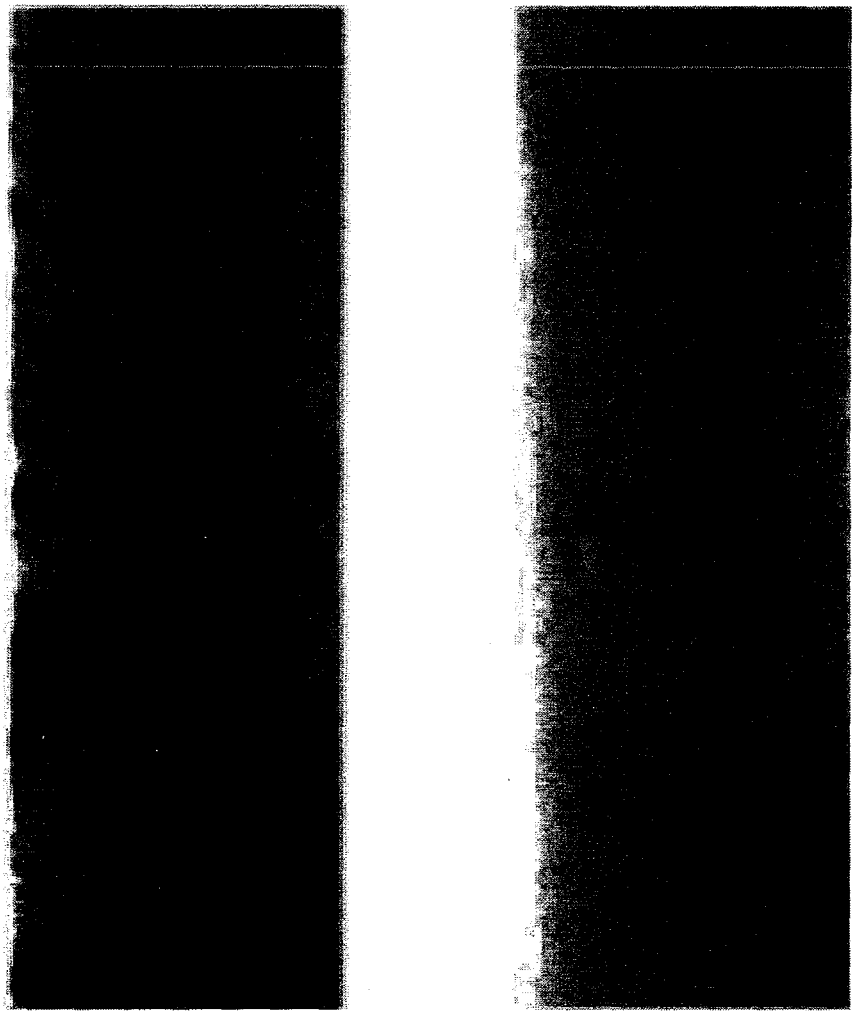

Segment 24-9
Subimage between
2.8" and 5.6"

Segment 24-16
Subimage between
8.5" and 11.3"

Figure 4.12. Two Subimages from Segments 24-9 and 24-16 Showing Distribution of Phases

As in the results presented for AW-101, the contribution of gas to the mean waste density was removed by correcting the averaging volume based on the measured void fraction of gases (Table 4.16). Note that with the exception of segment 15-8, which has a questionable calibration image, the remaining segments appear to have very similar density of the slurry (gas-free solid-liquid mixture), ranging from 1.67 to 1.73 (not including segment 8). These results suggest that the layers are stable, and no buoyant instability based on density inversion exist in this tank.

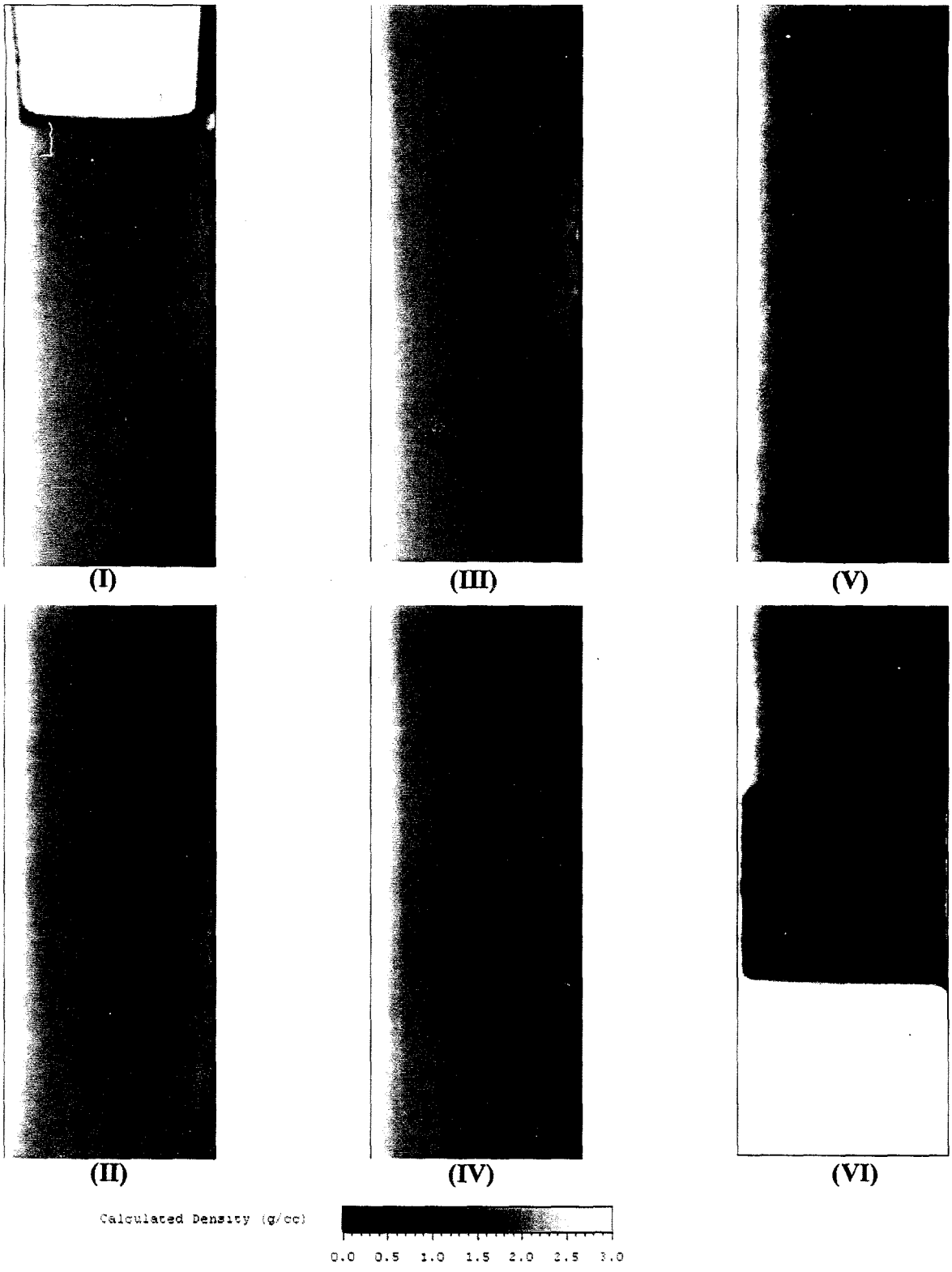

Figure 4.13a. Density Image Calculated from X-Ray Images of Segment 16, Riser 24, Tank A-101

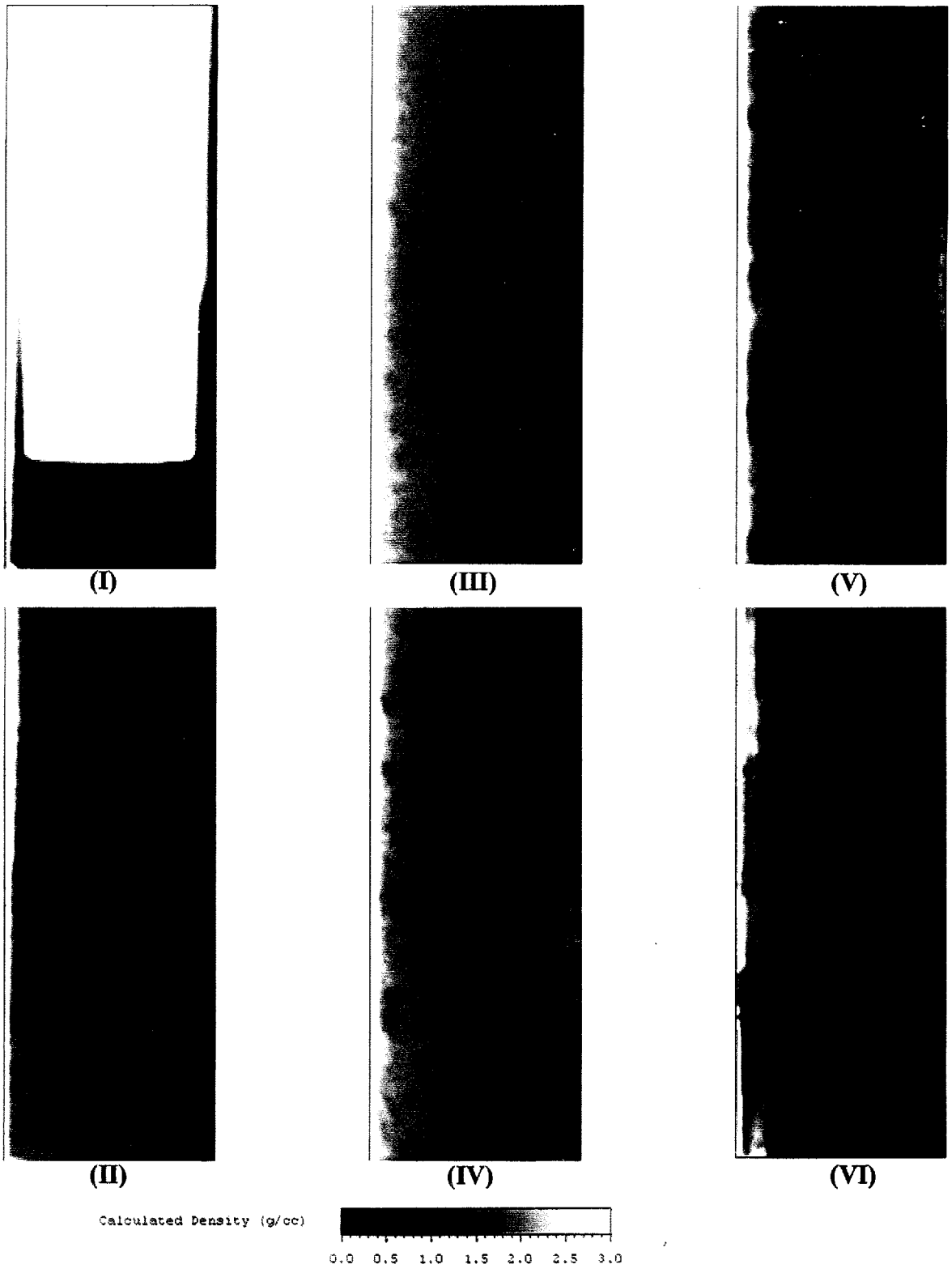

Figure 4.13b. Density Image Calculated from X-Ray Image of Segment 9, Riser 24, Tank A-101

Table 4.18. Summary of X-Ray Densitometry Results for Tank A-101

Segment	Mean Density (g/cc)	Density STD (%)	Mean Slurry Density (g/cc)	Slurry Density STD (%)
15-2	N/A	N/A	N/A	N/A
24-5	1.44	7.08	1.67	7.08
15-8	1.23	10.1	1.46	10.1
24-9	1.42	9.15	1.73	9.15
24-12	1.73	6.13	1.73	6.13
24-16	1.67	6.11	1.68	6.11
15-19	N/A	N/A	N/A	N/A

4.2.9 Other Discussions of RGS Results for Tank 241-A-101

4.2.9.1 Entrainment/Contamination

Table 4.11 shows that, as in Tank AW-101, oxygen and argon were present in the A-101 samples. In most cases (with the egregious exception of segment 2) the A-101 samples show less oxygen and more argon than the AW-101 samples did; one possibility is that the argon purge gas displaced some of the entrained air. Argon is especially noticeable in riser 24 samples. The N_2/Ar and N_2/O_2 ratios for the seven A-101 samples are given in Table 4.19. Most of the samples show evidence of considerable "native" nitrogen content, beyond what could have been obtained from air contamination.

Table 4.19. Ratios of N_2/Ar and N_2/O_2 in Tank A-101

Segment	N_2/O_2	N_2/Ar
15-5	31	74
15-8	36	151
15-12	7.5	2.1
24-2	4.4	83
24-9	194	7.1
24-16	12	1.0
24-19	8.4	2.3

Segment 2 of A-101 stands out from the other samples because both ratios are nearly equal to those for atmospheric air ($N_2/Ar = 83.5$ and $N_2/O_2 = 3.7$). A large part of this sample is probably atmospheric air hypothetically leaked into the RGS extractor rather than entrained during tank sampling. This hypothesis is based on three facts: 1) oxygen has apparently not been depleted by reaction with waste despite the 21-day lag time; 2) the oxygen content of the sample increases during the extraction process (compare O_2 mol% values in canisters J1, J2, and J3 in Table C.2.7); 3) the collection-canister pressure (proportional to the amount of gas extracted) increases during the extraction process as though gas were being added to the sample (Tables C.2.3, C.2.4, and C.2.5). Since the leak check (performed between 8:57 and 10:35 am on August 12, 1996) was acceptable, the leakage (assuming this hypothesis is correct) must have occurred during sample handling (10:45 am to 2:24 pm the same day). The leak rate must have been

$$= [(2074\ \mu mol\ O_2/L\ waste)(0.313\ L\ waste) / (0.21\ O_2\ in\ air)] / 3.7\ hr$$

$$= 0.23\ \mu mol\ air/s.$$

This is about 80 times the acceptance limit for the system. Although the inleakage hypothesis matches the chemical data, it is only a hypothesis because it is not clear what might have caused the leak rate to increase so overwhelmingly after the acceptance limit had been met. (The leak rate is tested and confirmed below the limit before each segment is processed.) Another possible explanation is related to the porous structure of the salt material in the sampler. The pores may trap headspace gas, which is mostly air, and then become sealed by further salt formation. As the sample was heated the pores reopened, releasing the trapped air. This hypothesis implies a porosity of greater than 0.3 for the waste (Table 4.16).

4.2.9.2 Ratio Between Hydrogen and Nitrous Oxide

Table 4.20 lists the ratios between hydrogen and nitrous oxide in Tank A-101. The ratios occupy the same general range as for Tank AW-101,(a) though A-101 exhibits both higher and lower values than AW-101. There is considerable consistency among the values within a layer; that is, the ratio of hydrogen to nitrous oxide concentration for the upper layer range between 8.4 and 14 while in the lower layer this ratio is 1.1 and smaller.

4.2.9.3 Concentration Variation in Lower Layer

Table 4.11 shows that the concentration differences within the lower layer of A-101 waste (segments 15-12, 24-16 and 24-19) exceeded the instrumental error band. This is true even for segments from the same riser (24-14 and 24-19). Such concentration variation may provide a clue as to the extent or the type of convection in the lower layer. However, we do not have multiple RGS samples from liquid layers in other tanks to provide a comparison with typical supernatant behavior. The lower layer in A-101 does behave like supernatant layers in other tanks in that it retains very little gas.

4.3 Tank 241-AN-105

4.3.1 Sampling Locations

Push mode sampling of Tank AN-105, the third tank sampled, was carried out in risers 12A and 7B. The approximate locations of these risers are depicted in Figure 4.14. Four segments

(a) This ratio ranges between 3.7 to 9.0 in riser 24A and 0.9 to 2.3 in riser 24B within Tank AW-101.

Table 4.20. Ratios of H_2/N_2O in Tank A-101

Segment	H_2/N_2O
15-5	13
15-8	14
15-12	0.5
24-2	8.4
24-9	14
24-16	0.7
24-19	1.1

of the first core (riser 12A) and four segments of the second core (7B) in Tank AN-105 were sampled and analyzed in late FY 1996. Riser 12A was sampled first because of its proximity to the MIT in riser 15A. Riser 12A is also close to riser 1B, where the VFI/ball rheometer measurements are made.

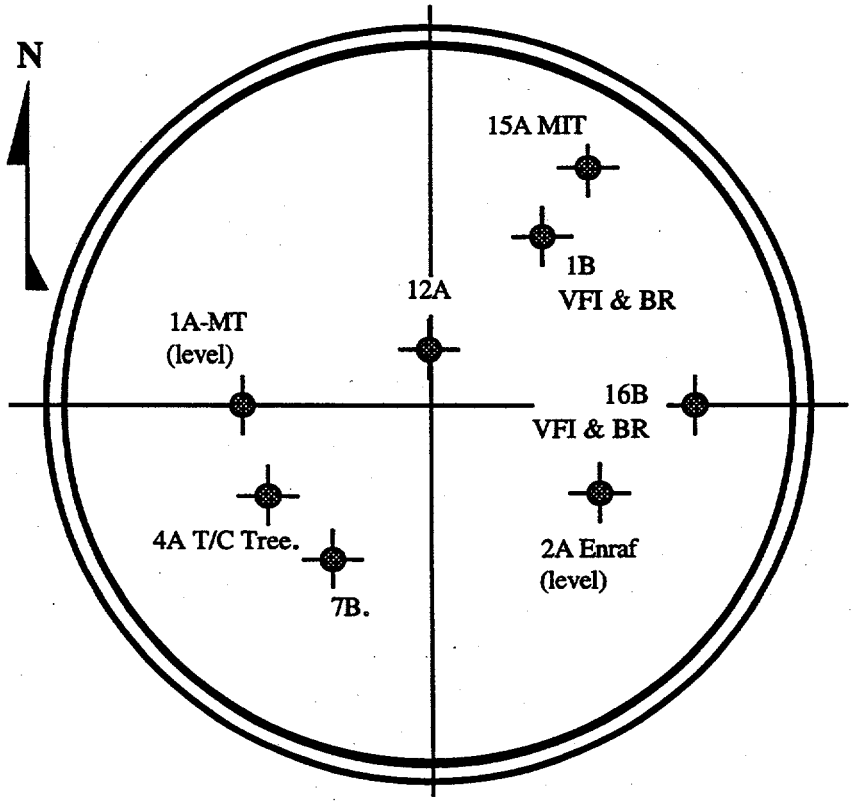

Figure 4.14. Schematic Diagram of Riser Locations for Tank AN-105

The total depth of waste in Tank AN-105 is approximately 1040 cm (410 in.). Figure 4.15 shows the available information on tank content layering as derived from the riser 4A thermocouple tree and riser 15A MIT measured temperature profiles, in concurrence with the VFI/ball rheometer data for this tank. The nonconvective layer is believed to be about 430 cm (170 in.) in depth, with the convective, supernatant liquid layer and a 50–100 cm (20–40 in.) thick crust forming the balance of the contents. Twenty-one full and one half-length sampler cores were required. The sampling levels for RGS in each of the two selected risers are graphically depicted in Figure 4.15.(a)

4.3.2 Pertinent Tank Characterization Information

Figure 4.16 is a temperature profile in this tank taken with the thermocouple tree located in riser 4A. The data points show the distribution of temperature, as measured over several months in 1995 and 1996. The thickness of the three zones, namely crust, supernatant liquid layer, and the nonconvective layer, can be approximated from these temperature profiles. Variation in the depth of the nonconvective layer may be indicated by the change in temperature profile over time.

The average density in the convective layer is 1.43 ± 0.03 g/cc as determined with the ball rheometer (Stewart et al. 1996a). The same reference specified a density of 1.59 ± 0.04 g/cc for the nonconvective layer. These densities, rather than the values obtained by x-ray image processing, were used in RGS data analysis for AN-105; this choice was made because ball rheometer and core sample densities are obtained by recognized methods and so are preferred (when available).

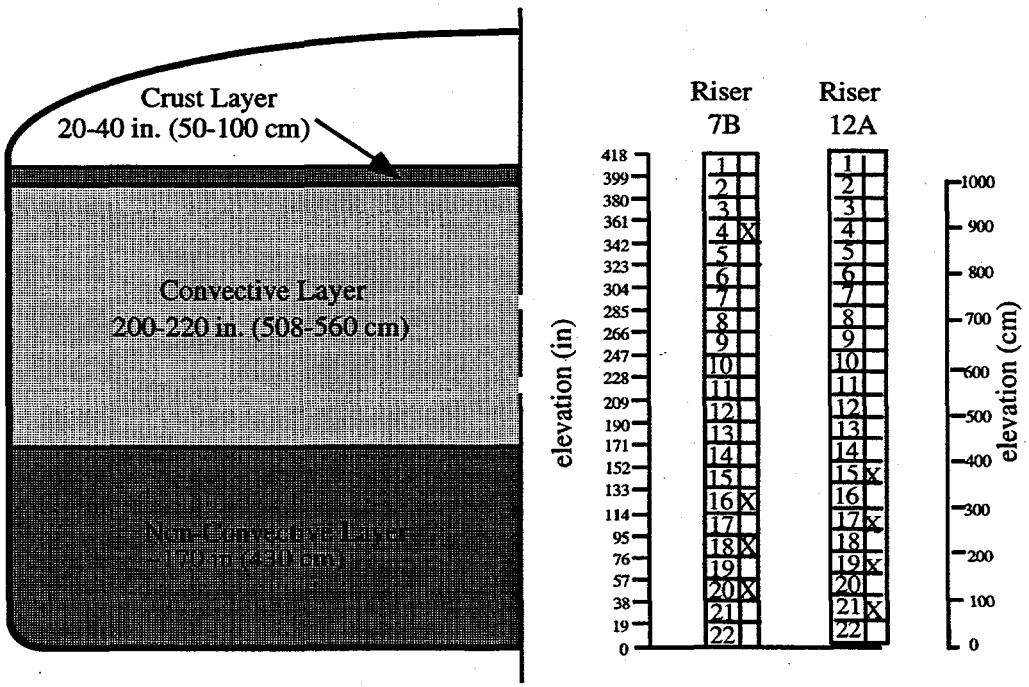

Figure 4.15. Diagram of the As-Sampled RGS Sample Elevations for Tank AN-105

(a) Phillips JR, R Shekarriz, and JM Bates. 1996. *Sampling Plan for Tank 241-AN-105 Retained Gas Sampler Deployment.* PNNL-MIT-030796, Pacific Northwest National Laboratory, Richland, Washington.

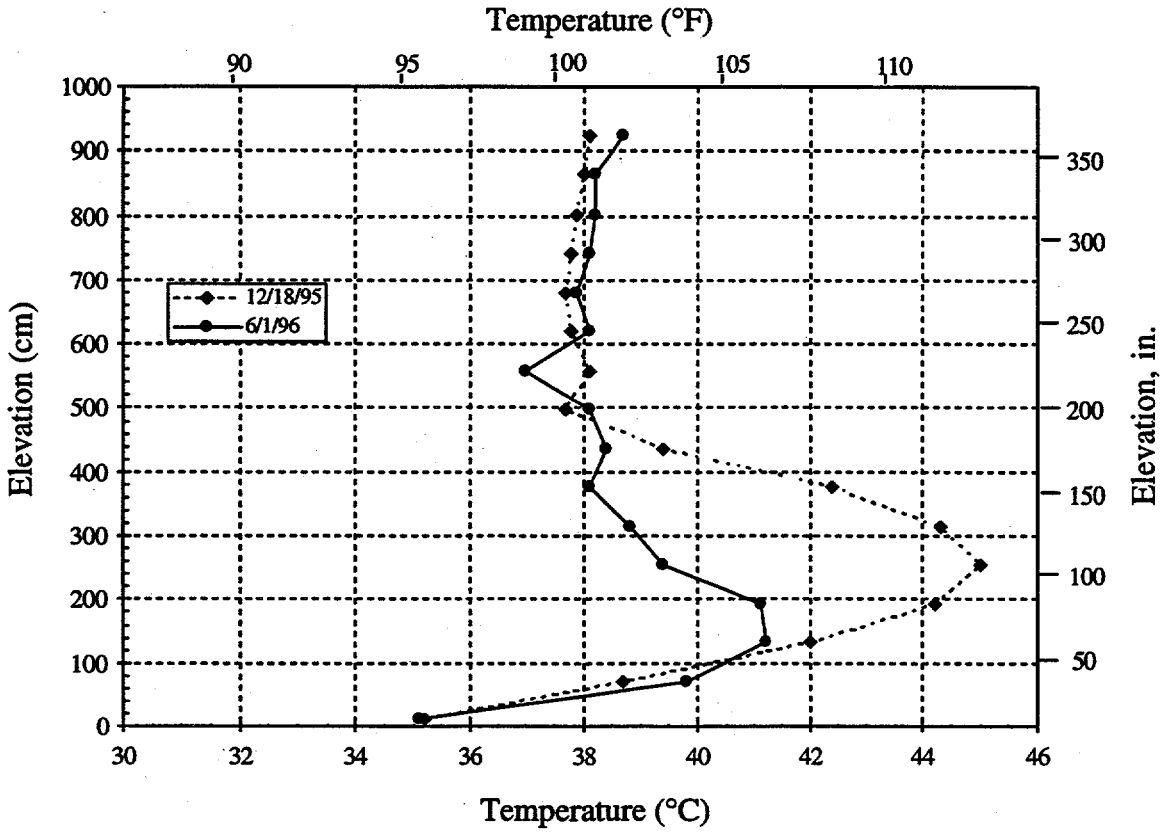

Figure 4.16. Profile of Temperature in Tank AN-105 Taken with Thermocouple Tree

4.3.3 RGS Sampling Process Information

Of the samples shown in Figure 4.15, that from segment 20, was lost because of sampler valve problems. The lag times (delay between sample acquisition and processing) for the remaining samples are shown in Table 4.21. The maximum hold time allowed by the sampling plan is 24 days, based on measured sampler leakage rates during acceptance testing. The hold time for samples 12A-21 and 7B-4 exceeded this limit, but the sample was accepted based on calculations which indicated that the estimated leakage was still negligible.

4.3.4 RGS Results Summary

The retained gas measurement data (Table 4.22), after averaging (by integration over the nonconvective layer) and correction for entrained air (Table 4.25), show three major constituents in the in-situ gas/vapor phase: 24.5 ± 2.0 mol% nitrogen, 62.4 ± 3.6 mol% hydrogen, and 11.8 ± 0.8 mol% nitrous oxide. For the retained gas/vapor in the convective layer (Table 4.26), the major constituents have a composition of 67 ± 32 mol% nitrogen, 24.3 ± 8.3 mol% hydrogen, and 3.7 ± 1.3 mol% nitrous oxide. The remainder of the gas is composed of ammonia, methane, and other hydrocarbons.

The lower-bound ammonia concentrations in AN-105 were found to range from 890 ± 230 to 2100 ± 400 μmol/L of waste (Table 4.23); more than 99.9% of this ammonia is dissolved in the waste. These concentrations integrate to a lower-bound nonconvective layer ammonia inventory that, if it were present as vapor, would occupy 54 ± 47 m^3 (1900 ± 1600 ft^3) at STP (Table 4.25);

Table 4.21. Lag Times for Processing of RGS Samples from AN-105

Sample	Acquisition Date	Processing Date	Lag (days)
12A-15	June 13, 1996	June 18, 1996	5
12A-17	June 14, 1996	June 18, 1996	14
12A-19	June 14, 1996	July 2, 1996	18
12A-21	June 17, 1996	July 12, 1996	25
7B-4	June 26, 1996	July 25, 1996	29
7B-16	June 28, 1996	July 10, 1996	12
7B-18	June 28, 1996	July 16, 1996	18

the corresponding lower-bound convective layer ammonia inventory (Table 4.26) would have a volume of 45 ± 14 m^3 (1600 ± 490 ft^3) at STP. The limitations in the measurement accuracy are similar to those discussed in the previous sections (4.1.4 and 4.2.4).

RGS data (Table 4.27, Figure 4.17) give a corrected in-situ void fraction of 0.003 ± 0.001 for the convective layer and void fractions from 0.004 ± 0.001 to 0.111 ± 0.009 (with a volume-averaged void fraction of 0.045 ± 0.005) for the nonconvective layer. The volume-averaged void fraction for the nonconvective layer (an average obtained by integrating over the depth of the layer) is 0.045 ± 0.005. The VFI data for the tank show in-situ void fractions of 0.001 to 0.004 in the convective layer and 0.001 to 0.068 in the nonconvective layer (Stewart et al. 1996a).

The STP hydrogen inventory retained in the nonconvective layer of AN-105 is 93 ± 16 m^3 (3300 ± 570 ft^3), based on a hydrogen mole fraction that is an arithmetic average of the RGS data for both risers, and on a total gas volume of 148 ± 24 m^3 that was calculated from VFI data by Stewart et al. (1996a). The nonconvective gas volume estimate from RGS data alone is 156 ± 37 m^3 at STP; the STP hydrogen inventory, calculated by integrating RGS hydrogen concentrations over depth and using data from both risers, is ~97 ± 23 m^3 (Table 4.25).

The STP hydrogen inventory retained in the convective layer of AN-105 is 1.7 ± 6.3 m^3 (60 ± 220 ft^3), based on a hydrogen mole fraction from the single sample taken from the layer and on a total gas volume of 7 ± 26 m^3 that was calculated from VFI data by Stewart et al. (1996a). The convective gas volume estimate from RGS data alone is 10 ± 3.5 m^3 at STP; the STP hydrogen inventory, calculated from the single datum, is 2.3 ± 0.6 m^3 (Table 4.26).

Note that the hydrogen concentration differences between the two risers (Table 4.22) are such as to strongly indicate lateral variability in hydrogen concentrations. Accordingly, the hydrogen inventory must be considered to contain substantially more uncertainty than the stated ± values (which only account for instrument precision and layer interface uncertainty). The same is true for void fraction and total void volume, as the VFI data further indicate.

4.3.5 Retained Gas Concentrations

Table 4.22 presents the estimated concentrations of the insoluble and low-solubility gases in AN-105. No corrections for air entrainment have been made in Table 4.22. Such a correction would consist of removing all the O_2 and Ar and subtracting (3.71 x O_2) from the N_2, consistent with the molar N_2/O_2 ratio in atmospheric air.

Table 4.22. Concentrations of Insoluble Constituents (μmoles/liter of waste) in Tank 241-AN-105, Without Entrainment Correction

Segment	N_2	H_2	N_2O	O_2	CH_4	Ar	Other Nit. Ox	C_2H_x	C_3H_x	Other Hyd.
12A-15	790±100	66±8	100±10	160±20	4.7±1.3	9.3±1.2	2.8±1.9	1.7±0.7	1.4±0.4	3.1±0.8
12A-17	1340±60	3100±100	550±30	74±6	29±4	7.5±0.7	6.5±1.0	7.9±2.2	2.2±0.9	11.3±1.9
12A-19	2370±80	6300±200	1230±40	80±3	60±6	8.4±0.5	13.1±6.0	7.0±1.1	5.1±0.80	14.1±1.4
12A-21	1400±60	3460±120	1220±60	15±1	48±2	380±20	13.0±1.2	3.7±1.0	2.8±0.8	5.8±1.3
7B-4	440±60	72±10	68±11	74±11	3.6±1.0	110±20	2.5±1.0	1.6±0.5	1.1±0.4	2.2±0.6
7B-16	550±60	84±10	68±10	64±7	3.2±1.0	89±10	2.6±1.2	0.9±0.4	1.0±0.5	2.5±0.8
7B-18	780±50	1040±70	260±20	54±4	13.6±1.3	46±4	4.6±0.5	7.8±1.2	1.2±0.2	11.9±1.9

Table 4.23 presents the total ammonia concentration per liter of waste under in-tank conditions. The average and standard deviation over the nonconvective layer (all segments except segment 4) are 1500 ± 490 μmol/L of waste. If, based on their very low gas content (Figure 4.17), segments 15 and 16 are considered to be part of the convective layer, then the average and standard deviations over the nonconvective layer are 1700 ± 400 μmol/L of waste. This standard deviation is less than or equal to the uncertainty in individual samples, so the concentration of ammonia can be considered constant throughout the nonconvective layer. The ammonia concentration in the convective layer (segment 4) appears to be significantly lower, as it does in segments 15 and 16. (The average and standard deviation for segments 4, 15 and 16 are 970 ± 120 μmol/L of waste.) These concentrations must be regarded as lower bounds, as mentioned in the previous sections, because they do not account for ammonia lost to condensation in the RGS system.

Table 4.23. Total Ammonia Concentrations in Tank AN-105

Segment	NH_3* (μmole/liter)
12A-15	1100±200
12A-17	2000±4600
12A-19	2100±400
12A-21	1300±1300
7B-4	920±230
7B-16	890±230
7B-18	1500±1200

* These lower-bound values do not account for ammonia in the condensate in the collector side of the RGS system; they are expected to be 1/2 to 1/3 of the actual in-tank values.

4.3.6 Gas Inventory

Table 4.24 compares the layer gas inventories that are calculated entirely from RGS data, with and without correction for entrained air, to the gas inventories calculated from VFI data by Stewart et al. (1996a). The RGS data uncertainty in the convective layer contain only the known instrument precision and layer thickness uncertainties for a single point, while the VFI data uncertainty additionally contain the standard deviation for a large number of measurements. The air correction can be seen to make a greater change in the convective layer inventory than the nonconvective.

Table 4.25 shows estimates of STP volumes of gas constituents in the nonconvective layer of AN-105. The RGS/VFI inventories were calculated from concentration data in Tables 4.22 and 4.23 by taking an arithmetic average of the mole-fractions of constituents in the gas and multiplying that average by the volume of gas measured by VFI (Stewart et al. 1996a). The RGS inventories were calculated by integrating RGS data over depth, as discussed in Section 3.4.1. Although a significant difference in the hydrogen concentrations was measured by the two risers, data from both risers have been used to generate Table 4.25 without any attempt to account for possible concentration variations in the horizontal plane. Table 4.26 is the same sort of table, but for the convective upper layer; the concentrations are based on the single sample taken in the layer.

The error bands in Tables 4.25 and 4.26 represent only the uncertainty that carries through from instrument error and uncertainty in layer interface location. Temporal and lateral variability are not included, and the resulting inventories may not be conservative. The values in Tables 4.25 and 4.26 include the effect of corrections to remove the (assumed) entrained air. The tables give the volume (at standard conditions) and the volume percent of each gas. It is interesting to note that, although ammonia is still the dominant soluble gas, nitrous oxide constitutes approximately 12% of the dissolved gases in the nonconvective and 6% of the dissolved gases in the convective waste.

4.3.7 Retained Void Fraction

The method by which the in-situ void fractions were calculated is given in Section 3.3. The results are presented in Table 4.27, showing the difference between entrainment-corrected and uncorrected in-situ void fractions.

Table 4.24. STP Gas Inventories in Tank AN-105, According to Different Methods

Layer	STP Gas Volume (m^3)		
	Uncorrected RGS	Corrected RGS	VFI (Stewart et al. 1996a)
Crust	---	---	30 ± 14
Upper (convective)	33 ± 8	10 ± 4	7 ± 26
Lower (nonconvective)	175 ± 42	156 ± 37	148 ± 24
Total	208 ± 43 (no crust)	166 ± 37 (no crust)	155 ± 35 (no crust) 184 ± 44 (crust)

Table 4.25. Nonconvective Layer Gas Inventory in Tank AN-105 at STP

Gas	RGS (corrected)		RGS (corrected)/VFI
	m^3 (mole %) in gas/vapor phase	m^3 (mole %) dissolved in liquid phase	m^3 (mole %) in gas/vapor phase
Ammonia	0.029 ±0.026 (0.02%)	54 ± 47 (83.0%)	0.031 (0.02%)
Nitrogen	38 ± 9.3 (24.5%)	1.0 ± 0.3 (1.5%)	37 (24.9%)
Hydrogen	97 ± 23 (62.4%)	2.5 ± 0.6 (3.8%)	93 (62.9%)
Nitrous Oxide	18 ± 4.4 (11.8%)	7.6 ± 1.8 (11.6%)	16 (10.9%)
Methane	1.1 ± 0.3 (0.7%)	0.038 ± 0.01 (0.06%)	1.0 (0.7%)
C_2H_x*	0.18 ± 0.06 (0.1%)	0	0.20 (0.1%)
C_3H_x*	0.10 ± 0.03 (0.1%)	0	0.09 (0.1%)
Other*	0.62 ± 0.20 (0.4%)	0	0.62 (0.4%)
Total	156 ± 37 m^3	65 ± 50 m^3	148 m^3

* These gases were assumed to be entirely insoluble.

Figure 4.17 presents the corrected void fractions found from RGS, plotted against the results found using VFI (Stewart et al. 1996a). This figure shows that the data from the retained gas sampler agree reasonably well with the VFI results. Given that both measurement techniques have finite uncertainty, and that the measurements were made at different points in the tank with possible lateral variations, the agreement between the two sets of data is acceptable.

Table 4.26. Convective Layer Gas Inventory in Tank AN-105 at STP

Gas	RGS (corrected)		RGS (corrected)/VFI
	m^3 (mole %) in gas/vapor phase	m^3 (mole %) dissolved in liquid phase	m^3 (mole %) in gas/vapor phase
Ammonia	0.001±0.0003 (0.01%)	45 ± 14 (88.6%)	0.001 (0.01%)
Nitrogen	6.4 ± 2.7 (67%)	1.5 ± 0.6 (3.0%)	4.7 (67%)
Hydrogen	2.3 ± 0.6 (24.3%)	1.2 ± 0.3 (2.3%)	1.7 (24.3%)
Nitrous Oxide	0.35 ± 0.09 (3.7%)	3.0 ± 0.7 (5.9%)	0.26 (3.7%)
Methane	0.12 ± 0.04 (1.3%)	0.054 ± 0.018 (0.1%)	0.09 (1.3%)
C_2H_x*	0.078 ± 0.03 (0.8%)	0	0.057 (0.8%)
C_3H_x*	0.053 ± 0.02 (0.6%)	0	0.038 (0.6%)
Other*	0.23 ± 0.09 (2.4%)	0	0.16 (2.4%)
Total	10 ± 3.5 m^3	51 ± 16 m^3	7 m^3

* These gases were assumed to be entirely insoluble.

Table 4.27. In-Situ Void Fractions in Tank AN-105

Segment	Sample Central Height (cm)	Hydrostatic Pressure (atm)	Temperature (°C)	Corrected Void Fraction (In-Tank Conditions)	Uncorrected Void Fraction (In-Tank Conditions)
12A-15	362	1.95	43.0	0.003 ± 0.001	0.014
12A-17	265	2.10	46.0	0.057 ± 0.006	0.062
12A-19	169	2.25	46.0	0.111 ± 0.009	0.116
12A-21	72	2.40	39.0	0.061 ± 0.006	0.066
7B-4	893	1.21	39.0	0.004 ± 0.001	0.015
7B-16	314	2.02	44.0	0.005 ± 0.001	0.010
7B-18	217	2.17	46.0	0.021 ± 0.003	0.024

Most of the data for segments 4 through 18, independent of the riser sampled, overlap the widely ranging data from VFI measurements for this tank. The exception is the void fraction measured in segment 19, with a value of 0.11. This is approximately 60% higher than the maximum void fraction measured with VFI at comparable depth, which was 0.068. The RGS measurement and x-ray (Figure 4.18b) indicated that this may represent a local gas pocket.

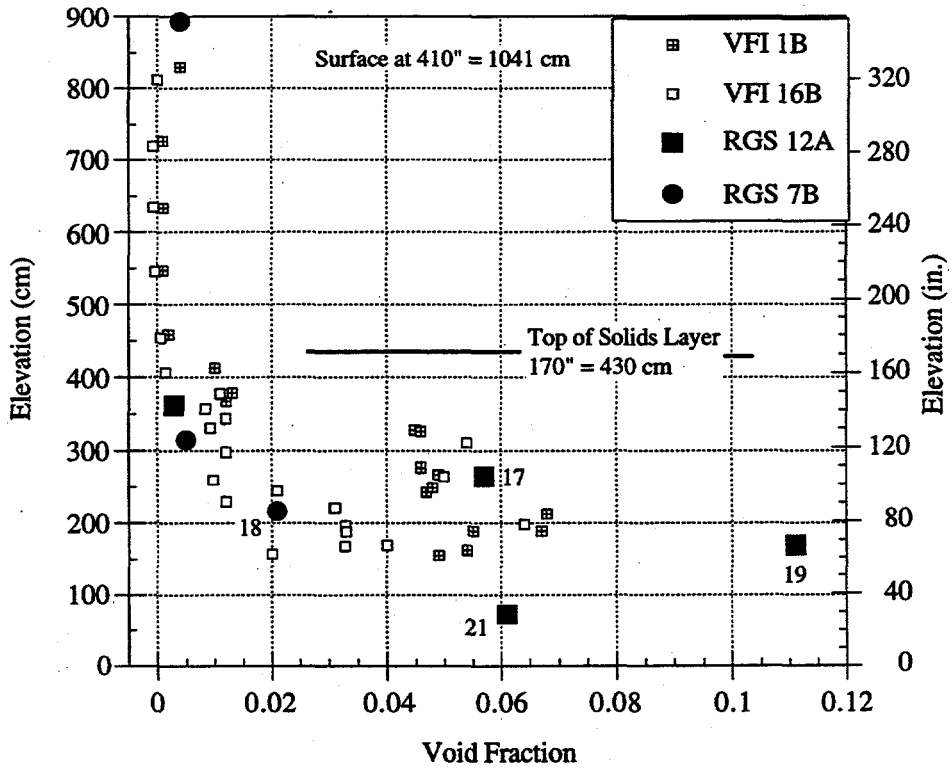

Figure 4.17. Void Fractions in Tank AN-105 (RGS data were taken for riser 12A in June-July and for riser 7B in July 1996; VFI data in December 1995)

4.3.8 X-Ray Results

Eight RGS segments from Tank AN-105 were radiographed with x-rays. A summary of the observations of these images is provided in Table 4.28. A discussion of the observations is provided in the next section. Unfortunately, several segments radiographed for this tank did not have calibration images, and the remainder were difficult to quantify. As a result, the quantitative data for this tank may be more questionable than those presented for Tanks AW-101 and A-101. However, the qualitative observations made for various segments obtained from this tank are considered important and are not affected by a lack of reliable calibration data.

4.3.8.1 Phase Distribution

Table 4.28 is a summary of the observations made from the x-ray images of the RGS segments in AN-105. The features observed in these images are very similar to those observed in the AW-101 waste. The bubbles were mostly round and smaller than approximately 5 mm in diameter. A large void below the piston was observed for several of the segments. It was previously established that entrained air would account for only a small void of less than 1.8% of the total sampler volume (see Section 4.1.8). The void present in segment 19, for example, exceeds 10% of the sampler volume (see Figure 4.18). These large voids are speculated to be caused by migration of the trapped gases to the top of the sampler, primarily during sampling. This speculation is based on the assumption that the vertical position of the large gas pockets in this tank are random and may not coincide with the position of the RGS piston for all the segments.

Table 4.28. Summary of Observations from X-Ray Images for Tank AN-105

Segment	Comments / Observations
7B-4	Homogeneous sample, no noticeable void under piston. Calibration questionable.
12A-15	No calibration data available for this segment. Few small bubbles, no noticeable void below piston.
7B-16	Few medium size bubbles. No noticeable void under piston.
12A-17	No calibration data available for this segment. Very many medium bubbles and voids, large void below piston.
7B-18	No calibration data available for this segment. Many small to large bubbles, no noticeable void below piston.
12A-19	Many small to medium voids, large void under piston (~2 in. height).
7B-20	Homogeneous sample. Large void under piston
12A-21	Many small to medium bubbles and medium-sized odd-shaped voids. Medium void below piston.

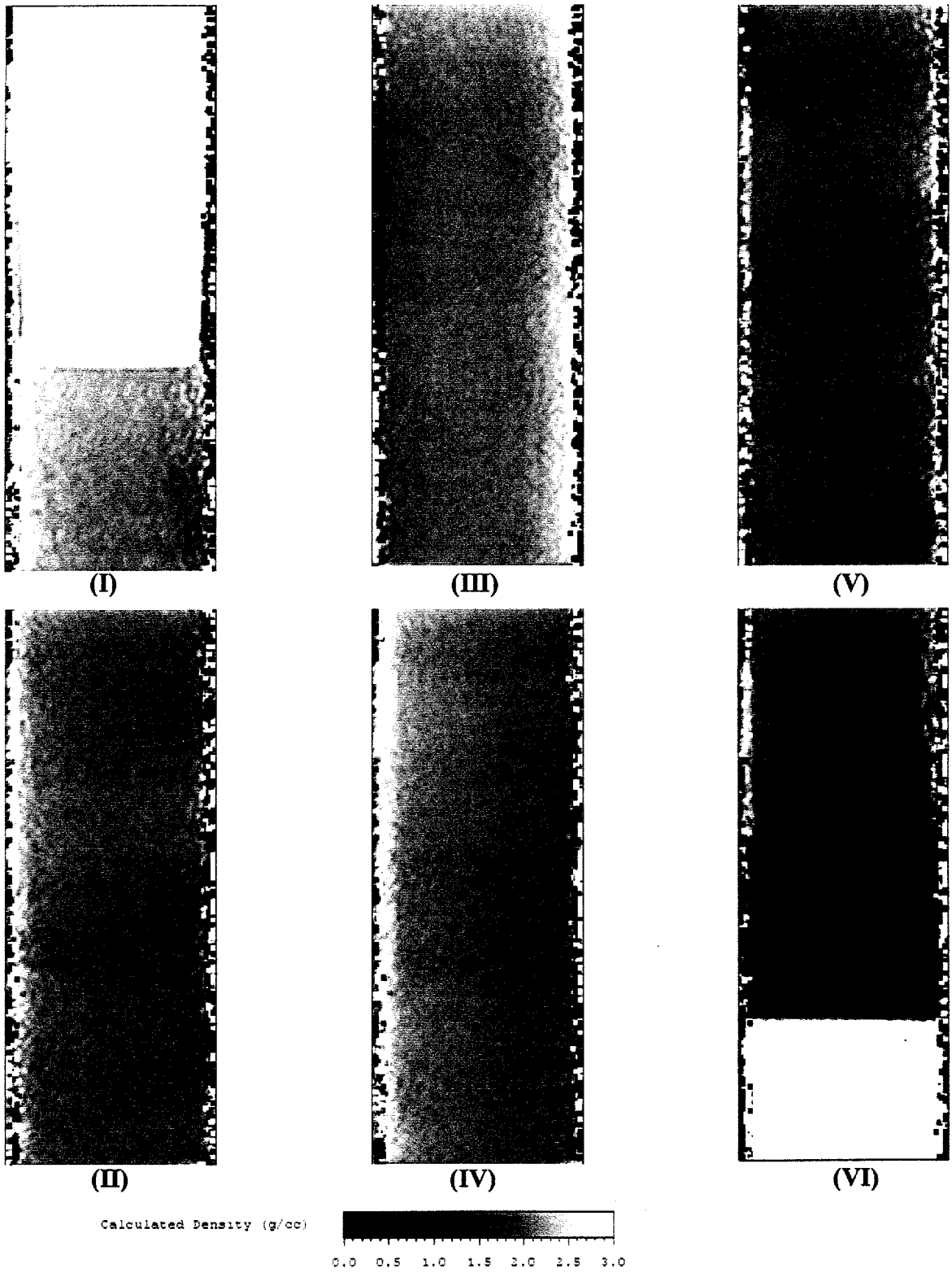

Figure 4.18a. Density Image Calculated from X-Ray Images of Segment 14, Riser 7B, Tank AN-105

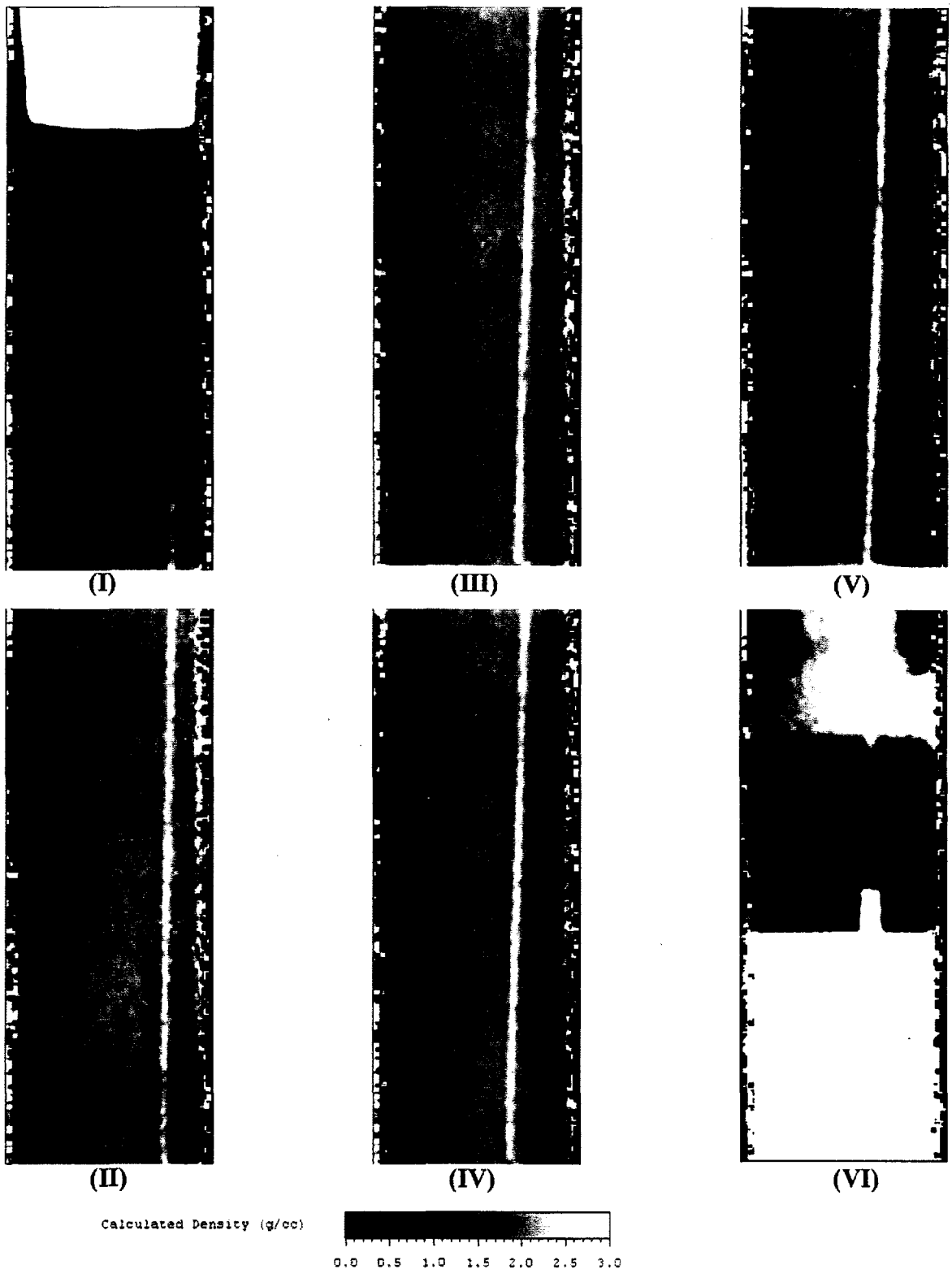

Figure 4.18b. Density Image Calculated from X-Ray Images of Segment 19, Riser 12A, Tank AN-105

The current results are significantly different from those of the previous two tanks in several ways:

1) Large gas pockets are observed in Tank AN-105, which account for a large portion of the measured void fraction. This is in contrast with the observations made for AW-101 waste that the major portion of the gas was observed to be smaller than the detection threshold of the x-ray imaging system (<0.5 mm).

2) No fractures or irregularly shaped bubbles were observed in this tank, unlike what was observed in Tank A-101 waste.

Clearly, the retention mechanisms of the gas phase within the waste in this tank are different from those in Tank A-101 waste. The distinction is not as clear between this tank and AW-101. However, assuming the accuracy of our hypothesis about migration of gases to the top of the sampler, then the strength of the disturbed waste would fall below what is required to support a gas bubble smaller than the characteristic scale of the sampler (~3 cm bubbles). This value would be on the order of 100 Pa, which is consistent with the ball rheometer results for this tank, reporting yield strength greater than 150 Pa in the nonconvective layer (Stewart et al. 1996a). This is a crude observation but worthy of attention.

4.3.8.2 Waste Density

Similar to the previous two tanks, the density was found for several RGS segments (except segment 20 which is a regular core sample). Table 4.29 is a summary of the findings for those segments for which calibration data were available. The density of the four segments shown in this table range between 1.65 to 1.83 g/cc with a mean of 1.7 ± 0.19 g/cc. Although the standard deviation within each image is high due to the presence of gas bubbles, the segment-to-segment standard deviation was calculated to be 0.07 g/cc.

4.3.9 Other Discussion of RGS Results for Tank 241-AN-105

4.3.9.1 High Void Fraction

Of the RGS void fraction data shown in Figure 4.17, only segment 19 (at 11.1% void) seems to be significantly different from the results given by VFI (Stewart et al. 1996a). There are several possible causes for such a discrepancy. Of these, massive air contamination does not match the composition data. In addition, the major constituent ratios for segment 19 are not very different from those of its nearest neighbors, as shown in Table 4.30; this argues against some other kind of gross contamination or other non-representativeness.

Table 4.29. Summary of X-Ray Densitometry Results for Tank AN-105

Segment	Mean Density (g/cc)	Density STD (%)
7B-16	1.68	7.08
12A-19	1.83	13.3
7B-20	1.67	8.8
1 2A-21	1.65	12.8

Table 4.30. Constituent Ratios for Tank AN-105

Segment	N_2/H_2	H_2/N_2O
12A-15	12	0.65
12A-17	0.43	5.6
12A-19	0.37	5.1
12A-21	0.41	2.8
7B-4	6.1	1.05
7B-16	6.5	1.25
7B-18	0.75	4.0

X-rays of segment 19 (see Subsection 4.3.8.1) show a large void at the top of the segment underneath the piston. It therefore seems plausible that the excess gas in the segment was in fact present in the tank near riser 12A, but not near enough to riser 1B to be captured by the VFI.

4.4 Tank 241-AN-104

4.4.1 Sampling Locations

Push-mode sampling of Tank AN-104, the fourth tank sampled, was carried out in risers 10A and 12A. The approximate locations of these risers are depicted in Figure 4.19. Six segments of the first core (riser 10A) and one segment of the second core (12A) in Tank AN-104 were sampled and analyzed in FY 1996. Laboratory and sampling schedules did not permit more segments to be sampled from riser 12A.

The total depth of waste in Tank AN-104 is approximately 978 cm (385 in.). Figure 4.20 shows the available information on tank content layering as derived from the riser 4A thermocouple tree and riser 15A MIT measured temperature profiles, in conjunction with the VFI/BR data for this tank. The nonconvective layer is believed to be about 445 cm (175 in.) in depth, with the convective, supernatant liquid layer forming the balance of the contents (the crust layer is of essentially zero thickness). Twenty full sampler cores and one partial sampler core were required. The sampling levels for RGS in each of the two selected risers are depicted in Figure 4.20.(a)

4.4.2 Pertinent Tank Characterization Information

Figure 4.21 is a temperature profile in the tank taken with the MIT located in riser 15A. The data points show the distribution of temperature, as measured over several months in 1995 and 1996. The thickness of the supernatant liquid layer and the nonconvective layer can be approximated from temperature profiles, which appear to show some temporal variation in the depth of the nonconvective layer.

(a) Shekarriz R and JM Bates. 1996. *Sampling Plan for Tank 241-AN-104 Retained Gas Sampler Deployment.* TWS-MIT-041796, Pacific Northwest National Laboratory, Richland, Washington.

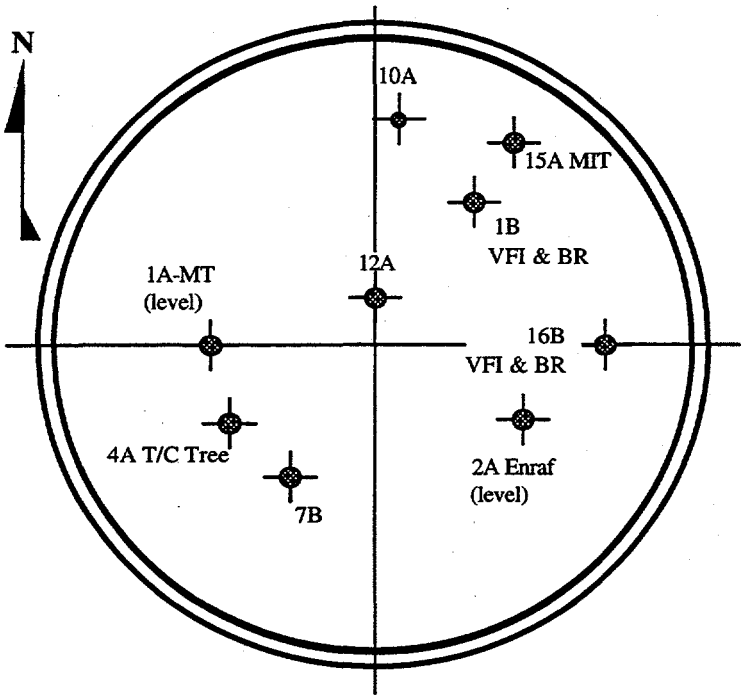

Figure 4.19. Schematic Diagram of Riser Locations for Tank AN-104

The average density in the convective layer is 1.44 ± 0.03 g/cc as determined with the ball rheometer (Stewart et al. 1996a). The same reference specified a density of 1.59 ± 0.04 g/cc for the nonconvective layer. These densities, rather than the values obtained by x-ray image processing, were used in RGS data analysis for AN-104 because ball rheometer and core samples densities are obtained by recognized methods and so are preferred (when available).

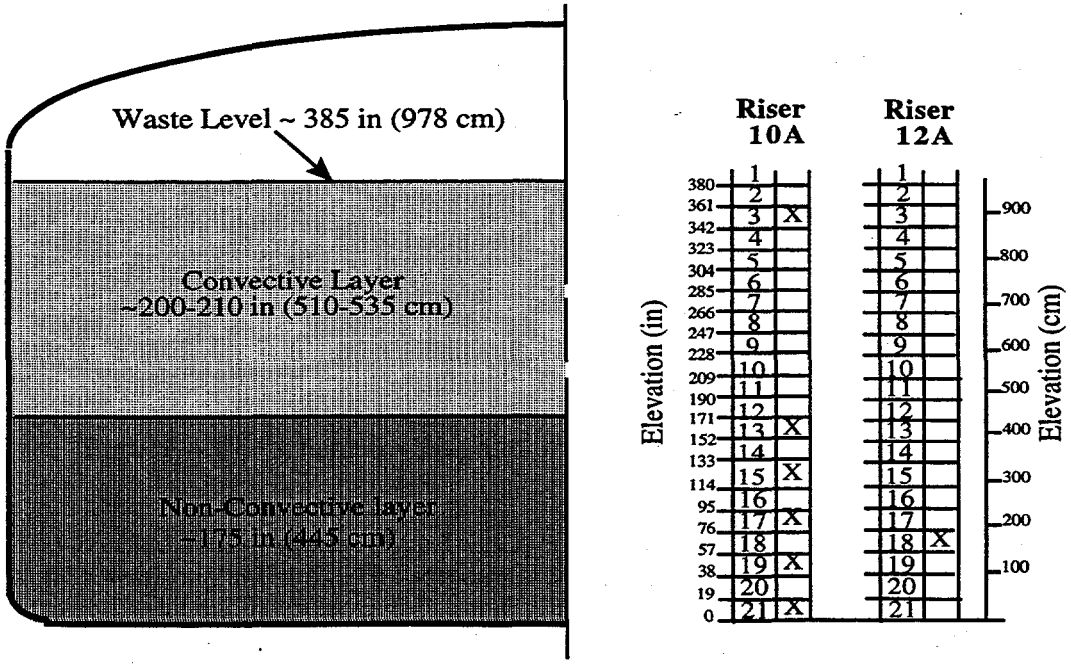

Figure 4.20. Diagram of the As-Sampled RGS Sample Elevations for Tank AN-104

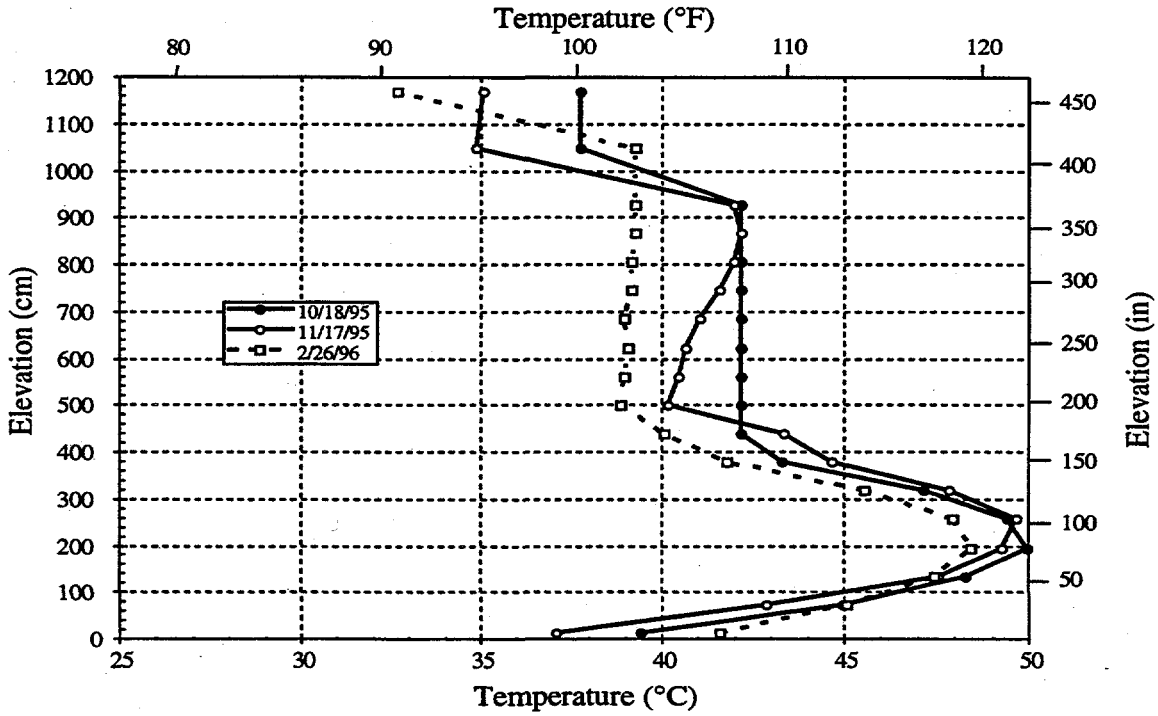

Figure 4.21. Profile of Temperature in Tank AN-104 Taken with MIT

4.4.3 RGS Sampling Process Information

The lag times (delay between sample acquisition and processing) for the AN-104 samples are shown in Table 4.31. The maximum hold time allowed by the sampling plan is 24 days, based on measured sampler leakage rates during acceptance testing. The hold time for sample 10A-21 exceeded this limit, but the sample was accepted based on calculations that indicated the estimated leakage was still negligible.

Table 4.31. Lag Times for Processing of RGS Samples from AN-104

Sample	Acquisition Date	Processing Date	Lag (days)
10A-3	Sept. 9, 1996	Sept. 18, 1996	9
10A-13	Sept. 11, 1996	Sept. 19, 1996	8
10A-15	Sept. 11, 1996	Sept. 20, 1996	9
10A-17	Sept. 11, 1996	Sept. 23, 1996	12
10A-19	Sept. 11, 1996	Sept. 25, 1996	14
10A-21	Sept. 12, 1996	Oct. 7, 1996	25
12A-18	Aug. 14, 1996	Aug. 22, 1996	8

4.4.4 RGS Results Summary

The retained gas measurement data (Table 4.32), when averaged by integration over the nonconvective layer and corrected for entrainment (Table 4.35), show three major constituents in the in-situ gas/vapor phase: 31.2 ± 2.9 mol% nitrogen, 47.3 ± 3.8 mol% hydrogen, and 19.8 ± 1.6 mol% nitrous oxide. For the retained gas/vapor in the convective layer (Table 4.36), the major constituents have a composition of 65.6 ± 37 mol% nitrogen, 25.1 ± 9.3 mol% hydrogen, and 4.5 ± 1.7 mol% nitrous oxide. The remainder of the gas is composed of ammonia, methane, and other hydrocarbons.

The lower-bound ammonia concentrations in AN-104 were found to range from 1100 ± 700 to 3700 ± 6100 μmol/L of waste (Table 4.33); more than 99.9% of this ammonia is dissolved in the waste. These concentrations integrate to a lower-bound nonconvective layer ammonia inventory that, if it were present as vapor, would occupy 89 ± 76 m^3 (3100 ± 2700 ft^3) at STP (Table 4.35); the corresponding lower-bound convective layer ammonia inventory (Table 4.36) would have a volume of 54 ± 35 m^3 (1900 ± 1200 ft^3) at STP. The limitations in the measurement accuracy are similar to those discussed in Sections 4.1.4 and 4.2.4.

RGS data (Table 4.37, Figure 4.22) gives a corrected in-situ void fraction of 0.005 ± 0.001 for the convective layer and void fractions ranging from 0.016 ± 0.003 to 0.133 ± 0.013 for the nonconvective layer. The volume-averaged void fraction for the nonconvective layer (an average obtained by integrating over the depth of the layer) is 0.057 ± 0.010. The VFI data for the tank show in-situ void fractions of 0.002 to 0.005 in the convective layer and 0.012 to 0.099 in the nonconvective layer (Stewart et al. 1996a).

The STP hydrogen inventory retained in the nonconvective layer of AN-104 is 92 ± 9.8 m^3 (3200 ± 340 ft^3), based on a hydrogen mole fraction that is an arithmetic average of the RGS data for both risers, and on a total gas volume of 197 ± 13 m^3 that was calculated from VFI data by Stewart et al. (1996a). The nonconvective gas volume estimate from RGS data alone is 202 ± 26 m^3 at STP; the STP hydrogen inventory, calculated by integrating RGS hydrogen concentrations over depth and using data from both risers, is 96 ± 12 m^3 (Table 4.35).

The STP hydrogen inventory retained in the convective upper layer of AN-104 is 2.8 ± 4.4 m^3 (97 ± 150 ft^3), based on a hydrogen mole fraction from the single sample taken from the layer and on a total gas volume of 11 ± 17 m^3 that was calculated from VFI data by Stewart et al. (1996a). The convective gas volume estimate from RGS data alone is 10 ± 3.8 m^3 at STP; the STP hydrogen inventory, calculated from the single datum, is 2.6 ± 0.4 m^3 (Table 4.36).

Note that, because of sample extraction scheduling constraints, there is only one sample from one of the risers, making it impossible to gauge the lateral variability in hydrogen concentrations. Accordingly, the hydrogen inventory may contain substantially more uncertainty than the ± error bands that have been cited above (which only account for instrument error and layer interface uncertainty). The same is true for void fraction and total void volume.

4.4.5 Retained Gas Concentrations

Table 4.32 presents the estimated concentrations of the insoluble and low-solubility gases in AN-104. No corrections for air entrainment have been made in Table 4.32. Such a correction would consist of removing all the O_2 and Ar and subtracting (3.71 x O_2) from the N_2, consistent with the molar N_2/O_2 ratio in atmospheric air.

Table 4.32. Concentrations of Insoluble Constituents (μmoles/liter of waste) in Tank AN-104, Without Entrainment Correction

Segment	N_2	H_2	N_2O	O_2	CH_4	Ar	Other Nit. Ox	C_2H_x	C_3H_x	Other Hyd.
10A-3	550±70	76±10	72±10	100±20	4.9±1.1	7±1	1.5±0.6	1.2±0.4	0.68±0.26	3.3±0.8
10A-13	790±60	520±40	200±20	76±6	14±2	8.4±0.7	2.3±1.3	6.0±1.9	1.3±0.4	9.8±2.2
10A-15	1190±90	1520±110	430±40	58±4	32±5	9.0±0.8	0.4±0.3	14±3	2.2±0.7	21±4
10A-17	2850±200	1000±70	530±40	290±20	51±6	20±2	0.3±0.3	22±3	3.5±0.8	28±5
10A-19*										
10A-21	2900±200	6100±300	4000±20	48±6	77±9	140±10	4.5±2.3	11±3	8.8±3.2	20±4
12A-18	2100±70	2220±80	760±30	79±3	50±5	21±1	0.5±0.4	21±2	3.8±0.8	29±3

* The data from segment 19 could not be used because of a valving problem in the extraction procedure.

Table 4.33 presents the total ammonia concentration per liter of waste under in-tank conditions. We can test the hypothesis that the ammonia concentration in the tank is uniform by taking the layer averages of the concentrations in Table 4.33. The average and standard deviation over the nonconvective layer (all samples except segment 3) are 2300 ± 900 μmol/L of waste. This standard deviation is larger than the error bands on most of the individual samples, so it is not clear whether the concentration of ammonia can be considered constant throughout the nonconvective layer or whether the concentrations in the convective layer are lower. All of these concentrations must be regarded as lower bounds (probably by a factor of 2–3) because they do not account for ammonia lost to condensation in the RGS system.

Table 4.33. Total Ammonia Concentrations in Tank AN-104

Segment	NH_3* (μmole/liter)
10A-3	1100±700
10A-13	2200±1300
10A-15	2500±500
10A-17	1800±400
10A-19	
10A-21	1300±400
12A-18	3700±6100

* These lower-bound values do not account for ammonia in the condensate in the collector side of the RGS system; they are expected to be one-half to one-third of the actual in-tank values.

4.4.6 Gas Inventory

Table 4.34 compares the layer gas inventories that are calculated entirely from RGS data, with and without corrections for entrained air, to the gas inventories calculated from VFI data by Stewart et al. (1996a). It can be noted that the air entrainment correction has a greater impact on the convective layer inventory than the nonconvective. The RGS data uncertainty in the convective layer contains only the instrument precision and layer thickness uncertainties for a single point, while the VFI data uncertainty additionally contains the standard deviation for a large number of measurements.

Table 4.35 shows estimates of the STP volumes of gas constituents in the nonconvective layer in AN-104. The RGS/VFI inventories were calculated from the concentration data presented in Tables 4.32 and 4.33 by taking an arithmetic average of the mole-fractions of constituents in the gas and multiplying that average composition by the volume of gas measured by VFI (Stewart et al. 1996a). The RGS inventories were calculated by integrating RGS data over depth, as discussed in Section 3.4.1. Although there was a significant difference in the hydrogen concentrations measured by the two risers, data from both risers have been used to generate Table 4.35 without any attempt to account for possible concentration variations in the horizontal plane. Table 4.36 presents similar results as Table 4.35, but for the convective layer; the concentrations are based on the single sample taken in this layer.

The values in Tables 4.35 and 4.36 all include the effect of corrections to remove the presumed entrained air. The table gives the volume (at standard conditions) and the volume percent of each gas. The uncertainty in the table represent only the uncertainty that carries through from instrument precision and uncertainty in layer interface location. Temporal and lateral variability in composition are not included.

Again, similar to Tank AN-105, Table 4.35 shows that the nitrous oxide in solution in Tank AN-104 constitutes approximately 5 to 10% of the dissolved gases in the waste.

Table 4.34. STP Gas Inventories in Tank AN-104, According to Different Methods

Layer	STP Gas Volume (m^3)		
	Uncorrected RGS	Corrected RGS	VFI (Stewart et al. 1996a)
Crust	---	---	39 ± 16
Upper (convective)	36 ± 5.9	10 ± 3.8	11 ± 17
Lower (nonconvective)	225 ± 29	202 ± 26	197 ± 13
Total	261 ± 30 (no crust)	212 ± 26 (no crust)	208 ± 21 (no crust) 247 ± 26 (crust)

Table 4.35. Nonconvective Layer Gas Inventory in Tank AN-104 at STP*

Gas	RGS (corrected)		RGS (corrected)/VFI
	m^3 (mol%) in gas/vapor phase	m^3 (mol%) dissolved in liquid phase	m^3 (mol%) in gas/vapor phase
Ammonia	0.046 ± 0.046 (0.02%)	89 ± 76 (86.8%)	0.045 (0.02%)
Nitrogen	63 ± 8.5 (31.2%)	0.86 ± 0.12 (0.8%)	63 (32.1%)
Hydrogen	96 ± 12 (47.3%)	2.2 ± 0.3 (2.2%)	92 (46.7%)
Nitrous Oxide	40 ± 5.1 (19.8%)	10 ± 1.4 (10.1%)	38 (19.4%)
Methane	1.8 ± 0.3 (0.9%)	0.043 ± 0.007 (0.04%)	1.8 (0.9%)
C_2H_x**	0.60 ± 0.13 (0.3%)	0	0.61 (0.3%)
C_3H_x**	0.16 ± 0.05 (0.1%)	0	0.16 (0.1%)
Other**	0.94 ± 0.22 (0.5%)	0	0.95 (0.5%)
Total	202 ± 26 m^3	103 ± 78 m^3	197 m^3

* The error bands in the table represent only the uncertainty that carries through from instrument error and uncertainty in layer interface location. Temporal and lateral variability are not included, and the resulting inventories may not be conservative.
**These gases were assumed to be entirely insoluble.

Table 4.36. Convective Layer Gas Inventory in Tank AN-104 at STP*

Gas	RGS (corrected)		RGS (corrected)/VFI
	m^3 (mol%) in gas/vapor phase	m^3 (mol%) dissolved in liquid phase	m^3 (mol%) in gas/vapor phase
Ammonia	0.002 ± 0.001 (0.02%)	54 ± 35 (90.8%)	0.002 (0.02%)
Nitrogen	6.9 ± 3.1 (65.6%)	1.3 ± 0.6 (2.2%)	7.2 (65.6%)
Hydrogen	2.6 ± 0.43 (25.1%)	1.1 ± 0.2 (1.8%)	2.8 (25.1%)
Nitrous Oxide	0.47 ± 0.08 (4.5%)	3.0 ± 0.5 (5.1%)	0.49 (4.5%)
Methane	0.18 ±0.04 (1.7%)	0.06 ± 0.01 (0.1%)	0.19 (1.7%)
C_2H_x**	0.059 ± 0.023 (0.6%)	0	0.062 (0.6%)
C_3H_x**	0.033 ± 0.013 (0.3%)	0	0.035 (0.3%)
Other**	0.24 ± 0.07 (2.3%)	0	0.25 (2.3%)
TOTAL	10 ± 3.8 m^3	60 ± 36 m^3	11 m^3

* The uncertainty in the table represent only the uncertainty that carries through from instrument precision and uncertainty in layer interface location. Temporal and lateral variability in composition are not included, and the resulting inventories may not be conservative.
** These gases were assumed to be entirely insoluble.

4.4.7 Retained Void Fraction

The method by which the in-situ void fractions were calculated is given in Section 3.3. The results are presented in Table 4.37, showing the difference between entrainment-corrected and uncorrected in-situ void fractions.

Figure 4.22 presents the corrected void fractions found from RGS, plotted against the results found using VFI (Stewart et al. 1996a). This figure shows that the data from the retained gas sampler agree reasonably well with the VFI results. Given that both measurement techniques have finite uncertainty, and that the measurements were made at different points in the tank with possible lateral variations, the agreement between the two sets of data is reasonable. The VFI data show an apparent maximum in void fraction of approximately 0.1 at ~100 cm (40 in.). But since the measurements do not go below about 80 cm, VFI data do not rule out the possibility that a higher void fraction at lower elevations could exist. The maximum void fraction found with the RGS is 0.133 in the bottom segment (segment 21), which may be consistent with VFI data based on the trend in the VFI data.

4.4.8 X-Ray Results

Six RGS segments from Tank AN-104 were radiographed with x-rays. A summary of the observations of these images are provided in Table 4.38. A discussion of the observations is provided in the next section. The measurements in this tank were more carefully performed as is evident from the observations provided in the following section.

4.4.8.1 Phase Distribution

Similar to Tank AN-105, the bubbles in the waste within the nonconvective layer were mostly round and smaller than approximately 5 mm in diameter. A large void below the piston was observed for several of the segments. Some of these features and those summarized in Table 4.38 are evident on the images provided in Figure 4.23.

Table 4.37. Corrected In-Situ Void Fractions in Tank AN-104

Segment	Sample Central Height (cm)	Hydrostatic Pressure (atm)	Temperature (°C)	Corrected Void Fraction (In-Tank Conditions)	Uncorrected Void Fraction (In-Tank Conditions)
10A-3	893	1.12	42.2	0.005 ± 0.001	0.018
10A-13	410	1.80	42.2	0.016 ± 0.003	0.021
10A-15	314	1.94	46.7	0.038 ± 0.006	0.042
10A-17	217	2.09	48.9	0.040 ± 0.005	0.059
10A-19	121	2.24	46.7		
10A-21	24	2.39	40.0	0.133 ± 0.013	0.137
12A-18	169	2.17	47.8	0.057 ± 0.005	0.062

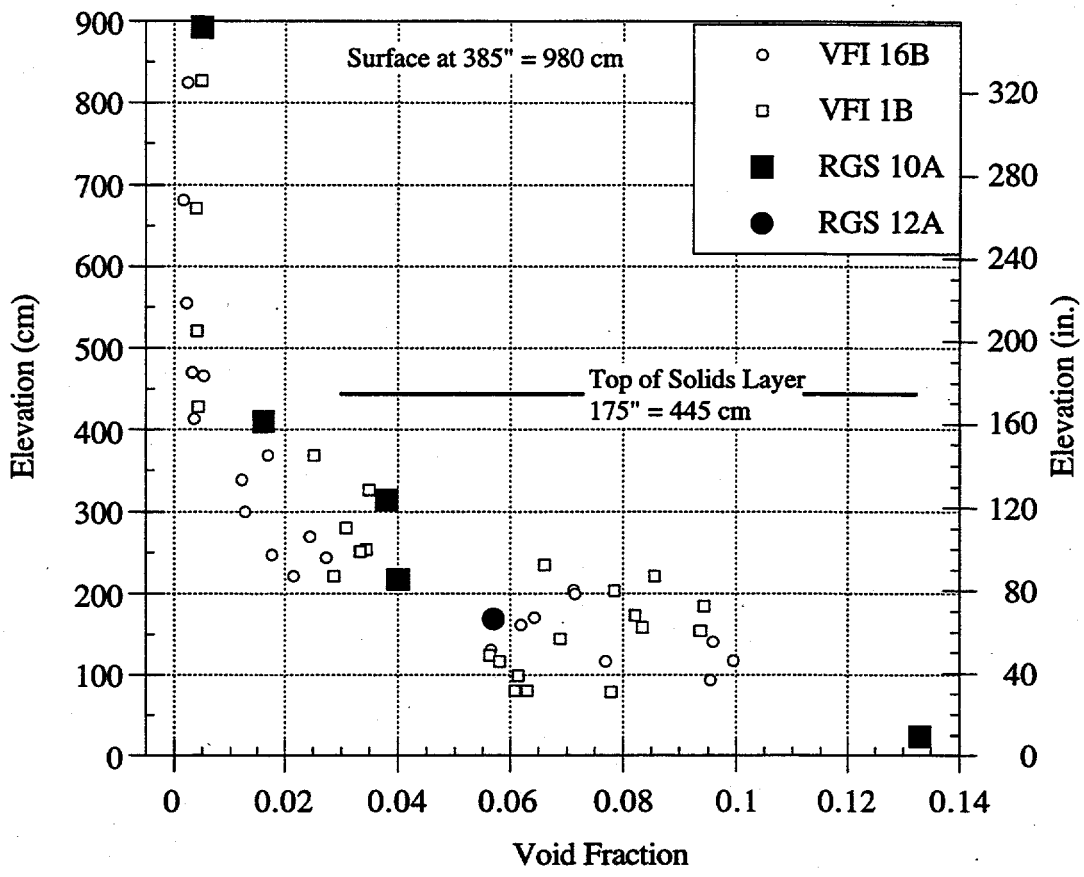

Figure 4.22. Void Fractions in Tank 241-AN-104 (RGS data were taken for riser 10A in September-October, riser 12A in August, and VFI data in April 1996)

Also similar to the results of observations of Tank AN-105 x-ray images, we summarize our observations for Tank AN-104 as:

1) Large gas pockets are observed in Tank AN-104, which account for a large portion of the measured void fraction. This is in contrast with the observations made for AW-101 waste that the major portion of the gas was observed to be smaller than the detection threshold of the x-ray imaging system (<0.5 mm).

2) No fractures or irregularly shaped bubbles were observed in this tank, unlike what was observed in Tank A-101 waste.

We therefore conclude that the retention mechanism of the gas phase within the waste in this tank is different from that in Tank A-101 and AW-101 wastes.

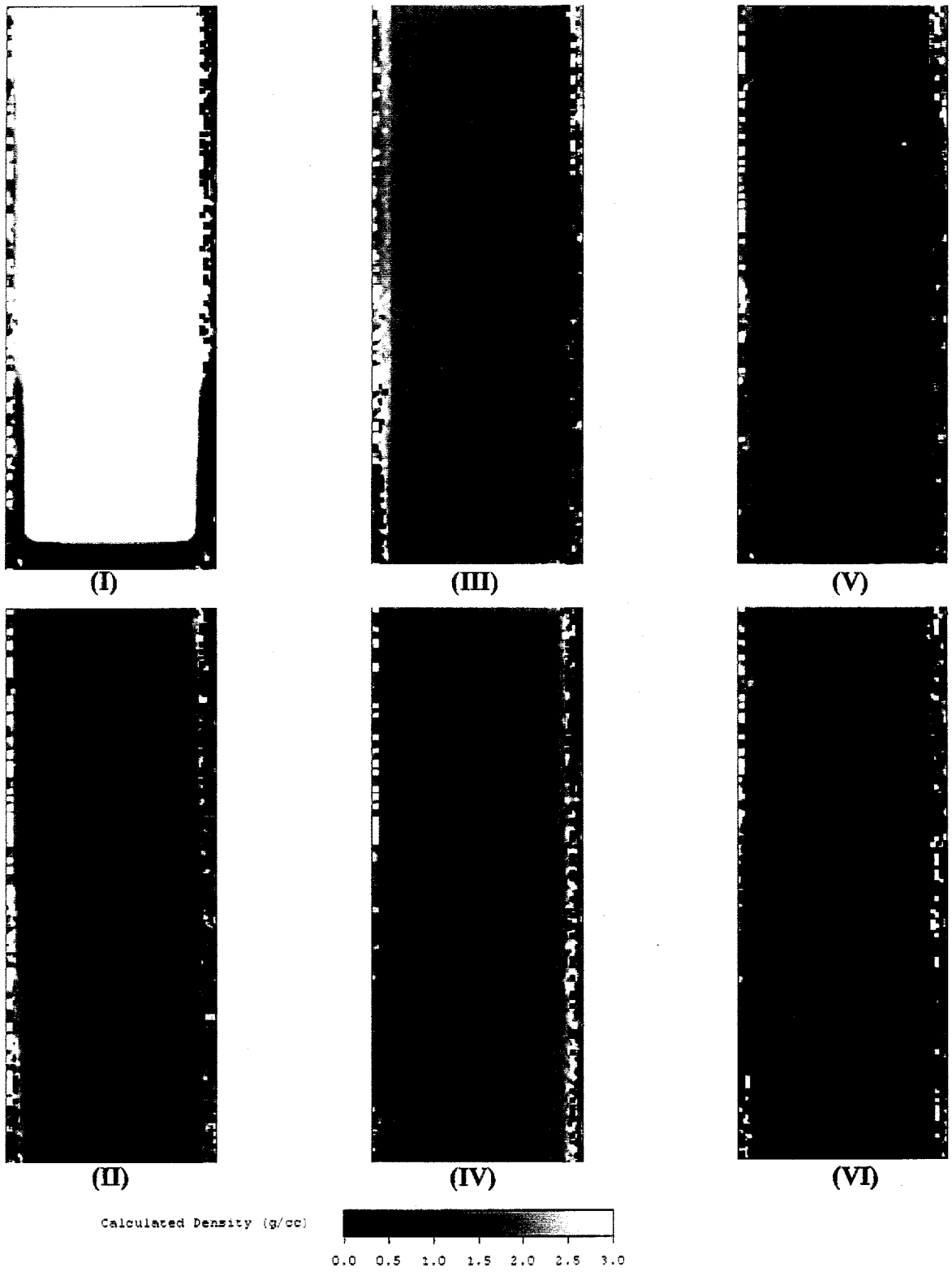

Figure 4.23a. Density Image Calculated from X-Ray Images of Segment 3, Riser 10A, Tank AN-104

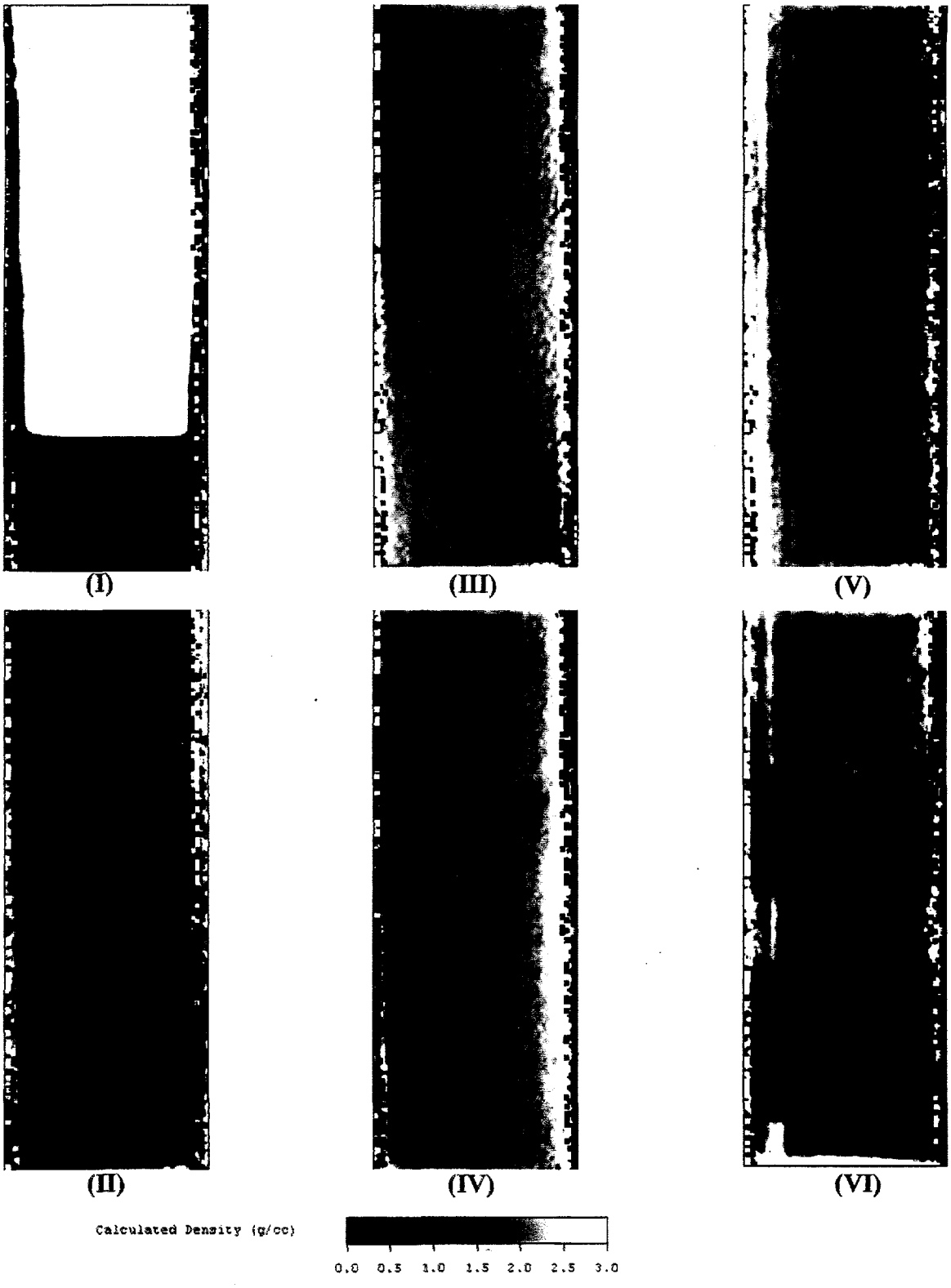

Figure 4.23b. Density Image Calculated from X-Ray Images of Segment 21, Riser 10A, Tank AN-104

Table 4.38. Summary of Observations from X-Ray Images for Tank AN-104

Segment	Comments/Observations
10A-3	Homogenous sample, very small void under piston.
10A-13	Some small bubbles, small void under piston.
10A-15	Many medium to large bubbles and voids. Small void below piston.
10A-17	Many small to medium bubbles throughout. Small void below piston.
10A-19	Many small to medium bubbles throughout. Medium void below piston.
10A-21	Many small to medium bubbles. Medium void below piston.

4.4.8.2 Waste Density

Similar to the previous three tanks, the density was found for all RGS segments taken in this tank (except for segment 18). Table 4.39 is a summary of the findings for those segments for which calibration data were available. The density of the five segments in the nonconvective layer, as shown in this table, range between 1.72 to 2.09 g/cc with a mean of 1.84 ± 0.16 g/cc (mean standard deviation of ~8.7%). The supernatant liquid (convective layer) density was determined to be 1.41 ± 0.05 g/cc.

4.4.9 Other Discussion of RGS Results for Tank 241-AN-104

Tank AN-104 contains one segment (segment 21 at 13.3% void) that is significantly higher than any results given by VFI (Stewart et al. 1996a). In this case, the high void value could be interpreted as the extrapolation of the VFI trend to increasing void fraction with depth, and therefore as having no implications of localized gas concentration. However, localized gas is another possible explanation. Table 4.40 shows the ratios of the major chemical constituents of the insoluble gas in AN-104.

Table 4.39. Summary of X-Ray Densitometry Results for Tank AN-104

Segment	Mean Density (g/cc)	Density STD (%)
10A-3	1.41	3.78
10A-13	1.79	6.17
10A-15	1.72	8.66
10A-17	2.09	9.54
10A-19	1.74	9.71
10A-21	1.85	8.27

Table 4.40. Constituent Ratios for Tank AN-104

Segment	N_2/H_2	H_2/N_2O
10A-3	7.2	1.06
10A-13	1.5	2.5
10A-15	0.78	3.5
10A-17	2.9	1.9
10A-21	0.47	1.5
12A-18	0.95	2.9

4.5 Tank 241-AN-103

4.5.1 Sampling Locations

Push mode sampling of Tank AN-103, the fifth (and last) tank sampled, was carried out in risers 21A and 12A. The approximate locations of these risers are depicted in Figure 4.24. Three segments of the first core (riser 12A) and four segments of the second core (21A) in AN-103 were sampled and analyzed in FY 1996. Riser 12A was chosen to be sampled first because of its proximity to the MIT tree in riser 15A and the VFI/ball rheometer measurements in riser 1B.

The total depth of waste in Tank AN-103 is approximately 884 cm (348 in.). Figure 4.25 shows the available information on tank content layering as derived from the riser 4A thermocouple tree and riser 15A MIT measured temperature profiles, in conjunction with the VFI/ball rheometer data for this tank. The nonconvective layer is believed to be about 378 ± 29 cm (149 ± 12 in.) in depth, with the convective, supernatant liquid layer forming the balance of the contents and a 92 ± 8 cm (36 ± 3 in) thick crust forming the balance of the contents.(a) Eighteen full sampler cores and one partial sampler core were required. The sampling levels for RGS in each of the two selected risers are graphically depicted in Figure 4.25.(b)

4.5.2 Pertinent Tank Characterization Information

Figure 4.26 is a temperature profile in the tank taken with the multi-instrument tree (MIT) located in riser 15A of Tank AN-103. The data points show the temperature profile for June 10, 1996. The thickness of the supernatant liquid layer and the nonconvective layers can be approximated from this temperature profile.

The average density in the convective layer is 1.53 ± 0.03 g/cc as determined with the ball rheometer (Stewart et al. 1996a). The same report specified a density of 1.80 ± 0.05 g/cc for the nonconvective layer based on a 1988 core sample. The densities, rather than values obtained by x-ray image processing, were used in RGS data analysis for AN-103 because ball rheometer and core sample densities are obtained by recognized methods and thus are preferred (when available).

(a) Private Communication with Chuck Stewart. Pacific Northwest National Laboratory, Richland, Washington.

(b) Shekarriz R and JM Bates. 1996. *Sampling Plan for Tank 241-AN-103 Retained Gas Sampler Deployment.* TWS-MIT-080196, Pacific Northwest National Laboratory, Richland, Washington.

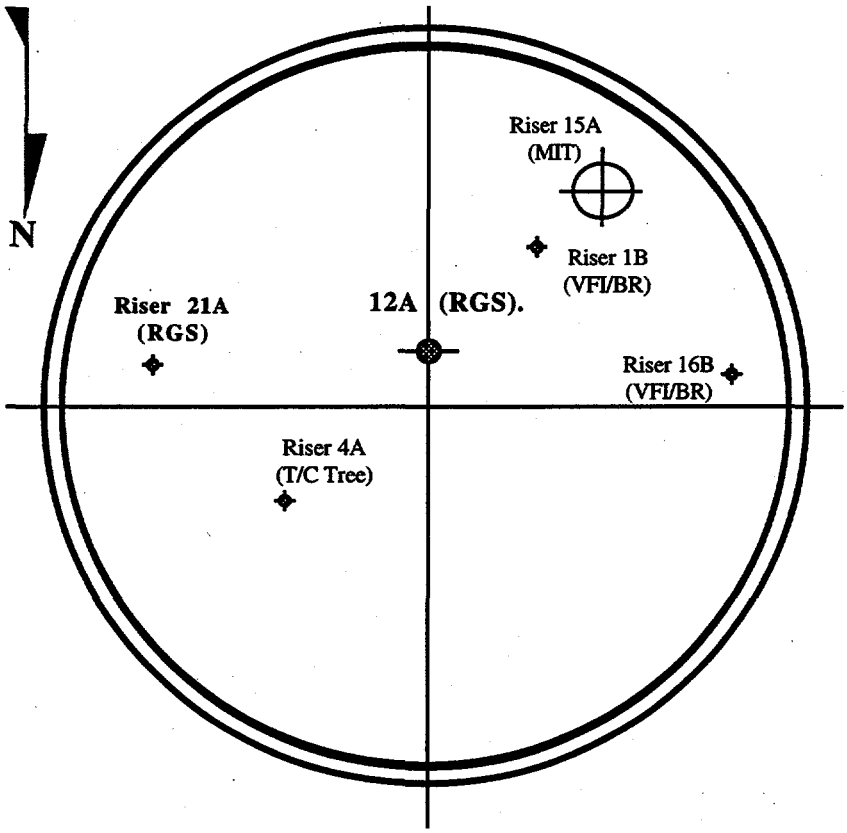

Figure 4.24. Schematic Diagram of Riser Locations for Tank 241-AN-103

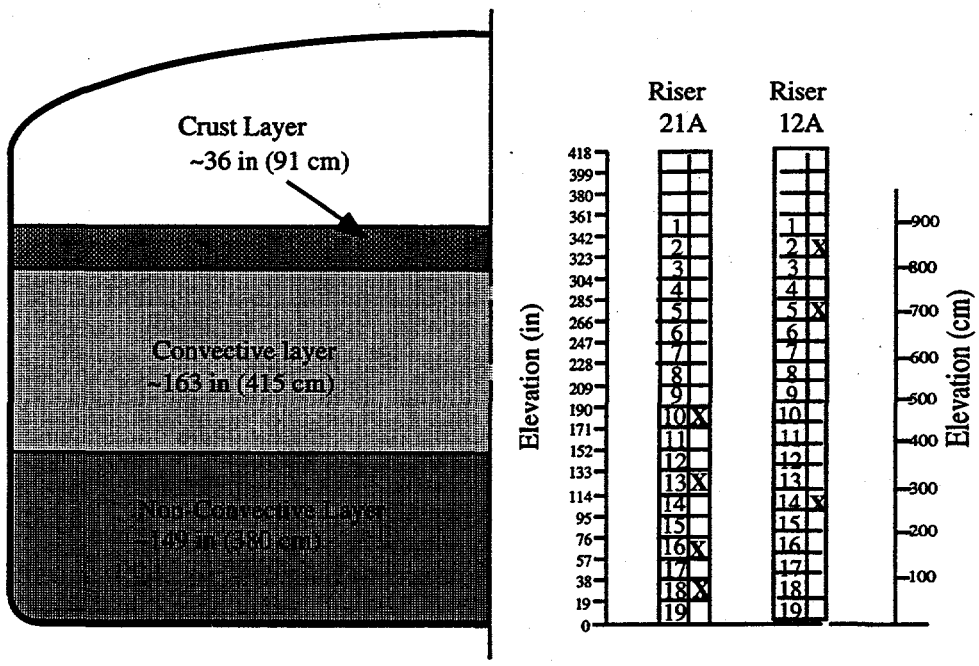

Figure 4.25. Diagram of the As-Sampled RGS Sample Elevations for Tank AN-103

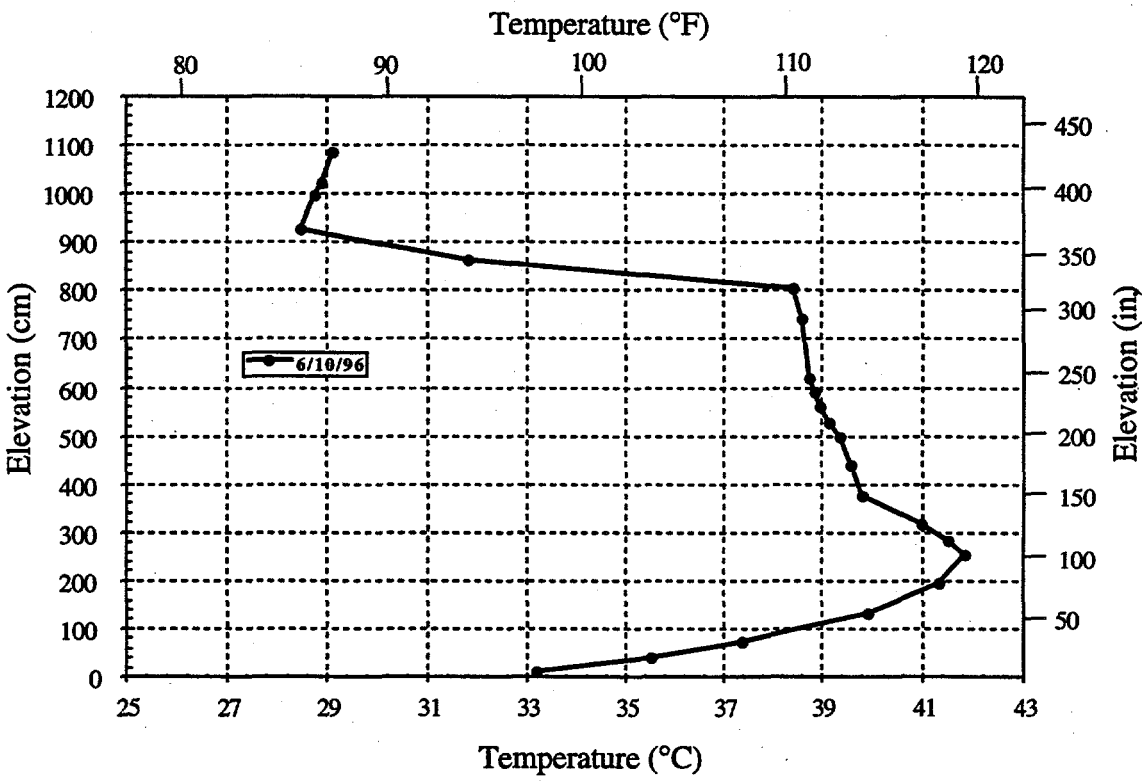

Figure 4.26. Profile of Temperature in Tank AN-103 Taken with MIT

4.5.3 RGS Sampling Process Information

Of the samples in Figure 4.25, segments 21A-13 and 21A-18 were lost because the sampler valve malfunctioned. The lag times (delay between sample acquisition and processing) for the remaining AN-103 samples are shown in Table 4.41. The maximum hold time allowed by the sampling plan is 24 days, based on measured sampler leakage rates during acceptance testing. The hold time for all the samples exceeded this limit, but the samples were accepted based on calculations that indicated the estimated leakage was still negligible. However, the long hold times increase the possibility that significant gas leakage has occurred.

Table 4.41. Lag Times for Processing of RGS Samples from AN-103

Sample	Acquisition Date	Processing Date	Lag (days)
12A-2	Sept. 13, 1996	Oct. 18, 1996	35
12A-5	Sept. 13, 1996	Oct. 22, 1996	39
12A-14	Sept. 16, 1996	Oct. 23, 1996	37
21A-10	Sept. 20, 1996	Oct. 24, 1996	34
21A-16	Sept. 20, 1996	Oct. 28, 1996	38

4.5.4 RGS Results Summary

The retained gas measurement data (Table 4.42), when averaged by integration over the nonconvective layer and corrected for entrainment (Table 4.45), show three major constituents in the in-situ gas/vapor phase: 33.1 ± 3.7 mol% nitrogen, 62.0 ± 6.6 mol% hydrogen, and 3.8 ± 0.4 mol% nitrous oxide. For the retained gas/vapor in the convective layer (Table 4.46), the major constituents have a composition of 76.3 ± 60 mol% nitrogen, 18.4 ± 10 mol% hydrogen, and 2.2 ± 1.2 mol% nitrous oxide. For the retained gas/vapor in the crust layer (Table 4.47), the major constituents have a composition of 29.3 ± 2.4 mol% nitrogen, 63.1 ± 1.7 mol% hydrogen, and 6.7 ± 0.2 mol% nitrous oxide. The remainder of the gas is composed of ammonia, methane, and other hydrocarbons.

The lower-bound ammonia concentrations in AN-103 were found to range from 1260 ± 350 to 3820 ± 3150 μmol/L of waste (Table 4.43); more than 99.9% of this ammonia is dissolved in the waste. These concentrations integrate to a lower-bound nonconvective layer ammonia inventory that, if it were present as vapor, would occupy 91 ± 59 m^3 (3200 ± 2100 ft^3) at STP (Table 4.45); the corresponding lower-bound convective layer ammonia inventory (Table 4.46) would have a volume of 75 ± 148 m^3 (2600 ± 5300 ft^3) at STP. The lower-bound crust ammonia inventory would have a volume of 9.0 ± 3.0 m^3 (320 ± 110 ft^3) at STP. The limitations on measurement accuracy are similar to those discussed in Sections 4.1.4 and 4.2.4.

RGS data (Table 4.48, Figure 4.27) give a corrected in-situ void fraction of 0.004 ± 0.001 for the convective layer; void fractions are 0.057 ± 0.008 and 0.094 ± 0.012 in the nonconvective layer (with only two samples); and the void fraction is 0.146 ± 0.015 for the crust. The volume-Averaged void fraction for the nonconvective layer (an average obtained by integrating over the depth of the layer) is 0.077 ± 0.012. The VFI data for the tank show in-situ void fractions of 0.001 to 0.013 in the convective layer and 0.004 to 0.15 in the nonconvective layer (Stewart et al. 1996a).

The STP hydrogen inventory retained in the nonconvective lower layer of AN-103 is 223 ± 25 m^3 (7900 ± 890 ft^3), based on a hydrogen mole fraction that is an arithmetic average of the RGS data for both risers, and on a total gas volume of 363 ± 10 m^3 that was calculated from VFI data by Stewart et al. (1996a). The nonconvective gas volume estimate from RGS data alone is 216 ± 22 m^3 at STP; the STP hydrogen inventory, calculated by integrating RGS hydrogen concentrations over depth and using both risers' data, is 134 ± 13 m^3 (Table 4.45).

The STP hydrogen inventory in the convective upper layer of AN-103 is 1.8 ± 2.9 m^3 (65 ± 100 ft^3), based on a hydrogen mole fraction from the single sample taken from the layer and on a total gas volume of 10 ± 15 m^3 that was calculated from VFI data by Stewart et al. (1996a). The convective gas volume estimate from RGS data alone is 8.8 ± 4.6 m^3 at STP; the STP hydrogen inventory, calculated from the single datum, is 1.6 ± 0.3 m^3 (Table 4.46).

The STP hydrogen inventory retained in the crust layer of AN-103 is 57 ± 20 m^3 (2000 ± 690 ft^3), based on a hydrogen mole fraction from the single sample taken from the layer and on a total gas volume of 91 ± 31 m^3 that was calculated by Stewart et al. (1996a). The crust gas volume estimate from RGS data alone is 48 ± 3.0 m^3 at STP; the STP hydrogen inventory, calculated from the single datum, is 30 ± 1.5 m^3 (Table 4.47).

Note that, because of sample losses caused by sampler valve malfunction, there is only one sample from each of the risers in the nonconvective layer, making it impossible to gauge the lateral variability in hydrogen concentrations. Accordingly, the hydrogen inventory may contain substantially more uncertainty than the ± values cited above (which only account for instrument precision and layer interface uncertainty). The same is true for void fraction and total void volume.

4.5.5 Retained Gas Concentrations

Table 4.42 presents the estimated concentrations of the insoluble and low-solubility gases in AN-103. No corrections have been made for air entrainment. Such a correction would consist of removing all the O_2 and Ar and subtracting (3.71 x O_2) from the N_2, consistent with the molar N_2/O_2 ratio in atmospheric air.

Table 4.43 presents the total ammonia concentration per liter of waste under in-tank conditions. With so few data points, there are no grounds for assessing the uniformity of the ammonia concentration in any layer. All of these concentrations must be regarded as lower bounds (probably by a factor of 2–3) because they do not account for ammonia lost to condensation in the RGS system.

4.5.6 Gas Inventory

Table 4.44 compares the layer gas inventories that are calculated entirely from RGS data, without and with air entrainment corrections, to the gas inventories calculated from VFI data by Stewart et al. (1996a). The air correction can be seen to make a greater change in the convective

Table 4.42. Concentrations of Insoluble Constituents (μmoles/liter of waste) in Tank AN-103, Without Entrainment Correction

Segment	N_2	H_2	N_2O	O_2	CH_4	Ar	Other Nit. Ox	C_2H_x	C_3H_x	Other Hyd.
12A-2	2000±100	3600±180	410±21	89±4.9	37±2.1	8.0±0.4	0.9±0.7	7.6±1.5	2.6±0.9	3.2±0.8
12A-5	520±67	49±5.8	28±3.2	93±12	2.4±0.3	6.1±0.8	0.9±0.7	0.3±0.2	0.6±0.2	0.3±0.1
12A-14	1860±170	2400±220	220±21	57±5.7	30±4.3	8.5±0.8	1.6±1.1	8.3±11.6	3.1±1.0	4.3±1.2
21A-10	610±130	62±12	40±7.5	110±23	3.7±0.9	21±4.4	1.3±0.4	0.8±0.3	1.2±0.3	1.0±0.3
21A-16	2400±170	5000±330	300±22	10±1.1	49±6.6	64±5.0	1.2±0.8	11±2.8	5.3±1.2	14±3.1

Table 4.43. Total Ammonia Concentrations in Tank AN-103

Segment	NH_3* (μmole/liter)
12A-2	1260±350
12A-5	
12A-14	3820±3150
21A-10	1980±3880
21A-16	2110±620

* These lower-bound values do not account for ammonia in the condensate in the collector side of the RGS system; they are expected to be one-half to one-third of the actual in-tank values.

layer inventory than the nonconvective. The RGS error bands in the convective layer contain only the instrument and layer thickness uncertainties for a single point, while the VFI error bands additionally contain the standard deviation for a large number of measurements.

Table 4.45 shows estimates of the STP volumes of gas constituents in the nonconvective layer in AN-103. The RGS/VFI inventories were calculated from the concentration data presented in Tables 4.42 and 4.43 by taking an arithmetic average of the mole fractions of constituents in the gas and multiplying that average composition by the volume of gas measured by VFI (Stewart et al. 1996a). The RGS inventories were calculated by integrating RGS data over depth, as discussed in Section 3.4.1. Although there was a significant difference in the hydrogen concentrations measured near the two risers, data from both risers have been used to generate Table 4.45 without any attempt to account for possible concentration variations in the horizontal plane. Tables 4.36 and 4.37 are the same sort of tables, but the concentration data from the convective upper layer and crust in each of these tables are based on the single sample taken in the layer.

The values in Table 4.45 include the effect of corrections to remove the (assumed) entrained air. The table gives the volume (at standard conditions) and the volume percent of each gas. The error bands in the table represent only the uncertainty that carries through from instrument error and uncertainty in layer interface location; temporal and lateral variability are not included.

4.5.7 Retained Void Fraction

The method by which the in-situ void fractions were calculated is given in Section 3.3. The results are presented in Table 4.48, showing the difference between entrainment-corrected and uncorrected in-situ void fractions.

Figure 4.27 presents the corrected void fractions found from RGS, plotted against the results found using VFI (Stewart et al. 1996a). This figure shows that the data from the retained gas sampler did not agree closely with the VFI results. The VFI data show a maximum of approximately 0.15 void fraction at approximately 200 cm (80 in.), while the maximum nonconvective-layer void fraction found with the RGS is 0.094.

Table 4.44. STP Gas Inventories in Tank AN-103, According to Different Methods

Layer	STP Gas Volume (m^3)		
	Uncorrected RGS	Corrected RGS	VFI (Stewart et al 1996a)
Crust	51 ± 3.1	48 ± 3.0	91 ± 31
Upper (convective)	29 ± 6.4	8.8 ± 4.6	10 ± 15
Lower (nonconvective)	222 ± 23	216 ± 22	363 ± 10
TOTAL	251 ± 24 (no crust) 309 ± 24 (crust)	225 ± 22 (no crust) 273 ± 23 (crust)	373 ± 18 (no crust) 464 ± 36 (crust)

Table 4.45. Nonconvective Layer Gas Inventory in Tank AN-103 at STP

Gas	RGS (corrected)		RGS (corrected)/VFI
	m^3 (mol%) in gas/vapor phase	m^3 (mol%) dissolved in liquid phase	m^3 (mol%) in gas/vapor phase
Ammonia	0.13 ± 0.06 (0.06%)	91 ± 59 (97.4%)	0.22 (0.06%)
Nitrogen	71 ± 7.6 (33.1%)	0.27 ± 0.04 (0.3%)	122 (33.6%)
Hydrogen	134 ± 13 (62.0%)	1.1 ± 0.1 (1.2%)	223 (61.4%)
Nitrous Oxide	8.2 ± 0.8 (3.8%)	1.1 ± 0.1 (1.1%)	14 (3.9%)
Methane	1.4 ± 0.2 (0.6%)	0.009 ± 0.002 (0.01%)	2.4 (0.6%)
C_2H_x*	0.34 ± 0.23 (0.2%)	0	0.59 (0.2%)
C_3H_x*	0.15 ± 0.04 (0.1%)	0	0.26 (0.1%)
Other*	0.38 ± 0.12 (0.2%)	0	0.63 (0.2%)
Total	216 ± 22 m^3	94 ± 60 m^3	363 m^3

* These gases were assumed to be entirely insoluble. The uncertainty in the table represent only the uncertainty that carries through from instrument precision and uncertainty in layer interface location. Temporal and lateral variability in composition are not included, and the resulting inventories may not be conservative.

Table 4.46. Convective Layer Gas Inventory in Tank AN-103 at STP

Gas	RGS (corrected)		RGS (corrected)/VFI
	m^3 (mol%) in gas/vapor phase	m^3 (mol%) dissolved in liquid phase	m^3 (mol%) in gas/vapor phase
Ammonia	0.002 ± 0.004 (0.02%)	75 ± 148 (95.7%)	0.002 (0.02%)
Nitrogen	6.7 ± 4.1 (76.3%)	1.3 ± 0.8 (1.7%)	7.6 (76.3%)
Hydrogen	1.6 ± 0.3 (18.4%)	0.73 ± 0.15 (0.9%)	1.8 (18.4%)
Nitrous Oxide	0.19 ± 0.04 (2.2%)	1.3 ± 0.3 (1.7%)	0.22 (2.2%)
Methane	0.10 ± 0.025 (1.2%)	0.036 ± 0.009 (0.05%)	0.12 (1.2%)
C_2H_x*	0.031 ± 0.01 (0.4%)	0	0.035 (0.4%)
C_3H_x*	0.046 ± 0.01 (0.5%)	0	0.052 (0.5%)
Other*	0.089 ± 0.03 (1.0%)	0	0.002 (1.0%)
Total	8.8 ± 4.6 m^3	79 ± 149 m^3	10 m^3

* These gases were assumed to be entirely insoluble. The uncertainty in the table represent only the uncertainty that carries through from instrument precision and uncertainty in layer interface location. Temporal and lateral variability in composition are not included, and the resulting inventories may not be conservative.

Table 4.47. Crust Layer Gas Inventory in Tank AN-103 at STP*

Gas	RGS (corrected)		RGS (corrected)/VFI
	m^3 (mol%) in gas/vapor phase	m^3 (mol%) dissolved in liquid phase	m^3 (mol%) in gas/vapor phase
Ammonia	0.024 ±0.008 (0.05%)	9.0 ± 3.0 (96.4%)	0.046 (0.05%)
Nitrogen	14 ± 1.3 (29.3%)	0.023 ± 0.002 (0.2%)	27 (29.3%)
Hydrogen	30 ± 1.5 (63.1%)	0.11 ± 0.01 (1.2%)	57 (63.1%)
Nitrous Oxide	3.2 ± 0.2 (6.7%)	0.19 ± 0.01 (2.1%)	6.1 (6.7%)
Methane	0.31 ± 0.02 (0.6%)	0.0009 ± 0.0001 (0.0%)	0.59 (0.6%)
C_2H_x**	0.064 ± 0.004 (0.1%)	0	0.12 (0.1%)
C_3H_x**	0.021 ± 0.003 (0.1%)	0	0.041 (0.1%)
Other**	0.034 ± 0.006 (0.1%)	0	0.065 (0.1%)
Total	48 ± 3.0 m^3	9.3 ± 3.0 m^3	91 m^3

* The error bands in the table represent only the uncertainty that carries through from instrument error and uncertainty in layer interface location. Temporal and lateral variability are not included, and the resulting inventories may not be conservative.
**These gases were assumed to be entirely insoluble.

4.5.8 X-Ray Results

Six RGS segments from Tank AN-103 were radiographed with x-rays. A summary of the observations of these images is provided in Table 4.49. A discussion of the observations is provided in the next section. The measurements in this tank were more carefully performed as is evident from the observations provided in the following section.

Table 4.48. In-Situ Void Fractions in Tank AN-103

Segment	Sample Central Height (cm)	Hydrostatic Pressure (atm)	Temperature (°C)	Corrected Void Fraction (In-Tank Conditions)	Uncorrected Void Fraction (In-Tank Conditions)
12A-2	844	1.00	37.8	0.146 ± 0.015	0.157
12A-5	700	1.27	42.2		
12A-14	265	1.94	42.8	0.057 ± 0.008	0.061
21A-10	458	1.63	42.2	0.004 ± 0.001	0.013
21A-16	169	2.11	41.7	0.094 ± 0.012	0.096

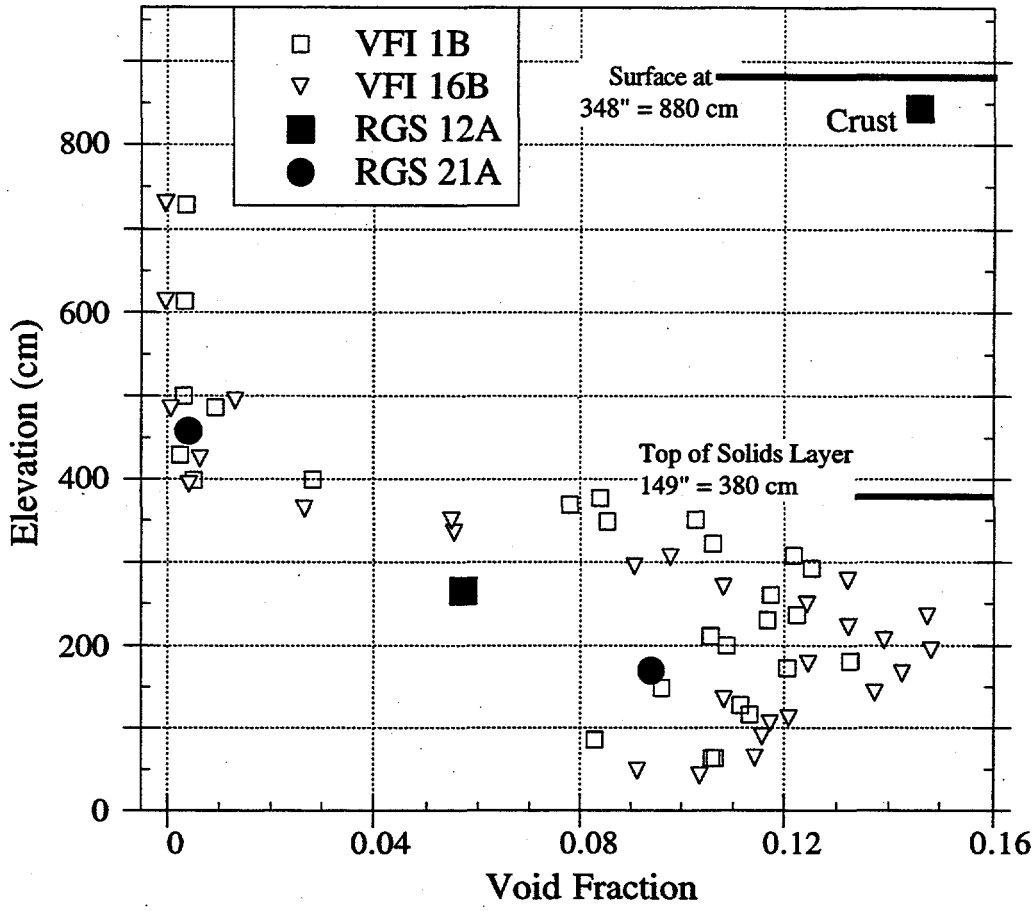

Figure 4.27. Void Fractions in Tank AN-103 (RGS riser 12A data taken in September 1996; VFI data in May 1996)

4.5.8.1 Phase Distribution

Similar to Tanks AN-105 and AN-104, the bubbles in the waste within the nonconvective layer were mostly round and smaller than approximately 5 mm in diameter. A large void below the piston was observed for two of the segments (5 and 13). Some of these features and those summarized in Table 4.49 are evident on the images provided in Figure 4.28.

Also similar to the results of observations of Tanks AN-105 and AN-104 x-ray images, we summarize our observations for Tank AN-103 as

1) Large gas pockets are observed in Tank AN-103, which account for a large portion of the measured void fraction. This is in contrast with the observations made for AW-101 waste that the major portion of the gas was observed to be smaller than the detection threshold of the x-ray imaging system (<0.5 mm).

2) No fractures or irregularly shaped bubbles were observed in this tank, unlike what was observed in Tank A-101 waste.

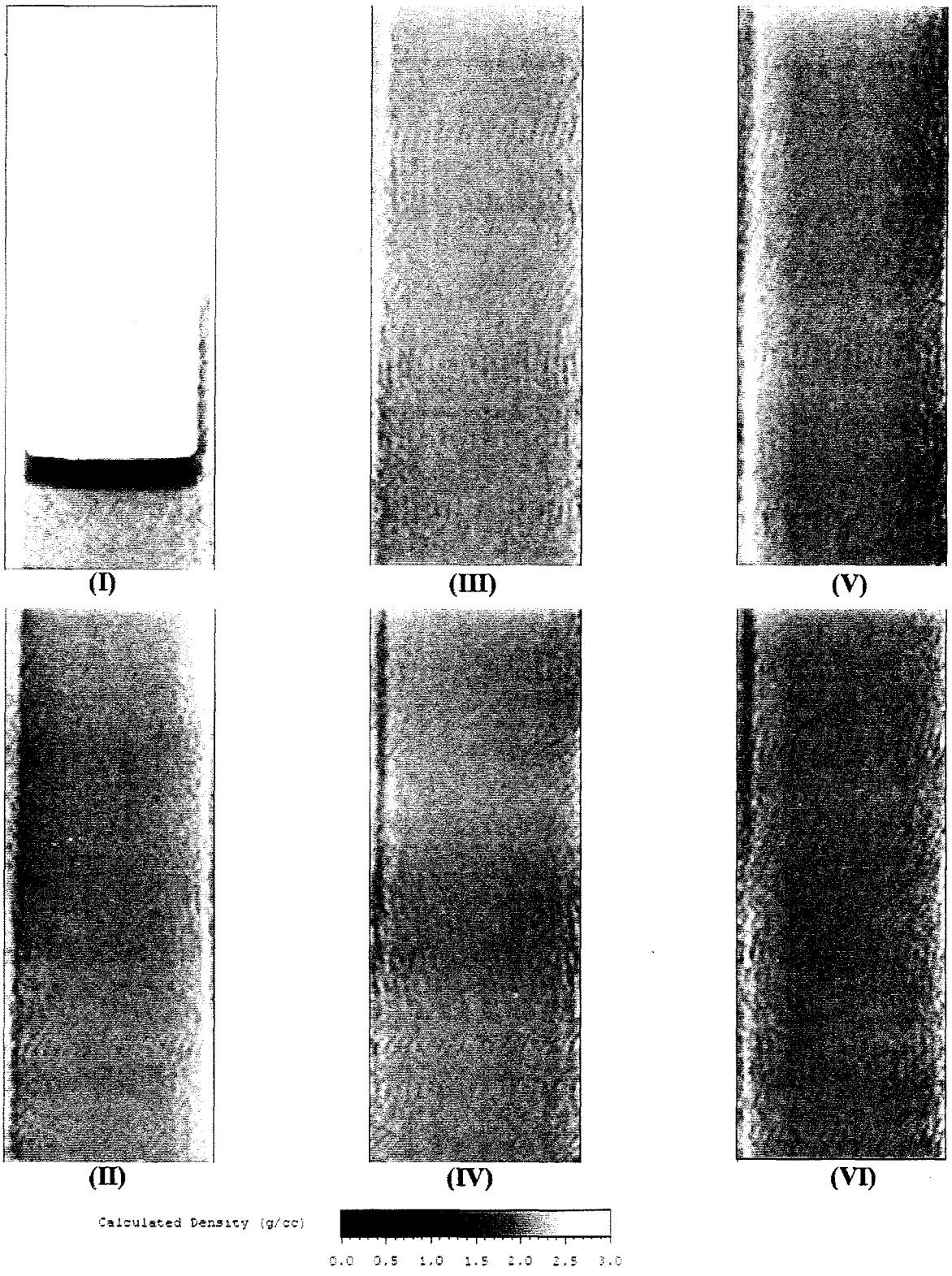

Figure 4.28a. Density Image Calculated from X-Ray Images of Segment 5, Riser 21A, Tank AN-103

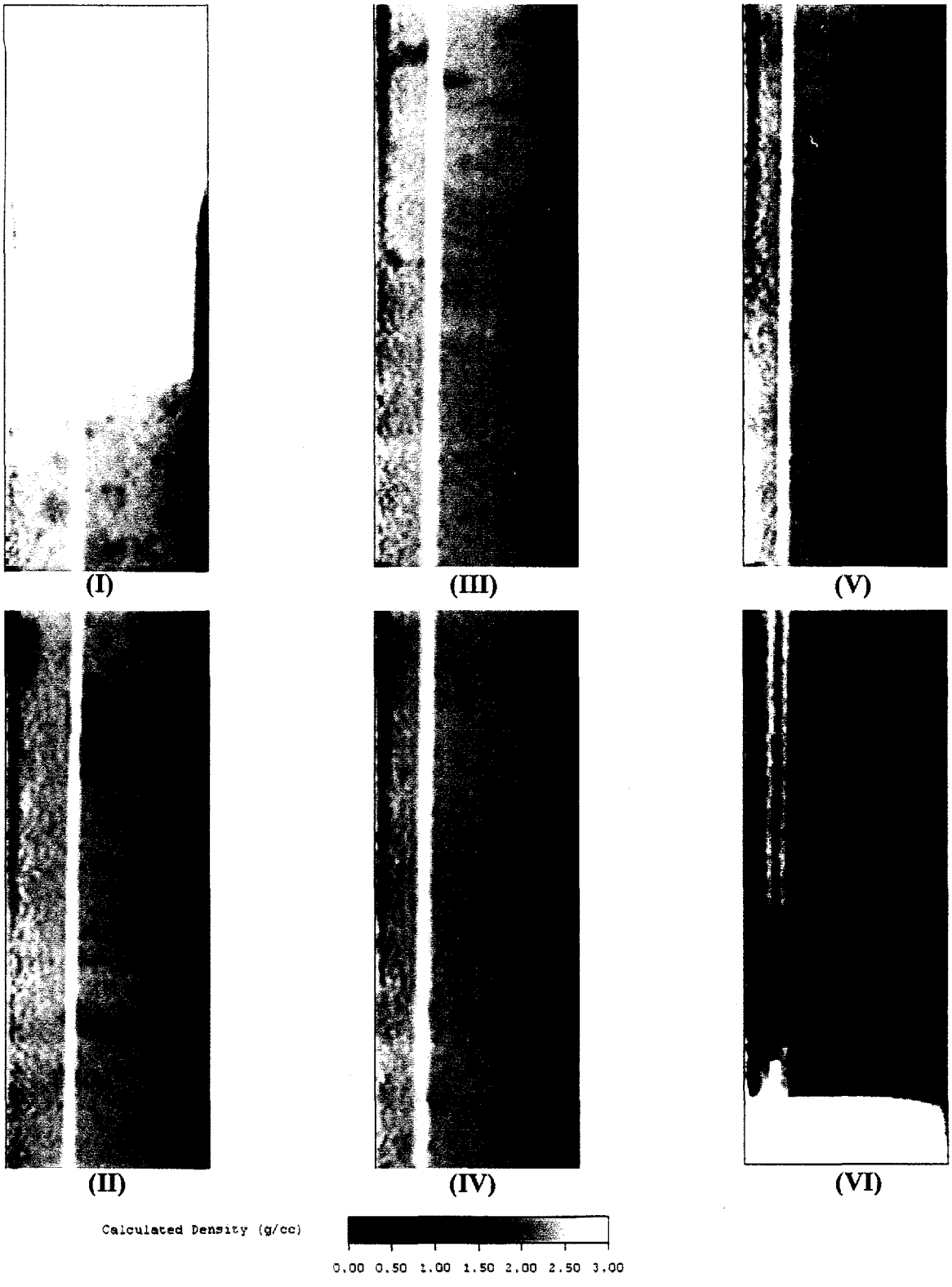

Figure 4.28b. Density Image Calculated from X-Ray Images of Segment 16, Riser 21A, Tank AN-103

Table 4.49. Summary of Observations from X-Ray Images for Tank AN-103

Segment	Comments/Observations
12A-2	Fairly homogeneous sample, changes composition at about L=1 ft. Looks like a slightly higher density plug on top of liquid sample. Large 3-in. void below piston.
12A-5	Homogeneous sample, small void below piston.
21A-13	Many small, medium, and large bubbles and voids, large void below piston.
12A-14	Many small irregular shaped voids, two large irregular voids near top of sample. Very small void below piston.
21A-16	Many small bubbles throughout, small void below piston.

We therefore conclude that the retention mechanism of the gas phase within the waste in this tank is different from that in Tank A-101 wastes.

4.5.8.2 Waste Density

Similar to the previous three tanks, the density was found for several RGS segments taken in this tank. Table 4.50 is a summary of the findings for those segments for which calibration data were available. The density of the five segments in the nonconvective layer, as shown in the table, range from 1.85 to 2.06 g/cc with a mean of 2.01 ± 0.18 g/cc (mean standard deviation of ~8.6%).

4.5.9 Other Discussion of RGS Results for Tank 241-AN-103

4.5.9.1 Effects of Sample Processing

It is worth noting that the RGS void fractions in Figure 4.27 are in no case higher than those measured by the VFI. This was not so consistently the case in the previous tanks. A hypothetical explanation of the low void fractions measured by RGS (compared to VFI data) might lie in the long lag times (Table 4.41) between sample acquisition and sample extraction. All of the samples had lag times of 34 days or more; it could be theorized that gases in the samplers (which

Table 4.50 Summary of X-Ray Densitometry Results for Tank AN-103

Segment	Mean Density (g/cc)	Density STD (%)
12A-2	2.07	8.1
12A-5	2.12	6.4
21A-13	2.01	11.1
12A-14	1.85	8.7
21A-16	2.06	8.4

were under pressure) leaked out, lowering the apparent void fractions. However, these samplers had shown acceptable leak rates during acceptance testing and, if those leak rates were maintained, the leakage would have been negligible.

Some of the difference between VFI and RGS could be lateral variability. Core profiles (a) show that while the nonconvective layer was composed of moist salt and wet salt at risers 12A and 21A, where RGS samples were taken, there was wet sludge from the top to the bottom of the layer at riser 7B (according to a 1986 core). This kind of difference in waste type might cause substantial variation in gas retention.

Another processing issue is the loss of the J3 canister of segment 5. This made ammonia estimation impossible and caused the insoluble gas to be underestimated by the amount in J3. Based on the distribution of gas between canisters J2 and J3 of segment 10 (also nonconvective), the gas losses might have ranged from 10 to 25% depending on the species.

4.5.9.2 Crust Data

Segment 12A-2 was part of the crust.. Its composition is comparable to the compositions of segments 12A-14 and 21A-16, in the nonconvective lower layer of the waste. Its gas content (in μmol/L) is about the same as that of 12A-14; the in-situ void fractions of 12A-2 and 12A-14 would be equal, within instrument error, if both segments were at the same pressure. In calculating the in-situ void fraction and volume, segment 2 was considered to be at atmospheric pressure. If, instead, the pressure was assumed to be that of the hydrostatic head of the bulk waste above the segment's center, the in-situ void fraction and volumes of segment 2 would decrease by about 6%.

4.5.9.3 Constituent Ratios

Table 4.51 shows the ratios of the major chemical constituents of the insoluble gas in Tank AN-103. The ratios are consistent within the convective and nonconvective layers, and the crust ratios strongly resemble those of the nonconvective layer.

Another feature of the AN-103 RGS data is the similarity of the N_2/Ar and N_2/O_2 ratios for two segments to the ratios for air. This is the result more of low nitrogen content, specifically for segments 5 and 10 (both supernatant), than of unusually high oxygen. This apparent contamination with leaked air (or entrained but unreacted air) probably did not occur during the extraction process. This is indicated because the O_2 mol% in each canister decreases from J1 to J3 (Table C.5.7) rather than increasing, as would result from inleakage.

Table 4.51. Constituent Ratios for Tank AN-103

Segment	N_2/H_2	H_2/N_20
12A-2	0.55	8.8
12A-5	11	1.7
12A-14	0.78	11
21A-10	9.9	1.5
21A-16	0.48	16

(a) Mousel, A. 1997. "AN-103 PMCS Core Profile." File AN103.CRD, created November 1, 1996, transmitted to L.A. Mahoney March 12, 1997.

4.6 Overview of All Tanks

4.6.1 Entrained Gas and Oxygen Reaction

The subject of RGS sample contamination by air or argon, entrained at sampling time, has already been discussed under individual tanks. A more encompassing examination has been reserved for this five-tank overview section.

The sampler "interface" volume into which gas can be entrained consists of spaces within the valve body. Laboratory tests, as well as volume calculations from design drawings, estimate a maximum interface volume of ~6 cc.(a) It appears that not all the gas entrained into this volume enters the RGS sample. Samplers that have been prepared in helium-filled gloveboxes and sealed with vacuum grease to keep the helium in the interface volume, have been used both in laboratory tests and in most recent RGS sampling campaign in Tank U-103. The results have been consistent with helium contamination volumes ranging from about 1.8 cc to 3.9 cc. (a)

The data from the five tanks covered in this report are also consistent with an entrainment volume of 2 to 4 cc entering the sample. Figure 4.29 is a plot of oxygen/argon concentration data versus lag time for all five tanks. The Y axis of this plot is in terms of "Equivalent O_2" concentrations, or (O_2+Ar/4.7). This sum includes O_2 from air, the associated N_2, and Ar scaled to put its volumetric contribution on the same basis as that of O_2.

The figure shows that nearly all of the five-tank data are within the same range of volume as the He backfill data. In most cases, the few samples with high values -- A-101-2, AN-105-15, AW-101-18, AN-104-17 -- are suspected to have suffered from air inleakage during extraction. This suspicion is based on the samples' typical tendency to show an increase in the mol% of O_2 with each successive canister extracted (see Tables C.n.7 in Appendix C).

Note that the preceding discussion of entrained volume depended on the assumption of N_2/O_2 equal to 3.7. Reacted air would have a different ratio. The possibility that entrained air has substantially reacted with sample waste cannot be conclusively proved or disproved from RGS data. Figure 4.30 shows the concentration of O_2 versus lag time. The plot shows considerable scatter and a slight overall tendency for O_2 to decrease with longer lag times. Considering the scatter, it is difficult to justify assuming that reaction rates were high enough to produce large increases in the estimated entrainment volumes, compared to those in Figure 4.29. Thus it seems likely that the assumption of near-atmospheric N_2/O_2 ratios is appropriate.

(a) Cannon NS. March 1997. *Retained Gas Sampler Interface Volume.* Letter report HNF-SD-WM-CN-092, SGN Eurisys Services Corporation, Richland, Washington.

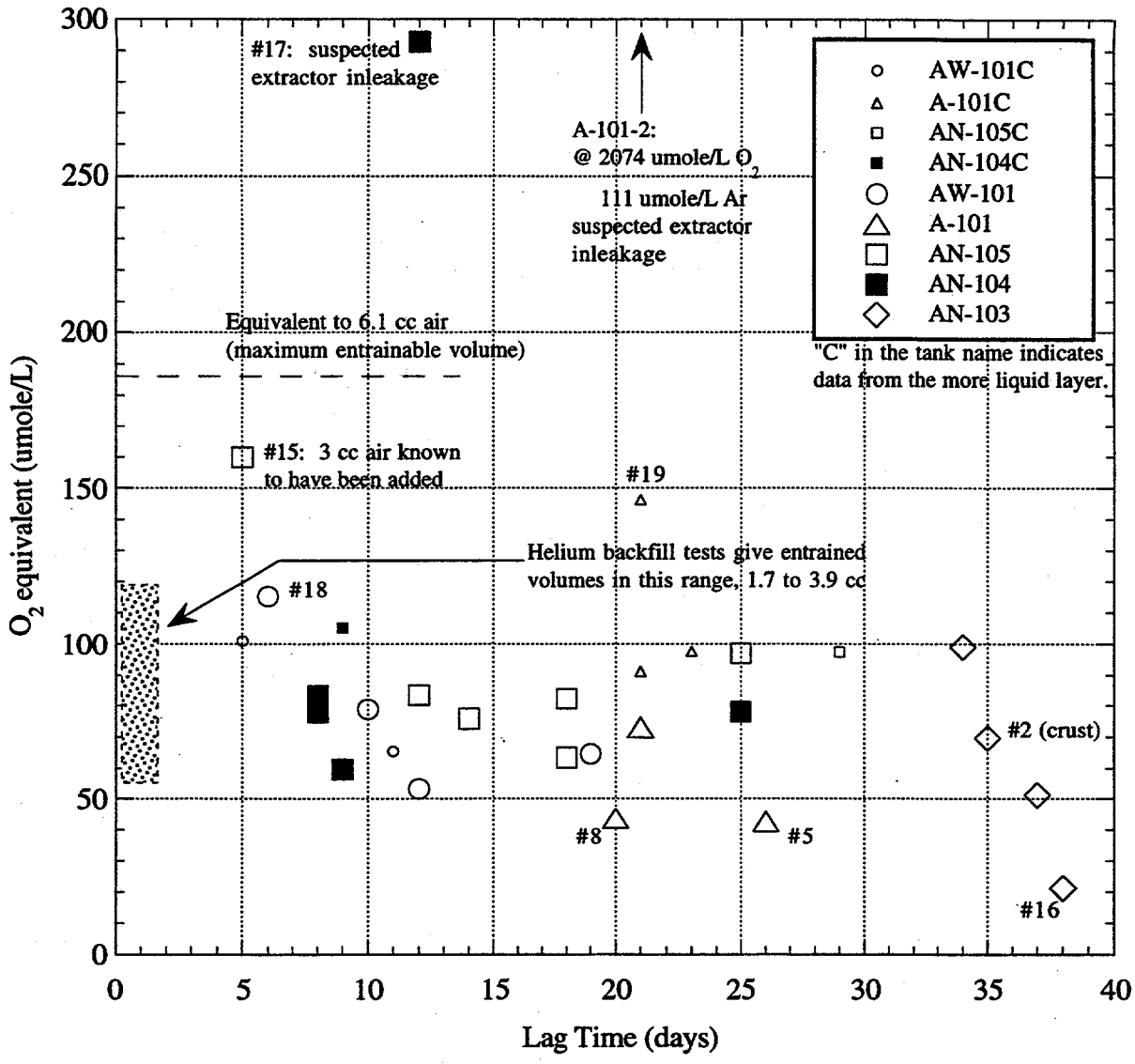

Figure 4.29. Equivalent Entrainment Volume Related to Lag Time

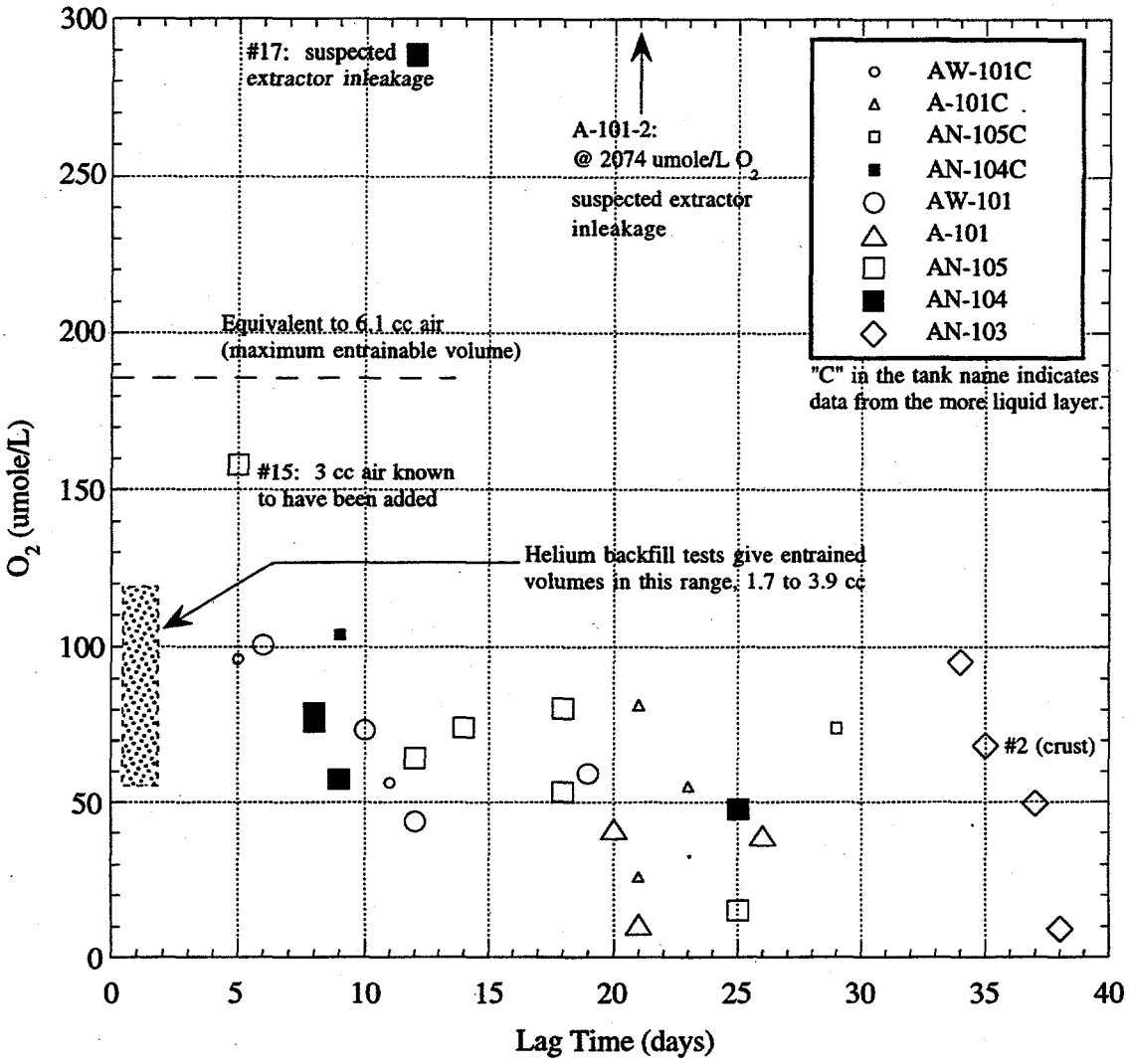

Figure 4.30. Oxygen Related to Lag Time

4.6.2 Five-Tank Data Observations

Observations made following a review of the RGS data presented in Section 4 include

- The mole fractions of several gas species for the convective layers of each tank appear to be significantly different than those for the nonconvective layers. The entrainment-corrected species mole fractions for nitrogen, hydrogen and nitrous oxide are presented for all five tanks in Table 4.52. In practically all cases, the nitrous oxide fraction increases and the hydrogen fraction decreases for the convective layer in each tank, compared to the nonconvective layer. This difference may be partly due to the fact that nitrous oxide has a greater solubility than hydrogen: the hydrogen gas bubbles which are generated collect in the nonconvective layer, while the dissolved portion of the nitrous oxide is distributed more evenly throughout the liquid in the tank.

- The RGS data for two of the tanks suggests that there may be significant lateral variations of void fraction and gas composition. For example, the void fractions and hydrogen concentrations in Tank AW-101 are substantially higher, at similar elevations, for samples taken from riser 24A (segments 17, 19, and 21) than for those taken from riser 24B (segments 18 and 22). This variation may be real: the core profiles for risers 24A and 24B, obtained from characterization of push mode samples,[a] indicates that the nonconvective layer was wet sludge at riser 24A and wet salt at riser 24B. Tank AN-105 also displays lateral variation, with higher H_2 in riser 12A (segments 17, 19, and 21) than in 7B (segment 18). Here the core profile[a] shows a less distinctive difference. At the pertinent depths, the two risers both contain wet salt and salt slurry.

  The number of RGS samples obtained in each tank is insufficient to quantify the lateral variation. (This is particularly true in Tank AN-104, with only one sample from riser 12A, and Tank AN-103, with only one sample in each riser in the nonconvective layer.) Therefore, care should be taken in using the calculated total tank gas inventories, since they are based on average nonconvective layer concentrations. Accumulated RGS data for many tanks may help show whether significant differences in concentrations between risers are common.

- In contrast, void fraction and gas compositions are expected to be relatively uniform throughout the convective layer in each tank; however, this expectation should be tested. Tanks A-101 and AN-105 both have more than one RGS sample taken from locations which, based on gas retention (in-situ void fraction), could be considered part of a convective layer. The corrected gas compositions for these samples are shown in Table 4.52. Note that the hydrogen gas mole fractions range from 12.1% to 18.4% for Tank A-101 and 17.1% to 22.9% for AN-105. The nitrous oxide mole fractions range from 16.8% to 23.2% for Tank A-101 and 14.3% to 26.3% for AN-105. The corrected void fractions range from 0.3% to 0.6% for A-101 and 0.3% to 0.5% for AN-105. (These differences may be due in part to uncertainties associated with the correction to nitrogen for entrained air.)

RGS results are summarized in Tables 4.53 and 4.54, which describe the nonconvective and convective layers of the five tanks. Tank A-101 stands out in several respects: it contains six to eight times as much ammonia as any other tank (based on current lower-bound estimation methods), and its upper layer contains higher void fractions and percentages of hydrogen. Tank AW-101, by contrast, has lower void fractions and percentages of hydrogen than the other tanks.

Figures 4.31 through 4.35 show a more detailed picture of the characteristics of the tanks, in terms of the elevation profiles of temperature, void fraction (RGS and, except for A-101, VFI data), composition, and top-down cumulative ammonia. The composition is expressed in volume percent (identical to mole percent) of dry, ammonia-free gases that have undergone entrainment correction. The ammonia plot (on the far right of each figure) has, on the x axis, the fraction of the total ammonia inventory that exists above any given elevation (y axis). The fraction is equal to zero at the top of the waste, and to 100% at the bottom. This type of integrated plot would be a straight line if the ammonia concentration were uniform. Instead, it is typically concave upward, suggesting that ammonia concentrations tend to be smaller near the top of the waste.

(a) Mousel, A. 1997. "AW-101 PMCS Core Profile." File AW101.CRD, created June 20, 1996, transmitted to L.A. Mahoney March 12, 1997.

Table 4.52. Corrected Dry Mole Fractions for Nitrogen, Hydrogen, and Nitrous Oxide

			Corrected Dry Mole Fraction (%)		
Tank	Segment	Type	N_2	H_2	N_2O
AW-101	8	Conv.	67.7	26.8	3.0
	17	Non.	60.1	29.6	6.0
	18	Non.	67.1	19.1	8.1
	19	Non.	47.7	43.5	5.9
	21	Non.	57.2	30.7	8.3
	22	Non.	66.2	13.0	14.2
A-101	2	Non.	27.9	63.6	7.6
	5	Non.	15.7	77.2	6.0
	8	Non.	16.3	77.2	5.5
	9	Non.	23.1	70.8	5.0
	12	Conv.(?)	59.8	12.1	23.2
	16	Conv.(?)	60.8	15.1	21.6
	19	Conv.(?)	63.0	18.4	16.8
AN-105	4	Conv.	51.9	22.9	21.7
	15	Conv.(?)	53.1	17.1	26.3
	16	Conv.(?)	65.8	17.8	14.3
	17	Non.	22.2	65.0	11.6
	18	Non.	30.3	54.1	13.6
	19	Non.	21.3	65.0	12.7
	21	Non.	22.1	56.7	20.0
AN-104	3	Conv.	51.1	23.3	22.0
	13	Non.	40.3	41.0	16.1
	15	Non.	32.6	50.6	14.3
	17	Non.	52.1	29.2	15.6
	18	Non.	36.9	45.3	15.6
	21	Non.	20.6	47.3	31.1
AN-103	2	Crust	29.1	62.9	7.1
	5	Conv.	68.6	18.9	10.9
	10	Conv.	65.9	19.2	12.4
	14	Non.	38.3	55.5	5.2
	16	Non.	30.6	64.4	3.9

Table 4.53. Summary of the Retained Gas Sampler Results for Nonconvective Layers

	AW-101	A-101 (upper layer)	AN-105	AN-104	AN-103
Maximum in-situ void fraction	0.044±0.004	0.178±0.011	0.111±0.009	0.133±0.013	0.094±0.012
Average mole% H_2 in free gas	32±2.4	75±3.8	62±3.6	47±3.8	62±6.6
Average mole% N_2O in free gas	7.0±0.6	5.6±0.3	12±0.8	20±1.6	3.8±0.4
Average mole% N_2 in free gas	56±4.6		24±2.0	31±2.9	33±3.7
Lower bound on average mole% NH_3 in free gas	0.06±0.05	2.4±1.3	0.02±0.02	0.02±0.01	0.06±0.03
Estimated H_2 Volume in Layer (STP m^3)	22±3	220±14	97±23	96±12	134±13
Lower bound on total NH_3 in layer (STP m^3)	59±32	280±120	54±46	89±76	92±59

Table 4.54. Summary of the Retained Gas Sampler Results for Convective Layers

	AW-101	A-101 (lower layer)	AN-105	AN-104	AN-103
Maximum in-situ void fraction	0.006±0.001	0.006±0.001	0.003±0.001	0.005±0.001	0.004±0.001
Average mole% H_2 in free gas	26±6.6	16±1.5	24±8.3	25±9.3	18±10
Average mole% N_2O in free gas	1.6±0.5	6.8±0.7	3.7±1.3	4.5±1.7	2.2±1.2
Average mole% N_2 in free gas	69±23	73±8.0	67±32	66±37	76±60
Lower bound on average mole% NH_3 in free gas	0.03±0.01	0.53±0.15	0.01±0.004	0.02±0.02	0.02±0.05
Estimated H_2 Volume in Layer (STP m^3)	5.6±0.8	2.2±0.2	2.4±0.6	2.6±0.4	1.6±0.3
Lower bound on total NH_3 in layer (STP m^3)	61±11	670±180	45±14	54±35	75±150

AW-101

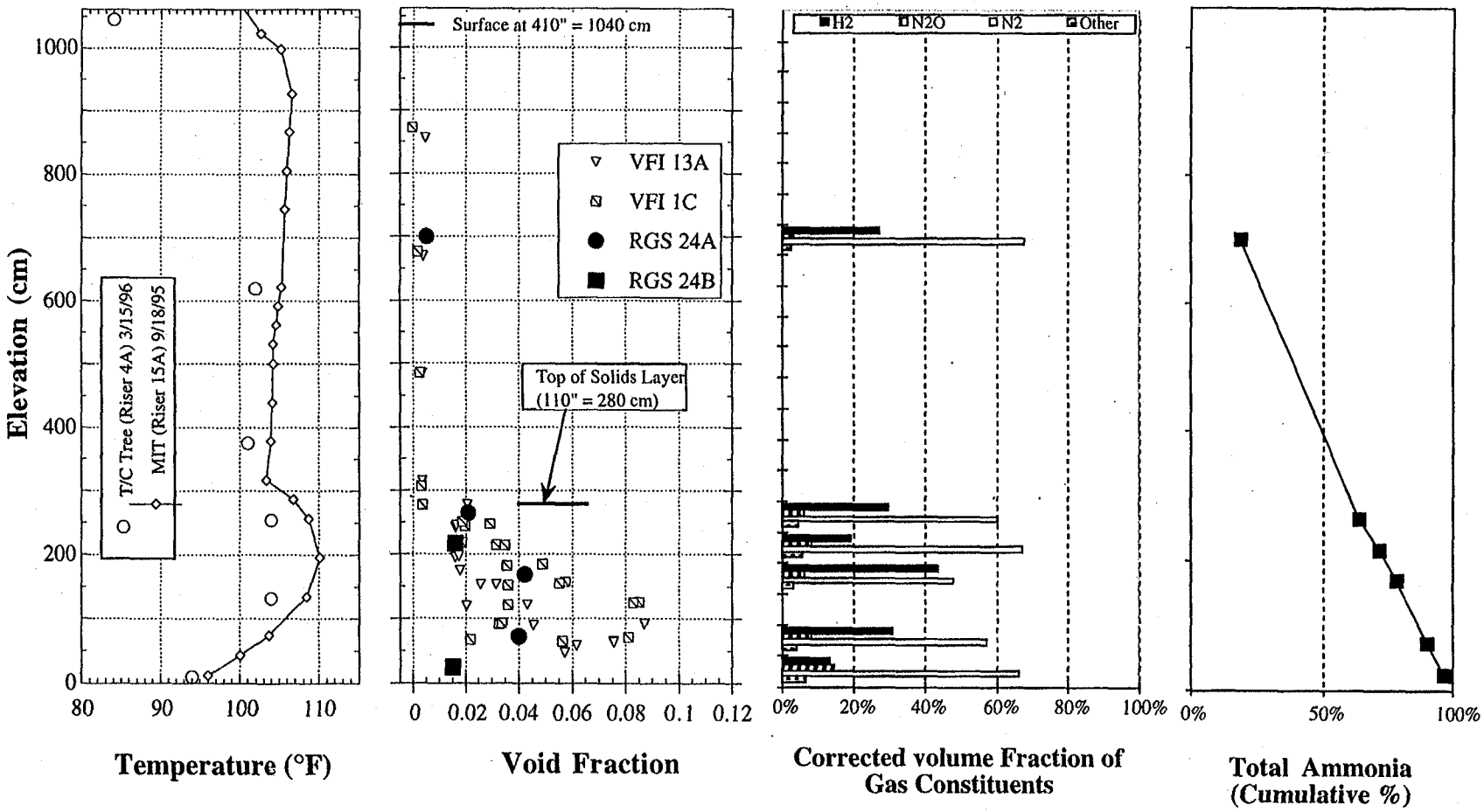

Figure 4.31. Temperature, Void, Composition, and Ammonia Inventory Profiles for Tank AW-101

A-101

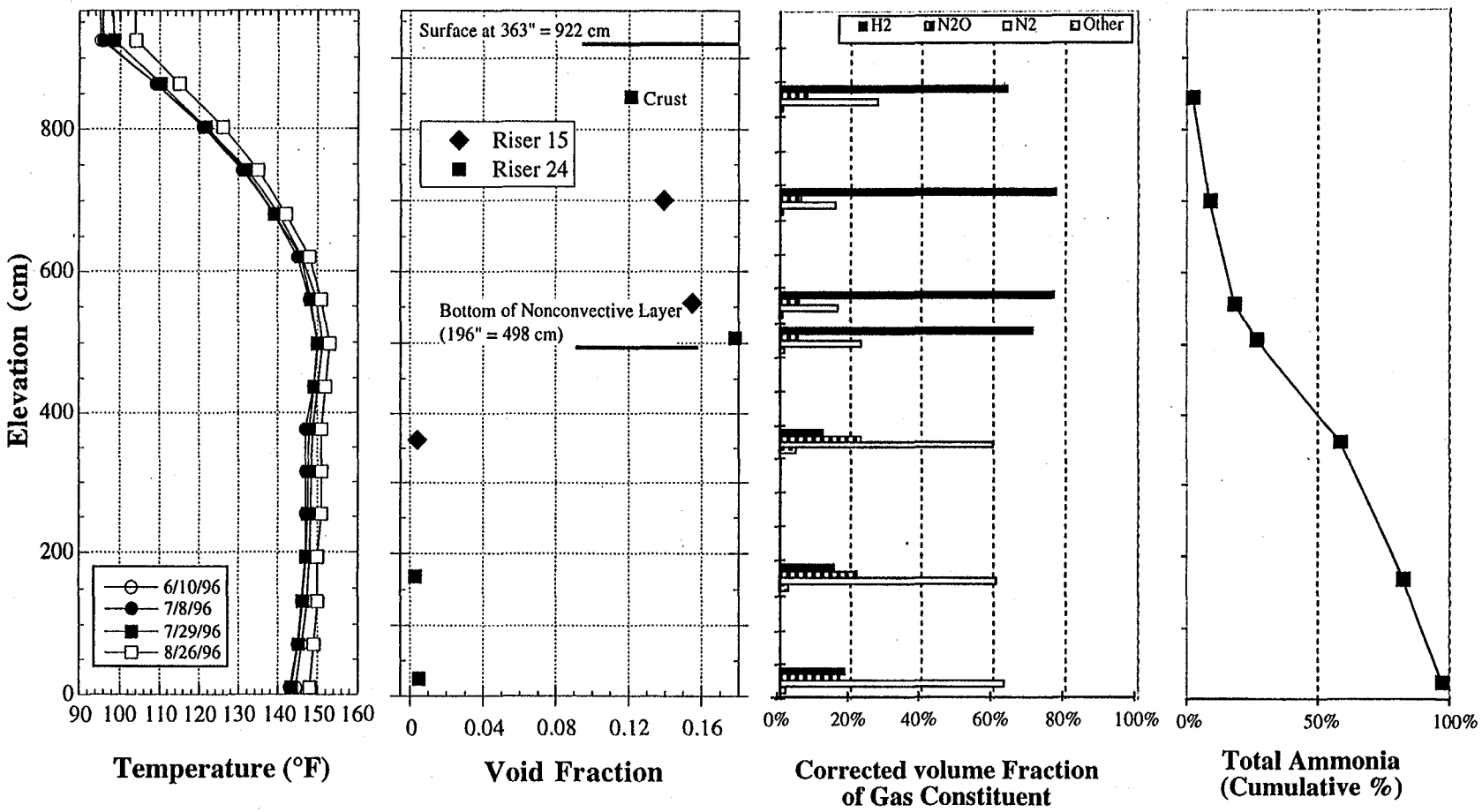

Figure 4.32. Temperature, Void, Composition, and Ammonia Inventory Profiles for Tank A-101

AN-105

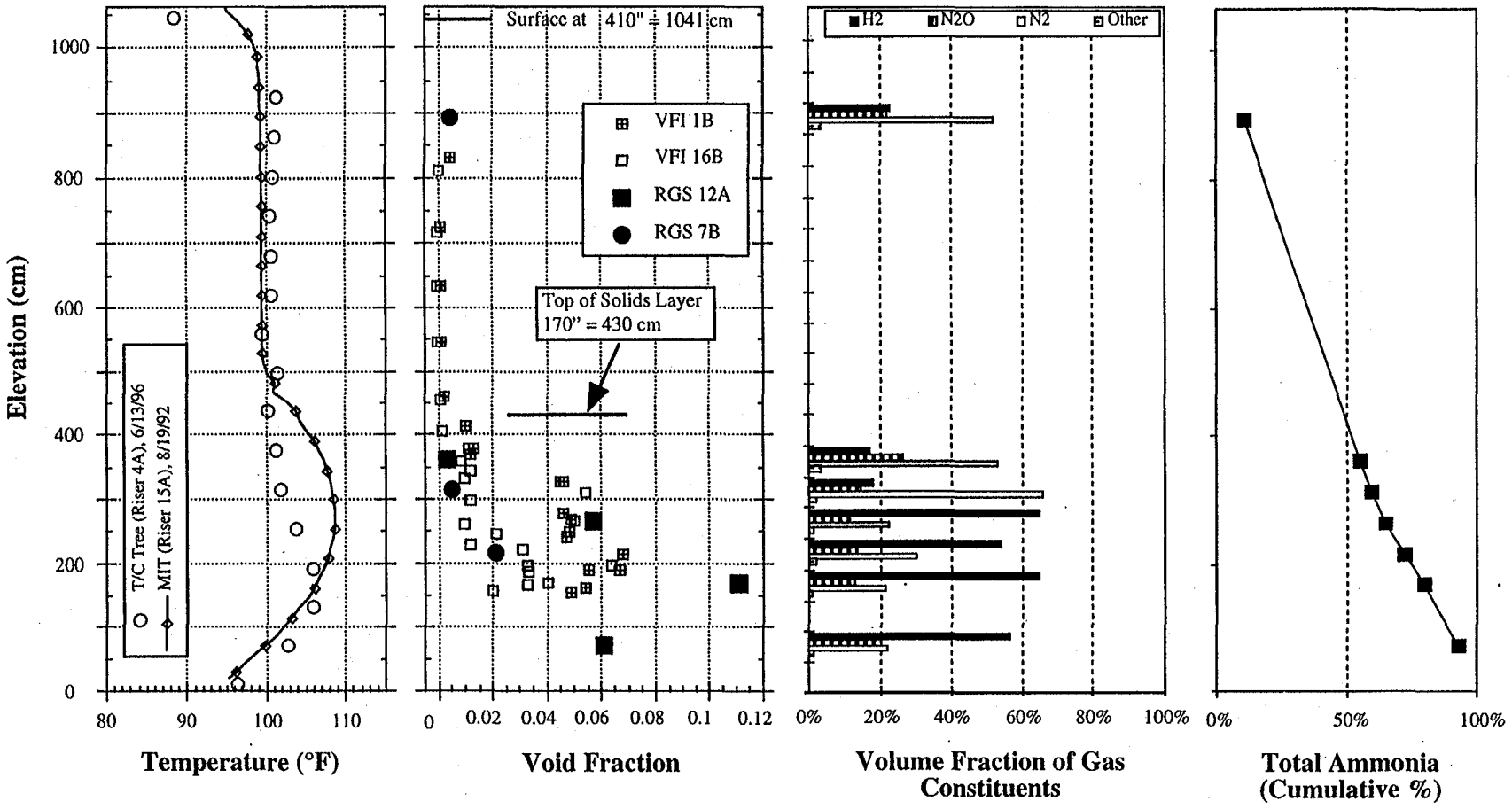

Figure 4.33. Temperature, Void, Composition, and Ammonia Inventory Profiles for Tank AN-105

AN-104

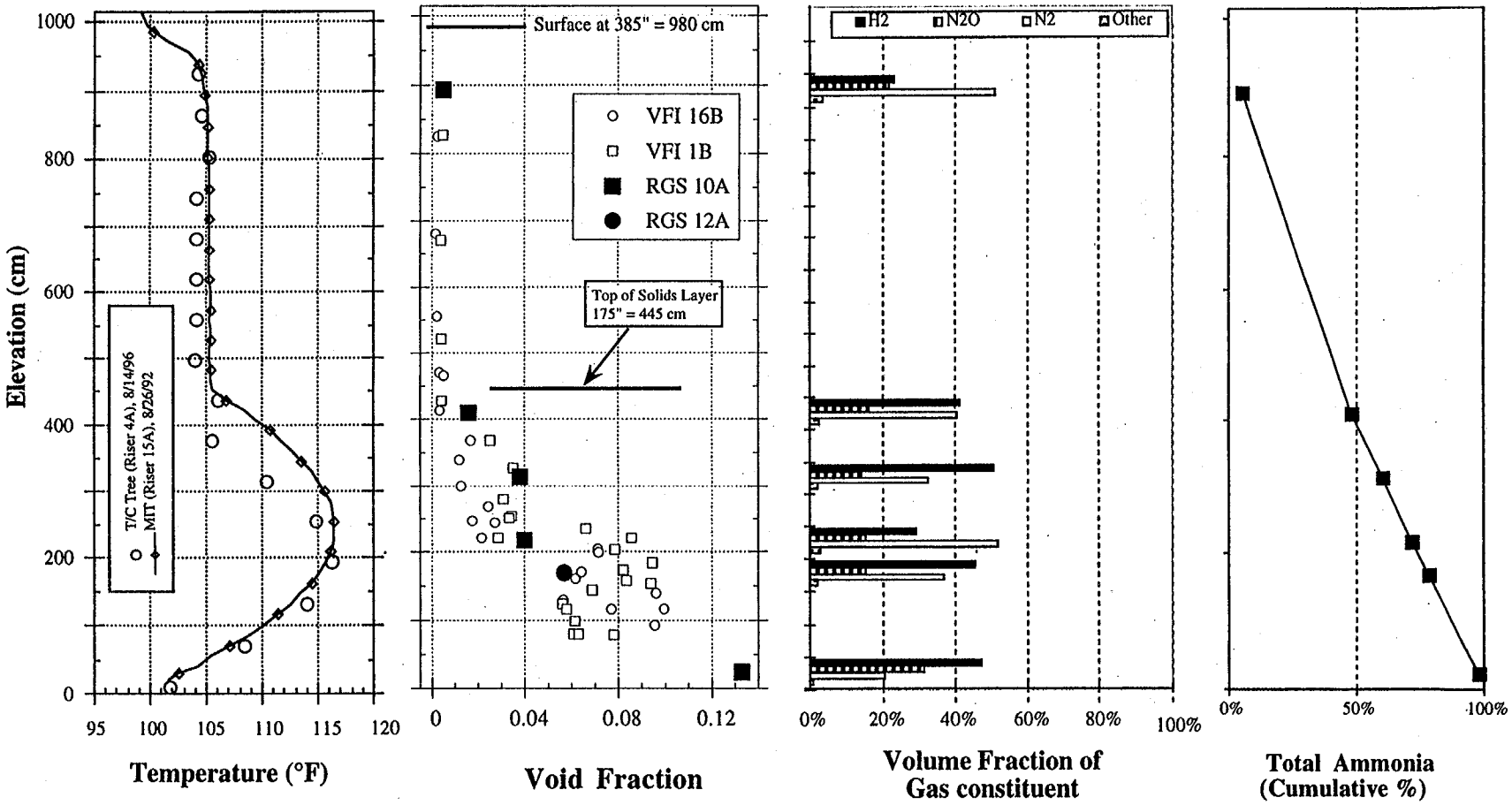

Figure 4.34. Temperature, Void, Composition, and Ammonia Inventory Profiles for Tank AN-104

AN-103

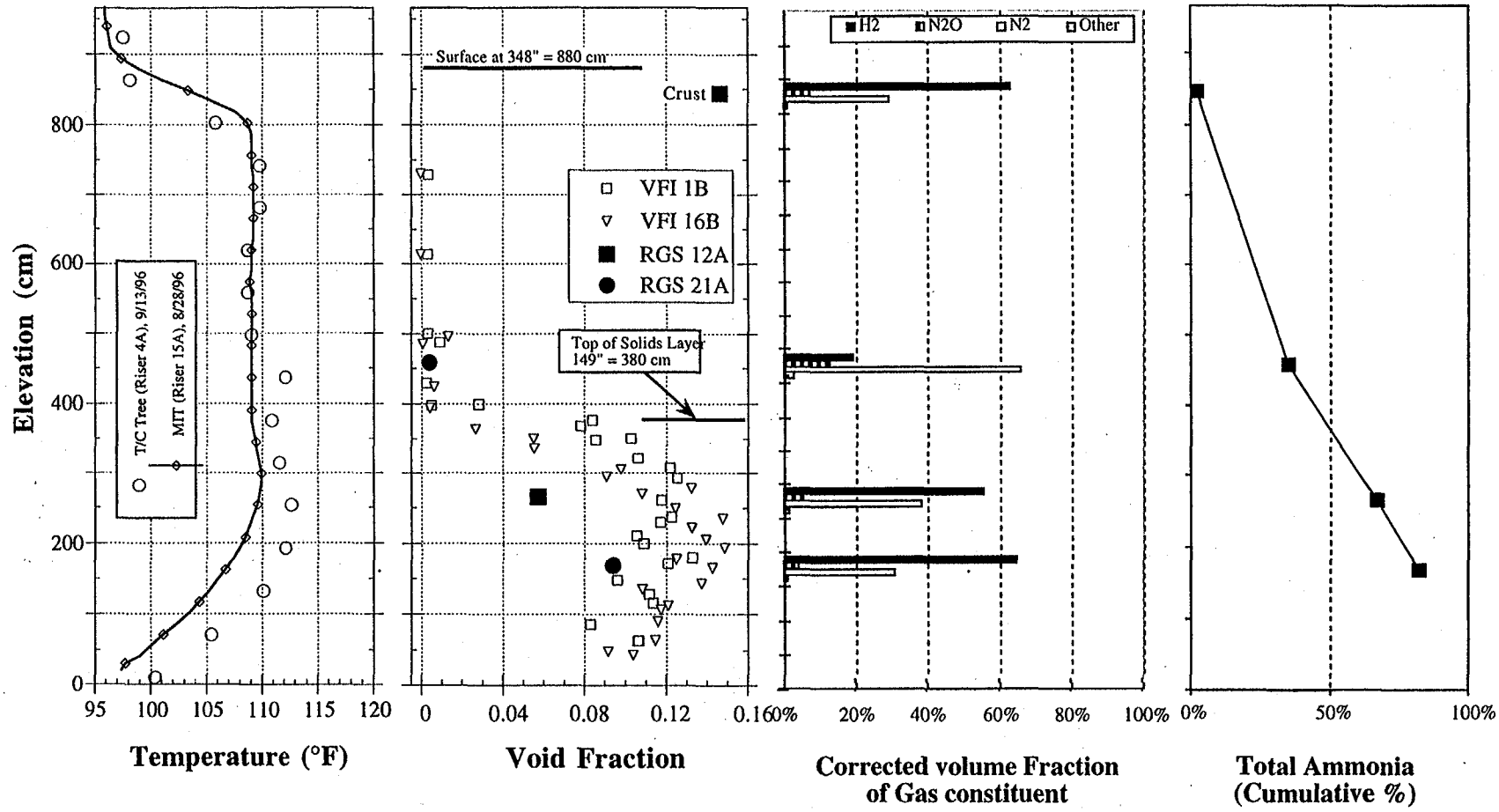

Figure 4.35. Temperature, Void, Composition, and Ammonia Inventory Profiles for Tank AN-103

The RGS and VFI data have already been compared and the differences discussed in Sections 4.n.7. Table 4.55 gives a summary of the RGS-VFI comparisons, broken out by the layers in each tank.

Table 4.55. Comparison of RGS Results with VFI Results (Stewart et al. 1996a)

	Integrated Average In-situ Void Fraction RGS / VFI	Maximum In-situ Void Fraction RGS / VFI	Total Free Gas in Layer (STP m^3) RGS / VFI	Total Free Hydrogen in Layer (STP m^3) RGS / VFI
AW-101 Nonconvective	0.031 / 0.047	0.044 / 0.087	69±11 / 115±12	22±3 / 35±4.6
AN-105 Nonconvective	0.045 / 0.038	0.111 / 0.068	160±37 / 148±24	97±23 / 93 ± 16
AN-104 Nonconvective	0.057 / 0.059	0.133 / 0.099	200±26 / 197±13	96±12 / 92±9.8
AN-103 Crust	0.146 / n/a	0.146 / n/a	48±3.0 / 91±31	30±1.5 / 57±20
AN-103 Nonconvective	0.077 / 0.122	0.094 / 0.15	216±22 / 363±10	134±13 / 222±25

5.0 Conclusions

In Section 4.6.2, we provided a summary of the quantitative results obtained from the RGS for the first five tanks sampled with this device, namely, AW-101, A-101, AN-105, AN-104, and AN-103. The results show the following conclusions, with evidence from various sources discussed throughout the report:

- Local measurements of void fraction with the RGS were consistent for all the DSTs, except AN-103, with the results obtained with the VFI. The highest void fraction was observed to be 0.178 in the upper waste layer of Tank A-101.

- The results consistently showed that more than 16% of the free gas in the nonconvective layer was nitrogen (N_2). The fraction of nitrogen gas is approximately 60% in AW-101. This finding shows that the free gases retained in tank wastes can have substantial nonflammable components.

- Tank A-101 appears to have the highest volume of hydrogen (220 m^3) and ammonia (>950 m^3) gas among the five tanks sampled. Its high ammonia concentrations and location of gas are unique in this set of tanks.

- Nitrous oxide mole fractions in the above tanks ranged between 3.8% in Tank AN-103 to approximately 19% in AN-104. In Tanks AN-104 and AN-105, nitrous oxide was approximated to compose nearly 10% of the gases in solution. The remainder of the tanks had much less dissolved nitrous oxide.

- Based on our measurements, ammonia constitutes more than 85% of the gases in solution. A very small fraction of the total ammonia exists in the form of vapor (gas phase) in the tanks sampled.

- Performance of RGS for measurement of composition of retained low solubility gases was concluded to be acceptable. As a result, such measurements will be carried out for several single-shell tanks at Hanford.

6.0 References

Ashby EC, DA Annis, EK Barefield, D Boatwright, F Doctorovich, CL Liotta, HM Newman, A Konda, DCF Yao, K Zhang, and NG McDuffie. 1994. *Synthetic Waste Chemical Mechanism Studies*. WHC-EP-0823, Westinghouse Hanford Company, Richland, Washington.

Benar CJ. January 1996. *Tank 241-AW-101 Push Mode Core Sampling and Analysis Plan.* WHC-SD-WM-TSAP-024 Rev 0, Westinghouse Hanford Company, Richland, Washington.

Brevick CH, LA Gaddis, and WW Pickett. 1995. *Historical Tank Content Estimate for the Northeast Quadrant of the Hanford 200E Area.* WHC-SD-WM-ER-349 Rev. 0, Westinghouse Hanford Company, Richland, Washington.

Bryan SA and LR Pederson. 1995. *Thermal and Combined Thermal and Radiolytic Reactions Involving Nitrous Oxide, Hydrogen ,and Nitrogen in the Gas Phase: Comparison of Gas Generation Rates in Supernate and Solid Fractions of Tank 241-SY-101 Simulated Wastes.* PNL-10490, Pacific Northwest Laboratory, Richland, Washington.

Bryan SA and LR Pederson. 1996. *Thermal and Combined Thermal and Radiolytic Reactions Involving Nitrous Oxide, Hydrogen, Nitrogen, and Ammonia in Contact with Tank 241-SY-101 Simulated Waste.* PNNL-10748, Pacific Northwest National Laboratory, Richland, Washington.

Bryan SA, CM King, LR Pederson, SV Forbes, and RL Sell. 1996. *Gas Generation from Tank 241-SY-103 Waste.* PNNL-10978, Pacific Northwest National Laboratory, Richland, Washington.

Bunker BC et al. 1995. *Colloidal Studies for Solid/Liquid Separation.* Tank Waste Treatment Science: Report for the First Quarter FY 1995, JP LaFemina, ed. PNL-10762, Pacific Northwest Laboratory, Richland, Washington.

Cannon NS and RC Knight. November 1995. *Retained Gas Sampler System Acceptance Test Report.* WHC-SD-WM-ATR-137, Rev 0, Westinghouse Hanford Company, Richland, Washington.

Cannon NS. 1996. *Retained Gas Sampler System Acceptance Test Report.* WHC-SD-WM-ATR-137 Rev. 1, Westinghouse Hanford Company, Richland, Washington.

Gauglitz PA, SD Rassat, PR Bredt, JH Konynenbelt, SM Tingey, and DP Mendoza. 1996. *Mechanisms of Gas Bubble Retention and Release: Results for Hanford Waste Tanks 241-S-102, 241-SY-103, and Single-Shell Tank Simulants.* PNNL-11298, Pacific Northwest National Laboratory, Richland, Washington.

Gauglitz PA, LA Mahoney, DP Mendoza, and MC Miller. 1994. *Mechanisms of Gas Bubble Retention.* PNL-10120, Pacific Northwest National Laboratory, Richland, Washington.

Hermann C, I Dewes, and A Schumpe. 1995. *Chemical Engineering Science,* 50:1673.

Hey BE. January 1996a. *Test Plan for the Authentic Application of the Retained Gas Sampler System.* WHC-SD-WM-TP-423 Rev. 0, Westinghouse Hanford Company, Richland, Washington.

Hey BE. January 1996b. *Retained Gas Sampler System Operation.* LT-160-101 BU, Westinghouse Hanford Company, Richland, Washington.

Holman JP. 1978. *Experimental Methods for Engineers.* McGraw-Hill, New York.

Krane KS. 1988. *Introductory Nuclear Physics.* John Wiley & Sons, New York, p. 196.

Los Alamos National Laboratory (LANL). 1994. *A Safety Assessment for Proposed Pump Mixing Operations to Mitigate Episodic Gas Releases in Tank 241-SY-101: Hanford Site, Richland, Washington.* LA-UR-92-3196 Rev. 13, Los Alamos National Laboratory, Los Alamos, New Mexico.

McDuffie NG. 1995. *Flammable Gas Tank Safety Program: Data Requirements for Core Sample Analysis Developed Through the Data Quality Objectives Process.* WHC-SD-WM-DQO-004 Rev 2, Westinghouse Hanford Company, Richland, Washington.

Mahoney LA and DS Trent. 1995. *Correlation Models for Waste Tank Sludges and Slurries.* PNL-10695, Pacific Northwest Laboratory, Richland, Washington.

Meisel D, CD Jonah, S Kapoor, MS Matheson, and MC Saucer Jr. 1993. *Radiolytic and Radiolytically Induced Generation of Gases From Synthetic Wastes.* ANL-93/43, Argonne National Laboratory, Argonne, Illinois.

Norton JD and LR Pederson. 1994. *Ammonia in Simulated Hanford Double-Shell Tank Wastes: Solubility and Effects on Surface Tension.* PNL-10173, Pacific Northwest Laboratory, Richland, Washington.

Norton JD and LR Pederson. 1995. *Solubilities of Gases in Simulated Tank 241-SY-101 Wastes.* PNL-10785, Pacific Northwest Laboratory, Richland, Washington.

Ogden DM. 1996. *Thermal Hydraulic Behavior of Tank A-101.* WHC-SD-WM-ER-555 Rev. 0, Westinghouse Hanford Company, Richland, Washington.

Onishi Y, A Shekarriz, KP Recknagle, PA Smith, J Liu, YL Chen, DR Rector, JD Hudson. 1996. *Tank SY-102 Waste Retrieval Assessment: Rheological Measurements and Pump Jet Mixing Simulations.* PNNL-11352, Pacific Northwest National Laboratory, Richland, Washington.

Palmer BJ, CM Anderson, G Chen, JM Cuta, TA Ferryman, and G Terrones. 1996. *Evaluation of the Potential Significant Ammonia Releases for Hanford Waste Tanks.* PNNL-11237, Pacific Northwest National Laboratory, Richland, Washington.

Person JC. 1996. *Effects of Oxygen Cover Gas and NaOH on GAs Generation in Tank 241-SY-101 Waste.* WHC-SD-WM-DTR-043, Westinghouse Hanford Company, Richland, Washington.

Press WH, BP Flannery, SA Teukolsky, and WT Vetterling. 1989. *Numerical Recipes: The Art of Scientific Computing.* Cambridge University Press, Cambridge, UK.

Schumpe A. 1993. *The Estimation of Gas Solubilities in Salt Solutions.* Chem. Eng. Sci., Vol. 48, p. 153.

Shekarriz A. 1994. *Retained Gas Sampler Flow Visualization Guide.* PNL-10138, Pacific Northwest Laboratory, Richland, Washington.

Stewart CW, JM Alzheimer, ME Brewster, G Chen, RE Mendoza, HC Reid, CL Shepard, and G Terrones. 1996a. *In Situ Rheology and Gas Volume in Hanford Double-Shell Waste Tanks.* PNL-11296, Pacific Northwest Laboratory, Richland, Washington.

Stewart CW, ME Brewster, PA Gauglitz, LA Mahoney, PA Meyer, KP Recknagle, and HC Reid. 1996b. *Gas Retention and Release Behavior in Hanford Single-Shell Waste Tanks.* PNNL-11391, Pacific Northwest National Laboratory, Richland, Washington.

Webb BJ. 1994. *Summary Report on the Design of the Retained Gas Sampler System.* WHC-SO-WM-ER-387, Westinghouse Hanford Company, Richland, Washington.

Weisenberger S and A Schumpe. 1996. *Estimation of Gas Solubilities in Salt Solutions at Temperatures from 273 K to 363 K.* AIChE J., 42(1):298-300.

Welsh TL. 1991. *Tank 241-AW-101 Characterization Results.* WHC-SD-WM-TRP-055 Rev 0, Westinghouse Hanford Company, Richland, Washington.

Appendix A

Retained Gas Sampler System Details

APPENDIX A

Retained Gas Sampler System Details

The requirements and functional design criteria for an RGS system (RGSS) have been specified in WHC-SD-WM-FRD-018. A brief (incomplete) synopsis of these criteria, particularly those important to data quality, are given as

- The extractor will have a design life of 30 gas extraction cycles or one year.
- The extractor will be capable of measuring the sample temperature and vapor space temperature over the range of 0–60°C with an accuracy of 2.2°C or better.
- The extractor will be able to measure the vapor space pressure over the range of 0–1.33×10^5 Pascal (0–1000 Torr) with an accuracy of 0.25% of reading or better.
- The extractor and associated analysis instrumentation will measure the void fraction of the sample with an absolute accuracy of 2% (e.g., if the actual void fraction is 20%, the measured void fraction would need to be between 18 and 22%).
- The extractor and associated analysis instrumentation will measure the hydrogen concentration in the collected gas with an absolute accuracy of 2%.
- The extractor and associated analysis instrumentation will measure the concentration of nitrogen, nitrous oxide, and ammonia with a relative accuracy of 20% or an absolute accuracy of 2%, whichever specification is the least stringent for a given case.
- The extractor vessel and lines will have helium leak rates of less than 10^{-6} atm-cc/sec.
- The extractor system will be able to provide a vacuum of 1.333 Pascal (10^{-2} Torr) or better.

The result is the RGSS, which has been designed to satisfy all these requirements. Figure 2.1 in the main report is a schematic of the RGSS assembled in the laboratory prior to deployment in the hot-cell facilities.

Before deployment of the RGSS to 222-S Laboratories[a] for field service, acceptance testing was performed to determine the compliance of the system with the functional design criteria specified in WHC-SD-WM-FRD-018. Results of these acceptance tests are reported in WHC-SD-ATR-137 (extruder results are reported separately in WHC-WM-ATR-495); exceptions to the respective acceptance test plans (ATPs) are also documented in these reports.

A.1 System Description

The RGSS consists of four main elements: the sampler, extruder, extractor, and collector. Each of these subsystems will be discussed individually. Figure A.1 is a drawing of the combined extractor, sampler, and extruder. The RGSS collector is shown in Figure A.2. In the following description of the RGSS, simplified testing procedures are suggested.

(a) Location of hot-cell facilities is in the 200 Area at Hanford, Washington.

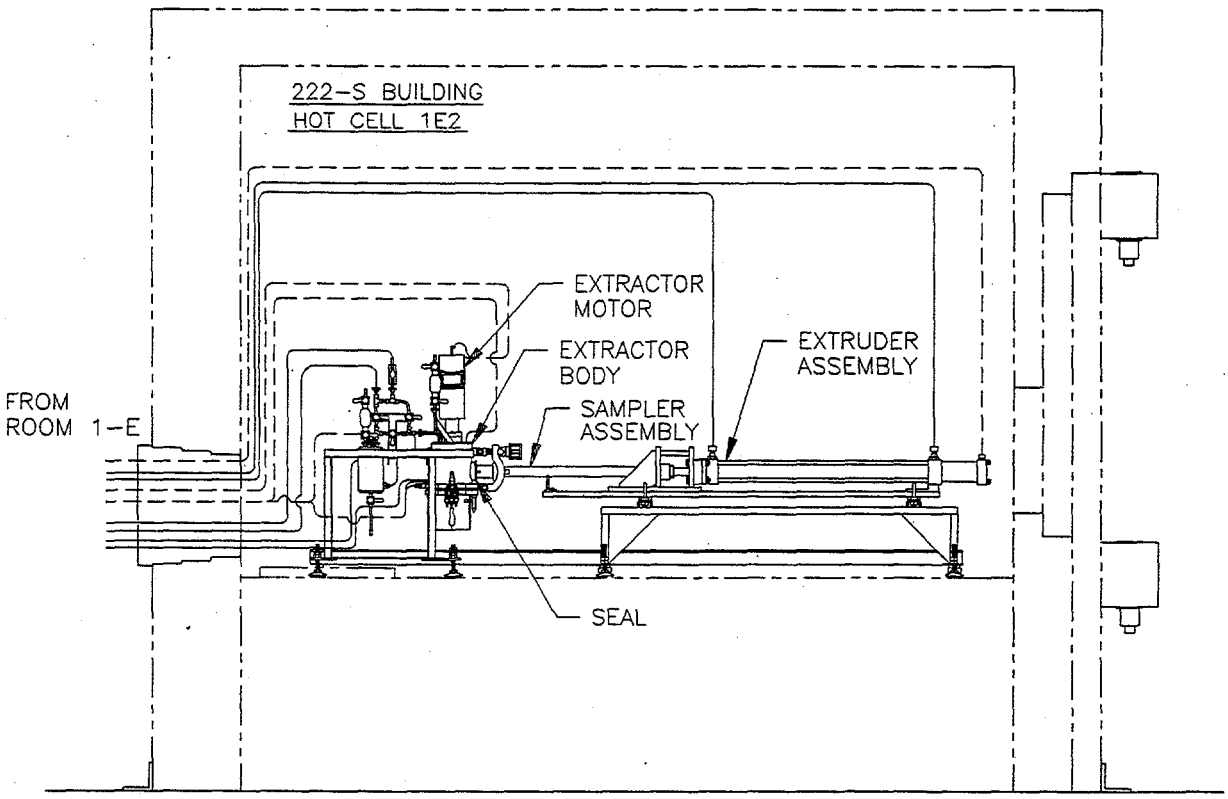

Figure A.1. Schematic of Assembled RGSS

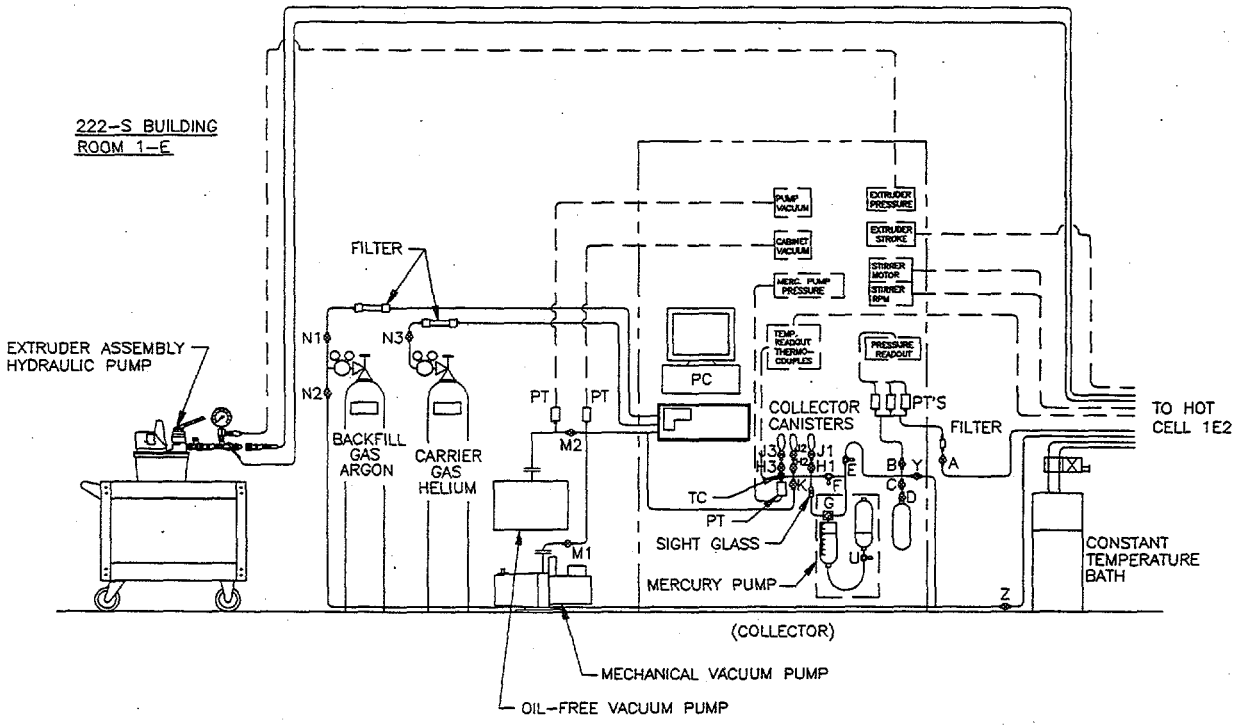

Figure A.2. Drawing of RGSS Collector

The RGS resulted from a redesign of the "universal sampler" already used in Hanford waste tanks. The purpose of the sampler redesign was to make the RGS hermetic or gas-tight so sample gases would not be lost during the delay between tank sampling and sample processing.

A.1.1 Retained Gas Sampler (RGS)

A sketch of the sampler is given in Figure A.3 (simplified from engineering drawings H-2-690140). Some features of the RGS operate exactly as the universal sampler. The sampler uses "keys" to stop the piston at the end of the sample stroke; these keys are left in to keep the piston in place until "piston sleeve" is inserted in the hot cell to perform this function and the sample can be extruded.

The performance of the sampler in capturing a representative sample was evaluated extensively using a transparent non-Newtonian slurry with nonlinear viscosity behavior similar to that of typical gas-retaining sludges in the Hanford double-shell tanks (Shekarriz 1994). In order to ensure that the retained gases are not lost during the sampling process, different sampler bit geometries were tested. Based on this study, a 60° bit angle was recommended, which is the final bit geometry currently used at the end of the drill string during sampling.

The RGS has some extra volume for piston/cylinder tolerances and ball valve operation that can trap atmospheric gases; a portion of these gases can contaminate the waste sample during the sampling process. An analysis in Appendix B suggests that this contamination is always less than 6 mL. Several options are currently under evaluation to minimize this problem, one of which is filling this "trapping volume" with an inert gas (not found in tank samples) and sealing it in place until sampling. However, these techniques have not been adequately tested, and none of them apply to the samplers used to obtain the data reported herein.

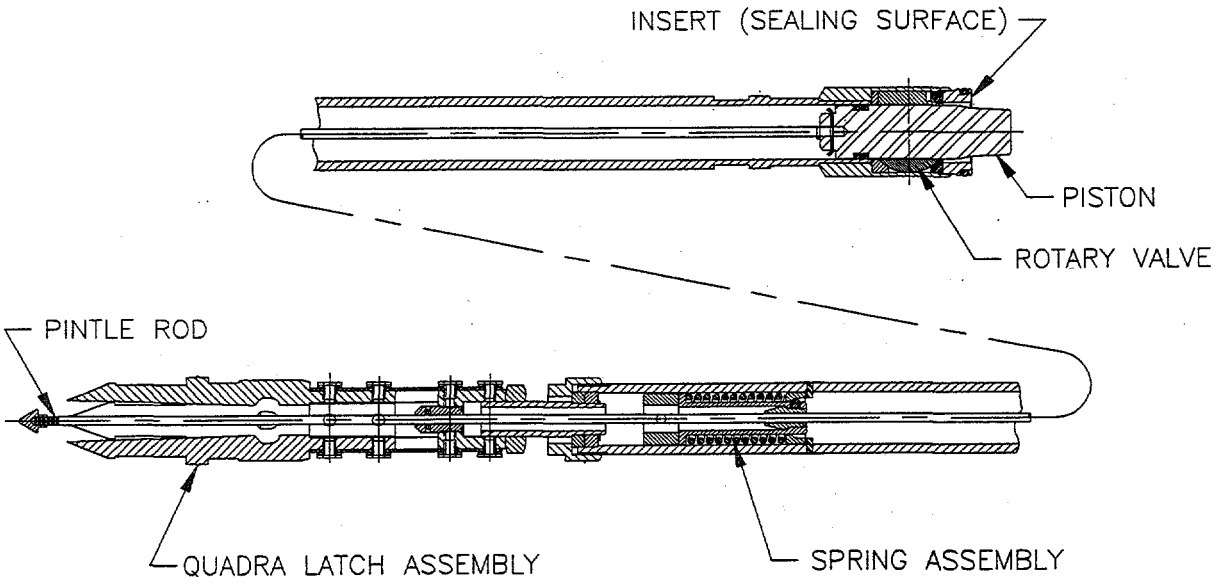

Figure A.3. Schematic Drawing of the Sampler

A.1.2 Extruder

The extruder is a high load (10000 lb) hydraulic ram of 1-inch diameter with a 27-inch stroke; the extruder is designed to push the sampler piston all the way forward to the ball valve, fully extruding the waste sample into the extractor. Some details of the extruder system can be seen in Figure A.1. The extruder ram is mounted on a four-legged table with each leg adjustable in height so that the ram can be leveled with respect to the extractor. The back end of a sampler is slotted into a bracket on the extruder table so that the "press nut" on the sampler holds it in place during extrusion. The front end of the sampler is clamped against the extractor (a seal makes this interface hermetic). A steel bar (bolted at the legs) connects the extruder table and the extractor. The hydraulic power supply is operated from outside the hot cell and is connected to the in-cell extruder ram by lines run through the cell wall.

A.1.3 Extractor

The extractor is designed to provide a hermetic, sealed container in which sample gases can be extracted from the bulk sample. The extractor gases can then be transferred to the collector for later composition analysis. An overview of the extractor subsystem (as part of the RGSS) is given in Figure A.1; more extractor details are shown in Figure A.4. The RGSS extractor subsystem is very versatile and has allowed changes in testing procedures (to meet new needs) with minimal hardware changes.

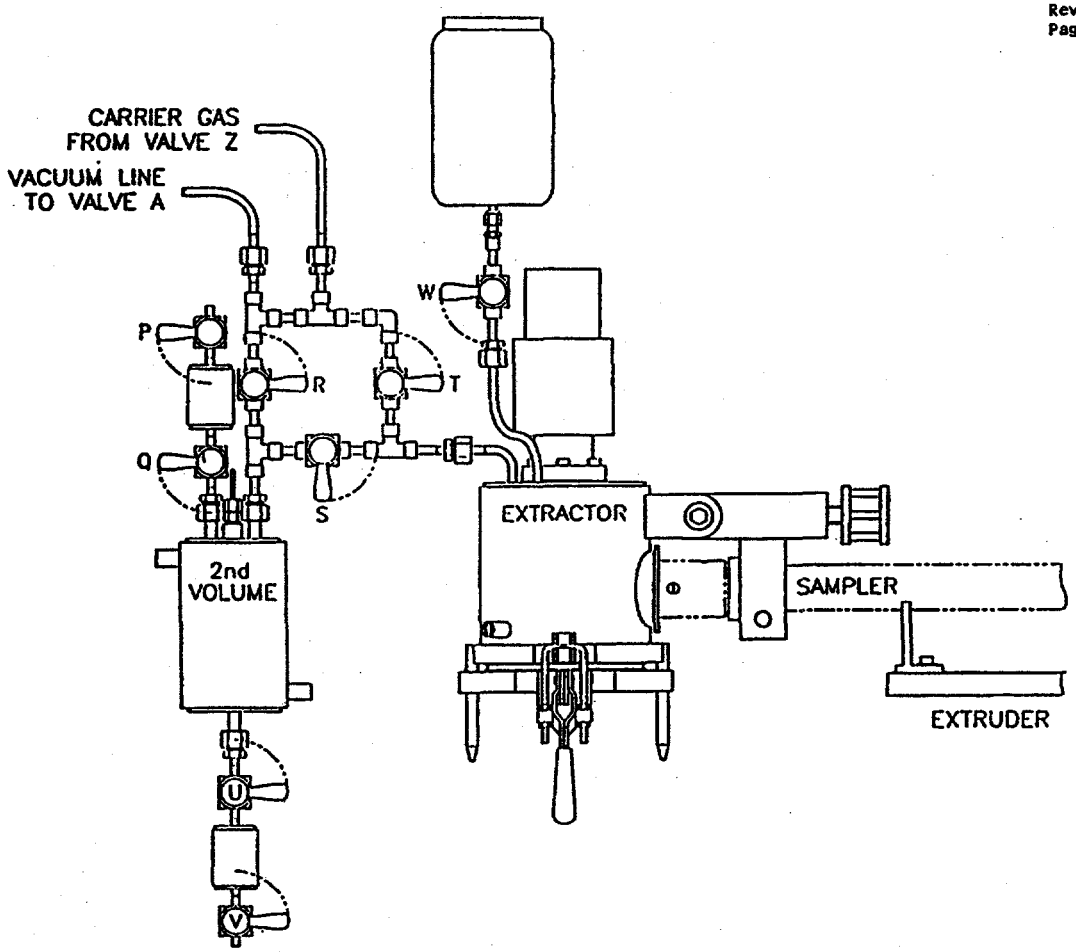

Figure A.4. Schematic Drawing of Extractor

A cut-away sketch of the extractor is given in Figure A.5 (based on drawing H-2-821610). During an RGS test, the sampler is attached to the extractor via a clamp and ring positioner that compress a seal making a gas-tight interface between the sampler and extractor. The base plate of the extractor is removable for removing the waste after an extraction process is complete and cleaning out the extractor with water. The extractor is then dried using dry pressurized air.

To assist in removing the gases trapped in the waste, the sampler is designed to agitate the slurry and to change the slurry temperature. In Figure A.5, a set of impellers is shown, attached to the motor shaft at three different heights, to provide sufficient mixing during extraction. Before the sample is extruded, the motor attached to the mixer blade assembly is turned on at about 3 rpm, providing a torque up to 20 ft-lb in case the slurry has high cohesiveness. A heating/cooling jacket is used for extractor temperature control. The temperature is controlled via a recirculating water system connected to a constant temperature bath. The extractor temperature can exceed 50°C and can be cooled to ambient temperature when necessary.

The RGSS includes ten Type K thermocouples (TCs) for system temperature measurement; nine are located inside the hot cell, and one is installed inside the collector cabinet. Extractor temperatures are measured by six of the TCs; with reference to Figure A.5, two are installed in the base-plate flange at sample level, two are just above the expected waste level surface, and two are installed in the top flange of the extractor (not shown in Figure A.5). Two thermocouples are also installed in V2. All of these TCs (as well as pressure transducers) are monitored by the computerized data acquisition system during testing.

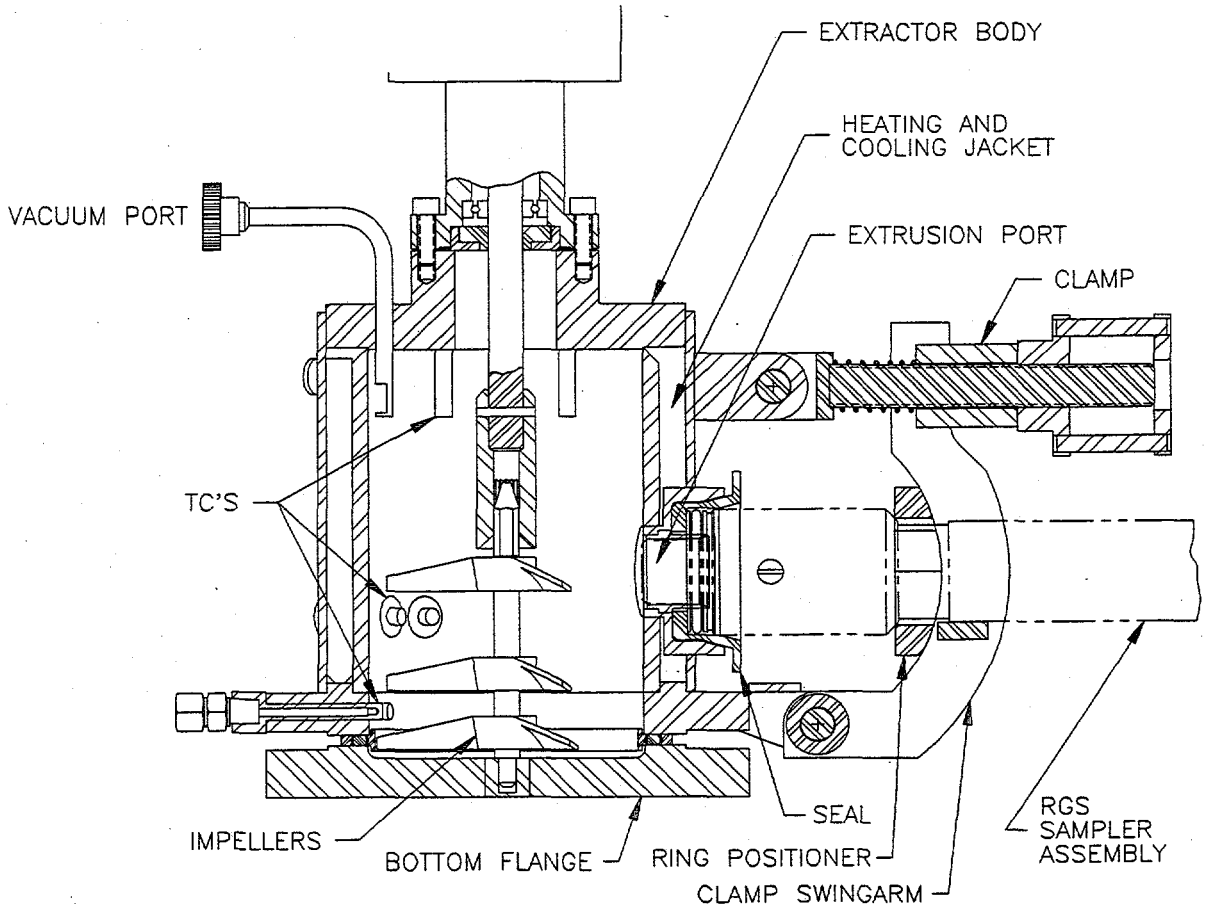

Figure A.5. Cut-Away View of Extractor

Extractor pressure is measured by three pressure transducers located outside of the hot cell beyond Valve A and the radiological filter (see Figure A.2). These transducers are rated to provide 0.25% accuracy and cover three full scale ranges (10, 100 and 1000 Torr).

A.1.4 Collector

The RGSS collector, as shown in Figure A.2, is enclosed in the instrumentation cabinet outside of the hot cell environment. A more detailed sketch of the collector is given in Figure A.6. The mercury (Hg) transfer pump is the heart of the collector, and moves the sample gas from the extractor into one of the collection (J) canisters. The procedure used for collection of the gases will be described in detail in Section A.3. The pressure of the collector-side vessels, J-canisters, are measured using a pressure transducer.

A.1.5 Laboratory Preparation for Deployment

Each sampler is custom-made and tested for quality assurance (QA). The retained gas sampler is fabricated to comply with drawing set H-2-821608, and in accordance with a Fabrication Traveler, which is a check list for inspection of various components and functionality of the sampler prior to field deployment.

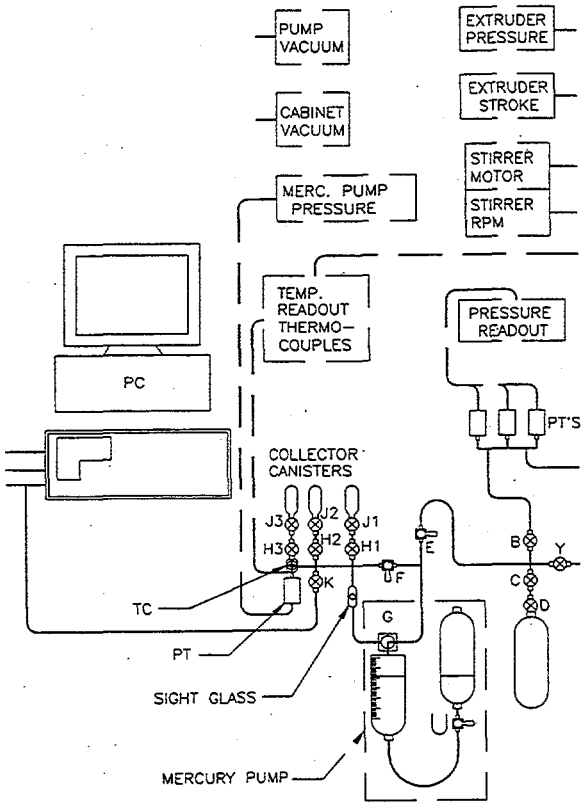

Figure A.6. Details of the RGSS Gas Collection System

Three types of tests are performed on each sampler during the QA testing: 1) water fill test to determine the sampler's internal volume, 2) load tests to verify cable and piston/pintle rod attachment load bearing capability, and 3) helium leak tests to verify seal integrity. During the helium leak test the sampler is internally pressurized with three atmospheres of helium, then placed in a leak detector vacuum chamber and the out-leakage rates measured. The sampler passes this test if the out-leakage rate is $\leq 10^{-6}$ cc/s of helium at STP. After a sampler passes this test, it is ready for deployment.

A.2 Tank to Laboratory Analysis Procedures

In this section, the steps taken to deploy the RGS into the tanks, capture and recover the tank waste sample, and then prepare that sample for quantitative analysis are presented. These steps are divided into the following five time-ordered categories:

A.2.1 Tank Preparation for Deployment of the RGS
A.2.2 The RGS Deployment and Sample Segment Recovery
A.2.3 Tank Farm Handling of "Filled" RGS
A.2.4 "Filled" RGS Retrieval from Tank Farm to 222S Lab

The specific time-ordered steps under each of these categories are presented below. In accordance with the overall objective to establish the capabilities and limitations of the RGSS and its "direct" data, the format used in these subsections is as follows: 1) mention briefly all the steps taken, regardless of how trivial, and provide rough estimates of values whenever possible; 2) identify and expand upon any possible activities that may influence the sampler contents for material loss or gain and changes in state; e.g., sample agitation and temperature variations. For the most part, the discussions of the steps will be brief if further details on the standard operating procedures can be obtained in other references. However, any deviations from the standard operating procedures will be discussed and entered into the tank-by-tank result sections.

A.2.1 Tank Preparation for Deployment of Retained Gas Sampling System

In this subsection, the field procedure steps are summarized, with emphasis on those that may affect the material captured by the RGS. For more details on all the steps for sampler insertion and recovery, see Section 5.2 through 5.6 of Operating Procedure TO-080-503, Rev.C8. Several changes have been made to the insertion and recovery procedure as more has been learned about the RGS and the data needs of the Flammable gas program. The initial version of this operating procedure (used for the first tank, AW-101) was TO-080-503 Rev. C-3, and the last tank, AN-103, used TO-080-503 Rev. C-8.

During the insertion and recovery process certain information is recorded by the operators on a Data Sheet 5 - Core Sampling Data Sheet (see Waste Tank Sampling Procedures) for each sampler. These Data Sheets contain values for specific operational parameters and in some cases additional field notes/observations recorded by the sampling crew. Some of the specific information includes sampler serial number, cask serial number, sample number, time and date of sampling (just after the pintle-rod has been pulled), drill string elevation encoder readings, amount of hydrostatic head fluid added, maximum force to unseat sampler/time, and radiation dose readings through drill string. These specific values are given in the tank-by-tank results section (Section 4) of the main document.

After a specific tank has been selected for push-mode core sampling with inclusion of retained gas sampling, the cognizant engineer (and usually two other members) of the Characterization Field Engineering Group (CFE Group) perform the following steps:

1) Determine Riser Availability: The OBJECTIVE is to locate and assess possible risers for drill truck (external) and ground-to-waste (internal) sampling ACCESSIBILITY. The PARAMETERS determining accessibility are: truck access to the riser, proximity of any high radiation zones, proximity to other instruments in the tank, and other physical obstructions that might prevent successful deployment of the RGS into the tank waste. These parameters are obtained from information appearing in previously written documents and current information gathered by a physical inspection of the tank under consideration.

The types of information obtained from previous documents includes in-tank photos, engineering change notices, surveys, etc. The Tank Characterization Resource Center (TCRC) files and other written sources are used to obtain this information.

The current physical information is obtained by a tank farm surface inspection and in-riser observations. A work package in the Job Control System (JCS) is used to document this information. The in-riser observations are performed by Operations personnel and referred to as part of the "Riser Prep" operation: opening the riser (and replacing the lid gasket if it is asbestos), inserting a "go no-go" gauge (PVC tube) to ensure the drill string can pass through the riser to the waste, and a "zip cord" reading of the actual liquid as well as the sludge (salt cake) levels. (The zip cord method uses electrical continuity to determine the riser-to-waste distance.)

2) Make Riser Selection: Once the prospective risers are identified and determined suitable for core sampling operations, the information is fed back to the program manager, who contacts program office for determination of which risers best meet the needs of the flammable gas program and the retained gas sampling efforts. If possible, three risers on a tank are identified for sampling with two designated as primary sample risers and one as a backup in the event of complications with either of the primary selections. When available, risers are selected to allow sampling from different quadrants and/or radii in the tank to better define horizontal distributions of tank waste and retained gases.

3) Perform Drill String Calculation: A preliminary drill string calculation is done to determine how much drill string to take to the field, and to what elevation to level the truck. Based on tank surface level and riser elevation measurements, the intent is to have a drill string length sufficient to complete a full depth core in the tank waste and to set up a reference elevation accurately. The first core taken from a tank is typically a partial length core such that an integer number of all subsequent full length (19 in.) cores is configured to reach the bottom of the tank (with a planned clearance from actual tank bottom). Details of the drill string calculation are included in Data Sheet 7 - Drill String Calculations Worksheet of the Push Mode Sampling of Hydrogen/Flammable Gas Watch-List Tanks and 241-C-103, WHC TO-080-503, Rev. C-8.

A.2.2 Retained Gas Sampler Deployment and Sample Segment Recovery

1) Sampler Receipt: After the specific tank risers for sampling and RGS deployment elevations and numbers have been determined (typically in the Tank Sampling Analysis Plan [TSAP]), the RGSs will be received by the CFE Group Cognizant Engineer for inspection and checkout. The sampler units have been assembled and inspected in the 306E laboratory prior to deployment to the field. The units pass dimensional and leak check inspections prior to shipment to the field and are again visually inspected in the field prior to use.

The first RGS units deployed had shear wires for tripping the ball valve at the bottom of the sampler. Because there are two "O-rings" on the piston in the RGS, it tends to "stick," i.e., requiring a relatively high force to start the piston moving. Many times when breaking the pistons loose the shear wire would be sheared, making it necessary to partially disassemble the sampler to reinstall a new shear wire. Thus the "breaking loose" of the sampler piston would be done just prior to sending the samplers to the field with the sampling crews.

2) Sampling Truck Deployment: The truck is deployed to the field and setup over the selected riser of the tank to be sampled. At this time the field crew notifies the CFE Group Cognizant Engineer if the value for the "Quill Rod to Riser" distance specified by the preliminary drill string calculation can be met [see Figure A.7 for distance being defined]. There are several reasons that the field crew may not be able to attain this value; and if it cannot be attained, a second calculation is performed to ensure that the proper amount of drill string is in the field. The purpose of the drill string calculation is to have just enough drill string in the field to reach from the top of the riser to the bottom of the tank. (Note that a hydraulic bottom detector is used to detect if an obstacle in the path of the drill string would cause the drill string to break due to excessive axial loading/bowing.)

3) Tank-Farm Operations/ Sampling Crew Operations and Procedures: When the crew arrives at the sampling site, the transport casks (with liners) are already at the site. After the truck is positioned and elevated for drilling operations, the casks are placed within reach of the truck rotating platform, and the RGSs are loaded into casks along with the other universal samplers [see Figure A.7 for reference to component labels mentioned in the following]

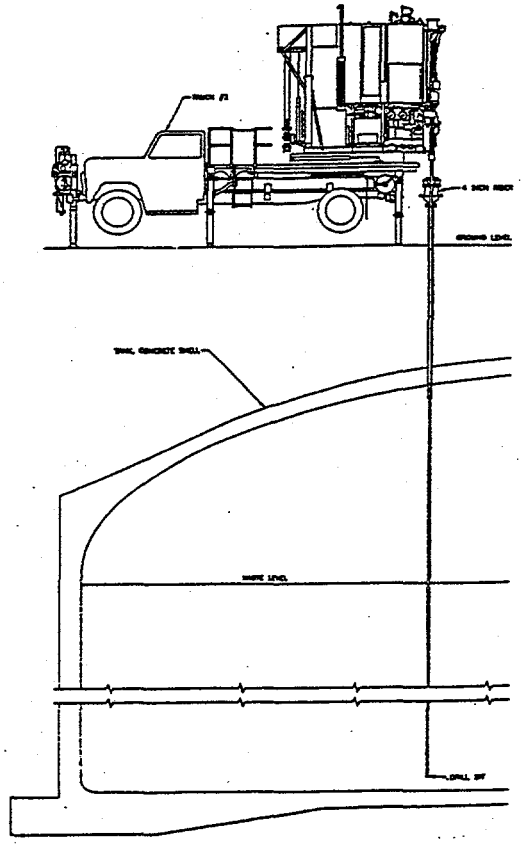

Figure A.7. Sampling Truck Deployment on Waste Tank

3a) RGS "Drop Off":
When an RGS is to be inserted into the drill string, it is picked up from the cask by the remote latch unit (RLU) and loaded into the shielded receiver. (This is the same procedure followed for universal samplers). The rotating platform on the truck is then rotated to the down-hole position, and the shielded receiver is attached to the drill string, which is a length of connected two-inch diameter pipe sections that have been inserted to a level just above the waste. A 19-inch section of drill string is added to the existing drill string, and RLU with the sampler attached is ready to be lowered from the shielded receiver into the tank. (Note that before any section of drill string is used, it is cleaned to ensure no foreign materials are present.)

Before any sampler (plus drill string segment) is pushed into the waste, gas from the drill string is sucked from the sample port on the Kamlok into an organic vapor meter (OVM), which measures total % lower flammability limit (LFL), and concentrations (in ppm) of total organic vapors and NH_3. This information may (or may not) be entered as a field observation on the data sheet. If the flammable gas concentration is <10% LFL, work continues. If the concentration is >10% but <25% of the LFL, work is stopped and the situation is evaluated before work continues. If the %LFL >25, then the standard operating procedure (purge gas procedure TO-020-002) followed during this sampling campaign calls for the use of an argon or argon + CO_2 purge.

[Note that the purge information may or may not be entered as a field observation on the data sheet used during this first RGS campaign. However, a revision 'Da' of the current Waste Sampling Procedure is currently in the approval process. Among other revisions, this latest version of the procedure will require documentation of any purging of the drill string on Data Sheet 1 - Ih&S Vapor and Gas Monitoring, the sheet used by the Industrial Health Technicians. It will contain the following information: tank being sampled, riser being sampled, segment # in the core, time & date, gas used for purge, average purge rate, and time drill string was purged. With this information, the amount of purge gas will be determined. Also on data sheet 1 are the readings for tank dome space flammability at 3 and 20 ft. into the tank, and information on other dome space gases, including organic vapors as well as ammonia. This information will also be in the work package used for the riser prep request.]

After the purge/no-purge step, an amount of fluid (H_2O+LiBr at a nominal 0.3 molar concentration) is poured down the drill string to assure a constant hydrostatic head (amounts dictated by the core sampling information sheet prepared by the cognizant engineer), and then the RLU plus RGS is lowered to the level of the waste to be sampled. The RLU is disconnected from the RGS and retracted back up the drill string into the shielded receiver. The rotating platform is then rotated to the Longyear ® push mode drill hardware and the drill string is then ready to be pushed into the waste by the Longyear hydraulics.

3b) Drill String "Push" & Sample Capture:
When the drill string is being pushed into the waste, the pintle rod stays stationary, causing the piston on the inside of the sampler to move upward relative to the wall of the sampler as the drill string is pushed into the waste. In this way, the desired core sample is captured with minimal disturbance to its in-situ conditions. At the end of the push stroke (a nominal 19 in.), the ball valve of the RGS is closed (by pulling up on the pintle rod, activating the "mouse trap" linkage with spring closure of the bottom ball valve). This seals the bottom and completes the sample capture process for the RGS. Throughout the insertion of the drill string, the down force required to push the drill string sections is continuously monitored. A record of this force per unit time is recorded on a strip chart, and this record has potential to provide some useful information about the nature of the waste.

3.c) RGS Recovery:

After the pintle rod is pulled, the rotating platform is rotated into to the sampler recovery position. Another gas sample is drawn from the drill string to ensure that the total flammable gas concentration is not above 25% LFL. Once the operating conditions are deemed safe, the RLU is sent back down into the drill string and attached to the RGS. After the RLU is attached, an upward force is applied to unseat the RGS and pull it back up the drill string into the shielded receiver. While the sampler is traveling up the drill string, a radiation dose rate instrument is placed next to the drill string just above the ground, and the observed dose rate is recorded. (Note that this measurement is of value to the RGS program in that it gives some reliable indication of the degree of waste recovery in the sampler.)

Before the sampler is retrieved into the shielded receiver, it passes by a glass observation port that enables visual inspection of the sampler to assess if it has been rinsed of unwanted tank waste material. This rinsing naturally occurs when the RGS passes through the hydrostatic head fluid. If needed, the sampler is sent back down into the head fluid for additional rinsing. Note that by following this procedure, no additional amounts of (spray wash) water are added to the tank.

Once in the shielded receiver, the shielded receiver ball valve is closed (to contain the liquid/sludge dripping from the sampler exterior), and the platform is rotated to the X-ray machine. The shielded receiver ball valve is opened and the RGS is lowered into the X-ray machine. After the RGS is x-rayed, it is pulled back into the shielded receiver and then the platform is positioned over the cask. The RGS is then lowered into the shipping cask, and the cask is sealed.

A.2.3 Tank Farm Handling of "Filled" RGS

Procedure TO-080-503 dictates that the sampler be placed in a cask stand next to the truck after the sample is x-rayed. Qualitative X-ray examination of the filled sampler is performed in the field for first indication of the % recovery for the sample and confirmation of proper operation of the sample capture hardware. Observations are recorded on the Chain of Custody form. X-ray analysis is presented in more detail in Section 3.5. Chain of Custody transfer protocols are followed in all subsequent transport/transfer of the sample to the 222S laboratory hot cells for extrusion/analysis. Once an RGS sampler has been successfully retrieved, the crew that does the transporting of the sampler to the lab is notified that there is an RGS sample in the farm ready to be picked up and delivered to the lab for analysis.

The TSAPs originally required that the sampler be delivered to the lab within 24 hours of pulling the pintle rod - this is the time that the sample has been taken and sealed into the sampler. Transportation will deliver the sample to the lab as soon as they can accept it. The lab must abide by their own requirements as to how much radioactive material they can have in their facility. In addition to this they have a limited number of storage locations to store the samplers before they are analyzed. Once delivered to the 222S laboratory, handling and analysis of the sample are as described in the following section II D.

A.2.4 RGS Retrieval from Tank Farm to 222-S Lab

At the completion of the sample recovery operation and the x-ray examination, the"filled" RGS is lowered into the lined shipping cask and the cask is sealed. Although the primary function of the cask liner is to prevent the cask from contamination from any material attached to the exterior of the sampler, the liner also acts to secure the RGS into a vertical position.

There is only one RGS per cask, and to enable the sampling crew to proceed with the next sampler, the filled cask is moved to a nearby (within 100 ft.) staging area and waits for truck transportation to one of the tank farm radiation buffer areas (RBA). The cask remains in the RBA (usually for a few hours) until a complete load of (three) casks are ready for transport to the 222-S Lab. Custody of the cask is transferred to the shipper, and the cask is shipped to the 222-S Lab. Upon arrival at 222-S, custody of the cask is transferred to the 222-S Sample Custodian, and the cask is staged inside the laboratory building until a request for "cask prep"is submitted. Note that throughout the entire transportation process, the RGS is kept in a vertical position. Also note that the period of time between the arrival of the cask at the 222-S Lab. Building and submittal of the cask prep request is sufficient for the temperature of the sample to equilibrate with the "room" temperature inside the building.

Several observations on the sampler handling are provided below:

* For all casks, no residual contamination (i.e., leakage) from the liner to the casks has been observed. Thus any change in RGS sample material would appear in the liner.

* Because the RGS sits well within the liner, it cannot be accessed directly for removal. The technique used is a tilting/ shaking of the liner until the RGS slides out onto the floor of the hot cell.

* After the RGS is removed from the liner, a 10-50 mL amount of "liner liquid" is usually observed, and a significant amount (~100 mL) of caked tank waste is lodged in the quadralatch assembly. Because this assembly is composed of high-carbon steel, and it has been exposed to the corrosive tank waste, it is also observed to be badly corroded. This observation for all of the samples indicates that there is a significant amount of waste material passing between the exterior of the RGS and the interior of the drill string during the sample capture operation. Thus the hydrostatic operation is not accomplishing its intended purpose and may need to be modified.

A.3 Sample Analytical Procedure

After the cask is received, it is prepped for the hot cell and transferred to 1E-2 hot cell airlock. The sampler is then transferred from cask to hot cell. The sampler is then prepped for RGS processing, following the procedure outlined in document LT-160-101, Section 8.

After preparation of the sampler for RGS processing, the sampler is assembled in the RGSS and the sample is extruded into a previously evacuated extractor, and thus far, the pressure within the extractor has remained below 20% of atmospheric pressure, even for samples with the greatest amount of entrained gas. These lower pressure levels enhance sample gas release into the extractor head space during mixing. Once mixing has been completed during a particular phase of the RGS test, the released insoluble sample gases are transferred to the collector subsystem (some soluble gas is usually transferred also).

There are two major phases for the gas extraction process: ambient temperature gas extraction and post heat cycle gas extraction. After the sample has been extruded into the extractor, it is mixed and the released gas transferred to a collection canister (all at ambient temperature). Then the sample is heated to nominally 50°C and mixed again to obtain additional gas release at a temperature closer to the in-situ tank temperature; the sample is then cooled back to ambient temperature, and the sample gases in the extractor are again extracted. The exact procedures used for specific RGS tests will be correlated and described in detail later in this report.

After a sample has been extruded and mixed at ambient temperature (Valve T open, Valves R, S closed), the previously evacuated 2nd Volume (V2) is exposed to the sample by opening Valve R; after equilibrium is approached, the resulting pressure change is used to determine (and separate) the insoluble gas quantity and vapor pressure (using ideal gas law considerations - see WHC-SD-WM-ATR-137).(a) Valve Q on PQ Canister 1 (see Figure A.4) is then closed to take a gas sample for later solution ammonia analysis (to be described in detail later). Then the Hg Transfer Pump is used to transfer the sample gas to the collector for storage in the J1 gas sample canister (as will be described in the next section), completing the ambient gas extraction phase.

Valve R is closed (isolating V2 from the rest of the system), and Valve T is also closed while the extractor is heated to nominally 50°C. (With Valves S and T closed, the extractor is completely isolated from the rest of the system; this is necessary to prevent water condensation at the radiological filter from plugging the line to the collector.) The heating is done using a heater/ chiller (Figure A.5) to move heated water through the extractor water jacket. After maintaining the peak temperature for at least 10 minutes while operating the mixer, the extractor is cooled back to ambient temperature, and valve T is opened.

A second solution ammonia (PQ canister 2) is taken, and the sample gas is then transferred to the collector into the J2 gas sample canister. An additional gas transfer is then performed which usually transfers mostly soluble gas (ammonia) into the J3 gas sample canister. Plots of the pressure variation during the gas transfer process for the J1 through J3 canisters provide information on the gas content of the sample (as described in detail in Section 3). In some cases there was too much sample gas at ambient temperature to fit into the J1 canister, and J2 was also used to store the extra gas; in these cases, there was only one post heat-cycle gas transfer into the J3 canister. The temperatures at the locations mentioned in Section A.1.1.3 are measured during the gas extraction and collection process.

Once sample gas transfer has been completed, V2 is filled with argon or air, Valves R and S closed, and the remainder of the system including the extractor is reduced in pressure (to a little above the sample vapor pressure). Valve R is opened and the resulting change in pressure recorded (along with temperatures). These steps are repeated at least two times, and a calculation of the sample's bulk volume (solids and liquids) can be made from the ideal gas law (see WHC-SD-WM-ATR-137). This completes the RGS test.

Cleanup is performed by removing the base plate flange (see Figure A.5), which also removes the mixer blade assembly. The sample drains into a catch pan from which it is poured into a plastic bottle, with a small portion saved separately for lithium bromide (LiBr) analysis. The level of LiBr found in the sample can be used to determine the maximum amount of drill string hydrostatic fluid (spiked with LiBr to a known concentration) that may have inadvertently entered the sampler.

A water jet is used to wash the remaining sample off all parts of the extractor, then an air jet is used to dry the extractor parts, including inside the housing. Dry argon is blown through the system lines to further dry the extractor and lines, then the base plate and mixer assembly are installed on the extractor, as is the next sampler to be tested. The extractor and V2 are heated toward 50°C (nominally for an hour) as evacuation of the system begins. It is usually necessary to evacuate the system at least four hours (preferably overnight) to reduce out-gassing of residual air and water vapor; if it is not pumped out long enough, the system can appear to fail the leak-rate test due to outgassing even when it is actually leak-tight.

The procedure to collect the gases into the J-canisters is as follows: Valves A, B, E, and H are open; Valve F is closed during a gas transfer operation; Valve G is a three way valve so that

(a) This method is used as a redundancy calculation to the approach described in Section 3.

RES 2 can be opened toward Valve E, or toward Valve H, or closed entirely. The first reservoir (RES 1) is lowered to a position much below the second reservoir (RES 2), so that all of the mercury is in RES 1. Valve G is opened toward Valve E, allowing gas from the extractor to flow into RES 2. Then Valve G is opened toward Valve H and RES 1 is raised above RES 2 to drive the mercury into RES 2. This pushes the sample gas through Valve H into the J canister. When the mercury reaches the sight glass, Valve G is closed; then RES 1 is lowered so that mercury flows out of RES 2. As the mercury drops out of RES 2, Valve G is opened toward Valve E, and extractor gas is pulled into RES 2. This process is repeated about 10 times for each gas transfer phase, depending on the canister pressure reading.

There are two NH_3 canisters used in the extraction side of the RGSS. They are labeled as "PQ" canisters in the Operation document for the extraction process (LT-160-101, D-0). One is attached to the extractor port and the other to the second volume port. (See Figures A.4 through A.6 for location of these ports.)

After the gas extraction process has been completed, both PQ canisters are removed from the hot cell and processed according to the procedures given in the WHC Internal Memo 75764-PCS96-007 entitled, "Test Plan for RGS Sample Preparation for Ammonia Analysis," by B.E. Hey.

The following is a brief outline of the procedure:

1) The canisters are moved by hand from the hot cell into a preparation hood/glovebox, appropriate for safe handling of these (radiation) contaminated vessels. Once in the hood, a hose is connected to the canister valve, and the other free end of the hose is inserted into an acid solution. The canister valve is then opened, and because the pressure within the canister is still at the level of vacuum attained during the RGSS extraction process, the acid is drawn into the canister. The role of the acid is to dissolve ammonia vapor into solution. The canister is shaken to enhance this process. Then the hose is disconnected from the canister and the acid wash is drained into a plastic vile. It is capped, labeled, and delivered to the ammonia analysis hood for further analysis.

2) After the gas extraction process has been completed (Sec.8.5 of LT-160-101, D-0), the next step is to begin the procedure for extractor "clean up" (Sec.8.6). As part of that process, a catch pan is placed under the extractor assembly. The bottom flange of the extractor is then removed, and the contents are allowed to fall into the catch pan. The contents are then poured into a 1-L poly bottle and a LiBr sample vial. These samples are labeled and sent on to the Analytical Services group at 222S, where they assign a "LABCOR" number to the samples and perform the analysis.

Of all the steps involved in the production of the direct RGS data, this part is perhaps the least likely to leave room for error and misinterpretation. The quality of the results has been established over years of experience. Moreover, from those years of experience with a wide variety of gas samples, the Mass Spectrometry laboratory was able to give the RGS program some comments that may be of use and are mentioned here. Before those comments, however, a brief description of the Mass Spectrometry Operation:

1) The samples are contained in 50 or 75 mL stainless steel cylinders (J canisters). The gas samples are delivered by hand to Room 421/320, Building 325. They are allowed to warm or cool to lab temperature. The Nupro valves on the cylinders are taped shut. An Analytical Chemistry Laboratory (ACL) Analytical Services Request (ASR) form is filled out with the sample identifications, etc. The samples are logged into the ACL system for tracking and for record storage.

2) Each gas sample cylinder is connected to the Finnigan MAT-271 quantitative gas mass spectrometer inlet system. The connecting vacuum/gas lines are evacuated and a subsample taken for mass analysis. Mass from 2 to 150 are scanned. The resultant mass run is checked and the 17 mass peak corrected for water. (The 17 mass peak is the ammonia parent mass peak.) The spectra is reduced by matrix calculations to give mole percent of each gas species detected and determined in the run. Organic gases are estimated using n-butane. The results are given to the ACL Laboratory Support Office [LSO]. LSO sends results out and files a copy of the results and data.

3) QA is assured with two weekly air standard runs and the results on nitrogen, oxygen, and argon are included the RGS report. In addition, the nitrogen is sensitivity checked at least once a day, and an organic calibration (methane, ethane, propane) is performed once a year.

4) Specific comments associated with the RGS samples: the RGS canisters were all very consistent. No observation of water vapor condensation resulting from water vapor trapped in the J-canister valves was experienced (as seen in from samples submitted by other projects.) The consensus was that the RGS sample status was very good.

A.4 X-Ray Data Acquisition

Immediately after recovery, each sampler is examined qualitatively using the x-ray radiography system. Figure A.8 shows a schematic diagram of the x-ray imaging system currently used in the field. This system is a state-of-the-art, real time, two-dimensional imaging system, specially designed for Hanford tank farm sampling operations. The primary purpose of the radiography is to immediately qualify the success of a sampling operation in capturing the desired amount of waste. Aside from sampling success, the radiograph images are also used for both qualitative observation of the phase distribution and quantification of density and phase distribution throughout the sampled waste.

Every core sample radiography session is recorded in real-time by the operator on a standard SVHS video tape. Each radiography session begins with the imaging of two calibration standards. Both standards consist of sections of sampler cylinder fixed vertically to a sliding mount so they can be moved in or out of view at will. One standard is filled with soil and air; the other is water and air. The radiography system is calibrated by setting the x-ray source energy (nominally 140 kV), adjusting the imaging camera iris, and setting the brightness and contrast of the display. After calibration, however, the x-ray source energy may be adjusted. Pertinent tank and core sample information and the x-ray source energy in kilovolts are recorded on the image using the image acquisition system. After the standards have been imaged, the core sample radiography begins. The sampler is lowered in front of the x-ray source such that the image of the sampler bottom (ball valve) is centered on the video monitor screen. The x-ray source energy is increased to approximately 160 kV to view the position of the valve and ensure it is properly closed. The position of the sampler is recorded on the video as 0.00 cm. The x-ray source energy is lowered back to 140 kV for the core sample radiography. The core sample is imaged in approximately 7.5 cm (3 in.) sections due to the limited field of view of the radiography system and elongated shape of the sampler. Imaging each subsection of the sampler proceeds as follows:

- Manually lower the sampler by approximately 7.5 cm (3 in.).
- Adjust side shutters to block extraneous x-rays.
- Maintain the sampler position for a few minutes.

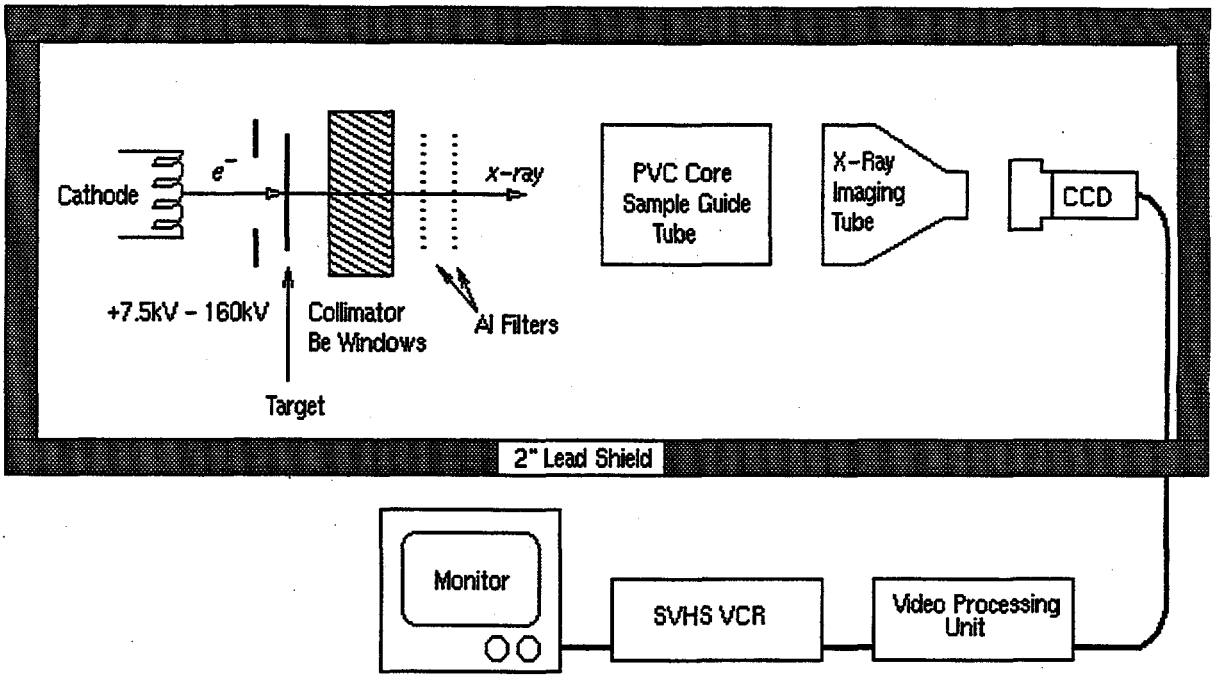

Figure A.8. Layout of the X-Ray Imaging System (portable core-sample radiography system)

- Note the vertical position of the sampler on the image.

This procedure is repeated until the entire sampler has been radiographed and recorded. Imaging the entire length of the sampler currently involves recording approximately six or seven subimages.

References

Hey BE. January 1996a. *Test Plan for the Authentic Application of the Retained Gas Sampler System.* WHC-SD-WM-TP-423 Rev. 0, Westinghouse Hanford Company, Richland, Washington.

Hey BE. January 1996b. *Retained Gas Sampler System Operation.* LT-160-101 BU, Westinghouse Hanford Company, Richland, Washington.

Shekarriz A. 1994. *Retained Gas Sampler Flow Visualization Guide.* PNL-10138, Pacific Northwest Laboratory, Richland, Washington.

Appendix B

System Volume Measurement and Uncertainty

APPENDIX B

System Volume Measurement and Uncertainty

The intent of the series of tests described in this appendix is to determine RGS sampler volume uncertainty. The setup assembled for performing these tests is shown in Figure B.1. The sampler (in a vertical orientation) was clamped in the structure shown in Figure B.1, and the assembly was immersed in water (water level about 6 in. up the RGS body) in a polyethylene drum. Pintle rod position, valve rotation and cylinder pressure/vacuum were measured using the instrumentation configuration shown in Figure B.2. The data collected by the measurement instruments was logged to a PC data acquisition system at 10 data points per channel per second. The pintle rod was drawn up vertically (like filling a syringe) at a programmed rate of 1±0.01 cm/s by a precision motion control system.

A prototypical RGS sampler was used for performing these tests.(a) This sampler was identified as being representative of RGSs used for the recent series of Tank AW-101 samples. To facilitate the tests, the four grapple fingers of the push mode quadralatch assembly were removed from the RGS. For tests 1 through 16, the shear wire method of piston-pintle rod retention was used, as was used in Tank AW-101.(b) After each test, the position of the valve was visually inspected and compared to the results obtained from the data acquisition system. Further, the final position of the piston was measured to within 1/32" using a standard measuring tape. Table B.1 provides a summary of the test results.

Starting with test 7, pintle rod draw force had been added to the data being sampled and logged. This allows to determine force profiles and relative timing to other data.

Tests 13 and 14 measured shear wire shear force profiles only. They both repeat at 72 lb peak force and have periods, measured at the baseline, of 1.0 and 0.7 seconds. If this had been pure shear, one would expect the time to be the wire diameter/pintle rod pull rate: .5mm/10mm/s = .05s. The shear wire "failure" was not pure shear but, due to the loose fit between the pintle rod and the socket, it fits into on top of the piston (where the shear wire is located), and the loose fit of the shear wire in the shear wire hole in the piston causes a combination of shear, bending, tension and smearing of the wire during its "failure." This combination of "failure" modes apparently stretches out the time of "failure."

To date, no separate force measurements have been made with the retention ring system. However, tests 17 through 22 involved this system and the information was obtained from the expanded data plots. These plots generally show a longer period force impulse in the region where the release disk is assumed to be releasing as opposed to a shorter period of force impulse for shear wire system tests. Also the release disk impulses tend to begin earlier than those of shear wire system tests. This appears to indicate an earlier initiation of piston release along with a longer release period for the retention disk system.

(a) The particulate RGS sampler used was labeled PROTOTYPE RGS, H-2-891608 Rev.1, FOR PNNL.

(b) Details of the apparatus and experimental procedure are covered in "Evaluation of RGS Volume Uncertainty," WTS-MIT-071596, by M White. July 1996, Pacific Northwest National Laboratory.

Most notably, tests 17, 18, 19, and 20 show a reduction in peak release forces of 91, 59, 56, and 18 lb, respectively. These data, taken with visual evidence of scraping and removal of metal on the bottom end of the pintle rod, indicate a wearing out of the retention system in just a few cycles. Since the RGS system needs to be tested before deployment to the field, this degree of wear-out-caused force reduction is unacceptable.

Since the data indicate the shear wire system to be stable in force over repeated cycles, this may be a better and simpler approach to piston retention than the retention ring method. It is expected that tightening up the clearance between the piston pintle rod socket and the pintle rod and similarly tightening up the clearance between the shear wire hole in the piston and the shear wire, that release force predictability at a desired level and short release periods could be obtained.

Instrumentation:

In order to expedite the tests the instrumentation was set up with reasonable, documented but non-traceable calibrations. The M&TE listing and the "Instrumentation Block Diagram" outline the instrumentation system used with the RGS tests.

Sampling Rate:

For tests 1 through 8, the sampling and logging rate was 10 Hz. This rate is probably not fast enough to catch the fast rising absolute peaks we are finding. Starting with test 9, all signals were sampled at 100 Hz, logged at 20 Hz, and signals averaged as tabulated below. Along with changes in electrical grounds, this produces data that are much less noisy. Averaging all the faster changing signals for the same period (.1 sec) does not change their relative delay and thus does not cause problems with comparing their relative timing. Nor does it appear to reduce peak detection appreciably.

Averaging the pintle rod stroke signal (the noisiest of the signals) for one second would tend to cause signal delay. Since this signal is not used for time comparisons in this analysis, this delay is of no concern.

Signal Noise:

More than desirable electrical noise is present on most of the signals as indicated by data plots through test 7. Most of this noise occurs when the motion control system's 3ϕ power is on. After test 7, electrical components and signal lines were grounded as follows:

> The grid turbulence tower, RGS unistrut frame, RGS clamp assembly & LVDT signal conditioner chassis are all connected to a common ground point (the building power ground via the electrical raceway in which the 3ϕ power is carried).

Data Acquisition sampling and averaging was set as tabulated:

Each channel has its - terminal strapped to the common terminal:

Ch.	Signal Samp.	Rate	Averaging	Log Rate
1	Stroke Pos.	100 Hz	1 sec	20/sec.
2	Valve Pos.	100 Hz	.1 sec	20/sec.
3	Pressure	100 Hz	.1 sec	20/sec.
4	Draw Force	100 Hz	.1 sec	20/sec.

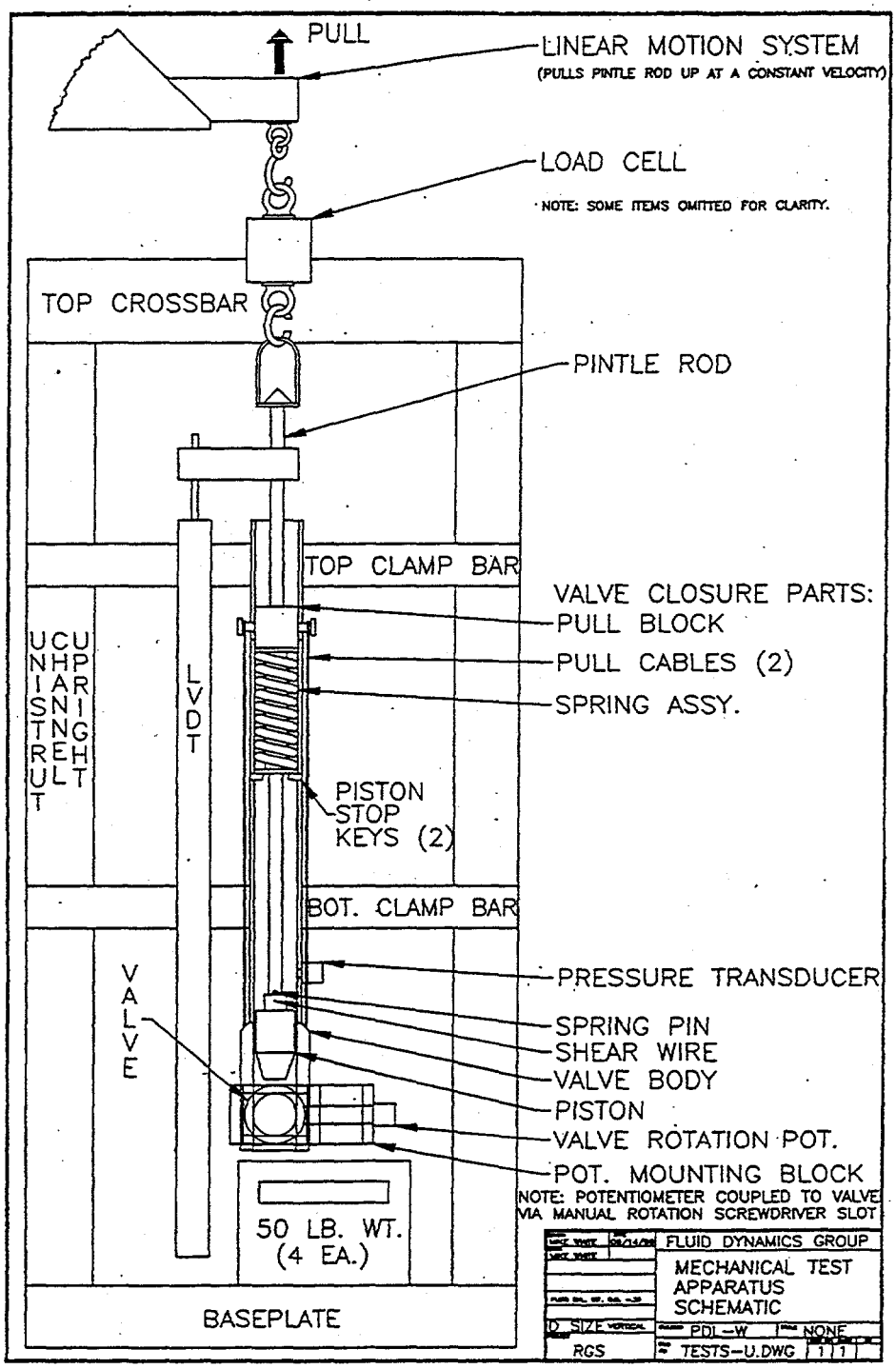

Figure B.1. Test Apparatus for Measurement of the RGS Volume Uncertainty

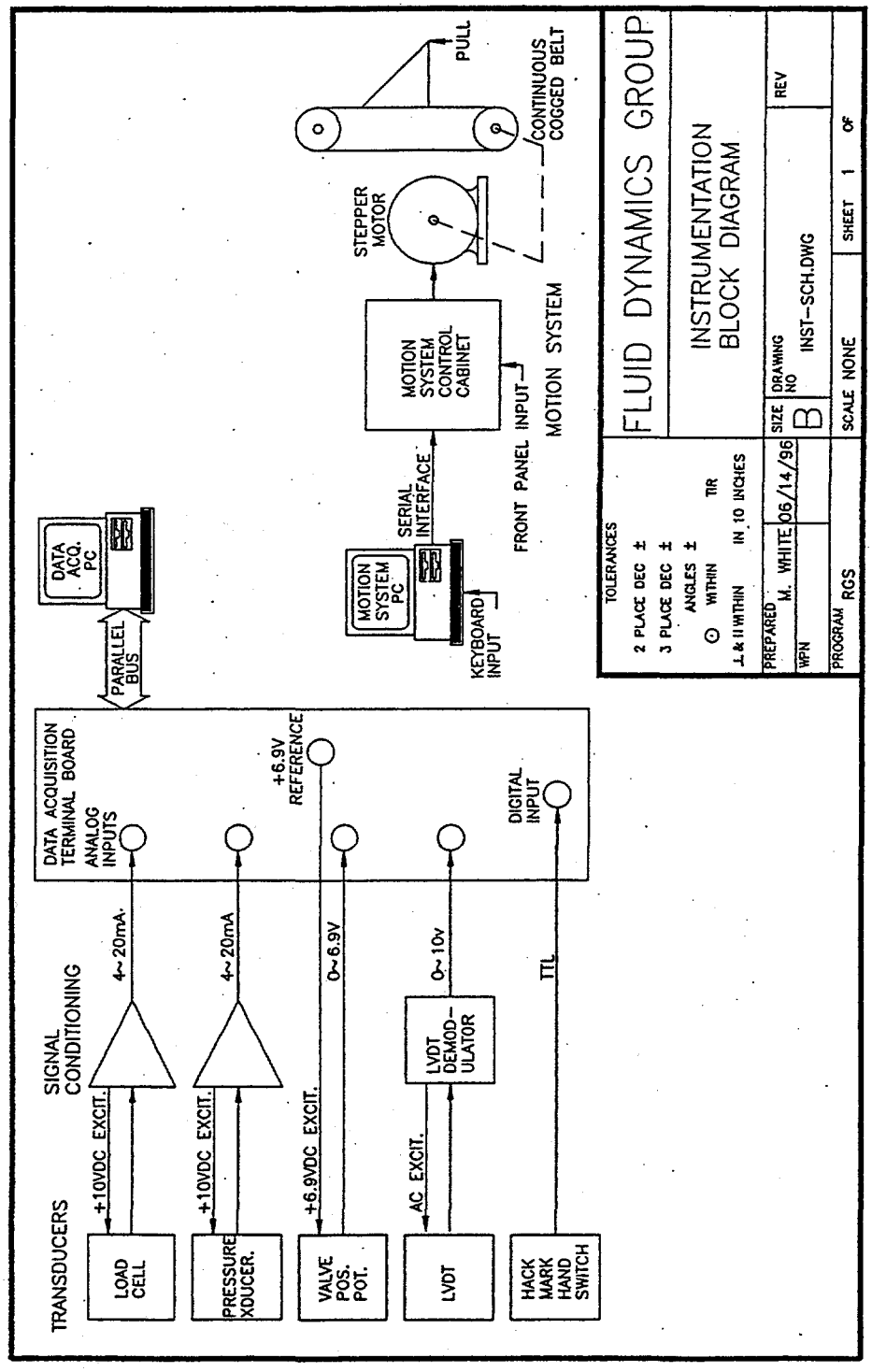

Figure B.2. Instrumentation Block Diagram for the RGS Volume Uncertainty

Table B.1. Summary of Test Results for Volume Uncertainty Measurements

Test No.	Date	Spring Color	Data Ends	Valve Full	Closure Gap(in.)	Piston Pos.(in.)	Water (cc)	Cyl. P. (psia)	Note
1	6/05	N/M	N/M	No	0.094	N/M	N/A	N/M	
2	6/05	N/M	N/M	No	0.28	19.31	N/A	N/M	Valve deemed too tight
3	6/06	N/M	Plain	Yes	0.00	N/M	N/M	N/M	Valve loosened
4	6/06	N/M	Flat-G	Yes	0.00	N/M	310	N/M	
5	6/07	N/M	Flat-G	Yes	0.00	19.12	312	16.7	Pressure channel may be saturated
6	6/07	N/M	Plain	Yes	0.00	19.12	310	6.9	
7	6/10	Yel.	Flat-G	Yes	0.00	N/M	312	17	PintleRod draw force inst. added
8	6/10	N/M	Plain	No	0.156	19.37	N/A	N/A	
9	6/18	Gold	Flat-G	No	0.067	19.28	N/A	N/A	Valve deemed too tight by WHC
10	6/19	Gold	Flat-G	Yes	0.00	19.28	317	16.8	Valve loosened by WHC
11	6/19	Gold	Flat-G	Yes	0.00	19.28	318	N/M	
12	6/20	Gold	Flat-G	No	N/A	N/M	N/A	N/A	Prototype alum. lower Spring stop, stop deformed, no trigger, motion system stalled
13	6/24	None	N/A	N/A	N/A		N/A		Shear Wire force only measured (72 lbs)
14	6/24	None	N/A	N/A	N/A		N/A		Shear Wire force only measured (72 lbs)
15	6/24	Gold	Flat-G	N/A	N/A		N/A		Spring mech. force measured (68 lbs)
16	6/25	Gold	Flat-G	Yes	N/A		N/A		Spring + valve force measured (68 lbs)

Notes: N/A = Not applicable N/M = not measured

Appendix C

Laboratory Data and Intermediate Results

APPENDIX C

Laboratory Data and Intermediate Results

C.1 Tank 241-AW-101

As described in Section 2.3, gases are extracted from waste samples into "J" canisters and then undergo analysis from mass spectroscopy to obtain the mole fraction composition of the extracted gas on a dry basis. (Water vapor is not measured.) The results, for Tank AW-101, are shown in Table C.1.1.

Table C.1.1. Mole Percents of Gases Measured in Tank AW-101 Dry Gas (obtained by mass spectroscopy)

Segment / Canister	N_2	H_2	N_2O	O_2	CH_4	Ar
8-J1	41±1.0	8.3±0.20	0.83±0.100	5.5±0.100	0.22±0.02	3.9±0.100
8-J2	9.4±0.2	2.43±0.05	0.41±0.040	0.74±0.020	0.05±0.05	0.87±0.020
8-J3*	20.8±0.4	0.022±0.00	0.033±0.002	8.7±0.200	0.02±0.01	69.4±0.400
17-J1	49±1.0	17.8±0.40	2.89±0.060	3.3±0.100	0.85±0.04	0.8±0.020
17-J2	10±0.2	4.33±0.09	2.21±0.050	0.67±0.020	0.47±0.02	0.24±0.005
17-J3*	36.5±0.7	0.19±0.00	0.34±0.020	13.8±0.300	0.13±0.02	48±0.900
19-J1	42.4±0.8	33.1±0.60	3.87±0.080	1.55±0.030	0.9±0.02	0.49±0.010
19-J2	12.5±0.2	11.1±0.20	3.45±0.070	0.39±0.010	0.56±0.06	0.235±0.004
19-J3*	42.2±0.8	0.394±0.01	0.52±0.020	14.1±0.300	0.2±0.02	42.4±0.900
21-J1	50.4±0.5	24.2±0.50	5.6±0.100	1.23±0.020	1.2±0.10	0.47±0.020
21-J2	15.2±0.3	8.7±0.20	5.8±0.100	0.374±0.008	0.62±0.60	0.28±0.030
21-J3*	41±0.8	0.45±0.01	0.65±0.020	10.8±0.200	0.27±0.03	46.4±0.800
18-J1	46.6±0.9	10.7±0.20	3.73±0.070	2.23±0.040	0.83±0.02	2.65±0.050
18-J2	15.7±0.3	2.11±0.04	1.97±0.040	2.38±0.050	0.44±0.02	0.54±0.010
18-J3	14.3±0.3	1.61±0.03	1.4±0.030	2.59±0.050	0.44±0.02	0.45±0.010
22-J1	48±1.0	8±0.20	7.4±0.200	1.7±0.060	1±0.10	1.62±0.060
22-J2	7.6±0.2	1.49±0.03	3.31±0.070	0.315±0.006	0.51±0.01	0.343±0.007
22-J3	5.5±0.1	1.28±0.03	2.67±0.050	0.117±0.002	0.54±0.01	0.311±0.006

* The J3 canisters of the first four samples processed were contaminated by gas in dilution water, and the data from them were not usable.

Table C.1.1 (contd)

Segment / Canister	Other NOx	C_2H_x	C_3H_x	Other HC	NH_3
8-J1	0.1±0.100	0.022±0.00	0.037±0.004	0.079±0.008	40±5.00
8-J2	0.1±0.100	0.14±0.02	0.051±0.005	0.26±0.030	86±5.00
8-J3*	0.1±0.100	0.01±0.01	0.02±0.010	0.01±0.010	1±0.40
17-J1	0.1±0.100	0.36±0.05	0.07±0.010	0.25±0.030	25±2.00
17-J2	0.1±0.100	0.58±0.05	0.18±0.020	1.1±0.100	80±5.00
17-J3*	0.1±0.100	0.07±0.01	0.07±0.010	0.14±0.020	0.68±0.05
19-J1	0.01±0.010	0.42±0.01	0.07±0.010	0.24±0.030	17±2.00
19-J2	0.01±0.010	0.67±0.09	0.21±0.020	1.1±0.100	70±5.00
19-J3*	0.01±0.010	0.1±0.10	0.044±0.004	0.15±0.070	0.01±0.01
21-J1	0.1±0.100	0.57±0.07	0.08±0.010	0.31±0.030	16±2.00
21-J2	0.1±0.100	0.96±0.09	0.28±0.030	1.53±0.030	66±5.00
21-J3*	0.01±0.010	0.02±0.01	0.06±0.010	0.26±0.030	0.01±0.01
18-J1	0.1±0.100	0.38±0.05	0.08±0.010	0.32±0.030	32±2.00
18-J2	0.01±0.010	0.47±0.05	0.16±0.020	0.91±0.020	75±5.00
18-J3	0.01±0.010	0.69±0.09	0.13±0.020	1.16±0.100	77±5.00
22-J1	0.01±0.007	0.5±0.10	0.09±0.010	0.43±0.040	31±8.00
22-J2	0.005±0.005	0.67±0.01	0.18±0.010	1.27±0.030	84±10.00
22-J3	0.005±0.005	1.02±0.02	0.136±0.003	1.75±0.040	87±10.00

* The J3 canisters of the first four samples processed were contaminated by gas in dilution water, and the data from them were not usable.

The pressure and temperature of the gas in the J canisters are measured at the time of collection. The collector volume always includes the canister volume and, in cases where the collector is pumped down to vacuum after a canister is valved closed, also includes the collector-side line volume. The water vapor pressure is assumed to be that of pure water rather than the much lower vapor pressure over the sample because, for AW-101, the collector-side is not in direct contact with the sample and is not in equilibrium with it. Table C.1.2 shows the canister (collector-side) conditions that prevailed for Tank AW-101 samples.

Table C.1.2. Canister Conditions at the Time of Collection, for Tank AW-101 Samples

Segment / Canister	Pressure (kPa)	Collector Volume (cc)	Temperature (°C)	Water Vapor Pressure (kPa)	Sampler Volume (L)
8-J1	16.353	56.1	25.8	3.321	0.31537
8-J2	12.84	56.5	26.3	3.421	0.31537
8-J3*					
17-J1	39.174	57.1	25.2	3.205	0.31482
17-J2	21.856	57.7	25.9	3.341	0.31482
17-J3*					
19-J1	64.19	56.1	25.2	3.205	0.31444
19-J2	23.303	56.5	26.8	3.523	0.31444
19-J3*					
21-J1	64.264	57.1	25.9	3.341	0.31448
21-J2	20.885	57.7	27.8	3.736	0.31448
21-J3*					
18-J1	34.347	56.1	25.6	3.282	0.31505
18-J2	25.598	39.9	27.6	3.692	0.31505
18-J3	17.022	55.8	27.4	3.650	0.31505
22-J1	34.681	57.1	24.6	3.189	0.31482
22-J2	25.139	41.1	25.2	3.205	0.31482
22-J3	14.689	57.2	24.9	3.149	0.31482

* The J3 canisters of the first four samples processed were contaminated by gas in dilution water, and the data from them were not usable.

Tables C.1.3 through C.1.5 give the peak collector-side pressures during the extraction pump cycling. Only the last five pressures are used for regression to get the pressure versus cycle derivatives.

Table C.1.3. Pump Cycle Peak Pressures (kPa) for Canister 1 of Each Segment of Tank AW-101

Cycle	8-J1	17-J1	19-J1	21-J1	18-J1	22-J1
1	9.039	15.395	23.208	19.361	13.404	13.454
2	12.48	22.924	35.559	32.578	19.922	20.211
3	14.166	26.862	42.95	40.526	23.527	23.866
4	14.979	29.311	46.783	45.4	25.68	26.397
5	15.25	30.829	51.025	49.201	27.556	28.037
6	15.576	32.017	53.997	52.205	28.945	29.681
7	15.756	33.119	56.691	55.366	30.18	30.796
8	15.985	34.268	58.995	57.657	31.344	31.974
9	16.353	35.462	60.748	59.597	32.335	32.942
10		36.163	62.424	61.742	33.257	33.762
11		37.157	64.19	64.264	34.347	34.681
12		38.171				
13		39.174				

Table C.1.4. Pump Cycle Peak Pressures (kPa) for Canister 2 of Each Segment of Tank AW-101

Cycle	8-J2	17-J2	19-J2	21-J2	18-J2	22-J2
1	9.234	11.705	12.137	9.715	12.553	11.863
2	11.395	15.938	17.166	13.437	17.751	16.555
3	12.186	17.826	19.422	15.638	20.467	19.234
4	12.529	18.943	20.683	16.441	21.909	20.796
5	12.637	19.651	21.314	17.736	22.907	21.87
6	12.823	20.004	21.797	18.405	23.857	22.655
7	12.84	20.423	22.098	19.053	24.433	22.991
8		20.891	22.423	19.299	24.564	23.44
9		21.251	22.435	19.935	25.031	23.952
10		21.418	22.862	20.274	25.598	24.521
11		21.856	23.303	20.885		25.139

Table C.1.5. Pump Cycle Peak Pressures (kPa) for Canister 3 of Each Segment of Tank AW-101

Cycle	8-J3	17-J3	19-J3	21-J3	18-J3	22-J3
1	25.524	21.594	22.788	20.989	9.248	9.928
2	35.346	28.212	30.329	33.187	11.877	11.198
3	39.309	30.606	32.388	38.11	13.313	12.014
4	42.353	32.053	33.153	40.433	14.03	12.489
5	44.088	33.04	33.75	41.74	14.542	12.818
6	45.189	33.795	34.229	42.894	14.991	13.094
7	46.2	34.672	34.604	43.75	15.135	13.355
8	47.137	35.211	34.916	44.149	15.289	13.504
9	47.597	35.634	35.307	44.582	15.558	13.638
10	48.601	36.013	35.014	44.768	15.717	13.826
11		36.763	36.421	45.53	15.699	13.996
12					15.922	13.995
13					16.127	14.077
14					16.154	14.157
15					16.352	14.246
16					16.405	14.299
17					16.528	14.475
18					16.653	14.469
19					16.647	14.627
20					17.022	14.689

Table C.1.6 shows the amounts of gases that are calculated based on the data presented earlier. The regression slopes in Table C.1.8 also play a part in the determination of the "residuals," which have meaning only for ammonia.

Table C.1.6. Quantities of Gases Found in Tank AW-101 Samples

Segment / Canister	N_2 (µmol)	H_2 (µmol)	N_2O (µmol)	O_2 (µmol)	CH_4 (µmol)	Ar (µmol)
8-J1	121±15	24.4±3.0	2.4±0.4	16.2±2.0	0.65±0.10	11.5±1.4
8-J2	20±3	5.2±0.8	0.9±0.2	1.6±0.3	0.12±0.12	1.9±0.3
8-J3*						
8-TOTAL*	141±18	29.6±3.9	3.3±0.6	17.8±2.3	0.76±0.22	13.3±1.7
17-J1	406±23	147±8	23.9±1.3	27.3±1.6	7.0±0.5	6.6±0.4
17-J2	43±4	19±2	9.5±0.9	2.9±0.3	2.0±0.2	1.0±0.1
17-J3*						
17-TOTAL*	449±27	166.0±10.0	33.4±2.2	30.2±1.9	9.06±0.70	7.7±0.5
19-J1	585±22	457±17	53.4±2.0	21.4±0.8	12.4±0.5	6.8±0.3
19-J2	56±5	50±4	15.5±1.4	1.7±0.2	2.5±0.3	1.1±0.1
19-J3*						
19-TOTAL*	641±27	506.3±21.2	68.8±3.4	23.1±1.0	14.92±0.83	7.8±0.3
21-J1	705±24	339±13	78.4±2.9	17.2±0.6	16.8±1.5	6.6±0.4
21-J2	60±6	34±3	22.9±2.2	1.5±0.1	2.5±2.4	1.1±0.2
21-J3*						
21-TOTAL*	765±30	373.0±16.3	101.3±5.1	18.7±0.8	19.24±3.88	7.7±0.5
18-J1	327±20	75.1±4.6	26.2±1.6	15.6±1.0	5.8±0.4	18.6±1.1
18-J2	55±4	7.4±0.6	6.9±0.6	8.3±0.7	1.5±0.1	1.9±0.2
18-J3	43±5	4.8±0.6	4.2±0.5	7.7±0.9	1.3±0.2	1.3±0.2
18-TOTAL	425±30	87.3±5.8	37.2±2.7	31.7±2.6	8.68±0.67	21.8±1.5
22-J1	349±22	58.1±3.7	53.8±3.4	12.3±0.8	7.3±0.8	11.8±0.8
22-J2	28±2	5.4±0.4	12.0±1.0	1.1±0.1	1.9±0.2	1.2±0.1
22-J3	15±2	3.4±0.5	7.1±1.0	0.3±0.0	1.4±0.2	0.8±0.1
22-TOTAL	391±26	66.9±4.6	72.9±5.4	13.8±1.0	10.56±1.2	13.8±1.0

* The J3 canisters of the first four samples processed were contaminated by gas in dilution water, and the data from them were not usable.

Table C.1.6 (contd)

Segment / Canister	Other NOx (µmol)	C_2H_x (µmol)	C_3H_x (µmol)	Other HC (µmol)	NH_3 (µmol)
8-J1	0.29±0.30	0.06±0.01	0.11±0.02	0.23±0.04	118±21
8-J2	0.21±0.22	0.30±0.06	0.11±0.02	0.56±0.11	184±31
8-J3*					
8-residual*					0±0
8-TOTAL*	0.51±0.51	0.36±0.07	0.22±0.04	0.79±0.14	301±51
17-J1	0.8±0.8	3.0±0.4	0.58±0.09	2.1±0.3	207±20
17-J2	0.4±0.4	2.5±0.3	0.77±0.11	4.7±0.6	344±38
17-J3*					
17-residual*					267±243
17-TOTAL*	1.26±1.26	5.47±0.76	1.35±0.20	6.80±0.88	818±301
19-J1	0.1±0.1	5.8±0.2	1.0±0.1	3.3±0.4	234±29
19-J2	0.0±0.0	3.0±0.5	0.9±0.1	4.9±0.6	314±35
19-J3*					
19-residual*					79±54
19-TOTAL*	0.18±0.18	8.80±0.71	1.91±0.26	8.24±1.04	627±118
21-J1	1.4±1.4	8.0±1.0	1.1±0.1	4.3±0.4	224±29
21-J2	0.4±0.4	3.8±0.5	1.1±0.2	6.1±0.6	261±32
21-J3*					
21-residual*					175±206
21-TOTAL*	1.79±1.80	11.77±1.52	2.23±0.30	10.39±1.04	660±266
18-J1	0.7±0.7	2.7±0.4	0.6±0.1	2.2±0.2	225±19
18-J2	0.0±0.0	1.6±0.2	0.6±0.1	3.2±0.3	262±27
18-J3	0.0±0.0	2.1±0.4	0.4±0.1	3.5±0.5	230±31
18-residual					199±1039
18-TOTAL	0.77±0.77	6.37±1.0	1.51±0.24	8.89±1.01	916±1116
22-J1	0.1±0.1	3.6±0.8	0.7±0.1	3.1±0.3	225±60
22-J2	0.0±0.0	2.4±0.2	0.7±0.1	4.6±0.4	305±44
22-J3	0.0±0.0	2.7±0.4	0.4±0.1	4.7±0.6	232±41
22-residual					70±199
22-TOTAL	0.10±0.08	8.78±1.3	1.67±0.2	12.40±1.4	832±343

* The J3 canisters of the first four samples processed were contaminated by gas in dilution water, and the data from them were not usable. The ammonia residuals are therefore also dubious.

Table C.1.7. Mole Percents of Gases in Tank AW-101 Dry Insoluble Gas

Segment / Canister	N_2	H_2	N_2O	O_2	CH_4	Ar
8-J1	68.3%±8.7%	13.8%±1.8%	1.4%±0.2%	9.2%±1.16%	0.37%±0.06%	6.50%±0.83%
8-J2	67.1%±4.2%	17.4%±1.1%	2.9%±0.3%	5.3%±0.34%	0.36%±0.36%	6.21%±0.39%
8-J3*	21.0%±8.4%	0.0%±0.0%	0.0%±0.0%	8.8%±3.52%	0.02%±0.01%	70.1%±28.04%
17-J1	65.3%±5.4%	23.7%±2.0%	3.9%±0.3%	4.4%±0.38%	1.13%±0.11%	1.07%±0.09%
17-J2	50.0%±3.3%	21.7%±1.4%	11.1%±0.7%	3.4%±0.23%	2.35%±0.18%	1.20%±0.08%
17-J3*	36.7%±2.8%	0.2%±0.0%	0.3%±0.0%	13.9%±1.07%	0.13%±0.02%	48.3%±3.67%
19-J1	51.1%±6.1%	39.9%±4.7%	4.7%±0.6%	1.9%±0.22%	1.08%±0.13%	0.59%±0.07%
19-J2	41.7%±3.0%	37.0%±2.7%	11.5%±0.9%	1.3%±0.10%	1.87%±0.24%	0.78%±0.06%
19-J3*	42.2%±42.2%	0.4%±0.4%	0.5%±0.5%	14.1%±14.10%	0.20%±0.20%	42.4%±42.41%
21-J1	60.0%±7.5%	28.8%±3.7%	6.7%±0.8%	1.5%±0.18%	1.43%±0.21%	0.56%±0.07%
21-J2	44.7%±3.5%	25.6%±2.0%	17.1%±1.3%	1.1%±0.09%	1.82%±1.77%	0.82%±0.11%
21-J3*	41.0%±41.0%	0.5%±0.5%	0.7%±0.7%	10.8%±10.80%	0.27%±0.27%	46.4%±46.41%
18-J1	68.5%±4.5%	15.7%±1.0%	5.5%±0.4%	3.3%±0.21%	1.22%±0.08%	3.90%±0.25%
18-J2	62.8%±4.4%	8.4%±0.6%	7.9%±0.5%	9.5%±0.67%	1.76%±0.14%	2.16%±0.15%
18-J3	62.2%±4.2%	7.0%±0.5%	6.1%±0.4%	11.3%±0.76%	1.91%±0.15%	1.96%±0.13%
22-J1	69.6%±18.0%	11.6%±3.0%	10.7%±2.8%	2.5%±0.64%	1.45%±0.40%	2.35%±0.61%
22-J2	47.5%±5.8%	9.3%±1.1%	20.7%±2.5%	2.0%±0.24%	3.19%±0.38%	2.14%±0.26%
22-J3	42.3%±4.9%	9.8%±1.2%	20.5%±2.4%	0.9%±0.10%	4.15%±0.48%	2.39%±0.28%

* The J3 canisters of the first four samples processed were contaminated by gas in dilution water, and the data from them were not usable.

Table C.1.7 (contd)

Segment / Canister	Other NOx	C_2H_x	C_3H_x	Other HC
8-J1	0.17%±0.17%	0.04%±0.01%	0.06%±0.01%	0.13%±0.02%
8-J2	0.71%±0.72%	1.00%±0.15%	0.36%±0.04%	1.86%±0.24%
8-J3*	0.10%±0.11%	0.01%±0.01%	0.02%±0.01%	0.01%±0.01%
17-J1	0.13%±0.13%	0.48%±0.08%	0.09%±0.02%	0.33%±0.05%
17-J2	0.50%±0.50%	2.90%±0.31%	0.90%±0.11%	5.50%±0.61%
17-J3*	0.10%±0.10%	0.07%±0.01%	0.07%±0.01%	0.14%±0.02%
19-J1	0.01%±0.01%	0.51%±0.06%	0.08%±0.02%	0.29%±0.05%
19-J2	0.03%±0.03%	2.23%±0.34%	0.70%±0.08%	3.67%±0.42%
19-J3*	0.01%±0.01%	0.10%±0.14%	0.04%±0.04%	0.15%±0.17%
21-J1	0.12%±0.12%	0.68%±0.12%	0.10%±0.02%	0.37%±0.06%
21-J2	0.29%±0.29%	2.82%±0.34%	0.82%±0.11%	4.50%±0.35%
21-J3*	0.01%±0.01%	0.02%±0.02%	0.06%±0.06%	0.26%±0.26%
18-J1	0.15%±0.15%	0.56%±0.08%	0.12%±0.02%	0.47%±0.05%
18-J2	0.04%±0.04%	1.88%±0.24%	0.64%±0.09%	3.64%±0.26%
18-J3	0.04%±0.04%	3.00%±0.44%	0.57%±0.09%	5.04%±0.54%
22-J1	0.01%±0.01%	0.72%±0.24%	0.13%±0.04%	0.62%±0.17%
22-J2	0.03%±0.03%	4.19%±0.50%	1.13%±0.15%	7.94%±0.96%
22-J3	0.04%±0.04%	7.85%±0.91%	1.05%±0.12%	13.5%±1.58%

* The J3 canisters of the first four samples processed were contaminated by gas in dilution water, and the data from them were not usable.

As discussed in Section 3.2, a regression was performed on the total pressures during the last several pump cycles (or "strokes") to find the residual ammonia content of the sample. The variables derived by, and used in, the regression are given in Table C.1.8.

Table C.1.8. Pressure Regression Variables for Tank AW-101 Sample Cycling

Segment / Canister	dp/dN (kPa/stroke)	p_{ins} (kPa)	N (number of strokes)	$(\Delta n/\Delta N)_{NH3}$ (mgmol NH3 per stroke)
8-J1	0.262±0.632	7.819	9	1.75E-06±4.25E-06
8-J2	0.160±0.632	1.319	7	3.64E-03±1.44E-02
8-J3*	0.822±0.632	44.942	10	1.85E-02±1.61E-02
17-J1	0.943±0.632	26.977	13	1.41E-02±9.53E-03
17-J2	0.339±0.632	3.703	11	6.15E-03±1.15E-02
17-J3*	0.498±0.632	33.155	11	-3.84E-03±4.89E-03
19-J1	1.843±0.632	50.618	11	1.87E-02±6.81E-03
19-J2	0.285±0.632	5.934	11	3.76E-03±8.35E-03
19-J3*	0.373±0.632	32.915	11	-6.44E-03±1.27E-02
21-J1	2.188±0.632	51.175	11	2.67E-02±8.44E-03
21-J2	0.464±0.632	5.831	11	1.07E-02±1.46E-02
21-J3*	0.418±0.632	41.680	11	9.54E-03±1.73E-02
18-J1	1.025±0.632	21.124	11	1.36E-02±8.45E-03
18-J2	0.408±0.632	5.476	10	6.51E-03±1.01E-02
18-J3	0.135±0.632	3.076	20	3.02E-03±1.41E-02
22-J1	0.956±0.632	21.730	11	2.20E-02±1.57E-02
22-J2	0.538±0.632	3.509	11	8.91E-03±1.06E-02
22-J3	0.093±0.632	1.500	20	2.07E-03±1.40E-02

*The J3 canisters of the first four samples processed were contaminated by gas in dilution water, and the data from them were not usable.

In order to estimate the void fraction and the distribution of gases between the void and slurry phases in each segment, the conditions under which the gas exists must be known. These are given in Table C.1.9 for Tank AW-101. The densities were taken from ball rheometer and core data in Stewart et al. (1996). The temperatures were based on a profile measured at the MIT tree; the profile is shown in Section 4.1.2. The pressures were derived from hydrostatic head, and are based on the depth of submergence of the segment and the thicknesses and gas-free densities of the waste layers. The solid volume fraction is estimated using 1420 kg/m^3 as the density of solid-free liquid, 1570 kg/m^3 as the density of gas-free slurry, and an assumed 2000 kg/m^3 as the intrinsic (not bulk) density of the solid material.

The water vapor pressure is the pressure in equilibrium with water in the waste; it is calculated using Equation 6.2 and Table 6.2 of Mahoney and Trent (1995), a correlation for water vapor pressure over concentrated homogeneous and non-homogeneous waste simulants. This correlation requires the weight fraction of water in the slurry, which is calculated using the solid

Table C.1.9. In-Tank Conditions Used for Tank AW-101 Phase Distribution Calculations

Segment	Density (kg/m^3)	Temperature (°C)	Pressure (atm)	Solid Volume Fraction	Water Vapor Pressure (atm)
8	1420	40.8	1.47	0	0.0436
17	1570	42.6	2.07	0.26	0.0299
19	1570	43.0	2.21	0.26	0.0305
21	1570	37.5	2.36	0.26	0.0228
18	1570	43.4	2.14	0.26	0.0311
22	1570	35.8	2.43	0.26	0.0207

volume fraction and density and the weight fraction of water in the solids-free solution. The latter value was estimated at 0.55, based on Equation 4.4 of Mahoney and Trent (1995), which allows the weight fraction of water in a simulant solution to be back-calculated from the solution density.

The average ionic concentrations in the drainable liquid in Tank AW-101 are given in Table C.1.10. They were taken from Table ES-1 of the AW-101 TCR document (WHC-SD-WM-ER-470, Rev. 0), and are based on supernatant samples taken in 1990.

Table C.1.10. Ionic Concentrations Used For Tank AW-101 Phase Distribution Calculations

Ion	gmol/L solution
Na^+	10.00
Al^{3+}	1.03
Fe^{3+}	0
Cr^{3+}	0.0030
Ni^{2+}	0
K^+	1.07
OH^-	5.07
NO_3^-	3.45
NO_2^-	2.22
CO_3^{2-}	0.21
PO_4^{3-}	0.02
SO_4^{2-}	0.01
F^-	0
Cl^-	0.15

The Henry's Law constants are necessary to estimate the in-tank phase distribution of gases (see Section 3.2). The intermediate steps in the Henry's Law constant calculation are shown in Table C.1.11. Note that the final Henry's Law constant is in terms of liters of gas-free waste slurry, while the Schumpe model is in terms of kg of water in the salt solution. Both the solid volume fraction and the weight percent of water in the solution are needed to put the Henry's Law constant in its final form. The gases not listed, argon and the minor gases, were assumed wholly insoluble with Henry's law constants of 10^{-10}.

The Henry's Law constant calculation is one method of calculating the ammonia partial pressure. Another method uses a grab-sample of extractor atmosphere, which is analyzed to find the ammonia content and hence the partial pressure at the time the sample was taken. Table C.1.12 shows the results of these analyses for AW-101 samples. In the table, "UBV" indicates unbound vapor, or the sample taken just before the J1 canister; "BV" means bound vapor, the sample taken just after the temperature ramp.

Table C.1.11. Henry's Law Constants For Tank AW-101 Phase Distribution Calculations

Segment	Condition	N_2	H_2	N_2O	O_2	CH_4	NH_3
8	Schumpe (K in water / K in solution)	81	34	60	107	102	30
	Waste Slurry K (mol/atm L waste)	5.4×10^{-6}	1.7×10^{-5}	2.1×10^{-4}	7.6×10^{-6}	8.7×10^{-6}	2.2
17	Schumpe (K in water / K in solution)	76	33	57	104	97	28
	Waste Slurry K (mol/atm L waste)	4.1×10^{-6}	1.3×10^{-5}	1.6×10^{-4}	5.7×10^{-6}	6.6×10^{-6}	1.5
19	Schumpe (K in water / K in solution)	75	33	57	103	96	27
	Waste Slurry K (mol/atm L waste)	4.2×10^{-6}	1.3×10^{-5}	1.6×10^{-4}	5.7×10^{-6}	6.7×10^{-6}	1.4
21	Schumpe (K in water / K in solution)	90	36	65	113	112	34
	Waste Slurry K (mol/atm L waste)	3.7×10^{-6}	1.2×10^{-5}	1.6×10^{-4}	5.5×10^{-6}	6.1×10^{-6}	1.8
18	Schumpe (K in water / K in solution)	74	33	56	102	95	27
	Waste Slurry K (mol/atm L waste)	4.2×10^{-6}	1.3×10^{-5}	1.6×10^{-4}	5.7×10^{-6}	6.7×10^{-6}	1.4
22	Schumpe (K in water / K in solution)	95	37	68	117	118	37
	Waste Slurry K (mol/atm L waste)	3.5×10^{-6}	1.2×10^{-5}	1.6×10^{-4}	5.5×10^{-6}	6.0×10^{-6}	2.0

Table C.1.12. Grab-Sample Data for Deriving Ammonia Partial Pressures in Tank AW-101

Sample	Grab-Sample Volume (cc)	Fill Temperature (°C)	Fill Pressure (kPa)	µmol NH_3	NH_3 Partial Pressure (atm)
8-UBV	52	22.5	2.03	8.19	0.0038
8-BV	52	26.7	2.5	11.6	0.0055
17-UBV	51.7	23.3	2.93	17.0	0.0080
17-BV	52	25.8	2.375	8.35	0.0039
19-UBV*					
19-BV*					
21-UBV*					
21-BV*					
18-UBV	38.6	24.7	2.922	6.52	0.0041
18-BV*					
22-UBV	51.7	24.1	2.894	12.3	0.0058
22-BV	52	25.4	2.385	23	0.011
* Grab-samples were lost in handling.					

C.2 Tank 241-A-101

As described in Section 2.3, gases are extracted from waste samples into "J" canisters and then undergo analysis from mass spectroscopy to obtain the mole fraction composition of the extracted gas on a dry basis. (Water vapor is not measured.) The results, for Tank A-101, are shown in Table C.2.1.

Table C.2.1. Mole Percents of Gases Measured in Tank A-101 Dry Gas (obtained by mass spectroscopy)

Segment / Canister	N_2	H_2	N_2O	O_2	CH_4	Ar
5-J1	13.1±0.300	55.6±0.090	4.34±0.090	0.41±0.010	0.41±0.050	0.17±0.010
5-J2	9.7±0.200	42.8±0.200	3.25±0.070	0.32±0.020	0.36±0.050	0.13±0.020
5-J3	1.72±0.030	7.8±0.200	0.73±0.020	0.078±0.003	0.27±0.050	0.031±0.003
8-J1	14.9±0.400	62.4±0.400	4.5±0.100	0.4±0.020	0.53±0.050	0.097±0.005
8-J2	11.7±0.300	50±0.300	3.5±0.100	0.35±0.007	0.43±0.009	0.076±0.008
8-J3	2.75±0.060	12.2±0.300	0.92±0.020	0.063±0.006	0.17±0.050	0.022±0.004
12-J1	9.2±0.200	0.91±0.020	1.36±0.050	1.3±0.040	0.12±0.050	4.63±0.090
12-J2	1.01±0.020	0.13±0.020	0.58±0.060	0.076±0.007	0.08±0.020	0.29±0.030
12-J3	0.69±0.020	0.084±0.008	0.37±0.040	0.044±0.004	0.09±0.020	0.16±0.020
2-J1*	42.8±0.900	32±0.600	3.81±0.080	7.7±0.200	0.19±0.050	0.52±0.020
2-J2*	39.9±0.500	25.2±0.500	2.96±0.060	8±0.200	0.05±0.050	0.48±0.020
2-J3*	64.8±0.300	1.55±0.030	0.245±0.005	17.1±0.300	0.000±0.000	0.78±0.020
9-J1	18±0.400	53±0.400	3.72±0.080	0.068±0.004	0.65±0.050	2.69±0.050
9-J2	14.1±0.300	42.6±0.300	2.91±0.060	0.082±0.004	0.51±0.050	2.04±0.040
9-J3	2.32±0.050	7.9±0.200	0.75±0.020	0.024±0.002	0.1±0.050	0.118±0.005
16-J1	6.9±0.200	1.17±0.020	1.45±0.030	0.55±0.010	0.053±0.005	6.8±0.200
16-J2	0.76±0.020	0.152±0.006	0.45±0.020	0.068±0.030	0.02±0.010	0.6±0.050
16-J3	0.51±0.010	0.104±0.005	0.32±0.010	0.06±0.020	0.012±0.005	0.35±0.010
19-J1	13.7±0.300	2.21±0.040	1.82±0.040	1.65±0.030	0.09±0.010	6.16±0.200
19-J2	1.42±0.030	0.279±0.006	0.47±0.010	0.152±0.004	0.000±0.000	0.57±0.020
19-J3	0.94±0.020	0.161±0.003	0.28±0.010	0.088±0.002	0.000±0.000	0.3±0.010
* Segment 2 is believed to have been contaminated by inleaked air during extraction.						

Table C.2.1 (contd)

Segment / Canister	Other NOx	C_2H_x	C_3H_x	Other HC	NH_3
5-J1	0.013±0.005	0.05±0.010	0.02±0.005	0.04±0.010	26±3.00
5-J2	0.02±0.010	0.05±0.010	0.03±0.010	0.04±0.010	43±4.00
5-J3	0.04±0.010	0.05±0.010	0.04±0.010	0.11±0.020	89±4.00
8-J1	0.05±0.010	0.06±0.010	0.02±0.010	0.04±0.010	17±3.00
8-J2	0.05±0.001	0.06±0.010	0.03±0.010	0.04±0.010	34±8.00
8-J3	0.06±0.020	0.05±0.010	0.03±0.010	0.05±0.010	84±8.00
12-J1	0.018±0.005	0.007±0.003	0.004±0.002	0.03±0.010	82±4.00
12-J2	0.04±0.020	0.000±0.000	0.011±0.005	0.04±0.010	98±1.00
12-J3	0.04±0.020	0.000±0.000	0.02±0.010	0.03±0.010	98±1.00
2-J1*	0.012±0.006	0.07±0.010	0.02±0.010	0.03±0.010	13±2.00
2-J2*	0.02±0.020	0.06±0.010	0.03±0.010	0.04±0.010	23±2.00
2-J3*	0.03±0.010	0.01±0.005	0.03±0.010	0.04±0.010	15±2.00
9-J1	0.000±0.000	0.1±0.002	0.014±0.005	0.03±0.010	22±2.00
9-J2	0.000±0.000	0.08±0.010	0.02±0.010	0.03±0.010	38±2.00
9-J3	0.02±0.010	0.02±0.010	0.02±0.010	0.04±0.010	88.7±0.90
16-J1	0.012±0.006	0.014±0.005	0.000±0.000	0.04±0.010	83±4.00
16-J2	0.03±0.010	0.000±0.000	0.011±0.005	0.03±0.010	97.9±0.50
16-J3	0.03±0.010	0.000±0.000	0.02±0.010	0.03±0.010	98.6±0.50
19-J1	0.011±0.006	0.02±0.010	0.000±0.000	0.03±0.010	74±2.00
19-J2	0.026±0.009	0.000±0.000	0.013±0.006	0.03±0.010	97±0.10
19-J3	0.029±0.009	0.000±0.000	0.02±0.010	0.02±0.010	98.2±0.10
* Segment 2 is believed to have been contaminated by inleaked air during extraction.					

The pressure and temperature of the gas in the J canisters are measured at the time of collection. The collector volume always includes the canister volume and, in cases where the collector is pumped down to vacuum after a canister is valved closed, also includes the collector-side line volume. The water vapor pressure is assumed to be that of pure water rather than the much lower vapor pressure over the sample because, for A-101, the collector-side is not in direct contact with the sample and is not in equilibrium with it. Table C.2.2 shows the canister (collector-side) conditions that prevailed for Tank A-101 samples.

Table C.2.2. Canister Conditions at the Time of Collection, for Tank A-101 Samples

Segment / Canister	Pressure (kPa)	Collector Volume (cc)	Temperature (°C)	Water Vapor Pressure (kPa)	Sampler Volume (L)
5-J1	98.35	39.5	23.9	2.968	0.3072
5-J2	69.423	56.5	23.8	2.950	0.3072
5-J3	57.659	55.8	24.2	3.022	0.3072
8-J1	99.17	40.5	24.4	3.059	0.3055
8-J2	72.55	57.7	24.8	3.132	0.3055
8-J3	52.59	57.2	25.3	3.228	0.3055
12-J1	56.366	57.1	25.2	3.208	0.3066
12-J2	59.199	41.1	25.8	3.324	0.3066
12-J3	39.598	57.2	25.8	3.324	0.3066
2-J1*	97.68	39.5	25	3.169	0.3068
2-J2*	92.815	56.5	25	3.169	0.3068
2-J3*	95.88	55.8	25	3.169	0.3068
9-J1	99.93	40.5	24.3	3.040	0.3071
9-J2	98.524	57.7	24.2	3.022	0.3071
9-J3	71.039	57.2	24.7	3.114	0.3071
16-J1	58.992	56.1	23.2	2.845	0.3063
16-J2	48.809	39.9	24.3	3.040	0.3063
16-J3	33.795	55.8	24.2	3.022	0.3063
19-J1	63.616	57.1	23.8	2.950	0.3077
19-J2	51.697	41.1	24.8	3.132	0.3077
19-J3	38.276	57.2	24.6	3.096	0.3077

* Segment 2 is believed to have been contaminated by inleaked air during extraction.

Tables C.2.3 through C.2.5 give the peak collector-side pressures during the extraction pump cycling. In most cases, the last five pressures are used for regression to get the pressure versus cycle derivatives. Where fewer points are used, the data on which regressions were performed are put in bold-face.

Table C.2.3. Pump Cycle Peak Pressures (kPa) for Canister 1 of Each Segment of Tank A-101

Cycle	5-J1	8-J1	12-J1	2-J1*	9-J1	16-J1	19-J1
1	36.107	38.516	17.947	46.517	47.325	17.178	19.015
2	60.881	61.994	27.958	76.06	78.156	26.628	29.421
3	89.016	77.918	33.762	97.728	99.972	32.214	35.736
4	98.364	90.503	38.047			36.753	40.128
5		99.242	41.37			40.196	44.526
6			44.853			44.697	48.645
7			47.334			48.312	52.259
8			50.593			51.706	55.63
9			53.536			54.867	59.898
10			56.366			58.992	63.616

* Segment 2 is believed to have been contaminated by inleaked air during extraction.

Table C.2.4. Pump Cycle Peak Pressures (kPa) for Canister 2 of Each Segment of Tank A-101

Cycle	5-J2	8-J2	12-J2	2-J2*	9-J2	16-J2	19-J2
1	27.058	30.785	20.728	44.149	45.793	19.419	20.326
2	39.155	41.902	32.421	57.36	60.16	28.245	29.352
3	47.39	48.725	39.01	67.205	**71.863**	33.054	34.317
4	53.701	**56.504**	43.221	**74.924**	**81.97**	36.071	37.955
5	**59.735**	**61.473**	46.708	**81.493**	**90.526**	39.049	40.506
6	**64.378**	**67.105**	49.06	**87.416**	**98.524**	40.948	42.976
7	**69.423**	**72.55**	51.635	**92.815**		**43.315**	45.169
8			54.339			**44.869**	46.673
9			56.542			**46.788**	49.375
10			59.199			**48.809**	51.697

* Segment 2 is believed to have been contaminated by inleaked air during extraction.

Table C.2.5. Pump Cycle Peak Pressures (kPa) for Canister 3 of Each Segment of Tank A-101

Cycle	5-J3	8-J3	12-J3	2-J3*	9-J3	16-J3	19-J3
1	49.158	19.337	22.547	46.994	21.381	19.03	19.796
2	25.718	28.094	26.085	76.317	34.049	21.992	23.161
3	33.446	33.237	28.459	95.871	41.323	23.575	25.647
4	38.121	35.973	30.233		46.169	24.759	27.386
5	42.067	39.496	31.89		50.957	26.37	26.969
6	45.877	41.676	33.477		55.324	27.887	29.436
7	48.461	44.251	35.113		59.714	29.372	31.38
8	52.069	**49.066**	36.714		63.667	30.938	33.11
9	54.585	**49.703**	38.177		67.391	32.158	35.064
10	57.659	**50.976**	39.598		71.039	33.795	36.536
11		**52.59**					38.276

* Segment 2 is believed to have been contaminated by inleaked air during extraction.

Table C.2.6 shows the amounts of gases that are calculated based on the data presented earlier. The regression slopes in Table C.2.8 also play a part in the determination of the "residuals," which have meaning only for ammonia.

Table C.2.6. Quantities of Gases Found in Tank A-101 Samples

Segment / Canister	N_2 (µmol)	H_2 (µmol)	N_2O (µmol)	O_2 (µmol)	CH_4 (µmol)	Ar (µmol)
5-J1	200±6	848±19	66.2±2.0	6.3±0.2	6.3±0.8	2.6±0.2
5-J2	148±5	651±20	49.4±1.8	4.9±0.3	5.5±0.8	2.0±0.3
5-J3	21.2±0.8	96±4	9.0±0.4	1.0±0.05	3.3±0.6	0.4±0.04
5-TOTAL	369±13	1595±42.4	125±4.2	12.1±0.6	15.1±2.18	5.0±0.5
8-J1	234±8	982±22.1	70.8±2.2	6.3±0.3	8.3±0.8	1.5±0.1
8-J2	189±7	808±23.6	56.6±2.3	5.7±0.2	7.0±0.2	1.2±0.1
8-J3	31.3±1.4	139±6.4	10.5±0.5	0.7±0.1	1.9±0.6	0.3±0.05
8-TOTAL	455±17	1929±52.1	138±4.9	12.7±0.6	17.2±1.62	3.0±0.3
12-J1	113±5	11.1±0.5	16.6±0.9	15.9±0.8	1.5±0.6	56.7±2.3
12-J2	9.3±0.4	1.2±0.2	5.4±0.6	0.7±0.1	0.7±0.2	2.7±0.3
12-J3	5.8±0.3	0.7±0.1	3.1±0.4	0.4±0.04	0.8±0.2	1.3±0.2
12-TOTAL	128±5	13.0±0.7	25.1±1.8	17.0±0.9	2.96±0.97	60.7±2.8
2-J1*	645±20	482±13.9	57.4±1.7	116±3.9	2.86±0.76	7.8±0.3
2-J2*	815±21	515±15.6	60.5±1.8	163±5.5	1.03±1.03	9.8±0.5
2-J3*	1352±31	32.3±1.0	5.1±0.2	357±10.1	0.00±0.00	16.3±0.6
2-TOTAL*	2812±71	1029±30.4	123±3.7	636±19.6	3.89±1.78	33.9±1.4
9-J1	286±9	841±19	59.0±1.8	1.1±0.1	10.3±0.8	42.7±1.2
9-J2	314±10	950±22	64.9±1.9	1.8±0.1	11.4±1.1	45.5±1.3
9-J3	36±1.3	124±5	11.8±0.5	0.4±0.0	1.6±0.8	1.9±0.1
9-TOTAL	636±20	1914±45.6	136±4.2	3.3±0.2	23.3±2.75	90.0±2.6
16-J1	88±4	15.0±0.6	18.5±0.7	7.0±0.3	0.7±0.1	86.9±4.0
16-J2	5.6±0.3	1.1±0.1	3.3±0.2	0.5±0.2	0.1±0.1	4.4±0.4
16-J3	3.5±0.2	0.7±0.1	2.2±0.1	0.4±0.1	0.1±0.0	2.4±0.2
16-TOTAL	97±4	16.8±0.7	24.1±1.1	8.0±0.6	0.91±0.2	93.8±4.5
19-J1	192±8	31.0±1.1	25.5±1.0	23.2±0.9	1.3±0.1	86.4±4.0
19-J2	11.4±0.5	2.2±0.1	3.8±0.2	1.2±0.1	0.0±0.00	4.6±0.2
19-J3	7.6±0.4	0.2±0.1	2.3±0.1	0.7±0.0	0.0±0.00	2.4±0.2
19-TOTAL	211±8	33.5±1.3	31.6±1.3	25.1±1.0	1.26±0.15	93.5±4.4
* Segment 2 is believed to have been contaminated by inleaked air during extraction.						

Table C.2.6 (contd)

Segment / Canister	Other NOx (µmol)	C_2H_x (µmol)	C_3H_x (µmol)	Other HC (µmol)	NH_3 (µmol)
5-J1	0.2±0.1	0.8±0.2	0.31±0.08	0.6±0.2	397±47
5-J2	0.3±0.2	0.8±0.2	0.46±0.15	0.6±0.2	654±64
5-J3	0.5±0.1	0.6±0.1	0.49±0.12	1.4±0.3	1098±63
5-residual					0±0
5-TOTAL	1.00±0.35	2.14±0.43	1.25±0.35	2.58±0.56	2148±173
8-J1	0.8±0.2	0.9±0.2	0.3±0.2	0.6±0.2	267±48
8-J2	0.8±0.03	1.0±0.2	0.5±0.2	0.6±0.2	550±130
8-J3	0.7±0.2	0.6±0.1	0.3±0.1	0.6±0.1	956±98
8-residual					549±386
8-TOTAL	2.28±0.42	2.48±0.4	1.14±0.43	1.85±0.44	2322±662
12-J1	0.2±0.1	0.1±0.04	0.0±0.02	0.4±0.1	1003±61
12-J2	0.4±0.2	0.0±0.00	0.1±0.0	0.4±0.1	905±33
12-J3	0.3±0.2	0.0±0.00	0.2±0.1	0.3±0.1	818±43
12-residual					2221±1727
12-TOTAL	0.92±0.41	0.09±0.04	0.32±0.15	0.99±0.30	4948±1863
2-J1*	0.18±0.09	1.05±0.15	0.30±0.15	0.45±0.15	196±30
2-J2*	0.41±0.41	1.23±0.21	0.61±0.20	0.82±0.21	470±42
2-J3*	0.63±0.21	0.21±0.10	0.63±0.21	0.83±0.21	313±42
2-residual*					0±0
2-TOTAL*	1.22±0.71	2.49±0.46	1.54±0.56	2.10±0.57	979±115
9-J1	0.0±0.00	1.6±0.05	0.2±0.1	0.5±0.2	349±33
9-J2	0.0±0.00	1.8±0.2	0.4±0.2	0.7±0.2	847±48
9-J3	0.3±0.2	0.3±0.2	0.3±0.2	0.6±0.2	1392±43
9-residual					7539±8803
9-TOTAL	0.31±0.16	3.68±0.43	0.98±0.46	1.77±0.54	10126±8927
16-J1	0.2±0.1	0.2±0.1	0.0±0.00	0.5±0.1	1061±63
16-J2	0.2±0.1	0.0±0.0	0.1±0.04	0.2±0.1	723±30
16-J3	0.2±0.1	0.0±0.0	0.1±0.1	0.2±0.1	685±41
16-residual					910±441
16-TOTAL	0.58±0.22	0.18±0.1	0.22±0.1	0.94±0.3	3379±576
19-J1	0.2±0.1	0.3±0.1	0.0±0.00	0.4±0.1	1038±44
19-J2	0.2±0.1	0.0±0.00	0.1±0.05	0.2±0.1	782±31
19-J3	0.2±0.1	0.0±0.00	0.2±0.1	0.2±0.1	798±42
19-residual					1311±576
19-TOTAL	0.60±0.23	0.28±0.1	0.27±0.13	0.83±0.30	3929±692

Table C.2.7. Mole Percents of Gases in Tank A-101 Dry Insoluble Gas

Segment / Canister	N_2	H_2	N_2O	O_2	CH_4	Ar
5-J1	17.7%±2.1%	75.1%±8.7%	5.9%±0.7%	0.6%±0.07%	0.55%±0.09%	0.23%±0.03%
5-J2	17.0%±1.6%	75.1%±7.0%	5.7%±0.5%	0.6%±0.06%	0.63%±0.11%	0.23%±0.04%
5-J3	15.6%±0.8%	70.9%±3.7%	6.6%±0.3%	0.7%±0.04%	2.45%±0.47%	0.3%±0.03%
8-J1	18.0%±3.2%	75.2%±13.3%	5.4%±1.0%	0.5%±0.09%	0.64%±0.13%	0.12%±0.02%
8-J2	17.7%±4.2%	75.8%±17.8%	5.3%±1.3%	0.5%±0.13%	0.65%±0.15%	0.12%±0.03%
8-J3	17.2%±1.7%	76.3%±7.5%	5.8%±0.6%	0.4%±0.05%	1.06%±0.33%	0.14%±0.03%
12-J1	51.1%±2.7%	5.1%±0.3%	7.6%±0.5%	7.2%±0.42%	0.67%±0.28%	25.7%±1.35%
12-J2	50.5%±1.1%	6.5%±1.0%	29.0%±3.0%	3.8%±0.35%	4.00%±1.00%	14.5%±1.51%
12-J3	34.5%±1.1%	4.2%±0.4%	18.5%±2.0%	2.2%±0.20%	4.50%±1.00%	8.0%±1.00%
2-J1*	49.2%±7.6%	36.8%±5.7%	4.4%±0.7%	8.9%±1.38%	0.22%±0.07%	0.60%±0.09%
2-J2*	51.8%±4.6%	32.7%±2.9%	3.8%±0.3%	10.4%±0.94%	0.06%±0.07%	0.62%±0.06%
2-J3*	76.2%±10.2%	1.8%±0.2%	0.3%±0.0%	20.1%±2.71%	0.00%±0.00%	0.9%±0.12%
9-J1	23.1%±2.2%	67.9%±6.2%	4.8%±0.4%	0.1%±0.01%	0.83%±0.10%	3.45%±0.32%
9-J2	22.7%±1.3%	68.7%±3.6%	4.7%±0.3%	0.1%±0.01%	0.82%±0.09%	3.29%±0.18%
9-J3	20.5%±0.5%	69.9%±1.9%	6.6%±0.2%	0.2%±0.02%	0.88%±0.44%	1.0%±0.05%
16-J1	40.6%±2.3%	6.9%±0.4%	8.5%±0.4%	3.2%±0.17%	0.31%±0.03%	40.0%±2.26%
16-J2	36.2%±1.0%	7.2%±0.3%	21.4%±1.0%	3.2%±1.43%	0.95%±0.48%	28.6%±2.39%
16-J3	36.4%±0.7%	7.4%±0.4%	22.9%±0.7%	4.3%±1.43%	0.86%±0.36%	25.0%±0.73%
19-J1	52.7%±1.8%	8.5%±0.3%	7.0%±0.2%	6.3%±0.21%	0.35%±0.04%	23.7%±1.00%
19-J2	47.3%±1.0%	9.3%±0.2%	15.7%±0.3%	5.1%±0.13%	0.00%±0.00%	19.0%±0.67%
19-J3	52.2%±1.1%	8.9%±0.2%	15.6%±0.6%	4.9%±0.11%	0.00%±0.00%	16.7%±0.56%

* Segment 2 is believed to have been contaminated by inleaked air during extraction.

Table C.2.7 (contd)

Segment / Canister	Other NOx	C_2H_x	C_3H_x	Other HC
5-J1	0.02%±0.01%	0.07%±0.02%	0.03%±0.01%	0.05%±0.01%
5-J2	0.04%±0.02%	0.09%±0.02%	0.05%±0.02%	0.07%±0.02%
5-J3	0.36%±0.09%	0.45%±0.09%	0.36%±0.09%	1.00%±0.19%
8-J1	0.06%±0.02%	0.07%±0.02%	0.02%±0.01%	0.05%±0.01%
8-J2	0.08%±0.02%	0.09%±0.03%	0.05%±0.02%	0.06%±0.02%
8-J3	0.38%±0.13%	0.31%±0.07%	0.19%±0.07%	0.31%±0.07%
12-J1	0.10%±0.03%	0.04%±0.02%	0.02%±0.01%	0.17%±0.06%
12-J2	2.00%±1.00%	0.00%±0.00%	0.55%±0.25%	2.00%±0.50%
12-J3	2.00%±1.00%	0.00%±0.00%	1.00%±0.50%	1.50%±0.50%
2-J1*	0.01%±0.01%	0.08%±0.02%	0.02%±0.01%	0.03%±0.01%
2-J2*	0.03%±0.03%	0.08%±0.01%	0.04%±0.01%	0.05%±0.01%
2-J3*	0.04%±0.01%	0.01%±0.01%	0.04%±0.01%	0.05%±0.01%
9-J1	0.00%±0.00%	0.13%±0.01%	0.02%±0.01%	0.04%±0.01%
9-J2	0.00%±0.00%	0.13%±0.02%	0.03%±0.02%	0.05%±0.02%
9-J3	0.18%±0.09%	0.18%±0.09%	0.18%±0.09%	0.35%±0.09%
16-J1	0.07%±0.04%	0.08%±0.03%	0.00%±0.00%	0.24%±0.06%
16-J2	1.43%±0.48%	0.00%±0.00%	0.52%±0.24%	1.43%±0.48%
16-J3	2.14%±0.71%	0.00%±0.00%	1.43%±0.71%	2.1%±0.71%
19-J1	0.04%±0.02%	0.08%±0.04%	0.00%±0.00%	0.1%±0.04%
19-J2	0.87%±0.30%	0.00%±0.00%	0.43%±0.20%	1.0%±0.33%
19-J3	1.61%±0.50%	0.00%±0.00%	1.11%±0.56%	1.1%±0.56%

* Segment 2 is believed to have been contaminated by inleaked air during extraction.

As discussed in Section 3.2, a regression was performed on the total pressures during the last several pump cycles (or "strokes") to find the residual ammonia content of the sample. The variables derived by, and used in, the regression are given in Table C.2.8. For segments 2,5,8, and 9, the gas content of the samples was so great that the pressure limit of 90 kPa was exceeded within a few pump cycles on canister J1, too few to allow a usable regression.

Table C.2.8. Pressure Regression Variables for Tank A-101 Sample Cycling

Segment / Canister	dp/dN (kPa/stroke)	p_{ins} (kPa)	N (number of strokes)	$(\Delta n/\Delta N)_{NH3}$ (mgmol NH3 per stroke)
5-J1		70.583	4	
5-J2	4.844±1.414	37.889	7	6.09E-02±1.87E-02
5-J3	2.969±0.632	6.01	10	6.35E-02±1.40E-02
8-J1		79.772	5	
8-J2	5.377±0.894	45.816	7	6.53E-02±1.89E-02
8-J3	1.185±0.894	7.898	11	2.38E-02±1.82E-02
12-J1	2.923±0.632	9.568	10	6.18E-02±1.39E-02
12-J2	2.519±0.632	1.117	10	
12-J3	1.531±0.632	0.725	10	3.48E-02±1.45E-02
2-J1*		82.224	3	
2-J2*	5.96±0.894	69.027	7	
2-J3*		78.804	3	
9-J1		75.574	3	
9-J2	8.854±0.894	59.211	6	1.02E-01±1.18E-02
9-J3	3.911±0.632	7.676	10	8.59E-02±1.42E-02
16-J1	3.515±0.632	9.545	10	7.46E-02±1.41E-02
16-J2	1.84±0.894	0.961	10	2.93E-02±1.43E-02
16-J3	1.46±0.632	0.431	10	3.27E-02±1.43E-02
19-J1	3.758±0.632	15.773	10	7.79E-02±1.35E-02
19-J2	2.165±0.632	1.457	10	3.53E-02±1.04E-02
19-J3	1.722±0.632	0.633	11	3.95E-02±1.47E-02

* Segment 2 is believed to have been contaminated by inleaked air during extraction.

In order to estimate the void fraction and the distribution of gases between the void and slurry phases in each segment, the conditions under which the gas exists must be known. These are given in Table C.2.9 for Tank A-101. The densities were taken from x-ray measurements (Section 4.2.8). The temperatures were based on a profile measured at the MIT tree; the profile is shown in Section 4.2.2. The pressures were derived from hydrostatic head, and are based on the depth of submergence of the segment and the thicknesses and gas-free densities of the waste layers. The solid volume fraction is estimated using 1700 kg/m^3 as the density of solid-free liquid (from x-ray data), 1350 kg/m^3 as the density of gas-free slurry (from x-ray data), and an assumed 1280 kg/m^3 as the intrinsic (not bulk) density of the solid material. This solid density is taken from Brevick and Gaddis (1995).

The water vapor pressure is the pressure in equilibrium with water in the waste; it is calculated using Equation 6.2 and Table 6.2 of Mahoney and Trent (1995), a correlation for water vapor pressure over concentrated homogeneous and non-homogeneous waste simulants. This correlation requires the weight fraction of water in the slurry, which is calculated using the solid volume fraction and density and the weight fraction of water in the solids-free solution. The latter value was estimated at 0.25, based on Equation 4.4 of Mahoney and Trent (1995), which allows the weight fraction of water in a simulant solution to be back-calculated from the solution density.

Table C.2.9. In-Tank Conditions Used for Tank A-101 Phase Distribution Calculations

Segment	Density (kg/m^3)	Temperature (°C)	Pressure (atm)	Solid Volume Fraction	Water Vapor Pressure (atm)
5	1350	46	1.29	0.83	0.0109
8	1350	57	1.48	0.83	0.0188
12	1700	62	1.78	0	0.0531
2	1350	33	1.10	0.83	0.00546
9	1350	63	1.54	0.83	0.0249
16	1700	61	2.09	0	0.0506
19	1700	60	2.33	0	0.0483

The average ionic concentrations in the drainable liquid in Tank A-101 are given in Table C.2.10. They are based on the A-101 solution density of 1700 kg/m^3 and Tables 11 and 13 of WHC-SD-WM-DP-192 Rev. 0, data for µg/g ionic concentrations from 1996 core sample analyses for Risers 24A and 24B of Tank AW-101.

Table C.2.10. Ionic Concentrations Used For Tank A-101 Phase Distribution Calculations

Ion	gmol/L solution
Na^+	3.28
Al^{3+}	2.02
Fe^{3+}	0
Cr^{3+}	0.0037
Ni^{2+}	0.00020
K^+	1.59
OH^-	1.21
NO_3^-	4.39
NO_2^-	3.66
PO_4^{3-}	0
SO_4^{2-}	0
F^-	0
Cl^-	0.24

The Henry's Law constants are necessary to estimate the in-tank phase distribution of gases (see Section 3.2). The intermediate steps in the Henry's Law constant calculation are shown in Table C.2.11. Note that the final Henry's Law constant is in terms of liters of gas-free waste slurry, while the Schumpe model is in terms of kg of water in the salt solution. Both the solid volume fraction and the weight percent of water in the solution are needed to put the Henry's Law constant in its final form. The gases not listed, argon and the minor gases, were assumed wholly insoluble with Henry's law constants of 10^{-10}.

Table C.2.11. Henry's Law Constants For Tank A-101 Phase Distribution Calculations

Segment	Condition	N_2	H_2	N_2O	O_2	CH_4	NH_3
5	Schumpe (K in water / K in solution)	15.5	9.0	12.9	20	18.7	4.2
	Waste Slurry K (mol/atm L waste)	2.4×10^{-6}	5.8×10^{-6}	8.1×10^{-5}	3.5×10^{-6}	4.1×10^{-6}	0.41
8	Schumpe (K in water / K in solution)	12.1	8.0	10.6	17.4	15.0	4.2
	Waste Slurry K (mol/atm L waste)	3.0×10^{-6}	6.6×10^{-6}	8.0×10^{-5}	3.7×10^{-6}	4.7×10^{-6}	0.26
12	Schumpe (K in water / K in solution)	10.8	7.5	9.7	16.3	13.6	4.2
	Waste Slurry K (mol/atm L waste)	2.0×10^{-5}	4.2×10^{-5}	4.8×10^{-4}	2.3×10^{-5}	3.0×10^{-5}	1.3
2	Schumpe (K in water / K in solution)	21	10.4	16.4	24	24	4.2
	Waste Slurry K (mol/atm L waste)	2.0×10^{-6}	5.2×10^{-6}	8.6×10^{-5}	3.5×10^{-6}	3.7×10^{-6}	0.71
9	Schumpe (K in water / K in solution)	10.5	7.4	9.5	16.1	13.4	4.2
	Waste Slurry K (mol/atm L waste)	3.3×10^{-6}	7.1×10^{-6}	8.1×10^{-5}	3.8×10^{-6}	5.1×10^{-6}	0.21
16	Schumpe (K in water / K in solution)	11.0	7.6	9.9	16.6	13.9	4.2
	Waste Slurry K (mol/atm L waste)	1.9×10^{-5}	4.1×10^{-5}	4.8×10^{-4}	2.3×10^{-5}	3.0×10^{-5}	1.3
19	Schumpe (K in water / K in solution)	11.3	7.7	10.0	16.8	14.2	4.2
	Waste Slurry K (mol/atm L waste)	1.9×10^{-5}	4.1×10^{-5}	4.8×10^{-4}	2.2×10^{-5}	2.9×10^{-5}	1.4

The Henry's Law constant calculation is one method of calculating the ammonia partial pressure. Another method uses a grab-sample of extractor atmosphere, which is analyzed to find the ammonia content and hence the partial pressure at the time the sample was taken. Table C.2.12 shows the results of these analyses for A-101 samples. In the table, "UBV" indicates unbound vapor, or the sample taken just before the J1 canister; "BV" means bound vapor, the sample taken just after the temperature ramp.

Table C.2.12. Grab-Sample Data for Deriving Ammonia Partial Pressures in Tank A-101

Sample	Grab-Sample Volume (cc)	Fill Temperature (°C)	Fill Pressure (kPa)	µmol NH_3	NH_3 Partial Pressure (atm)
5-UBV	51.7	23.4	6.609	38.2	0.018
5-BV	52	24.9	4.03	63.8	0.030
8-UBV	154.8	24	6.862	67.0	0.011
8-BV	52	25	3.865	43.8	0.021
12-UBV	51.7	23.9	3.729	50.6	0.024
12-BV	40.5	25.5	4.517	43.1	0.026
2-UBV*	38.6	24.4	7.727	21.4	0.014
2-BV*	52	24.9	7.878	25.3	0.012
9-UBV	154.8	23.7	8.062	56.5	0.009
9-BV	52.2	24.3	3.989	42.7	0.020
16-UBV	52	23.1	3.57	57.0	0.027
16-BV	51.7	23.9	4.064	47.7	0.023
19-UBV	52	23.2	3.947	60.7	0.028
19-BV	51.7	23.3	4.026	55.5	0.026
*Segment 2 is believed to have been contaminated by inleaked air during extraction.					

C.3 Tank 241-AN-105

As described in Section 2.3, gases are extracted from waste samples into "J" canisters and then undergo analysis from mass spectroscopy to obtain the mole fraction composition of the extracted gas on a dry basis. (Water vapor is not measured.) The results, for Tank AN-105, are shown in Table C.3.1.

Table C.3.1. Mole Percents of Gases Measured in Tank AN-105 Dry Gas (obtained by mass spectroscopy)

Segment / Canister	N_2	H_2	N_2O	O_2	CH_4	Ar
15-J1	44±1.000	4.7±0.100	5.6±0.100	7.6±0.200	0.17±0.050	0.52±0.020
15-J2	7.8±0.200	1.95±0.040	5.3±0.100	1.23±0.020	0.3±0.050	0.11±0.010
15-J3	41±1.000	0.86±0.020	2.25±0.050	10.3±0.200	0.2±0.050	0.47±0.020
17-J1	23.2±0.500	53.9±0.500	8.8±0.200	1.3±0.100	0.45±0.050	0.12±0.010
17-J2	8.5±0.400	19.7±0.400	6.9±0.100	0.5±0.010	0.36±0.040	0.081±0.004
17-J3	7.2±0.300	16.3±0.300	5.9±0.100	0.27±0.010	0.43±0.040	0.099±0.005
19-J1	23±0.500	60.7±0.600	11.5±0.200	0.66±0.010	0.54±0.050	0.074±0.003
19-J2	21.5±0.400	57.5±0.600	10.8±0.200	0.78±0.020	0.51±0.050	0.069±0.003
19-J3	5.3±0.100	16.1±0.300	5.2±0.100	0.35±0.010	0.34±0.030	0.063±0.003
21-J1	20.4±0.400	50.2±0.500	16.1±0.300	0.2±0.010	0.67±0.010	5.7±0.100
21-J2	8.8±0.200	22.5±0.500	16.2±0.300	0.18±0.010	0.41±0.010	1.9±0.040
21-J3	7.4±0.100	18.8±0.600	13.4±0.300	0.21±0.010	0.43±0.010	1.6±0.030
4-J1	38.2±0.200	5.9±0.100	4.7±0.100	6.6±0.200	0.17±0.040	9.6±0.200
4-J2	11±0.200	2.28±0.050	3.43±0.070	1.6±0.030	0.05±0.050	2.5±0.050
4-J3	8.2±0.200	1.84±0.040	2.86±0.060	1.32±0.030	0.32±0.060	2.01±0.040
16-J1	43±1.000	6.3±0.100	4.2±0.100	5.1±0.100	0.16±0.050	7.1±0.200
16-J2	6.9±0.200	1.78±0.050	3.8±0.100	0.66±0.030	0.23±0.040	0.79±0.050
16-J3	3.6±0.100	1.05±0.020	2.15±0.040	0.28±0.010	0.25±0.005	0.45±0.020
18-J1	28.9±0.600	37.4±0.700	8.2±0.200	2±0.100	0.36±0.010	1.7±0.100
18-J2	4.2±0.100	8.1±0.200	5±0.100	0.24±0.005	0.39±0.010	0.26±0.005
18-J3	3.5±0.070	7±0.100	4.3±0.090	0.21±0.004	0.42±0.010	0.25±0.005

Table C.3.1 (contd)

Segment / Canister	Other NOx	C_2H_x	C_3H_x	Other HC	NH_3
15-J1	0.12±0.080	0.02±0.001	0.04±0.010	0.07±0.010	37±8.00
15-J2	0.16±0.090	0.16±0.050	0.09±0.010	0.25±0.050	83±8.00
15-J3	0.11±0.080	0.1±0.050	0.07±0.030	0.16±0.050	45±5.00
17-J1	0.09±0.005	0.07±0.020	0.02±0.010	0.05±0.002	12±3.00
17-J2	0.13±0.050	0.18±0.050	0.06±0.030	0.5±0.100	63±6.00
17-J3	0.12±0.050	0.48±0.080	0.11±0.010	0.83±0.020	68±7.00
19-J1	0.1±0.050	0.02±0.001	0.031±0.006	0.025±0.005	3±1.00
19-J2	0.11±0.050	0.022±0.001	0.033±0.006	0.03±0.006	9±2.00
19-J3	0.13±0.050	0.27±0.050	0.1±0.010	0.63±0.010	72±7.00
21-J1	0.15±0.010	0.02±0.010	0.03±0.010	0.02±0.010	7±2.00
21-J2	0.26±0.010	0.13±0.010	0.06±0.010	0.3±0.010	49±5.00
21-J3	0.28±0.010	0.27±0.010	0.08±0.010	0.42±0.010	57±6.00
4-J1	0.1±0.050	0.02±0.010	0.04±0.010	0.05±0.010	35±8.00
4-J2	0.18±0.040	0.15±0.030	0.08±0.020	0.2±0.040	79±8.00
4-J3	0.25±0.050	0.26±0.050	0.12±0.040	0.28±0.040	83±8.00
16-J1	0.12±0.050	0.00±0.000	0.04±0.020	0.07±0.020	34±8.00
16-J2	0.2±0.100	0.14±0.050	0.09±0.020	0.31±0.060	85±8.00
16-J3	0.23±0.050	0.18±0.050	0.12±0.040	0.31±0.060	91±4.00
18-J1	0.1±0.005	0.06±0.005	0.02±0.001	0.05±0.001	21±4.00
18-J2	0.17±0.005	0.48±0.010	0.06±0.001	0.82±0.020	80±8.00
18-J3	0.2±0.004	0.71±0.010	0.06±0.001	1.2±0.020	82±8.00

The pressure and temperature of the gas in the J canisters are measured at the time of collection. The collector volume always includes the canister volume and, in cases where the collector is pumped down to vacuum after a canister is valved closed, also includes the collector-side line volume. The water vapor pressure is assumed to be that of pure water rather than the much lower vapor pressure over the sample because, for AN-105, the collector-side is not in direct contact with the sample and is not in equilibrium with it. Table C.3.2 shows the canister (collector-side) conditions that prevailed for Tank AN-105 samples.

Table C.3.2. Canister Conditions at the Time of Collection, for Tank AN-105 Samples

Segment / Canister	Pressure (kPa)	Collector Volume (cc)	Temperature (°C)	Water Vapor Pressure (kPa)	Sampler Volume (L)
15-J1	18.56	56.1	26.9	3.544	0.3146
15-J2	13.066	39.9	27	3.565	0.3146
15-J3	13.228	55.8	26.9	3.544	0.3146
17-J1	75.938	57.1	26	3.361	0.3151
17-J2	18.448	41.1	26.6	3.482	0.3151
17-J3	11.354	57.2	26.5	3.462	0.3151
19-J1	96.79	39.5	25.7	3.302	0.3073
19-J2	76.57	56.5	26.1	3.381	0.3073
19-J3	28.12	55.8	26.8	3.523	0.3073
21-J1	89.381	56.1	25.4	3.243	0.3073
21-J2	18.671	39.9	26.8	3.523	0.3073
21-J3	10.544	55.8	26.6	3.482	0.3073
4-J1	16.04	56.1	24.5	3.074	0.3059
4-J2	11.33	39.9	25	3.167	0.3059
4-J3	7.157	55.8	25.1	3.186	0.3059
16-J1	19.386	57.1	25.6	3.282	0.3058
16-J2	9.177	41.1	26.9	3.544	0.3058
16-J3	6.682	57.2	26.8	3.523	0.3058
18-J1	37.097	57.1	24.8	3.13	0.3064
18-J2	16.079	41.1	26	3.361	0.3064
18 -J3	8.897	57.2	25.8	3.321	0.3064

Tables C.3.3 through C.3.5 give the peak collector-side pressures during the extraction pump cycling. Only the last five pressures are used for regression to get the pressure versus cycle derivatives.

Table C.3.3. Pump Cycle Peak Pressures (kPa) for Canister 1 of Each Segment of Tank AN-105

Cycle	15-J1	17-J1	19-J1	21-J1	4-J1	16-J1	18-J1
1	9.482	26.322	42.607	26.502	8.91	10.196	15.5
2	12.9	40.615	67.034	45.559	11.96	13.92	22.884
3	14.805	48.819	82	56.647	13.445	15.718	26.984
4	15.858	54.223	96.794	63.484	14.198	16.304	29.273
5	16.447	58.342		68.257	14.657	16.806	30.578
6	17.041	61.369		73.038	14.961	17.45	32.161
7	17.369	64.219		75.752	15.201	17.695	33.523
8	17.734	66.779		81.636	15.453	18.153	34.269
9	17.835	70.936		84.449	15.675	18.502	35.288
10	18.188	72.853		86.28	15.888	18.838	36.121
11	18.549	75.938		89.831	16.041	19.386	37.097

Table C.3.4. Pump Cycle Peak Pressures (kPa) for Canister 2 of Each Segment of Tank AN-105.

Cycle	15-J2	17-J2	19-J2	21-J2	4-J2	16-J2	18-J2
1	8.233	10.138	37.572	10.981	7.825	7.045	9.887
2	10.784	13.459	45.105	14.978	9.872	8.355	12.873
3	11.922	15.373	50.605	16.548	10.411	8.654	14.274
4	12.352	16.181	54.538	17.252	10.804	8.845	14.761
5	12.571	16.849	58.402	17.433	10.894	8.975	14.991
6	12.776	17.132	61.511	17.637	11.073	8.896	15.33
7	12.916	17.174	64.735	17.934	11.089	9.04	15.496
8	12.992	17.836	67.757	18.169	11.168	9.084	15.304
9	13.066	18.163	70.822	18.331	11.167	9.097	15.81
10	13.125	18.26	73.568	18.454	11.191	9.098	16.079
11	13.066	18.448	76.568	18.671	11.326	9.119	
12						9.177	

Table C.3.5. Pump Cycle Peak Pressures (kPa) for Canister 3 of Each Segment of Tank AN-105

Cycle	15-J3	17-J3	19-J3	21-J3	4-J3	16-J3	18-J3
1	10.869	18.437	12.574	6.166	5.43	4.685	7.074
2	11.859	8.081	17.107	8.16	6.132	5.861	8.059
3	12.113	9.395	19.659	9.121	6.506	6.242	8.416
4	12.655	10.084	20.416	9.729	6.689	6.36	8.567
5	12.693	10.32	21.367	10.035	6.806	6.475	8.703
6	12.829	10.519	22.031	10.23	6.876	6.548	8.793
7	12.991	10.652	22.596	10.341	6.916	6.574	8.823
8	12.965	10.86	23.014	10.284	7.177	6.597	8.935
9	13.108	11.007	23.631	10.45	7.042	6.669	8.93
10	13.228	11.001	23.846	10.522	7.157	6.682	8.897
11		11.157	24.388	10.544			
12		11.354	24.679				
13			24.924				
14			25.425				
15			25.908				
16			26.361				
17			26.674				
18			26.678				
19			27.365				
20			27.578				
21			28.121				

Table C.3.6 shows the amounts of gases that are calculated based on the data presented earlier. The regression slopes in Table C.3.8 also play a part in the determination of the "residuals," which have meaning only for ammonia.

Table C.3.6. Quantities of Gases Found in Tank AN-105 Samples

Segment / Canister	N_2 (µmol)	H_2 (µmol)	N_2O (µmol)	O_2 (µmol)	CH_4 (µmol)	Ar (µmol)
15-J1	149±16	16±2	18.9±2.1	25.7±2.9	0.6±0.2	1.8±0.2
15-J2	12±1.8	3.0±0	8.1±1.2	1.9±0.3	0.5±0.1	0.2±0.03
15-J3	88.8±13.6	1.9±0	4.9±0.7	22.3±3.41	0.4±0.1	1.0±0.16
15-TOTAL	249±32	21±2.5	32±4.1	49.8±6.5	1.5±0.41	2.9±0.4
17-J1	387±13	898±26	147±5.2	21.7±1.8	7.5±0.9	2.0±0.2
17-J2	21±2.5	49±5	17.0±1.9	1.2±0.1	0.9±0.1	0.2±0.02
17-J3	13±2.4	30±5	10.7±1.9	0.5±0.1	0.8±0.2	0.2±0.03
17-TOTAL	421±18	976±36.6	174±9.0	23.4±2.0	9.2±1.2	2.4±0.2
19-J1	342±11	902±21.8	171±4.8	9.8±0.3	8.0±0.8	1.1±0.05
19-J2	357±12	956±27.8	180±5.9	13.0±0.5	8.5±0.9	1.1±0.06
19-J3	29.2±2.2	88.6±6.5	28.6±2.1	1.9±0.15	1.9±0.2	0.3±0.03
19-TOTAL	728±25	1946±56	379±12.8	24.7±0.9	18.37±1.8	2.6±0.14
21-J1	397±12	977±25	313±9.4	3.9±0.2	13.0±0.4	111.0±3.3
21-J2	21.3±2.3	54.5±6.0	39.3±4.3	0.4±0.05	1.0±0.11	4.6±0.5
21-J3	11.7±2.2	0.4±5.7	21.2±4.1	0.3±0.06	0.7±0.13	2.5±0.5
21-TOTAL	430±17	1032.3±36.8	373.9±17.8	4.7±0.3	14.72±0.60	118.1±4.3
4-J1	112±14	17±2.2	13.8±1.8	19±2.5	0.50±0.13	28.2±3.6
4-J2	14±3	3.0±0.5	4.5±0.8	2.1±0.4	0.09±0.09	3.3±0.6
4-J3	7.3±2.1	1.6±0.5	2.6±0.7	1.2±0.3	0.29±0.10	1.8±0.5
4-TOTAL	134±19	22±3.2	21±3.3	23±3.2	0.87±0.32	33.3±4.7
16-J1	159±17	23±2.4	15.5±1.7	18.9±2.0	0.6±0.2	26.3±2.8
16-J2	6.4±1.4	1.7±0.4	3.5±0.8	0.6±0.1	0.2±0.1	0.7±0.2
16-J3	2.6±0.8	0.8±0.2	1.6±0.5	0.2±0.1	0.2±0.1	0.3±0.10
16-TOTAL	168±19	26±3.0	21±2.9	19.7±2.2	1.0±0.31	27.3±3.1
18-J1	226±13	293±16.9	64.2±3.8	15.7±1.2	2.8±0.2	13.3±1.1
18-J2	8.8±1.1	17.0±2.2	10.5±1.3	0.5±0.1	0.8±0.1	0.5±0.07
18-J3	4.5±1.0	9.0±2.0	5.5±1.2	0.3±0.06	0.5±0.1	0.3±0.07
18-TOTAL	240±15	319±21.0	80.2±6.4	16.4±1.3	4.2±0.40	14.2±1.2

Table C.3.6 (contd)

Segment / Canister	Other NOx (µmol)	C_2H_x (µmol)	C_3H_x (µmol)	Other HC (µmol)	NH_3 (µmol)
15-J1	0.4±0.3	0.1±0.01	0.14±0.04	0.2±0.04	125±30
15-J2	0.2±0.1	0.2±0.08	0.14±0.03	0.4±0.1	126±23
15-J3	0.2±0.2	0.2±0.11	0.15±0.07	0.3±0.1	97±18
15-residual					0±0
15-TOTAL	0.89±0.59	0.53±0.21	0.42±0.13	0.96±0.26	349±71
17-J1	1.5±0.09	1.2±0.33	0.3±0.2	0.8±0.04	200±50
17-J2	0.3±0.13	0.4±0.1	0.1±0.1	1.2±0.3	155±22
17-J3	0.2±0.1	0.9±0.2	0.2±0.04	1.5±0.3	123±25
17-residual					154±1337
17-TOTAL	2.04±0.32	2.48±0.68	0.68±0.28	3.57±0.59	632±1435
19-J1	1.5±0.7	0.3±0.02	0.5±0.09	0.4±0.07	45±15
19-J2	1.8±0.8	0.4±0.02	0.5±0.10	0.5±0.10	150±33
19-J3	0.7±0.3	1.5±0.3	0.6±0.1	3.5±0.3	396±48
19-residual					56±30
19-TOTAL	4.03±1.86	2.15±0.3	1.56±0.3	4.34±0.4	646±126
21-J1	2.9±0.2	0.4±0.2	0.6±0.20	0.4±0.2	136±39
21-J2	0.6±0.07	0.3±0.04	0.1±0.03	0.7±0.08	119±18
21-J3	0.4±0.09	0.4±0.08	0.1±0.03	0.7±0.13	90±20
21-residual					41±320
21-TOTAL	3.99±0.36	1.13±0.3	0.86±0.25	1.78±0.40	386±396
4-J1	0.29±0.15	0.06±0.03	0.12±0.03	0.15±0.03	103±27
4-J2	0.24±0.07	0.20±0.05	0.11±0.03	0.26±0.07	104±21
4-J3	0.22±0.08	0.23±0.08	0.11±0.05	0.25±0.08	74±22
4-residual					0±0
4-TOTAL	0.75±0.30	0.49±0.16	0.33±0.11	0.66±0.18	281±70
16-J1	0.4±0.2	0.0±0.0	0.1±0.1	0.3±0.1	126±32
16-J2	0.2±0.10	0.1±0.1	0.1±0.0	0.3±0.1	79±19
16-J3	0.2±0.1	0.1±0.1	0.1±0.0	0.2±0.1	66±20
16-residual					0±0
16-TOTAL	0.80±0.35	0.26±0.1	0.32±0.14	0.77±0.24	271±71
18-J1	0.8±0.1	0.5±0.05	0.2±0.01	0.4±0.02	164±33
18-J2	0.4±0.0	1.0±0.13	0.1±0.02	1.7±0.2	168±27
18-J3	0.3±0.1	0.9±0.21	0.1±0.02	1.5±0.3	105±26
18-residual					34±290
18-TOTAL	1.40±0.16	2±0.38	0.36±0.04	3.65±0.59	471±376

Table C.3.7. Mole Percents of Gases in Tank AN-105 Dry Insoluble Gas

Segment / Canister	N_2	H_2	N_2O	O_2	CH_4	Ar
15-J1	69.8%±15.2%	7.5%±1.6%	8.9%±1.9%	12.1%±2.63%	0.27%±0.10%	0.83%±0.18%
15-J2	45.9%±4.6%	11.5%±1.1%	31.2%±3.1%	7.2%±0.71%	1.76%±0.34%	0.65%±0.09%
15-J3	74.5%±8.5%	1.6%±0.2%	4.1%±0.5%	18.7%±2.11%	0.36%±0.10%	0.9%±0.10%
17-J1	26.4%±6.6%	61.3%±15.3%	10.0%±2.5%	1.5%±0.39%	0.51%±0.14%	0.14%±0.04%
17-J2	23.0%±2.4%	53.2%±5.2%	18.6%±1.8%	1.4%±0.13%	0.97%±0.14%	0.22%±0.02%
17-J3	22.5%±2.5%	50.9%±5.3%	18.4%±1.9%	0.8%±0.09%	1.34%±0.19%	0.3%±0.04%
19-J1	23.7%±7.9%	62.6%±20.9%	11.9%±4.0%	0.7%±0.23%	0.56%±0.19%	0.1%±0.03%
19-J2	23.6%±5.3%	63.2%±14.1%	11.9%±2.6%	0.9%±0.19%	0.56%±0.14%	0.1%±0.02%
19-J3	18.9%±1.9%	57.5%±5.7%	18.6%±1.8%	1.3%±0.13%	1.21%±0.16%	0.2%±0.02%
21-J1	21.9%±6.3%	54.0%±15.4%	17.3%±5.0%	0.2%±0.06%	0.72%±0.21%	6.1%±1.75%
21-J2	17.3%±1.8%	44.1%±4.6%	31.8%±3.3%	0.4%±0.04%	0.80%±0.08%	3.7%±0.39%
21-J3	17.2%±1.8%	43.7%±4.8%	31.2%±3.4%	0.5%±0.06%	1.00%±0.11%	3.7%±0.40%
4-J1	58.8%±13.4%	9.1%±2.1%	7.2%±1.7%	10.2%±2.34%	0.26%±0.09%	14.77%±3.39%
4-J2	52.4%±5.4%	10.9%±1.1%	16.3%±1.7%	7.6%±0.78%	0.24%±0.24%	11.90%±1.23%
4-J3	48.2%±4.8%	10.8%±1.1%	16.8%±1.7%	7.8%±0.77%	1.88%±0.40%	11.8%±1.16%
16-J1	65.2%±15.4%	9.5%±2.3%	6.4%±1.5%	7.7%±1.82%	0.24%±0.09%	10.76%±2.55%
16-J2	46.0%±4.5%	11.9%±1.2%	25.3%±2.5%	4.4%±0.46%	1.53%±0.30%	5.27%±0.60%
16-J3	40.0%±2.1%	11.7%±0.6%	23.9%±1.1%	3.1%±0.18%	2.78%±0.13%	5.00%±0.31%
18-J1	36.6%±7.0%	47.3%±9.1%	10.4%±2.0%	2.5%±0.50%	0.46%±0.09%	2.2%±0.43%
18-J2	21.0%±2.2%	40.5%±4.2%	25.0%±2.5%	1.2%±0.12%	1.95%±0.20%	1.3%±0.13%
18-J3	19.4%±1.9%	38.9%±3.8%	23.9%±2.4%	1.2%±0.12%	2.33%±0.23%	1.4%±0.14%

Table C.3.7 (contd)

Segment / Canister	Other NOx	C_2H_x	C_3H_x	Other HC
15-J1	0.19%±0.13%	0.03%±0.01%	0.06%±0.02%	0.11%±0.03%
15-J2	0.94%±0.54%	0.94%±0.31%	0.53%±0.08%	1.47%±0.33%
15-J3	0.20%±0.15%	0.18%±0.09%	0.13%±0.06%	0.29%±0.10%
17-J1	0.10%±0.03%	0.08%±0.03%	0.02%±0.01%	0.06%±0.01%
17-J2	0.35%±0.14%	0.49%±0.14%	0.16%±0.08%	1.35%±0.30%
17-J3	0.38%±0.16%	1.50%±0.29%	0.34%±0.05%	2.59%±0.27%
19-J1	0.10%±0.06%	0.02%±0.01%	0.03%±0.01%	0.03%±0.01%
19-J2	0.12%±0.06%	0.02%±0.01%	0.04%±0.01%	0.03%±0.01%
19-J3	0.46%±0.18%	0.96%±0.20%	0.36%±0.05%	2.3%±0.22%
21-J1	0.16%±0.05%	0.02%±0.01%	0.03%±0.01%	0.0%±0.01%
21-J2	0.51%±0.06%	0.25%±0.03%	0.12%±0.02%	0.6%±0.06%
21-J3	0.65%±0.07%	0.63%±0.07%	0.19%±0.03%	1.0%±0.11%
4-J1	0.15%±0.08%	0.03%±0.02%	0.06%±0.02%	0.08%±0.02%
4-J2	0.86%±0.21%	0.71%±0.16%	0.38%±0.10%	0.95%±0.21%
4-J3	1.47%±0.33%	1.53%±0.33%	0.71%±0.24%	1.65%±0.28%
16-J1	0.18%±0.09%	0.00%±0.00%	0.06%±0.03%	0.11%±0.04%
16-J2	1.33%±0.68%	0.93%±0.34%	0.60%±0.14%	2.07%±0.44%
16-J3	2.56%±0.57%	2.00%±0.56%	1.33%±0.45%	3.44%±0.68%
18-J1	0.13%±0.02%	0.08%±0.02%	0.03%±0.00%	0.06%±0.01%
18-J2	0.85%±0.09%	2.40%±0.25%	0.30%±0.03%	4.10%±0.42%
18-J3	1.11%±0.11%	3.94%±0.39%	0.33%±0.03%	6.67%±0.66%

As discussed in Section 3.2, a regression was performed on the total pressures during the last several pump cycles (or "strokes") to find the residual ammonia content of the sample. The variables derived by and used in the regression are given in Table C.3.8.

Table C.3.8. Pressure Regression Variables for Tank AN-105 Sample Cycling

Segment / Canister	dp/dN (kPa/stroke)	p_{ins} (kPa)	N (number of strokes)	$(\Delta n/\Delta N)_{NH3}$ (mgmol NH3 per stroke)
15-J1	0.2814±0.632	9.460	11	2.26E-03±5.1E-03
15-J2	0.0433±0.632	1.615	11	1.98E-04±2.9E-03
15-J3	0.0915±0.632	5.326	10	-9.02E-04±6.2E-03
17-J1	2.9512±0.632	63.868	11	3.97E-02±1.3E-02
17-J2	0.2972±0.632	5.537	11	3.15E-03±6.7E-03
17-J3	0.1138±0.632	2.526	12	1.75E-03±9.7E-03
19-J1		90.684	4	
19-J2	2.9477±0.632	66.602	11	6.69E-02±2.1E-02
19-J3	0.3794±0.632	6.887	21	8.23E-03±1.4E-02
21-J1	3.2802±0.632	80.108	11	3.95E-02±1.4E-02
21-J2	0.1759±0.632	7.725	11	4.49E-04±1.6E-03
21-J3	0.0644±0.632	3.037	11	1.41E-04±1.4E-03
4-J1	0.2115±0.632	8.428	11	9.38E-04±2.8E-03
4-J2	0.0497±0.632	1.714	11	8.00E-04±1.0E-02
4-J3	0.0688±0.632	0.675	10	1.55E-03±1.4E-02
16-J1	0.4067±0.632	10.629	11	4.67E-03±7.4E-03
16-J2	0.0208±0.632	0.845	12	3.43E-04±1.0E-02
16-J3	0.0363±0.632	0.284	10	8.33E-04±1.5E-02
18-J1	0.9±0.632	26.834	11	8.91E-03±6.5E-03
18-J2	0.1812±0.632	2.544	10	2.99E-03±1.0E-02
18-J3	0.0315±0.632	1.004	10	7.25E-04±1.5E-02

In order to estimate the void fraction and the distribution of gases between the void and slurry phases in each segment, the conditions under which the gas exists must be known. These are given in Table C.3.9 for Tank AN-105. The densities were taken from ball rheometer and core data in Stewart et al. (1996). The temperatures were based on a profile measured at the MIT tree; the profile is shown in Section 4.3.2. The pressures were derived from hydrostatic head, and are based on the depth of submergence of the segment and the thicknesses and gas-free densities of the waste layers. The solid volume fraction is estimated using 1430 kg/m^3 as the density of solid-free liquid, 1590 kg/m^3 as the density of gas-free slurry, and an assumed 2000 kg/m^3 as the intrinsic (not bulk) density of the solid material.

The water vapor pressure is the pressure in equilibrium with water in the waste; it is calculated using Equation 6.2 and Table 6.2 of Mahoney and Trent (1995), a correlation for water vapor pressure over concentrated homogeneous and non-homogeneous waste simulants. This correlation requires the weight fraction of water in the slurry, which is calculated using the solid volume fraction and density and the weight fraction of water in the solids-free solution. The latter value was estimated at 0.54, based on Equation 4.4 of Mahoney and Trent (1995), which allows the weight fraction of water in a simulant solution to be back-calculated from the solution density.

Table C.3.9. In-Tank Conditions Used for Tank AN-105 Phase Distribution Calculations

Segment	Density (kg/m^3)	Temperature (°C)	Pressure (atm)	Solid Volume Fraction	Water Vapor Pressure (atm)
15	1590	43	1.95	0.28	0.0288
17	1590	46	2.10	0.28	0.0336
19	1590	46	2.25	0.28	0.0336
21	1590	39	2.40	0.28	0.0233
4	1430	39	1.20	0	0.0389
16	1590	44	2.02	0.28	0.0303
18	1590	46	2.17	0.28	0.0336

The average ionic concentrations in the drainable liquid in Tank AN-105 are given in Table C.3.10. Most of them are based on the AN-105 solution density of 1430 kg/m^3 and Tables 11 and 13 of WHC-SD-WM-DP-192 Rev. 0, data for µg/g ionic concentrations from 1996 core sample analyses for Risers 24A and 24B of Tank AW-101. The concentrations of Ni^{2+}, F^-, Cl^-, NO_3^-, NO_2^-, and SO_4^{2-} were taken from preliminary data for AN-105 core analyses performed in 1996.(a)

(a) Personal cc:mail communication from J. Jo to L.A. Mahoney, October 1996.

Table C.3.10. Ionic Concentrations Used For Tank AN-105 Phase Distribution Calculations

Ion	gmol/L solution
Na^+	2.76
Al^{3+}	1.70
Fe^{3+}	0
Cr^{3+}	0.0031
Ni^{2+}	0.00017
K^+	1.34
OH^-	1.02
NO_3^-	2.64
NO_2^-	2.71
PO_4^{3-}	0
SO_4^{2-}	0.011
F^-	0.013
Cl^-	0.27

The Henry's Law constants are necessary to estimate the in-tank phase distribution of gases (see Section 3.2). The intermediate steps in the Henry's Law constant calculation are shown in Table C.3.11. Note that the final Henry's Law constant is in terms of liters of gas-free waste slurry, while the Schumpe model is in terms of kg of water in the salt solution. Both the solid volume fraction and the weight percent of water in the solution are needed to put the Henry's Law constant in its final form. The gases not listed, argon and the minor gases, were assumed wholly insoluble with Henry's law constants of 10^{-10}.

Table C.3.11. Henry's Law Constants For Tank AN-105 Phase Distribution Calculations

Segment	Condition	N_2	H_2	N_2O	O_2	CH_4	NH_3
15	Schumpe (K in water / K in solution)	10.1	6.5	8.7	12.0	11.5	3.6
	Waste Slurry K (mol/atm L waste)	3.0×10^{-5}	6.3×10^{-5}	9.9×10^{-4}	4.7×10^{-5}	5.4×10^{-5}	4.2
17	Schumpe (K in water / K in solution)	9.6	6.4	8.3	11.6	11.0	3.6
	Waste Slurry K (mol/atm L waste)	3.1×10^{-5}	6.4×10^{-5}	9.7×10^{-4}	4.7×10^{-5}	5.4×10^{-5}	3.7
19	Schumpe (K in water / K in solution)	9.6	6.4	8.3	11.6	11.0	3.6
	Waste Slurry K (mol/atm L waste)	3.1×10^{-5}	6.4×10^{-5}	9.7×10^{-4}	4.7×10^{-5}	5.4×10^{-5}	3.7
21	Schumpe (K in water / K in solution)	10.8	6.7	9.2	12.4	12.3	3.6
	Waste Slurry K (mol/atm L waste)	2.9×10^{-5}	6.1×10^{-5}	1.0×10^{-3}	4.7×10^{-5}	5.3×10^{-5}	5.0
4	Schumpe (K in water / K in solution)	10.8	6.7	9.2	12.4	12.3	3.6
	Waste Slurry K (mol/atm L waste)	4.0×10^{-5}	8.5×10^{-5}	1.4×10^{-3}	6.6×10^{-5}	7.3×10^{-5}	7.0
16	Schumpe (K in water / K in solution)	9.9	6.5	8.6	11.8	11.4	3.6
	Waste Slurry K (mol/atm L waste)	3.0×10^{-5}	6.3×10^{-5}	9.8×10^{-4}	4.7×10^{-5}	5.4×10^{-5}	4.1
18	Schumpe (K in water / K in solution)	9.6	6.4	8.3	11.6	11.0	3.6
	Waste Slurry K (mol/atm L waste)	3.1×10^{-5}	6.4×10^{-5}	9.7×10^{-4}	4.7×10^{-5}	5.4×10^{-5}	3.7

The Henry's Law constant calculation is one method of calculating the ammonia partial pressure. Another method uses a grab-sample of extractor atmosphere, which is analyzed to find the ammonia content and hence the partial pressure at the time the sample was taken. Table C.3.12 shows the results of these analyses for AN-105 samples. In the table, "UBV" indicates unbound vapor, or the sample taken just before the J1 canister; "BV" means bound vapor, the sample taken just after the temperature ramp.

Table C.3.12. Grab-Sample Data for Deriving Ammonia Partial Pressures in Tank AN-105

Sample	Grab-Sample Volume (cc)	Fill Temperature (°C)	Fill Pressure (kPa)	µmol NH_3	NH_3 Partial Pressure (atm)
15-UBV	51.7	24.3	2.348	11.3	0.0054
15-BV	52	24.5	2.133	16.3	0.0076
17-UBV*					
17-BV	38.6	24.4	2.308	10.9	0.0069
19-UBV	40.5	24.2	7.167	11.6	0.0070
19-BV	51.7	26.7	2.822	16.8	0.0080
21-UBV	51.7	24.2	5.786	11.3	0.0053
21-BV	52	25.6	2.576	6.5	0.0031
4-UBV	51.7	23.9	2.205	10.2	0.0048
4-BV	52.2	24.2	2.312	15.7	0.0073
16-UBV	52	24.4	2.448	9.2	0.0043
16-BV	51.7	24.4	2.369	15.6	0.0074
18-UBV	52	24.1	2.992	12.3	0.0058
18-BV	38.6	25.5	2.743	15.1	0.0096

* Grab-sample was lost in handling.

C.4 Tank 241-AN-104

As described in Section 2.3, gases are extracted from waste samples into "J" canisters and then undergo analysis from mass spectroscopy to obtain the mole fraction composition of the extracted gas on a dry basis. (Water vapor is not measured.) The results, for Tank AN-104, are shown in Table C.4.1.

Table C.4.1. Mole Percents of Gases Measured in Tank AN-104 Dry Gas (obtained by mass spectroscopy)

Segment / Canister	N_2	H_2	N_2O	O_2	CH_4	Ar
3-J1	48.5±0.200	6.4±0.100	5.4±0.100	9.5±0.200	0.12±0.020	0.58±0.020
3-J2	9.8±0.200	1.73±0.040	2.28±0.050	1.56±0.030	0.05±0.050	0.13±0.010
3-J3	9.7±0.200	1.48±0.030	2.08±0.040	1.28±0.030	0.44±0.050	0.14±0.010
13-J1	38±0.800	24±0.500	6.8±0.200	3.68±0.070	0.35±0.050	0.38±0.010
13-J2	4.66±0.090	4.04±0.080	5.1±0.100	0.4±0.010	0.35±0.050	0.073±0.007
13-J3	3.28±0.070	3.2±0.060	3.74±0.070	0.31±0.010	0.55±0.050	0.073±0.007
15-J1	29.9±0.600	37.6±0.600	9.2±0.200	1.46±0.030	0.53±0.050	0.2±0.004
15-J2	3.12±0.060	5.4±0.100	4.4±0.100	0.083±0.004	0.63±0.060	0.07±0.010
15-J3	2.9±0.060	4.6±0.100	3.8±0.100	0.174±0.003	0.63±0.060	0.076±0.008
17-J1	53.1±0.200	19.6±0.400	9.2±0.200	4.9±0.100	0.82±0.050	0.32±0.010
17-J2	17.8±0.400	4.2±0.080	5.8±0.100	2.7±0.050	0.64±0.060	0.23±0.020
17-J3	19.7±0.400	3.6±0.070	4.8±0.100	3.53±0.070	0.72±0.070	0.27±0.010
21-J1	22.1±0.500	47±1.000	29.1±0.600	0.44±0.010	0.56±0.060	1.16±0.030
21-J2	20.7±0.400	45±1.000	28.9±0.600	0.3±0.030	0.54±0.050	1.04±0.040
21-J3	11.1±0.300	20.3±0.400	19.3±0.400	0.49±0.010	0.48±0.050	0.49±0.020
18-J1	35.3±0.700	36.7±0.700	11.5±0.200	1.31±0.030	0.7±0.050	0.33±0.010
18-J2	3.45±0.070	5±0.100	5.2±0.100	0.138±0.003	0.37±0.050	0.078±0.008
18-J3	1.66±0.030	3.75±0.080	3.8±0.080	0.163±0.003	0.64±0.050	0.103±0.005

Table C.4.1 (contd)

Segment / Canister	Other NOx	C_2H_x	C_3H_x	Other HC	NH_3
3-J1	0.06±0.010	0.03±0.010	0.02±0.010	0.08±0.010	29±7.00
3-J2	0.1±0.050	0.07±0.020	0.04±0.010	0.25±0.050	84±8.00
3-J3	0.1±0.050	0.14±0.050	0.07±0.020	0.3±0.050	84±8.00
13-J1	0.05±0.050	0.14±0.050	0.03±0.010	0.11±0.050	26±7.00
13-J2	0.08±0.020	0.16±0.050	0.03±0.010	0.42±0.050	85±8.00
13-J3	0.09±0.020	0.27±0.050	0.06±0.010	0.55±0.050	88±9.00
15-J1	0.005±0.005	0.15±0.030	0.03±0.010	0.11±0.020	21±5.00
15-J2	0.005±0.005	0.39±0.040	0.05±0.010	0.82±0.080	85±9.00
15-J3	0.02±0.010	0.46±0.050	0.06±0.010	0.88±0.090	86±9.00
17-J1	0.005±0.005	0.24±0.010	0.05±0.010	0.14±0.020	12±2.00
17-J2	0.005±0.005	0.55±0.050	0.06±0.010	1.07±0.020	67±7.00
17-J3	0.005±0.005	0.62±0.060	0.06±0.010	1.17±0.020	66±7.00
21-J1	0.01±0.010	0.06±0.020	0.05±0.020	0.05±0.020	0.1±0.10
21-J2	0.02±0.010	0.05±0.020	0.05±0.020	0.07±0.020	3±0.80
21-J3	0.12±0.060	0.27±0.030	0.14±0.030	0.65±0.060	47±12.00
18-J1	0.005±0.005	0.19±0.010	0.05±0.010	0.12±0.010	14±2.00
18-J2	0.011±0.006	0.24±0.010	0.03±0.010	0.73±0.020	85±4.00
18-J3	0.005±0.005	0.8±0.100	0.06±0.010	1.48±0.030	88±4.00

The pressure and temperature of the gas in the J canisters are measured at the time of collection. The collector volume always includes the canister volume and, in cases where the collector is pumped down to vacuum after a canister is valved closed, also includes the collector-side line volume. The water vapor pressure is assumed to be that of pure water rather than the much lower vapor pressure over the sample for all the segments of AN-104 except Segment 21. For these early segments, and for canisters J2 and J3 of Segment 21, the collector-side was not in direct contact with the sample and was not in equilibrium with it. For canister J1 of Segment 21, the collector-side was in equilibrium with the sample and the vapor pressure over the sample is used. Table C.4.2 shows the canister (collector-side) conditions that prevailed for Tank AN-104 samples.

Table C.4.2. Canister Conditions at the Time of Collection, Tank AN-104 Samples

Segment / Canister	Pressure (kPa)	Collector Volume (cc)	Temperature (°C)	Water Vapor Pressure (kPa)	Sampler Volume (L)
3-J1	16.221	57.1	26.8	3.523	0.3068
3-J2	14.277	41.1	26.6	3.482	0.3068
3-J3	8.303	57.2	26.4	3.441	0.3068
13-J1	29.479	56.1	26.8	3.523	0.3062
13-J2	21.911	39.9	26.7	3.503	0.3062
13-J3	12.561	55.8	26.5	3.462	0.3062
15-J1	30.603	105.1	25.6	3.282	0.306
15-J2	12.843	90.5	27.1	3.586	0.306
15-J3	9.706	109.9	27.6	3.692	0.306
17-J1	36.517	107.9	25.7	3.302	0.3065
17-J2	12.37	89.5	26.8	3.523	0.3065
17-J3	9.457	109.3	26.7	3.503	0.3065
21-J1	8.115	91.3	26.8	1.201	0.3067
21-J2	90.06	106.1	27	3.565	0.3067
21-J3	15.04	109.3	26.1	3.381	0.3067
18-J1	81.404	56.1	24.4	3.056	0.307
18-J2	27.235	39.9	25.2	3.205	0.307
18-J3	14.529	55.8	25.2	3.205	0.307

Tables C.4.3 through C.4.5 give the peak collector-side pressures during the extraction pump cycling. Only the last five pressures are used for regression to get the pressure versus cycle derivatives.

Table C.4.3. Pump Cycle Peak Pressures (kPa) for Canister 1 of Each Segment of Tank AN-104

Cycle	3-J1	13-J1	15-J1	17-J1	21-J1*	18-J1
1	9.527	13.367	12.916	15.207		26.83
2	12.856	19.042	18.608	22.043		42.405
3	14.265	21.639	21.756	26.129		51.628
4	14.772	23.067	23.714	28.574		58.732
5	14.998	24.196	25.262	30.304		63.633
6	15.226	25.267	26.812	31.714		67.434
7	15.316	26.357	27.715	33.013		70.524
8	15.49	27.163	28.796	34.275		73.169
9	15.732	27.696	29.689	35.456		76.483
10	16.011	28.629	30.603	36.517		78.377
11	16.221	29.479				81.404
* In accord with a procedure change, Canister J1 of Segment 21 was not pumped, but was acquired at extractor pressure.						

Table C.4.4. Pump Cycle Peak Pressures (kPa) for Canister 2 of Each Segment of Tank AN-104

Cycle	3-J2	13-J2	15-J2	17-J2	21-J2	18-J2
1	9.485	11.639	6.203	6.87	26.654	14.321
2	12.017	15.96	8.469	9.266	45.082	19.456
3	12.884	17.754	9.859	10.51	58.042	21.651
4	13.225	18.766	10.717	11.137	67.191	22.93
5	13.227	19.398	11.255	11.492	72.944	23.605
6	13.522	19.705	11.665	11.744	77.674	24.28
7	13.666	20.169	11.852	11.915	81.767	25.133
8	13.851	20.543	12.255	12.111	84.726	25.833
9	14.001	21.038	12.609	12.21	87.809	26.109
10	14.14	21.412	12.843	12.37	90.06	26.646
11	14.277	21.911				27.235

Table C.4.5. Pump Cycle Peak Pressures (kPa) for Canister 3 of Each Segment of Tank AN-104

Cycle	3-J3	13-J3	15-J3	17-J3	21-J3	18-J3
1	6.827	9.474	3.447	6.67	6.718	8.224
2	7.833	10.826	4.666	7.382	9.548	10.976
3	8.102	11.471	5.946	7.824	11.113	12.207
4	8.196	11.882	7.157	8.112	11.909	12.843
5	8.224	12.049	8.03	8.281	12.328	13.112
6	8.212	11.939	8.627	8.385	12.586	13.353
7	8.274	12.371	9.03	8.497	12.901	13.675
8	8.258	12.325	9.278	8.601	13.036	13.818
9	8.246	12.253	9.479	8.659	13.23	14.079
10	8.303	12.561	9.706	8.725	13.432	14.235
11				8.808	13.562	14.529
12				8.881	13.733	
13				8.939	13.93	
14				9.016	14.061	
15				9.088	14.15	
16				9.146	14.323	
17				9.223	14.459	
18				9.299	14.588	
19				9.356	14.772	
20				9.457	14.901	
21					15.04	

Table C.4.6 shows the amounts of gases that are calculated based on the data presented earlier. The regression slopes in Table C.4.8 also play a part in the determination of the "residuals," which have meaning only for ammonia.

Table C.4.6. Quantities of Gases Found in Tank AN-104 Samples

Segment / Canister	N_2 (µmol)	H_2 (µmol)	N_2O (µmol)	O_2 (µmol)	CH_4 (µmol)	Ar (µmol)
3-J1	141±17	18.6±2.3	15.7±2.0	27.6±3.5	0.35±0.07	1.7±0.2
3-J2	17.4±2.5	3.1±0.4	4.1±0.6	2.8±0.4	0.13±0.13	0.2±0.04
3-J3	10.8±2.6	1.7±0.4	2.3±0.6	1.4±0.3	0.49±0.13	0.2±0.04
3-TOTAL	169±23	23.3±3.2	22.1±3.1	32±4.2	0.97±0.33	2.1±0.3
13-J1	222±16	140±10	39.7±3.0	21.5±1.5	2.0±0.3	2.2±0.2
13-J2	13.7±1.3	11.9±1.1	15.0±1.4	1.2±0.1	1.03±0.2	0.2±0.03
13-J3	6.7±1.1	6.5±1.0	7.6±1.2	0.6±0.10	1.12±0.2	0.1±0.03
13-TOTAL	242±18	159±12.2	62±5.6	23.3±1.7	4.2±0.70	2.6±0.2
15-J1	346±24	435±29.4	106.4±7.4	16.9±1.2	6.1±0.7	2.3±0.2
15-J2	10.5±1.6	18.1±2.8	14.8±2.3	0.3±0.05	2.1±0.4	0.23±0.05
15-J3	7.7±1.6	12.2±2.5	10.0±2.1	0.5±0.10	1.7±0.4	0.20±0.05
15-TOTAL	364±27	465±34.8	131±11.8	17.6±1.3	9.9±1.47	2.7±0.3
17-J1	766±42	283±17	133±7.9	70.7±4.2	11.8±1.0	4.6±0.3
17-J2	56.5±9.2	13.3±2.2	18.4±3.0	8.6±1.4	2.0±0.4	0.7±0.13
17-J3	51.4±10.9	9.4±2.0	12.5±2.7	9.2±2.0	1.9±0.4	0.7±0.15
17-TOTAL	874±63	305±20.8	164±13.5	88.5±7.5	15.7±1.8	6.1±0.6
21-J1	55.9±14	119±29	74±18.2	1.1±0.3	1.4±0.4	2.9±0.7
21-J2	761±23.1	1655±53.4	1063±33.3	11.0±1.13	19.9±1.90	38.2±1.7
21-J3	56.9±7.7	0.6±14.0	98.9±13.3	2.5±0.34	2.5±0.42	2.5±0.3
21-TOTAL	874±45	1774±96.9	1235±64.8	14.7±1.7	23.7±2.69	43.7±2.8
18-J1	627±20	652±20.9	204.3±6.3	23.3±0.8	12.4±0.9	5.9±0.2
18-J2	13.3±1.0	19.3±1.5	20.1±1.5	0.5±0.0	1.4±0.2	0.30±0.04
18-J3	4.2±0.6	9.6±1.3	9.7±1.4	0.4±0.06	1.6±0.3	0.26±0.04
18-TOTAL	645±22	681±23.7	234.1±9.2	24.2±0.9	15.5±1.42	6.4±0.3

Table C.4.6 (contd)

Segment / Canister	Other NOx (µmol)	C_2H_x (µmol)	C_3H_x (µmol)	Other HC (µmol)	NH_3 (µmol)
3-J1	0.17±0.04	0.09±0.03	0.06±0.03	0.23±0.04	84±23
3-J2	0.18±0.09	0.12±0.04	0.07±0.02	0.45±0.11	150±25
3-J3	0.11±0.06	0.16±0.07	0.08±0.03	0.33±0.10	94±24
3-residual					16±145
3-TOTAL	0.46±0.19	0.37±0.14	0.21±0.08	1.01±0.25	343±218
13-J1	0.3±0.3	0.8±0.30	0.18±0.06	0.64±0.30	152±42
13-J2	0.2±0.06	0.5±0.15	0.09±0.03	1.2±0.2	250±33
13-J3	0.2±0.05	0.6±0.13	0.12±0.03	1.1±0.2	179±34
13-residual					82±298
13-TOTAL	0.71±0.41	1.84±0.59	0.39±0.12	3.00±0.69	663±407
15-J1	0.1±0.1	1.7±0.37	0.35±0.12	1.3±0.2	243±60
15-J2	0.0±0.02	1.3±0.24	0.17±0.04	2.8±0.5	285±54
15-J3	0.1±0.0	1.2±0.28	0.16±0.04	2.3±0.5	227±53
15-residual					0±0
15-TOTAL	0.13±0.10	4.26±0.9	0.67±0.20	6.35±1.29	755±166
17-J1	0.1±0.07	3.5±0.24	0.72±0.1	2.0±0.31	173±30
17-J2	0.0±0.02	1.7±0.3	0.19±0.0	3.4±0.6	213±41
17-J3	0.0±0.01	1.6±0.4	0.16±0.04	3.1±0.6	172±41
17-residual					0±0
17-TOTAL	0.10±0.10	6.83±0.94	1.07±0.24	8.47±1.51	558±112
21-J1	0.0±0.0	0.2±0.1	0.13±0.06	0.13±0.1	0±0
21-J2	0.7±0.37	1.8±0.74	1.8±0.74	2.6±0.74	110±30
21-J3	0.6±0.32	1.4±0.24	0.7±0.18	3.3±0.54	241±69
21-residual					39±36
21-TOTAL	1.38±0.71	3.37±1.0	2.68±0.98	6.03±1.34	391±135
18-J1	0.09±0.1	3.4±0.20	0.9±0.18	2.1±0.19	249±36
18-J2	0.04±0.0	0.9±0.08	0.1±0.04	2.8±0.2	329±29
18-J3	0.01±0.0	2.0±0.38	0.2±0.03	3.8±0.5	224±33
18-residual					326±1783
18-TOTAL	0.14±0.13	6±0.66	1.16±0.25	8.72±0.93	1127±1881

Table C.4.7. Mole Percents of Gases in Tank AN-104 Dry Insoluble Gas

Segment / Canister	N_2	H_2	N_2O	O_2	CH_4	Ar
3-J1	68.3%±16.5%	9.0%±2.2%	7.6%±1.8%	13.4%±3.24%	0.17%±0.05%	0.82%±0.20%
3-J2	61.3%±6.0%	10.8%±1.1%	14.3%±1.4%	9.8%±0.95%	0.31%±0.31%	0.81%±0.10%
3-J3	60.6%±5.9%	9.3%±0.9%	13.0%±1.3%	8.0%±0.78%	2.75%±0.41%	0.9%±0.10%
13-J1	51.4%±13.9%	32.4%±8.8%	9.2%±2.5%	5.0%±1.34%	0.47%±0.14%	0.51%±0.14%
13-J2	31.1%±3.0%	26.9%±2.6%	34.0%±3.3%	2.7%±0.26%	2.33%±0.40%	0.49%±0.07%
13-J3	27.3%±2.9%	26.7%±2.8%	31.2%±3.2%	2.6%±0.28%	4.58%±0.63%	0.6%±0.09%
15-J1	37.8%±9.0%	47.6%±11.4%	11.6%±2.8%	1.8%±0.44%	0.67%±0.17%	0.25%±0.06%
15-J2	20.8%±2.2%	36.0%±3.9%	29.3%±3.2%	0.6%±0.06%	4.20%±0.60%	0.47%±0.08%
15-J3	20.7%±2.2%	32.9%±3.5%	27.1%±2.9%	1.2%±0.13%	4.50%±0.64%	0.54%±0.08%
17-J1	60.3%±10.1%	22.3%±3.7%	10.5%±1.8%	5.6%±0.93%	0.93%±0.17%	0.36%±0.06%
17-J2	53.9%±5.8%	12.7%±1.4%	17.6%±1.9%	8.2%±0.87%	1.94%±0.27%	0.70%±0.09%
17-J3	57.9%±6.3%	10.6%±1.1%	14.1%±1.5%	10.4%±1.12%	2.12%±0.30%	0.8%±0.09%
21-J1	22.1%±22.1%	47.0%±47.1%	29.1%±29.1%	0.4%±0.44%	0.56%±0.56%	1.2%±1.16%
21-J2	21.3%±5.7%	46.4%±12.4%	29.8%±8.0%	0.3%±0.09%	0.56%±0.16%	1.1%±0.29%
21-J3	20.9%±5.4%	38.3%±9.8%	36.4%±9.3%	0.9%±0.24%	0.91%±0.25%	0.9%±0.24%
18-J1	41.0%±5.9%	42.7%±6.2%	13.4%±1.9%	1.5%±0.22%	0.81%±0.13%	0.4%±0.06%
18-J2	23.0%±1.2%	33.3%±1.7%	34.7%±1.8%	0.9%±0.05%	2.47%±0.35%	0.5%±0.06%
18-J3	13.8%±0.7%	31.3%±1.6%	31.7%±1.6%	1.4%±0.07%	5.33%±0.48%	0.9%±0.06%

Table C.4.7 (contd)

Segment / Canister	Other NOx	C_2H_x	C_3H_x	Other HC
3-J1	0.08%±0.02%	0.04%±0.02%	0.03%±0.02%	0.11%±0.03%
3-J2	0.63%±0.32%	0.44%±0.13%	0.25%±0.07%	1.56%±0.35%
3-J3	0.63%±0.32%	0.88%±0.32%	0.44%±0.13%	1.88%±0.36%
13-J1	0.07%±0.07%	0.19%±0.08%	0.04%±0.02%	0.15%±0.08%
13-J2	0.53%±0.14%	1.07%±0.35%	0.20%±0.07%	2.80%±0.42%
13-J3	0.75%±0.18%	2.25%±0.48%	0.50%±0.10%	4.58%±0.63%
15-J1	0.01%±0.01%	0.19%±0.06%	0.04%±0.02%	0.14%±0.04%
15-J2	0.03%±0.03%	2.60%±0.38%	0.33%±0.08%	5.47%±0.79%
15-J3	0.14%±0.07%	3.29%±0.50%	0.43%±0.08%	6.29%±0.92%
17-J1	0.01%±0.01%	0.27%±0.05%	0.06%±0.01%	0.16%±0.03%
17-J2	0.02%±0.02%	1.67%±0.23%	0.18%±0.04%	3.24%±0.34%
17-J3	0.01%±0.01%	1.82%±0.26%	0.18%±0.03%	3.44%±0.37%
21-J1	0.01%±0.01%	0.06%±0.06%	0.05%±0.05%	0.1%±0.05%
21-J2	0.02%±0.01%	0.05%±0.02%	0.05%±0.02%	0.1%±0.03%
21-J3	0.23%±0.13%	0.51%±0.14%	0.26%±0.09%	1.2%±0.33%
18-J1	0.01%±0.01%	0.22%±0.03%	0.06%±0.01%	0.14%±0.02%
18-J2	0.07%±0.04%	1.60%±0.10%	0.20%±0.07%	4.87%±0.27%
18-J3	0.04%±0.04%	6.67%±0.89%	0.50%±0.09%	12.33%±0.61%

As discussed in Section 3.2, a regression was performed on the total pressures during the last several pump cycles (or "strokes") to find the residual ammonia content of the sample. The variables derived by, and used in, the regression are given in Table C.4.8.

Table C.4.8. Pressure Regression Variables for Tank AN-104 Sample Cycling

Segment / Canister	dp/dN (kPa/stroke)	p_{ins} (kPa)	N (number of strokes)	$(\Delta n/\Delta N)_{NH3}$ (mgmol NH3 per stroke)
3-J1	0.2331±0.632	9.015	11	1.39E-03±3.8E-03
3-J2	0.1511±0.632	1.727	11	2.49E-03±1.0E-02
3-J3	0.0154±0.632	0.778	10	3.54E-04±1.5E-02
13-J1	0.771±0.632	19.207	11	9.07E-03±7.9E-03
13-J2	0.4353±0.632	2.761	11	6.12E-03±8.9E-03
13-J3	0.1126±0.632	1.092	10	1.92E-03±1.1E-02
15-J1	0.9556±0.632	21.584	10	1.78E-02±1.3E-02
15-J2	0.3113±0.632	1.389	10	1.13E-02±2.3E-02
15-J3	0.2607±0.632	0.842	10	1.15E-02±2.8E-02
17-J1	1.2049±0.632	29.229	10	2.09E-02±1.2E-02
17-J2	0.1547±0.632	2.919	10	2.96E-03±1.2E-02
17-J3	0.0755±0.632	2.025	20	3.12E-03±2.6E-02
21-J1*				
21-J2	3.0814±0.632	83.900	10	4.27E-02±1.4E-02
21-J3	0.1475±0.632	6.179	21	6.02E-03±2.6E-02
18-J1	2.6968±0.632	67.379	11	3.19E-02±8.8E-03
18-J2	0.5017±0.632	3.605	11	8.07E-03±1.0E-02
18-J3	0.2125±0.632	1.359	11	4.78E-03±1.4E-02

* In accord with a procedure change, Canister J1 of Segment 21 was not pumped, but was acquired at extractor pressure.

In order to estimate the void fraction and the distribution of gases between the void and slurry phases in each segment, the conditions under which the gas exists must be known. These are given in Table C.4.9 for Tank AN-104. The densities were taken from ball rheometer and core data in Stewart et al. (1996). The temperatures were based on a profile measured at the MIT tree; the profile is shown in Section 4.4.2. The pressures were derived from hydrostatic head, and are based on the depth of submergence of the segment and the thicknesses and gas-free densities of the waste layers. The solid volume fraction is estimated using 1440 kg/m^3 as the density of solid-free liquid, 1590 kg/m^3 as the density of gas-free slurry, and an assumed 2000 kg/m^3 as the intrinsic (not bulk) density of the solid material.

The water vapor pressure is the pressure in equilibrium with water in the waste; it is calculated using Equation 6.2 and Table 6.2 of Mahoney and Trent (1995), a correlation for water vapor pressure over concentrated homogeneous and non-homogeneous waste simulants. This correlation requires the weight fraction of water in the slurry, which is calculated using the solid

Table C.4.9. In-Tank Conditions Used for Tank AN-104 Phase Distribution Calculations

Segment	Density (kg/m^3)	Temperature (°C)	Pressure (atm)	Solid Volume Fraction	Water Vapor Pressure (atm)
3	1440	42.2	1.12	0	0.0448
13	1590	42.2	1.80	0.27	0.0277
15	1590	46.7	1.94	0.27	0.0348
17	1590	48.9	2.09	0.27	0.0390
19	1590	46.7	2.24	0.27	0.0348
21	1590	40	2.39	0.27	0.0246
18	1590	47.8	2.17	0.27	0.0368

volume fraction and density and the weight fraction of water in the solids-free solution. The latter value was estimated at 0.53, based on Equation 4.4 of Mahoney and Trent (1995), which allows the weight fraction of water in a simulant solution to be back-calculated from the solution density.

The average ionic concentrations in the drainable liquid in Tank AN-104 are given in Table C.4.10. They are based on the AN-104 solution density of 1440 kg/m^3 and Tables 11 and 13 of WHC-SD-WM-DP-192 Rev. 0, data for µg/g ionic concentrations from 1996 core sample analyses for Risers 24A and 24B of Tank AW-101.

Table C.4.10. Ionic Concentrations Used For Tank AN-104 Phase Distribution Calculations

Ion	gmol/L solution
Na^+	2.77
Al^{3+}	1.71
Fe^{3+}	0
Cr^{3+}	0.0031
Ni^{2+}	0.00017
K^+	1.34
OH^-	1.02
NO_3^-	3.72
NO_2^-	3.10
PO_4^{3-}	0
SO_4^{2-}	0
F^-	0
Cl^-	0.21

The Henry's Law constants are necessary to estimate the in-tank phase distribution of gases (see Section 3.2). The intermediate steps in the Henry's Law constant calculation are shown in Table C.4.11. Note that the final Henry's Law constant is in terms of liters of gas-free waste slurry, while the Schumpe model is in terms of kg of water in the salt solution. Both the solid volume fraction and the weight percent of water in the solution are needed to put the Henry's Law constant in its final form. The gases not listed, argon and the minor gases, were assumed wholly insoluble with Henry's law constants of 10^{-10}.

The Henry's Law constant calculation is one method of calculating the ammonia partial pressure. Another method uses a grab-sample of extractor atmosphere, which is analyzed to find the ammonia content and hence the partial pressure at the time the sample was taken. Table C.4.12 shows the results of these analyses for AN-104 samples. In the table, "UBV" indicates unbound vapor, or the sample taken just before the J1 canister; "BV" means bound vapor, the sample taken just after the temperature ramp.

Table C.4.11. Henry's Law Constants For Tank AN-104 Phase Distribution Calculations

Segment	Condition	N_2	H_2	N_2O	O_2	CH_4	NH_3
3	Schumpe (K in water / K in solution)	11.0	6.7	9.3	13.2	12.7	3.4
	Waste Slurry K (mol/atm L waste)	3.8×10^{-5}	8.4×10^{-5}	1.3×10^{-3}	5.9×10^{-5}	6.7×10^{-5}	6.3
13	Schumpe (K in water / K in solution)	11.0	6.7	9.3	13.2	12.7	3.4
	Waste Slurry K (mol/atm L waste)	2.8×10^{-5}	6.2×10^{-5}	9.5×10^{-4}	4.3×10^{-5}	4.9×10^{-5}	4.6
15	Schumpe (K in water / K in solution)	10.1	6.4	8.6	12.6	11.8	3.4
	Waste Slurry K (mol/atm L waste)	2.9×10^{-5}	6.4×10^{-5}	9.2×10^{-4}	4.3×10^{-5}	5.0×10^{-5}	3.8
17	Schumpe (K in water / K in solution)	9.6	6.3	8.4	12.3	11.4	3.4
	Waste Slurry K (mol/atm L waste)	3.0×10^{-5}	6.5×10^{-5}	9.2×10^{-4}	4.3×10^{-5}	5.1×10^{-5}	3.5
21	Schumpe (K in water / K in solution)	11.5	6.8	9.6	13.5	13.2	3.4
	Waste Slurry K (mol/atm L waste)	2.7×10^{-5}	6.0×10^{-5}	9.6×10^{-4}	4.3×10^{-5}	4.8×10^{-5}	5.1
18	Schumpe (K in water / K in solution)	9.9	6.3	8.5	12.4	11.6	3.4
	Waste Slurry K (mol/atm L waste)	3.0×10^{-5}	6.4×10^{-5}	9.2×10^{-4}	4.3×10^{-5}	5.1×10^{-5}	3.7

Table C.4.12. Grab-Sample Data for Deriving Ammonia Partial Pressures in Tank AN-104

Sample	Grab-Sample Volume (cc)	Fill Temperature (°C)	Fill Pressure (kPa)	μmol NH_3	NH_3 Partial Pressure (atm)
3-UBV	52	24.2	2.331	12.0	0.0056
3-BV	51.7	24.2	2.696	7.0	0.0033
13-UBV	52	24.2	2.831	15.7	0.0074
13-BV	52	24.3	2.671	9.3	0.0044
15-UBV	52.2	24.2	3.037	43.8	0.0205
15-BV	40.5	25.8	2.927	1.9	0.0011
17-UBV*					
17-BV	51.7	24.1	2.502	28.6	0.0135
19-UBV*					
19-BV	51.7	23.9	2.867	16.6	0.0078
21-UBV*					
21-BV	52	24.2	2.692	15.5	0.0073
18-UBV	52.2	24.2	4.613	36.5	0.0171
18-BV	40.5	24	3.14	12.3	0.0074
* Grab-samples were lost in handling.					

C.5 Tank 241-AN-103

As described in Section 2.3, gases are extracted from waste samples into "J" canisters and then undergo analysis from mass spectroscopy to obtain the mole fraction composition of the extracted gas on a dry basis. (Water vapor is not measured.) The results, for Tank AN-103, are shown in Table C.5.1.

Table C.5.1. Mole Percents of Gases Measured in Tank AN-103 Dry Gas (obtained by mass spectroscopy)

Segment / Canister	N_2	H_2	N_2O	O_2	CH_4	Ar
2-J1	33.3±0.700	56.3±0.800	6.8±0.100	1.45±0.030	0.57±0.010	0.131±0.003
2-J2	29.9±0.600	52.6±0.700	6.1±0.100	1.24±0.020	0.01±0.010	0.116±0.002
2-J3	11.6±0.200	28.3±0.600	2.39±0.050	1±0.020	0.413±0.008	0.078±0.002
5-J1	76.1±0.400	5±0.100	2.32±0.050	13.8±0.300	0.33±0.010	0.87±0.020
5-J2	35±0.700	3.34±0.070	1.93±0.040	6.2±0.100	0.159±0.003	0.407±0.008
5-J3*	6±0.100	0.92±0.020	1.12±0.020	0.87±0.020	0.271±0.005	0.074±0.001
14-J1	40±1.000	47±1.000	4.7±0.100	1.42±0.030	0.55±0.050	0.178±0.006
14-J2	30.7±0.600	39.3±0.800	3.55±0.070	0.92±0.020	0.43±0.040	0.136±0.003
14-J3	3.04±0.060	5.32±0.100	0.75±0.030	0.097±0.005	0.26±0.030	0.027±0.003
10-J1	75.1±0.400	5.2±0.100	2.32±0.050	13.9±0.300	0.27±0.030	2.52±0.050
10-J2	32.3±0.600	3.21±0.060	1.89±0.040	5.6±0.100	0.1±0.010	1.11±0.020
10-J3	6.4±0.100	0.94±0.020	1.05±0.020	1.24±0.020	0.24±0.005	0.206±0.004
16-J1	31.4±0.700	62.6±0.700	4.03±0.090	0.072±0.005	0.53±0.050	0.92±0.020
16-J2	25.8±0.500	53.2±0.500	3.21±0.070	0.094±0.005	0.49±0.050	0.68±0.020
16-J3	7.9±0.200	20.1±0.200	1.49±0.030	0.2±0.010	0.47±0.050	0.22±0.010

* During acquisition of the J3 canister for Segment 5, the mercury pump overflowed and the pressure data were made unusable. Mole fraction data are probably sound but total moles could not be calculated.

Table C.5.1 (contd)

Segment / Canister	Other NOx	C_2H_x	C_3H_x	Other HC	NH_3
2-J1	0.005±0.005	0.13±0.020	0.03±0.010	0.04±0.010	1.3±0.30
2-J2	0.005±0.005	0.11±0.020	0.03±0.010	0.04±0.010	9±2.00
2-J3	0.05±0.030	0.06±0.010	0.06±0.020	0.06±0.010	56±14.00
5-J1	0.005±0.005	0.06±0.020	0.01±0.005	0.01±0.005	1.4±0.40
5-J2	0.06±0.001	0.02±0.010	0.04±0.010	0.02±0.010	53±13.00
5-J3*	0.08±0.020	0.03±0.010	0.06±0.010	0.04±0.010	91±5.00
14-J1	0.01±0.010	0.15±3.000	0.03±0.010	0.05±0.010	6±2.00
14-J2	0.01±0.010	0.12±0.020	0.03±0.010	0.04±0.010	25±6.00
14-J3	0.06±0.030	0.07±0.010	0.08±0.020	0.11±0.030	90±5.00
10-J1	0.01±0.010	0.04±0.010	0.02±0.010	0.02±0.010	0.6±0.20
10-J2	0.04±0.010	0.03±0.010	0.04±0.010	0.03±0.010	56±14.00
10-J3	0.08±0.020	0.04±0.010	0.07±0.010	0.07±0.010	90±5.00
16-J1	0.05±0.050	0.1±0.050	0.04±0.010	0.04±0.010	0.2±0.10
16-J2	0.01±0.005	0.08±0.020	0.05±0.010	0.08±0.020	16±4.00
16-J3	0.01±0.010	0.36±0.040	0.09±0.010	0.63±0.060	68±17.00

* During acquisition of the J3 canister for Segment 5, the mercury pump overflowed and the pressure data were made unusable. Mole fraction data are probably sound but total moles could not be calculated.

The pressure and temperature of the gas in the J canisters are measured at the time of collection. The collector volume always includes the canister volume and, in cases where the collector is pumped down to vacuum after a canister is valved closed, also includes the collector-side line volume. For the J2 and J3 canisters of AN-103, the water vapor pressure is assumed to be that of pure water rather than the much lower vapor pressure over the sample because the collector-side is not in direct contact with the sample and is not in equilibrium with it. This is not the case for the J1 canisters, which are at equilibrium with the sample; for these the water vapor pressures over the sample are used. Table C.5.2 shows the canister (collector-side) conditions that prevailed for Tank AN-103 samples.

Table C.5.2. Canister Conditions at the Time of Collection, for Tank AN-103 Samples

Segment / Canister	Pressure (kPa)	Collector Volume (cc)	Temperature (°C)	Water Vapor Pressure (kPa)	Sampler Volume (L)
2-J1	3.507	57.1	22.6	0.364	0.308
2-J2	82.552	41.1	23.7	2.930	0.308
2-J3	18.547	57.2	24.9	3.149	0.308
5-J1	1.876	56.1	24.8	1.376	0.3073
5-J2	22.563	39.9	25.1	3.186	0.3073
5-J3*					
14-J1	3.45	105.1	24.8	0.540	0.30636
14-J2	41.745	90.5	25	3.167	0.30636
14-J3	15.47	109.9	25.8	3.321	0.30636
10-J1	1.854	107.9	24.9	1.384	0.3068
10-J2	14.726	89.5	25.2	3.205	0.3068
10-J3	8.85	109.3	25.8	3.321	0.3068
16-J1	5.032	108.2	25	0.546	0.3074
16-J2	60.595	94	25.1	3.186	0.3074
16-J3	10.945	106.1	26.1	3.381	0.3074

* During acquisition of the J3 canister for Segment 5, the mercury pump overflowed and the pressure data were made unusable.

Tables C.5.3 through C.5.5 give the peak collector-side pressures during the extraction pump cycling. In some cases pressures are given only for the latter cycles, because only the last five pressures are used for regression to get the pressure versus cycle derivatives.

Table C.5.3. Pump Cycle Peak Pressures (kPa) for Canister 1 of Each Segment of Tank AN-103 (This table number is included to make the AN-103 format easily comparable to that of the other tanks; however, there are no data because the J1 canisters of AN-103 were not pumped.)

Table C.5.4. Pump Cycle Peak Pressures (kPa) for Canister 2 of Each Segment of Tank AN-103

Cycle	2-J2	5-J2	14-J2	10-J2	16-J2
1	23.915	9.639	11.499	5.77	16.306
2	41.848	14.331	19.882	8.965	28.854
3	51.909	17.399	26.08	10.765	37.805
4	57.011	18.987	30.063	11.829	44.332
5	63.848	20.072	32.946	12.553	48.845
6	67.892	20.397	34.793	13.061	51.844
7	70.537	21.059	36.282	13.434	54.058
8	72.744	21.434	37.46	13.709	55.607
9	75.855	21.923	38.861	13.847	56.967
10	78.266	22.065	39.431	14.093	58.074
11	79.01	22.34	40.271	14.285	59.475
12	81.139	22.563	40.972	14.366	60.595
13	82.552		41.745	14.635	
14				14.726	

Table C.5.5. Pump Cycle Peak Pressures (kPa) for Canister 3 of Each Segment of Tank AN-103

Cycle	2-J3	5-J3*	14-J3	10-J3	16-J3
1	8.202		7.201	2.672	20.79
2	12.022		10.088	4.98	27.019
3	14.063		11.599	6.511	30.426
4	14.883		12.447	7.289	31.712
5	15.431		12.893	7.707	31.252
6	15.841		13.167	7.899	33.244
7	16.152		13.37	8.022	33.617
8	16.171		13.575	8.143	33.454
9	16.572		13.779	8.232	33.189
10	16.726		13.915	8.283	33.761
11	16.941		14.073	8.316	34.094
12	17.035		14.256	8.384	34.215
13	17.301		14.394	8.431	34.311
14	17.523		14.576	8.466	34.449
15	17.617		14.715	8.492	34.425
16	17.777		14.904	8.569	34.304
17	17.98		15.033	8.615	34.568
18	18.122		15.124	8.642	34.272
19	18.267		15.291	8.706	34.743
20	18.467		15.47	8.707	34.659
21	18.547			8.85	7.385**
22					8.676
23					9.427
24					9.899
25					10.215
26					10.39
27					10.513
28					10.625
29					10.795
30					10.83
31					10.945

* During acquisition of the J3 canister for Segment 5, the mercury pump overflowed and the pressure data were made unusable.
** At this point, it was discovered that the canister was closed off from the rest of the collector; the valve was opened and pumping resumed at lower pressure.

Table C.5.6 shows the amounts of gases that are calculated based on the data presented earlier. The regression slopes in Table C.5.8 also play a part in the determination of the "residuals," which have meaning only for ammonia.

Table C.5.6. Quantities of Gases Found in Tank AN-103 Samples

Segment / Canister	N_2 (μmol)	H_2 (μmol)	N_2O (μmol)	O_2 (μmol)	CH_4 (μmol)	Ar (μmol)
2-J1	17±10	29.1±16.6	3.5±2.0	0.75±0.4	0.30±0.17	0.07±0.04
2-J2	557±18.0	979±28.1	113.6±3.4	23.1±0.7	0.31±0.31	2.2±0.07
2-J3	41.2±4.5	100.6±11.1	8.5±0.9	3.6±0.39	1.47±0.16	0.28±0.03
2-TOTAL	615±32	1109±55.8	126±6.4	27±1.5	2.07±0.64	2.5±0.14
5-J1	6.1±6.5	0.4±0.42	0.18±0.20	1.1±1.2	0.03±0.03	0.07±0.07
5-J2	155±14.1	14.7±1.3	8.5±0.78	27.4±2.5	0.70±0.06	1.8±0.16
5-J3*						
5-TOTAL*	161±21	15.1±1.8	8.7±1.0	28.5±3.6	0.73±0.09	1.9±0.24
14-J1	42±24	49±28	4.9±2.8	1.5±0.9	0.57±0.34	0.19±0.11
14-J2	512±26.7	655±34.4	59.2±3.1	15.3±0.8	7.2±0.8	2.3±0.12
14-J3	16.3±2.1	28.6±3.7	4.0±0.5	0.52±0.07	1.4±0.2	0.15±0.02
14-TOTAL	570±53	732±66.5	68±6.5	17.3±1.7	9.1±1.3	2.6±0.3
10-J1	13.0±14.0	0.90±1.0	0.40±0.43	2.4±2.6	0.05±0.05	0.44±0.5
10-J2	159±21.9	15.8±2.2	9.3±1.3	27.6±3.79	0.49±0.08	5.47±0.75
10-J3	15.6±3.5	2.3±0.52	2.6±0.58	3.0±0.68	0.58±0.13	0.50±0.11
10-TOTAL	188±39	19.0±3.7	12.3±2.3	33.0±7.1	1.1±0.27	6.4±1.3
16-J1	52±21	104±42.2	6.7±2.7	0.12±0.05	0.88±0.37	1.5±0.6
16-J2	661±25.8	1362±47.8	82.2±3.3	2.4±0.15	12.5±1.3	17.41±0.78
16-J3	25.5±4.7	64.8±11.9	4.8±0.9	0.65±0.12	1.5±0.32	0.71±0.13
16-TOTAL	738±52	1531±101.9	93.7±6.9	3.2±0.3	14.9±2.04	19.6±1.5

* During acquisition of the J3 canister for Segment 5, the mercury pump overflowed and the pressure data were made unusable. The total moles could not be calculated.

Table C.5.6 (contd)

Segment / Canister	Other NOx (µmol)	C_2H_x (µmol)	C_3H_x (µmol)	Other HC (µmol)	NH_3 (µmol)
2-J1	0.00±0.00	0.07±0.04	0.02±0.01	0.02±0.01	0.67±0.41
2-J2	0.09±0.09	2.05±0.38	0.56±0.19	0.74±0.19	199±37
2-J3	0.18±0.11	0.21±0.04	0.21±0.07	0.21±0.04	199±54
2-residual					20±16
2-TOTAL	0.27±0.20	2.33±0.46	0.79±0.27	0.98±0.24	387±108
5-J1	0.00±0.00	0.00±0.01	0.00±0.00	0.00±0.00	0.11±0.12
5-J2	0.26±0.02	0.09±0.04	0.18±0.05	0.09±0.05	234±61
5-J3*					
5-residual*					
5-TOTAL*	0.27±0.02	0.09±0.05	0.18±0.05	0.09±0.05	234±61
14-J1	0.01±0.01	0.16±3.12	0.03±0.02	0.05±0.03	6.2±4.2
14-J2	0.17±0.17	2.0±0.3	0.50±0.17	0.7±0.2	417±102
14-J3	0.32±0.17	0.4±0.07	0.43±0.12	0.6±0.2	483±68
14-residual					264±790
14-TOTAL	0.50±0.35	2.53±3.54	0.96±0.31	1.31±0.38	1170±964
10-J1	0.00±0.00	0.01±0.01	0.00±0.00	0.00±0.00	0.10±0.12
10-J2	0.20±0.06	0.15±0.05	0.20±0.06	0.15±0.05	276±79
10-J3	0.19±0.1	0.10±0.03	0.17±0.05	0.17±0.05	219±51
10-residual					113±1060
10-TOTAL	0.39±0.12	0.25±0.09	0.37±0.11	0.32±0.10	608±1189
16-J1	0.08±0.09	0.17±0.11	0.07±0.03	0.07±0.03	0.33±0.21
16-J2	0.26±0.13	2.0±0.52	1.3±0.26	2.0±0.5	410±103
16-J3	0.03±0.03	1.2±0.25	0.29±0.06	2.0±0.4	219±68
16-residual					20±20
16-TOTAL	0.37±0.25	3±0.87	1.64±0.35	4.15±0.97	649±192

* During acquisition of the J3 canister for Segment 5, the mercury pump overflowed and the pressure data were made unusable. The total moles could not be calculated.

Table C.5.7. Mole Percents of Gases in Tank AN-103 Dry Insoluble Gas

Segment / Canister	N_2	H_2	N_2O	O_2	CH_4	Ar
2-J1	33.7%±7.8%	57.0%±13.2%	6.9%±1.6%	1.5%±0.34%	0.58%±0.13%	0.13%±0.03%
2-J2	32.9%±7.3%	57.8%±12.9%	6.7%±1.5%	1.4%±0.30%	0.01%±0.01%	0.13%±0.03%
2-J3	26.4%±6.6%	64.3%±16.1%	5.4%±1.4%	2.3%±0.57%	0.94%±0.24%	0.2%±0.04%
5-J1	77.2%±22.1%	5.1%±1.5%	2.4%±0.7%	14.0%±4.01%	0.33%±0.10%	0.88%±0.25%
5-J2	74.5%±18.3%	7.1%±1.7%	4.1%±1.0%	13.2%±3.24%	0.34%±0.08%	0.87%±0.21%
5-J3*	66.7%±3.8%	10.2%±0.6%	12.4%±0.7%	9.7%±0.58%	3.01%±0.17%	0.8%±0.05%
14-J1	42.6%±14.2%	50.0%±16.7%	5.0%±1.7%	1.5%±0.50%	0.59%±0.20%	0.19%±0.06%
14-J2	40.9%±9.9%	52.4%±12.6%	4.7%±1.1%	1.2%±0.30%	0.57%±0.15%	0.18%±0.04%
14-J3	30.4%±1.8%	53.2%±3.1%	7.5%±0.5%	1.0%±0.07%	2.60%±0.33%	0.3%±0.03%
10-J1	75.6%±25.2%	5.2%±1.7%	2.3%±0.8%	14.0%±4.67%	0.27%±0.10%	2.54%±0.85%
10-J2	73.4%±18.4%	7.3%±1.8%	4.3%±1.1%	12.7%±3.19%	0.23%±0.06%	2.52%±0.63%
10-J3	64.0%±3.7%	9.4%±0.6%	10.5%±0.6%	12.4%±0.72%	2.40%±0.14%	2.06%±0.12%
16-J1	31.5%±15.7%	62.7%±31.4%	4.0%±2.0%	0.1%±0.04%	0.53%±0.27%	0.9%±0.46%
16-J2	30.7%±7.7%	63.3%±15.8%	3.8%±1.0%	0.1%±0.03%	0.58%±0.16%	0.8%±0.20%
16-J3	24.7%±6.2%	62.8%±15.7%	4.7%±1.2%	0.6%±0.16%	1.47%±0.40%	0.7%±0.17%

* During acquisition of the J3 canister for Segment 5, the mercury pump overflowed and the pressure data were made unusable. Mole fraction data are probably sound but total moles could not be calculated.

Table C.5.7 (contd)

Segment / Canister	Other NOx	C_2H_x	C_3H_x	Other HC
2-J1	0.01%±0.01%	0.13%±0.04%	0.03%±0.01%	0.04%±0.01%
2-J2	0.01%±0.01%	0.12%±0.03%	0.03%±0.01%	0.04%±0.01%
2-J3	0.11%±0.07%	0.14%±0.04%	0.14%±0.06%	0.14%±0.04%
5-J1	0.01%±0.01%	0.06%±0.03%	0.01%±0.01%	0.01%±0.01%
5-J2	0.13%±0.03%	0.04%±0.02%	0.09%±0.03%	0.04%±0.02%
5-J3*	0.89%±0.23%	0.33%±0.11%	0.67%±0.12%	0.44%±0.11%
14-J1	0.01%±0.01%	0.16%±3.19%	0.03%±0.02%	0.05%±0.02%
14-J2	0.01%±0.01%	0.16%±0.05%	0.04%±0.02%	0.05%±0.02%
14-J3	0.60%±0.30%	0.70%±0.11%	0.80%±0.20%	1.10%±0.31%
10-J1	0.01%±0.01%	0.04%±0.02%	0.02%±0.01%	0.02%±0.01%
10-J2	0.09%±0.03%	0.07%±0.03%	0.09%±0.03%	0.07%±0.03%
10-J3	0.80%±0.20%	0.40%±0.10%	0.70%±0.11%	0.70%±0.11%
16-J1	0.05%±0.06%	0.10%±0.07%	0.04%±0.02%	0.04%±0.02%
16-J2	0.01%±0.01%	0.10%±0.03%	0.06%±0.02%	0.10%±0.03%
16-J3	0.03%±0.03%	1.13%±0.31%	0.28%±0.08%	1.97%±0.53%

* During acquisition of the J3 canister for Segment 5, the mercury pump overflowed and the pressure data were made unusable. Mole fraction data are probably sound but total moles could not be calculated.

As discussed in Section 3.2, a regression was performed on the total pressures during the last several pump cycles (or "strokes") to find the residual ammonia content of the sample. The variables derived by, and used in, the regression are given in Table C.5.8.

Table C.5.8. Pressure Regression Variables for Tank AN-103 Sample Cycling

Segment / Canister	dp/dN (kPa/stroke)	p_{ins} (kPa)	N (number of strokes)	$(\Delta n/\Delta N)_{NH3}$ (mgmol NH3 per stroke)
2-J2	1.6267±0.632	72.456	13	3.80E-02±1.7E-02
2-J3	0.1479±0.632	6.775	21	3.41E-03±1.5E-02
5-J2	0.2675±0.632	9.107	12	3.00E-03±7.2E-03
5-J3*				
14-J2	0.7309±0.632	28.933	13	1.71E-02±1.6E-02
14-J3	0.139±0.632	1.215	20	6.03E-03±2.7E-02
10-J2	0.1616±0.632	5.069	14	6.91E-03±2.7E-02
10-J3	0.0535±0.632	0.553	21	2.35E-03±2.8E-02
16-J2	1.2484±0.632	48.224	12	5.57E-02±3.2E-02
16-J3	0.1069±0.632	2.421	31	4.56E-03±2.7E-02

* During acquisition of the J3 canister for Segment 5, the mercury pump overflowed and the pressure data were made unusable.

In order to estimate the void fraction and the distribution of gases between the void and slurry phases in each segment, the conditions under which the gas exists must be known. These are given in Table C.5.9 for Tank AN-103. The densities were taken from ball rheometer and core data in Stewart et al. (1996). The temperatures were based on a profile measured at the MIT tree; the profile is shown in Section 4.5.2. The pressures were derived from hydrostatic head, and are based on the depth of submergence of the segment and the thicknesses and gas-free densities of the waste layers. In Segments 5, 10, 14, and 16, the solid volume fraction is estimated using 1530 kg/m^3 as the density of solid-free liquid, 1800 kg/m^3 as the density of gas-free slurry, and an assumed 2000 kg/m^3 as the intrinsic (not bulk) density of the solid material. In Segment 2, the crust, the solid fraction is roughly estimated at 0.6, leaving only a small volume fraction of liquid.

The water vapor pressure is the pressure in equilibrium with water in the waste; it is calculated using Equation 6.2 and Table 6.2 of Mahoney and Trent (1995), a correlation for water vapor pressure over concentrated homogeneous and non-homogeneous waste simulants. This correlation requires the weight fraction of water in the slurry, which is calculated using the solid volume fraction and density and the weight fraction of water in the solids-free solution. The latter value was estimated at 0.44, based on Equation 4.4 of Mahoney and Trent (1995), which allows the weight fraction of water in a simulant solution to be back-calculated from the solution density.

Table C.5.9. In-Tank Conditions Used for Tank AN-103 Phase Distribution Calculations

Segment	Density (kg/m^3)	Temperature (°C)	Pressure (atm)	Solid Volume Fraction	Water Vapor Pressure (atm)
2	1530	37.8	1.0	0.6	0.0085
5	1530	42.2	1.27	0	0.0357
14	1800	42.8	1.94	0.57	0.0144
10	1530	42.2	1.63	0	0.0357
16	1800	41.7	2.11	0.57	0.0136

The average ionic concentrations in the drainable liquid in Tank AN-103 are given in Table C.5.10. They are based on the AN-103 solution density of 1530 kg/m^3 and Tables 11 and 13 of WHC-SD-WM-DP-192 Rev. 0, data for µg/g ionic concentrations from 1996 core sample analyses for risers 24A and 24B of Tank AW-101.

Table C.5.10. Ionic Concentrations Used For Tank AN-103 Phase Distribution Calculations

Ion	gmol/L solution
Na^+	2.95
Al^{3+}	1.81
Fe^{3+}	0
Cr^{3+}	0.0033
Ni^{2+}	0.00018
K^+	1.43
OH^-	1.09
NO_3^-	3.95
NO_2^-	3.29
PO_4^{3-}	0
SO_4^{2-}	0
F^-	0
Cl^-	0.22

The Henry's Law constants are necessary to estimate the in-tank phase distribution of gases (see Section 3.2). The intermediate steps in the Henry's Law constant calculation are shown in Table C.5.11. Note that the final Henry's Law constant is in terms of liters of gas-free waste slurry, while the Schumpe model is in terms of kg of water in the salt solution. Both the solid volume fraction and the weight percent of water in the solution are needed to put the Henry's Law constant in its final form. The gases not listed, argon and the minor gases, were assumed wholly insoluble with Henry's law constants of 10^{-10}.

Table C.5.11. Henry's Law Constants For Tank AN-103 Phase Distribution Calculations

Segment	Condition	N_2	H_2	N_2O	O_2	CH_4	NH_3
2	Schumpe (K in water / K in solution)	14.0	7.9	11.4	16.3	16.1	3.7
	Waste Slurry K (mol/atm L waste)	1.1×10^{-5}	2.5×10^{-5}	4.1×10^{-4}	1.8×10^{-5}	2.0×10^{-5}	2.5
5	Schumpe (K in water / K in solution)	12.8	7.5	10.6	15.5	14.9	3.7
	Waste Slurry K (mol/atm L waste)	2.9×10^{-5}	6.6×10^{-5}	9.9×10^{-4}	4.4×10^{-5}	5.0×10^{-5}	5.1
14	Schumpe (K in water / K in solution)	12.6	7.5	10.6	15.4	14.8	3.7
	Waste Slurry K (mol/atm L waste)	1.3×10^{-5}	2.8×10^{-5}	4.2×10^{-4}	1.9×10^{-5}	2.1×10^{-5}	2.1
10	Schumpe (K in water / K in solution)	12.8	7.5	10.6	15.5	14.9	3.7
	Waste Slurry K (mol/atm L waste)	2.9×10^{-5}	6.6×10^{-5}	9.9×10^{-4}	4.4×10^{-5}	5.0×10^{-5}	5.1
16	Schumpe (K in water / K in solution)	12.9	7.5	10.7	15.6	15.1	3.7
	Waste Slurry K (mol/atm L waste)	1.2×10^{-5}	2.8×10^{-5}	4.2×10^{-4}	1.9×10^{-5}	2.1×10^{-5}	2.2

The Henry's Law constant calculation is one method of calculating the ammonia partial pressure. Another method uses a grab-sample of extractor atmosphere, which is analyzed to find the ammonia content and hence the partial pressure at the time the sample was taken. Table C.5.12 shows the results of these analyses for AN-103 samples. In the table, "UBV" indicates unbound vapor, or the sample taken just before the J1 canister; "BV" means bound vapor, the sample taken just after the temperature ramp.

Table C.5.12. Grab-Sample Data for Deriving Ammonia Partial Pressures in Tank AN-103

Sample	Grab-Sample Volume (cc)	Fill Temperature (°C)	Fill Pressure (kPa)	µmol NH_3	NH_3 Partial Pressure (atm)
2-UBV*					
2-BV	40.5	23.7	2.103	1.4	0.00082
5-UBV*					
5-BV	52.2	24	2.038	18.0	0.0085
14-UBV	52	24.2	3.829	16.2	0.0077
14-BV	52	24.5	2.354	0.4	0.00017
10-UBV*					
10-BV	51.7	23.5	1.768	16.2	0.0077
16-UBV	52.2	24.2	3.978	14.7	0.0070
16-BV*					

* Grab-samples were lost in handling.

References

Brevick, C.H., and L.A. Gaddis. 1995. *Historical Tank Contents Estimates for the Northeast Quadrant of the Hanford 200 East Area.* WHC-SD-WM-ER-349, Rev. 1A, ICF Kaiser Hanford Company, Richland, Washington.

Mahoney, L.A., and D.S. Trent. 1995. *Correlation Models for Waste Tank Sludges and Slurries.* PNL-10695, Pacific Northwest Laboratory, Richland, Washington.

Norton, J.D., and L.R. Pederson. 1994. *Ammonia in Simulated Hanford Double-Shell Tank Wastes: Solubility and Effects on Surface Tension.* PNL-10173, Pacific Northwest Laboratory, Richland, Washington.

Norton, J.D., and L.R. Pederson. 1995. *Solubilities of Gases in Simulated Tank 241-SY-101 Wastes.* PNL-10785, Pacific Northwest Laboratory, Richland, Washington.

Schumpe, A. 1993. "The Estimation of Gas Solubilities in Salt Solutions", Chem. Eng. Sci., Vol. 48, pg. 153.

Stewart, C.W., Alzheimer, J.M., Brewster, M.E., Chen, G., Mendoza, R.E., Reid, H.C., Shepard, C.L., and G. Terrones. 1996. *In Situ Rheology and Gas Volume in Hanford Double-Shell Waste Tanks.* PNL-11296, Pacific Northwest Laboratory, Richland, Washington.

Welsh, T.L. 1991. *Tank 241-AW-101 Characterization Results.* WHC-SD-WM-TRP-055, Rev 0, Westinghouse Hanford Company, Richland, Washington.

Distribution

No. of Copies

Offsite

2 DOE Office of Scientific and Technical Information

E. K. Barefield
Georgia Institute of Technology
Boggs Chemistry Building
225 North Avenue
Atlanta, GA 30332

M. J. Barnes
Savannah River Site
Aiken, SC 29802

D. O. Campbell
102 Windham Road
Oak Ridge, TN 37830

S.J. Eberlein
Westinghouse Savannah River
241-12H
Aiken, SC 29802

Charles W. Forsberg
Oak Ridge National Laboratory
P.O. Box 2008, MS-6495
Oak Ridge, TN 37831-6495

B. C. Hudson
P.O. Box 271
Lindsborg, KS 67456

M. S. Kazimi
Massachusetts Institute
of Technology
Department of Nuclear Engineering
77 Massachusetts Avenue
Cambridge, MA 02139

J. L. Kovach
P.O. Box 29151
70000 Huntley Road
Columbus, OH 43229

T. S. Kress
102-B Newridge Road
Oak Ridge, TN 37830

No. of Copies

T. E. Larson
2711 Walnut St.
Los Alamos, NM 87545

4 Los Alamos National Laboratory
P.O. Box 1663
Los Alamos, NM 87545

Attn:	W. L. Kubic	K575
	K. Pasamehmetoglu	K575
	C. Unal	K575
	JR White	K575

D. Meisel
Argonne National Laboratory
Chemistry Division
9700 S. Cass Avenue
Argonne, IL 60439

D. Pepson
U.S. Department of Energy
Trevion II Building, EM-35
Washington, D.C. 20585-0002

D. A. Powers
Sandia National Laboratory
Nuclear Facilities Safety Department
MS-0744
Albuquerque, NM 87185-0744

W. R. Rossen
University of Texas at Austin
Department of Petroleum/
Geosystems Engineering
Austin, TX 78712

S. E. Slezak
806 Hermosa NE
Albuquerque, NM 87110

Onsite

6 DOE Richland Operations Office

M. H. Campbell	S7-73
K. Chen	S7-54
J. M. Gray	S7-54
C. A. Groendyke	S7-54

No. of Copies

G. W. Rosenwald	S7-54
C. L. Sohn	S7-51

51 PHMC

R. P. Anantatmula	R1-30
S. A. Barker	R2-11
G. S. Barney	T5-12
W. B. Barton	R2-11
R. E. Bauer (10)	S7-14
C. J. Benar	R2-12
R. J. Cash	S7-14
N.S. Cannon	L6-38
A.F. Choho	H6-35
M. L. Dexter	R1-51
J. G. Field	R2-12
K. A. Gasper	G3-21
T. C. Geer	R1-43
J. M. Grigsby	R1-49
B. E. Hey	T6-07
K. M. Hodgson	H0-34
T. A. Hu	R2-12
J. R. Jewett	T6-07
J. Jo	R2-12
G. D. Johnson	S7-15
N. W. Kirch	R2-11
P. F. Kison	T4-07
G. M. Koreski	R2-11
J. G. Kristofzski	R2-12
C. E. Leach	R1-49
J. W. Lentsch	S2-48
C.G. Linschooten	S7-12
L. L. Lockrem	S3-90
J. E. Meacham	S7-14
W. H. Meader	S8-05
N. J. Milliken	A3-37
J. C. Person	T6-09
R. E. Raymond	S7-12

No. of Copies

D. A. Reynolds	R2-11
E. R. Siciliano	HO-31
B. C. Simpson	R2-12
L. M. Stock	S7-14
R. R. Thompson	R2-12
J. E. Van Beek	S2-48
R. J. Van Vleet	A3-34
A. B. Webb	A3-37
N. E. Wilkins	R2-11

45 Pacific Northwest National Laboratory

Z. I. Antoniak	K7-15
J. M. Bates	K7-15
B. O. Barnes	P7-41
M. E. Brewster	K1-96
J. W. Brothers (10)	K9-20
S. A. Bryan	P7-25
B. C. Bunker	K2-25
M.A. Chieda	K5-25
J. A. Fort	K7-15
P. A. Gauglitz	P7-41
J. L. Huckaby	K6-80
L. A. Mahoney	K7-15
P. A. Meyer	K7-15
B. J. Palmer	K7-15
L. R. Pederson	K2-44
K. P. Recknagle	K7-15
D. R. Rector	K7-15
H. C. Reid	K7-15
A. Shekarriz (10)	K7-15
C. W. Stewart	K7-15
G. Terrones	K7-15
P. D. Whitney	K5-12
Information Release (5)	K6-06